Novel Tools for Molecular Imaging and Bioconjugation

Synthesis and Characterization of New Probes and Tracers for the Visualization of β-Cells

Romain Bertrand

The research leading to these results has received funding from the People Program (Marie Curie Actions) of the European Union's Seventh Framework Program FP7/2007-2013/under REA Grant Agreement No. 289932.

Printing of this thesis was financially supported by Radboud University Nijmegen.

Cover design: Mathieu Bourlion

Printed by: Ipskamp Printing
ISBN: 978-94-028-0891-9

Novel tools for molecular imaging and bioconjugation

Synthesis and characterization of new probes and tracers for the visualization of β-cells

Doctoral Thesis

to obtain the degree of doctor
from the Radboud University Nijmegen
on authority of the Rector Magnificus prof. dr. J.H.J.M. van Krieken,
according to the decision of the Council of Deans
to be defended in public on Friday, February 2, 2018
at 16.30 hours

by

Romain Bertrand
born on September 29, 1989
in Neuilly sur Seine, France

Supervisors
Prof. dr. Martin Gotthardt
Prof. dr. Oliver Plettenburg (Leibniz Universität Hannover, Germany)

Co-supervisors
Dr. Volker Derdau (Sanofi, Germany)
Dr. Maarten Brom

Doctoral thesis committee
Prof. dr. Ir. Jan van Hest
Prof. dr. Roland Brock
Dr. Fijs van Leeuwen (Leiden University Medical Center)

Paranymphen
Romain Grosse
Marion Alriquet

Novel tools for molecular imaging and bioconjugation

Synthesis and characterization of new probes and tracers for the visualization of β-cells

Proefschrift

ter verkrijging van de graad van doctor
aan de Radboud Universiteit Nijmegen
op gezag van de rector magnificus prof. dr. J.H.J.M. van Krieken,
volgens besluit van het college van decanen
in het openbaar te verdedigen op vrijdag 2 februari 2018
om 16.30 uur precies

door

Romain Bertrand
geboren op 29 september 1989
te Neuilly sur Seine, France

Promotoren
Prof. dr. Martin Gotthardt
Prof. dr. Oliver Plettenburg (Leibniz Universität Hannover, Duitsland)

Copromotoren
Dr. Volker Derdau (Sanofi, Duitsland)
Dr. Maarten Brom

Manuscriptcommissie
Prof. dr. ir. Jan van Hest
Prof. dr. Roland Brock
Dr. Fijs van Leeuwen (LUMC)

Paranymphen
Romain Grosse
Marion Alriquet

« Connaître, ce n'est point démontrer, ni expliquer. C'est accéder à la vision »
Antoine de Saint Exupéry

This work is dedicated to Lise Deval

Table of content

Outline of the Thesis

Diabetes is a group of metabolic diseases characterized by a deficiency in control of glucose homeostasis which can have severe life-threatening consequences. To date, no cure for diabetes exists. The disease affects an increasing number of people and imposes a massive public health challenge for almost every country around the globe. Contrary to preconceived ideas, diabetes is not confined to western world countries, with lower socioeconomic groups being disproportionately affected in high-income countries, and with over three-quarters of the world's diabetic population living in low- and middle-income countries. Considering the serious human, societal, and economic consequences, major research efforts have been undertaken in the last decades to tackle the disease and its complications. However, our knowledge on the pathogenesis of diabetes remains limited. In type 1 diabetes, autoimmune destruction of insulin-producing cells, also called β-cells, leads to an insulin shortage and a subsequent glycemic dysregulation. In type 2 diabetes, insulin resistance of the target cells combined with an impaired β-cell function are the main causes of hyperglycemia. The changes in β-cell mass and function in the development and progression of diabetes are not well identified, nor well characterized. Imaging tools to visualize and monitor β-cells non-invasively would improve our understanding of the disease onset and progression. Furthermore, β-cell imaging might help in the development of novel anti-diabetic medication, or for therapies such as islet transplantation by providing information on the graft's survival. Due to β-cell sparsity, and to β-cell location, β-cell imaging faces numerous hurdles. Consequently, finding an ideal biological target that is highly and specifically expressed by the β-cells, and a suitable probe that binds tightly and exclusively to the β-cells, is a challenging process. As of today, despite extensive efforts from researchers worldwide, there is no probe or tracer that can precisely detect and quantify β-cells *in vivo*.

In this thesis, the design, the synthesis, and the characterization of novel fluorescent probes and radioactive tracers as new promising tools for β-cell imaging are described. The development of new imaging probes relies on the field of bioconjugation chemistry. The most widespread approaches to functionalize peptides rely on the chemistry of lysine and cysteine side chains. However, in some cases these conjugation strategies present shortcomings such as high abundance of lysine residues or the need of preliminary reductive treatment to cleave disulfide bridges. Therefore, we report a novel methodology to label unprotected peptides, based on the reactivity of tyrosine.

Diabetes and its consequences are presented in **Chapter 1**, and how non-invasive β-cell imaging could give a better understanding of the disease is discussed. We also reviewed potential targets and the most promising approaches for selective visualization of β-cells, with a particular emphasis on the free fatty acid receptor 1 (FFAR1/GPR40), which is predominantly expressed in human and rodent pancreatic β-cells. Accordingly, we report in **Chapter 2** the design and development of the first fluorescent probes targeting the FFAR1, which was until now unexplored for imaging purposes. The novel probes, which are based on the scaffold of TAK875, a synthetic FFAR1 agonist with high affinity and selectivity for the receptor, were characterized *in vitro* on different kind of β-cell models. Using the same scaffold, we synthesized the first [^{18}F]-radioactive analog of TAK875, as described in **Chapter 3**, which could serve as a potential PET tracer for selective β-cell imaging. Incretin derivatives such as Exendin-4, a potent agonist of the glucagon-like peptide 1 receptor (GLP-1R), are promising peptides for β-cell imaging. In the search of novel bioconjugation techniques to allow synthesis of new peptidic imaging probes, we examined in **Chapter 4** the mono-iodination of tyrosine residues on fully unprotected peptides. The introduced iodine can subsequently serve as a handle for further

functionalization such as for the introduction of fluorescent dyes. Finally, in **Chapter 5** the remaining, yet unpublished experimental results and future perspectives are discussed.

Chapter 1

General introduction

Introduction

Diabetes, a global burden

Diabetes mellitus, commonly referred to as diabetes, is a chronic, metabolic disease diagnosed by observing raised levels of glucose in the blood. Over time, these high blood glucose levels, known as hyperglycemia, damage many tissues in the body, leading to the development of disabling and life-threatening health complications.[1] Symptoms of the condition range from frequent urination, persistent thirst, increased hunger, fatigue, weight loss or blurry vision.[2] The disease is also associated with reduced life expectancy, significant morbidity due to specific diabetes related microvascular complications (retinopathy, neuropathy, nephropathy), increased risk of macrovascular complications (ischemic heart disease, stroke and peripheral vascular disease) and diminished quality of life.[3] Three ways to diagnose diabetes mellitus exist, and each, in the absence of unequivocal hyperglycemia, must be confirmed by any one of the three methods given in Figure 1.[4]

Symptoms of diabetes plus casual plasma glucose concentration ≥ 200 mg/dL (11.1 mmol/L)[a]
or
Fasting plasma glucose ≥ 126 mg/dL (7.0 mmol/L)[b]
or
2-h post load glucose ≥ 200 mg/dL (11.1 mmol/L) during an oral glucose tolerance test[c]

Figure 1 Criteria for the diagnosis of diabetes. a) Casual is defined as any time of day without regard to time since last meal. The classic symptoms of diabetes include polyuria, polydipsia, and unexplained weight loss. b) Fasting is defined as no caloric intake for at least 8 h. c) The test should be performed as described by the World Health Organization, using a glucose load containing the equivalent of 75 g anhydrous glucose dissolved in water.

Diabetes can be classified into three main categories: type 1 diabetes (T1D), type 2 diabetes (T2D) and gestational diabetes (GDM).

Type 1 diabetes (T1D), also called insulin-dependent diabetes, is an autoimmune disease[5] characterized by the expansion of pathogenic T effector cells which cause the irreversible destruction of insulin producing cells. As a consequence, insulin production is insufficient and thus glucose homeostasis uncontrolled.[6] T1D is usually observed in children, teens or young adults. Management of T1D requires the careful maintenance of near-normalized blood glucose levels while minimizing the risk of hypoglycemic episodes. These latter events can lead to symptoms varying from anxiety, palpitations, and tremor, to neurological impairments, including behavioral changes, cognitive dysfunction and seizures. Severe prolonged hypoglycemia can cause permanent brain damage.[7] As a result of insufficient insulin dosing, a person with T1D can also lapse into a life-threatening diabetic coma, also known as diabetic ketoacidosis.[8]

Type 2 diabetes (T2D) is the most prevalent form of the disease. In high-income countries, more than 91% of adults with diabetes have T2D.[9-12] It usually occurs in adults, but is increasingly seen in children and adolescents. In T2D, the body is able to produce insulin but is unable to respond to its effects: this is known as insulin resistance. Over time, insulin levels may also subsequently become insufficient. Both the insulin resistance and deficiency lead to high blood glucose levels. Although the exact causes for the development of T2D are still not fully identified, there are several known risk factors. The most important are excess body weight and obesity, sedentary lifestyle and unhealthy diet.[13-17] Many people with T2D remain unaware of their condition for a long time because the symptoms are usually less marked than in T1D and may take years to be recognized. However, during this time the body is already being damaged by excess blood glucose. In contrast to people with T1D, most people with T2D do not require daily insulin treatment to survive. The cornerstone of treatment of T2D is the adoption of a healthy diet, increased physical activity and maintenance of a normal body weight. If followed carefully, these three guidelines can yield to disease remission, for cases of T2D being diagnosed early enough.[18] In the absence of contraindications, an oral antidiabetic drug (such as metformin) is recommended as a first line treatment, when changes in lifestyle were inefficient in controlling glycemia (Figure 2). A second oral agent of another class (sulfonylureas, thiazolidinediones, dipeptidyl peptidase-4 inhibitors, SGLT2 inhibitors - Figure 2) may also be added for patients inadequately controlled with metformin monotherapy.

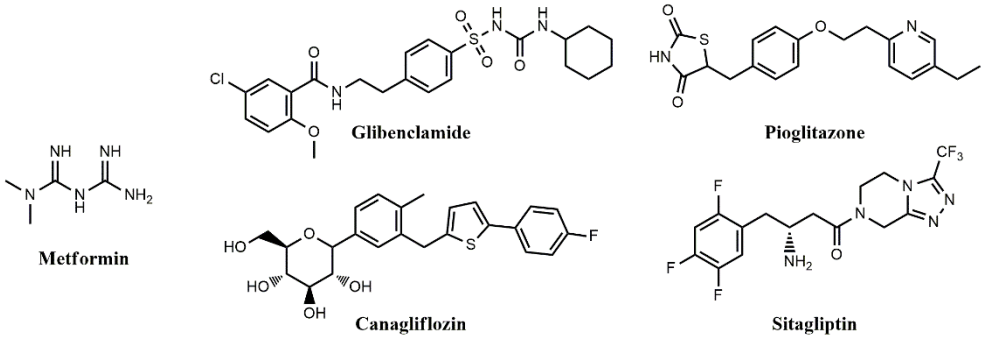

Figure 2 Examples of structures of oral antidiabetic drugs including metformin, glibenclamide (sulfonylurea), pioglitazone (thiazolidinediones), sitagliptin (dipeptidyl peptidase-4 inhibitors), and canaglifozin (SGLT2 inhibitor).

Gestational diabetes mellitus (GDM) is defined as glucose intolerance of various degrees which appears, or is first diagnosed, during pregnancy.[19] Approximately 7% of all pregnancies are affected by GDM[20] which engenders a risk of morbidity and mortality to mother, fetus and subsequent newborn.[21,22] Gestational diabetes normally disappears after birth. However, women with the history of gestational diabetes mellitus are at higher risk of being affected by gestational diabetes in subsequent pregnancies and of developing type 2 diabetes later in life. They have a 20 to 70% chance of developing T2D within the 5 to 10 years following delivery.[23] They also have a significantly increased risk of cardiovascular disease in the years after pregnancy.[24] It was also observed that offspring born to mothers with GDM also have a higher risk of developing T2D in their life.[25]

The two main subtypes of diabetes are summarized in Figure 3, and compared to the healthy situation.

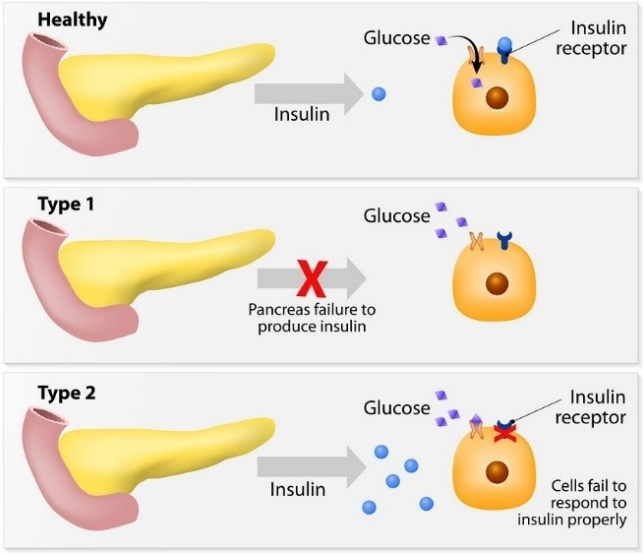

Figure 3 Schematic representation of the healthy situation compared to the main different types of diabetes. In normal situation, insulin acts as a key that lets the body's cells take in glucose and use it as energy. The lack of insulin (for T1D patients), or insulin resistance (for T2D and GDM patients) in a person with diabetes results in high circulating levels of blood glucose causing damages to many tissues in the body. Retrieved with permission from http://www.healthstyle.net.au/article/diabetes-the-tale-of-two-types as accessed on 2016, November 11).

A challenge arising in the last years is that more and more individuals are diagnosed with forms of diabetes that do not fit in the three above-mentioned categories. Other metabolic disorders of glucose include, for instance, monogenic diabetes (maturity onset diabetes of the young MODY) or latent autoimmune diabetes of adults (LADA) which is sometimes referred to as type 1.5 diabetes, as it is a form of T1D that shares some characteristics with T2D. Classification of diabetes is permanently evolving as efforts are undertaken to understand the pathogenesis of each form, with the purpose of gaining relevant information on the cause, natural history, genetics and heritability, clinical phenotype and, most importantly, to provide the patients with optimum treatments for the disease.[26]

In 2015, according to the International Diabetes Federation (IDF), 415 million adults were estimated to have diabetes worldwide and this number is expected to reach 642 million in 2040.[1] Notably, the IDF estimates that one in two adults with diabetes is undiagnosed. Diabetes is major causes of death in most countries: in 2013, the disease and its related complications engendered 5.1 million deaths,[27] which is more than HIV/AIDS (1.5 million[28]), tuberculosis (1.5 million[29]) or malaria (0.6 million[30]). In addition to the daunting human and social costs, the condition has heavy financial consequences. Not only does diabetes impose a large financial burden on individuals and their families due to the cost of healthcare, but it also has a substantial economic impact on communities and their national health systems.[31-36] This is due to the high and globally increasing prevalence of diabetes, the demand for multi-modal treatment, and the serious complications associated with long disease duration. The American Diabetes Association estimated the total economic cost of diagnosed diabetes in the United States in 2012 to be $245 billion.[37] Furthermore, the costs related to undiagnosed diabetes are considerable: they include medical (hospital inpatient, physician and emergency care, and retail prescriptions) and nonmedical (workdays absent or reduced performance at work). One study from the United States found that undiagnosed diabetes was responsible for an additional $18 billion in

healthcare costs in 2007.[38] In Europe, the ageing population will place an increasing number of people at risk of diabetes and, consequently, place a greater cost burden on health systems. A majority of countries already spend between 5% and 20% of their total health expenditure on diabetes.[1] With such a high cost, the disease is a major challenge for healthcare systems today and this challenge will grow greater in the future.

The link between insulin and pancreatic β-cells

Diabetes occurs when the body cannot produce enough insulin or because the body does not respond properly to insulin.[39] The link between insulin, the pancreas and diabetes was first postulated by Minkowski and Mering at the end of the 19th century when they noticed that a dog developed signs of diabetes after a total pancreatectomy.[40] A few years later, Hédon observed that grafting a small piece of pancreatic tissue under the skin after a total pancreatectomy relieved diabetes, but the disease promptly returned on removal of the tissue.[41] These results led Gustave-Edouard Laguesse to hypothesize that the small clusters of ductless cells within the pancreas - described by Paul Langerhans in 1869 and named Langerhans islets as a tribute to the discoverer[42] - could be the source of the substance involved in glucose control. In 1901, Opie finally confirmed the association between the islet cells and diabetes by connecting the degeneration of the islet cells to the appearance of diabetes.[43]
Human insulin is a polypeptide with a molecular mass of 5.808 g/mol, comprising an A and a B chain connected by two disulphide bridges (Figure 4). Within mammals, the amino acid sequence of insulin is highly conserved. The sequence of insulin was determined by British molecular biologist Frederick Sanger, while British biochemist Dorothy Hodgkin resolved the spatial conformation of the molecule by means of X-ray diffraction studies. They were respectively awarded the Nobel Prize in Chemistry in 1958 and 1964 for their work.

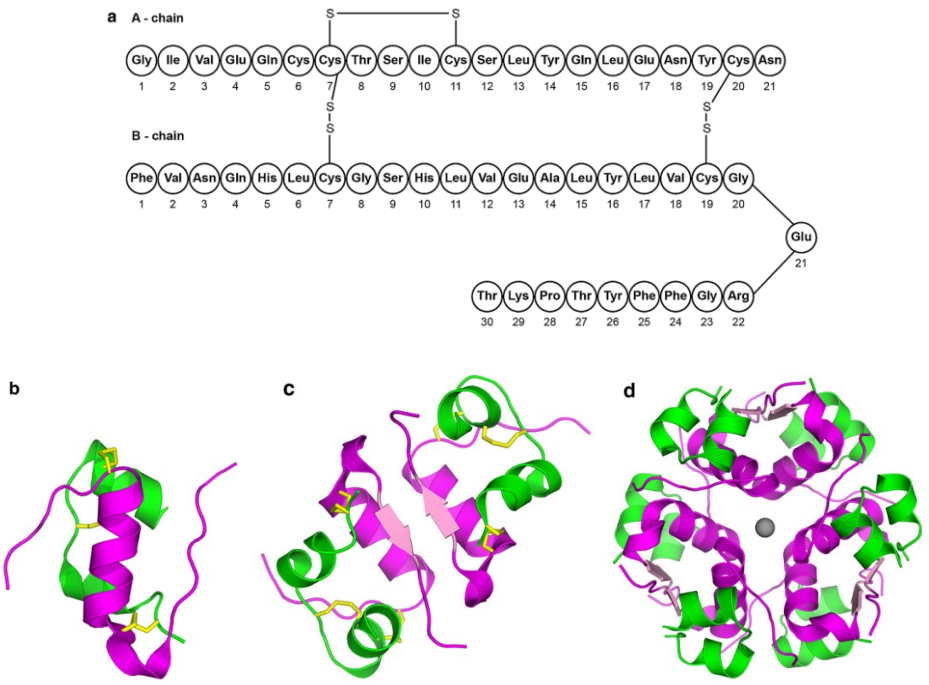

Figure 4 Structures of human insulin. Schematic structure of insulin (a), the three-dimensional structures of insulin monomer (b), dimer (c), and hexamer (d). In (b–d): A chain (green), B chain (magenta). In (d) two axial zinc ions (grey; overlaid at center for clarity) are coordinated by six histidine side chains from residue B10 (not shown for clarity). (Adapted from Hilgenfeld).[44]

Insulin has a key role in vertebrates' glucose homeostasis. It is primarily secreted in response to elevated blood concentrations of glucose, although some neural stimuli (e.g. sight and taste of food)[45] and increased blood concentrations of other molecules, including amino acids, fatty acids or incretins, can also increase glucose-induced insulin secretion.[46] The hormone helps regulate the metabolism of carbohydrates, fats and proteins by promoting the absorption of blood glucose into fat, liver and skeletal muscle cells. In these tissues the absorbed glucose is converted into either glycogen or fats (triglycerides), or in the case of the liver, into both.[47] When the islet cells are stimulated by glucose, insulin - which is stored as microcrystalline arrays of zinc insulin hexamers within secretory vescicles[48] - is released by exocytosis and diffuses into the blood after a complex signaling pathway involving glucose phosphorylation, closure of the ATP-gated potassium and a subsequent increase in cytosolic [Ca^{2+}] levels, as shown in Figure 5.

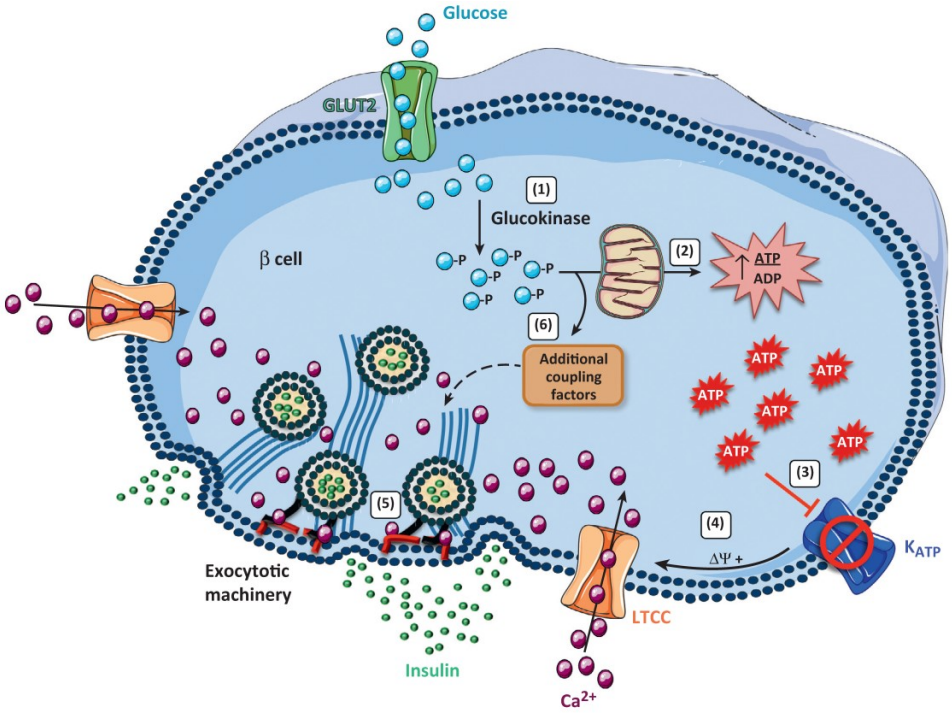

Figure 5 Mechanisms of glucose-stimulated insulin secretion. Increased blood glucose concentrations result in enhanced glucose uptake by β-cells through the glucose transporter GLUT2. Intracellular glucose is rapidly phosphorylated by glucokinase (1) and the product subsequently undergoes glycolysis to produce pyruvate which leads to elevated ATP production and a rise in the ATP/ADP ratio (2). Closure of ATP-gated potassium channels ensues (3), resulting in plasma-membrane depolarization and consequent opening of voltage-gated Ca^{2+} channels (L-type Ca^{2+} channels, LTCCs) (4). Finally, an influx of extracellular Ca^{2+} through LTCCs increases cytosolic Ca^{2+} levels, which promotes insulin secretion by activating the exocytotic machinery involved in fusion of insulin granules with the β-cell plasma membrane (5). Additional coupling factors emanating from glucose metabolism – the nature of which remains debated – amplify this main triggering pathway (6). (Adapted from Mancini).[49]

Insulin is exclusively secreted by β-cells from the islets of Langerhans, located in the pancreas. In humans, the pancreas is a yellowish organ about 12-15 cm long and 4 cm wide and around 98% of it is composed of exocrine tissue (pancreatic acini) and ductal systems. The islets of Langerhans constitute approximately 2% of the pancreatic mass: there are about one million islets distributed heterogeneously throughout the pancreas of a healthy human adult, each of which measures about

0.2 mm in diameter. The combined mass of the islets is estimated to be 1 to 1.5 grams in average.[50] The islets consist of three major cell types (α, β, and δ-cells) which produce important hormones (glucagon, insulin, and somatostatin respectively). In all species, the β-cells are the most abundant (55-75%) of the three, followed by the α-cells (15-30%) and the δ-cells (5-15%)(Figure 6).[51]

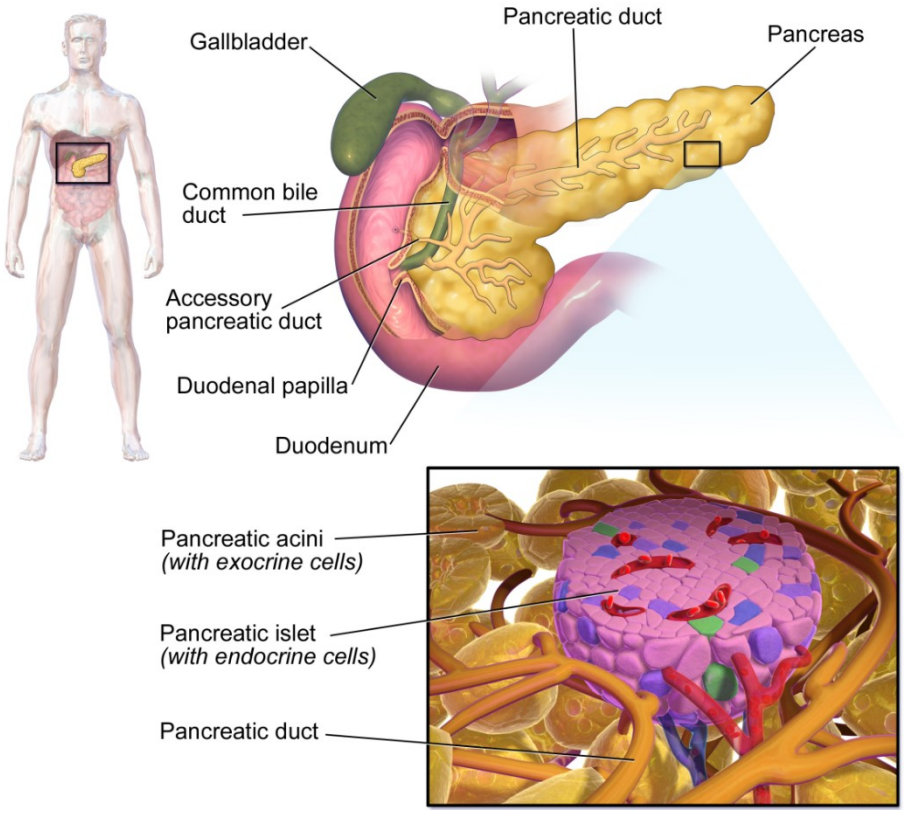

Figure 6 Schematic representations of human pancreas and islets of Langerhans. The pancreas is located in the upper part of the abdomen, surrounded by the stomach, the intestine and the liver. The Langerhans islets (magnified) are scattered throughout the pancreas and are mostly composed of β-cells (pink), α-cells (violet), δ-cells (green) and PP cells (blue). (Figure by Bruce Blaus, Wikiversity Journal of Medicine, 2014).

Why do we need β-cell imaging? Understanding the link between β-cell mass, function, and onset of diabetes

Glucose homeostasis disorders happen when the body cannot produce enough insulin or cannot use insulin effectively. Shortage of insulin production can be caused by both impaired β-cell function (BCF) - when the amount of insulin required to restore normoglycemia is not released, and a decrease in β-cell mass (BCM) which, though perfectly functional, do not produce enough hormone.[52] The total mass of pancreatic β-cells in humans generally increases rapidly from birth to adulthood.[53] Both T1D and T2D have been associated with a significant reduction of the BCM (from 0-65% for TD2 to and 70-99% for TD1 – Figure 7).[54] For children, teens or young adults affected by TD1, the β-cell mass declines over many years from a young age;[55] whereas for T2D patients, the functional sensitivity of β-cells to hyperglycemia tends to diminish with advancing age[56] and the BCM may have reduced significantly before the first symptoms are clinically diagnosed.[57-60]

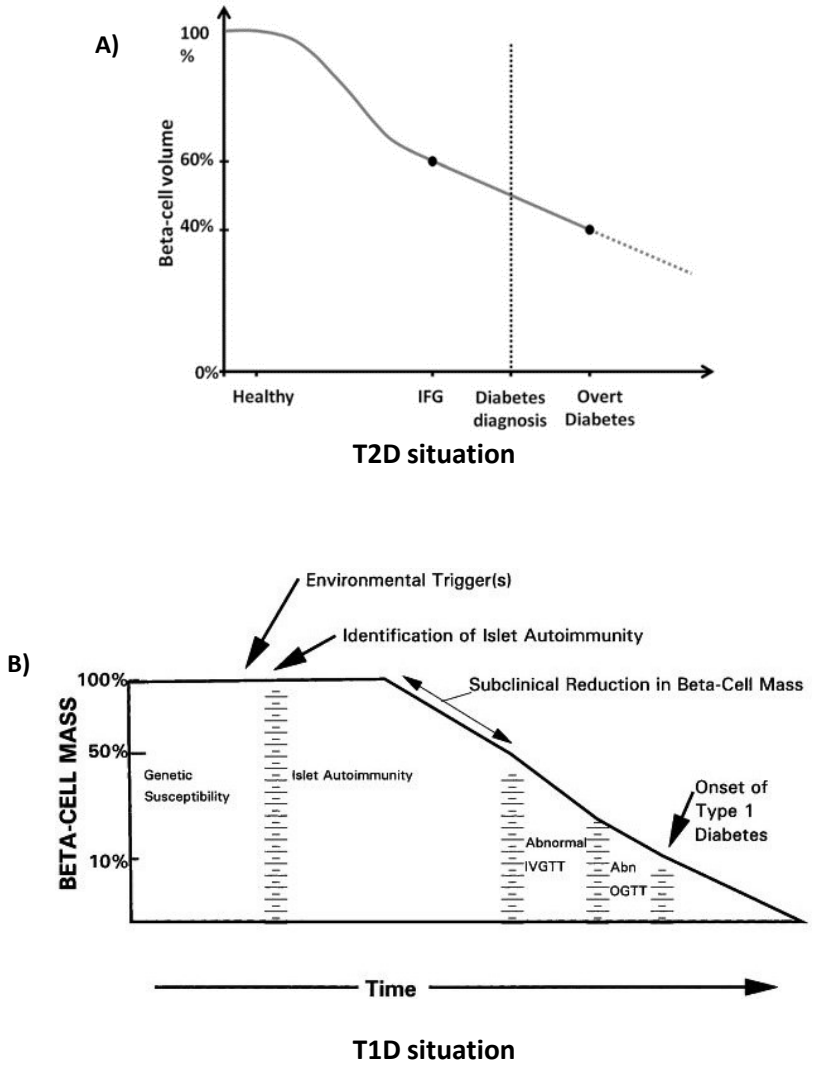

Figure 7 A)Postulated β-cell loss during disease progression in T2D. Impaired fasting glucose = IFG (Adapted from Neutzsky-Wulff).[57] B) Postulated β-cell loss during disease progression in T1D (Adapted from Fakhfakh)[61].

Currently, BCF is evaluated by blood glucose and insulin determination, HbA1C measurements and intraperitoneal or oral glucose-stimulated insulin secretion (GSIS)**.** Although the above-mentioned measurements may provide a surrogate assessment of the BCM, they do not afford its precise quantification. Insulin immunostaining for β-cells after pancreatic biopsy is the only available method to determine the BCM, but being invasive, unreliable and dangerous, its use as a standard to monitor the BCM before or during the progression of the disease is precluded. Furthermore, studies of BCM based on invasively extracted pancreatic tissues do not show the dynamics of the BCM over time.[62,63] Diabetes has been extensively studied for a long time, more than 100 years separates us from Langerhans', Hédon's, and Opie's discoveries, and yet the exact role of the BCM - and its link to the BCF - in the development and progression of diabetes is still poorly understood. For instance, it is still unknown whether the disease starts preferentially in individuals with only a deficit in β-cell number, leading to impaired cell activity due to cellular exhaustion over time. Or, on the other hand, whether aggressing factors (such as high levels of lipids, sugars, cytokines or amyloid polypeptide, metabolic and oxidative stress, etc.) disturb BCF, and then the subsequent hyperglycemia drive β-cell apoptosis.[64] One can also hypothesize that a modulation of both BCM and BCF occurs during the development of

the disease to compensate for high insulin demand, this ability is called plasticity, before eventually declining.
Specifically, although five stages[65] in the progression of diabetes is postulated (characterized by different changes in BCM and BCF), we do not know the natural evolution of β-cell mass, nor do we have convincing evidence on potential β-cell neogenesis and on the preserved β-cell mass in patients. The ability to evaluate independently BCF and BCM is therefore expected to play a pivotal role in future diabetes research. Furthermore, with the introduction of antidiabetic treatments suggesting modulating, preserving or even an increasing the BCM, it becomes clear that we are in need of reliable, sensitive, specific, and non-invasive methods to visualize living pancreatic β-cells in order to validate these claims.[66,67] Such imaging techniques might help to enhance our understanding of the pathophysiology of T2D and T1D, by getting more insights into the precise molecular mechanisms leading to the decrease in β-cell mass and function.

Non-invasively imaging pancreatic β-cells is a challenge hindered by many obstacles.[68] First, as described previously, β-cells comprise only 1-2% of the total pancreatic mass and are heterogeneously distributed in the organ. Distinguishing such a rare population of cells from the exocrine tissues in the pancreas is therefore extremely difficult; it was estimated that the uptake of β-cells specific probes must exceed the uptake of tracer in exocrine tissue cells by roughly 440-fold.[69] Second, in diabetics the BCM is likely to decrease over time, so the ability to monitor disease progression depends on detecting small variations. Third, the pancreas is surrounded by the gastrointestinal system and liver, and consequently, probe uptake in the latter organs complicates visualization of the pancreas.

Receptors or proteins that are highly expressed on β-cell membranes have been reported as potential targets for β-cell imaging. They include sulfonylurea receptor 1 (SUR1),[70,71] membrane protein IC2,[72,73] or transmembrane protein 27 (TMEM27).[74,75] However, the reported approaches focusing on SUR1, IC2 or TMEM27 showed limitations attributed either to the expression of the target (heterogeneous or non-β-cell specific expression) or to the developed tracer (low absolute uptake, or even unspecific accumulation of the tracer).[76] Nonetheless, in the past few years, several research groups have developed imaging tools for the visualization of pancreatic β-cells and transplanted islets. The three most promising approaches that are currently being investigated through clinical trials are targeting either the glucagon like peptide 1 receptor (GLP-1R), the vesicular monoamine transporter 2 (VMAT2) or tracing the serotonin biosynthesis via dopa decarboxylase (DDC).

The [^{11}C]-radiolabeled analog of 5-hydroxytryptophan ([^{11}C]-5-HTP) is a biogenic precursor for serotonin and was originally developed as a PET neuroimaging tracer to assess the rate of serotonin biosynthesis by DDC in the central nervous system. Since the full serotonergic metabolic pathway has been described in the pancreatic β-cells and has been implicated in insulin release and β-cell proliferation, the use of [^{11}C]-5-HTP was investigated .[77] The total pancreatic uptake of [^{11}C]-5-HTP was found to be reduced by 66% in humans with T1D compared with healthy volunteers. In two of the individuals with T1D enrolled in the study, total uptake decreased by more than 90%.[78] Inasmuch as the serotonin biosynthesis takes place in all pancreatic neuroendocrine tissue, and not exclusively in β-cells, the [^{11}C]-5-HTP radioligand should not serve as a BCM detecting tool but rather as a good biomarker of total endocrine mass.[77, 78]

Vesicular monoamine transporter is a transmembrane protein that translocates monoamines from the cytoplasm into secretory vesicles. The type 2 protein (VMAT2) is highly expressed in pancreatic β-cells.[79] PET-imaging of VMAT2 was made possible by the development of radiolabeled dihydrotetrabenazine (DTBZ) analogues such as [^{18}F]-FP-(+)-DTBZ, which specifically bind to VMAT2.[80] With this radioligand, significant differences in tracer uptake could be observed between healthy volunteers and people with T1D[81] as displayed in Figure 8. However, doubts on the specificity of VMAT2 ligands emerged recently, especially regarding unspecific binding to exocrine tissue in rodent models,[82] or to pancreatic PP cells.[83]

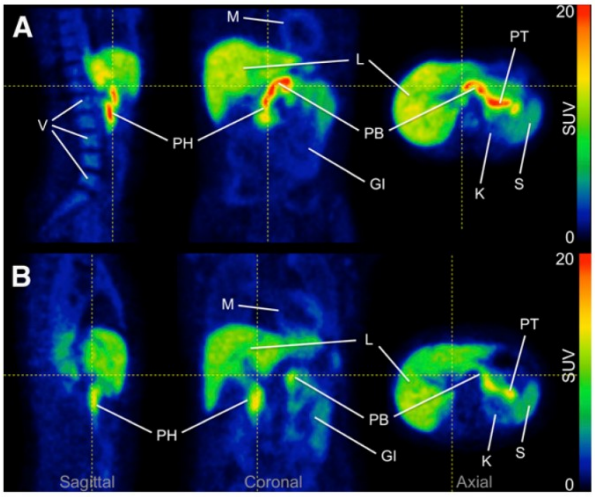

Figure 8 [^{18}F]-FP-(+)-DTBZ PET images of a healthy volunteer (A) and a patient with T1D (B). Pancreas uptake was clearly reduced in diabetic patient. PB, PH and PT = pancreas body, head, and tail. K = kidney. L = liver. M = myocardium. S = spleen. V = vertebrae. GI = gastrointestinal tract. (Adapted from Normandin).[81]

Glucagon like peptide 1 receptor (GLP-1R) is abundantly expressed on native islets,[84] and peptides targeting the GLP-1R are thus promising candidates for use in β-cell imaging. As well, GLP-1R agonists such as Lixisenatide, Exenatide, or Albiglutide are safe and already used clinically for the treatment of T2D. Exendin derivatives, which bind to the extracellular domain of GLP-1R with picomolar affinity, have been extensively used for visualization of β-cell using fluorescence microscopy,[85] MRI,[86] and nuclear imaging.[87-89] Notably, SPECT-imaging with [^{111}In]-Exendin-4 showed a marked reduction in pancreatic uptake in patients with T1D as shown in Figure 9, even if substantial inter-individual variability and overlap between diabetic and non-diabetic individuals was also observed.[90]

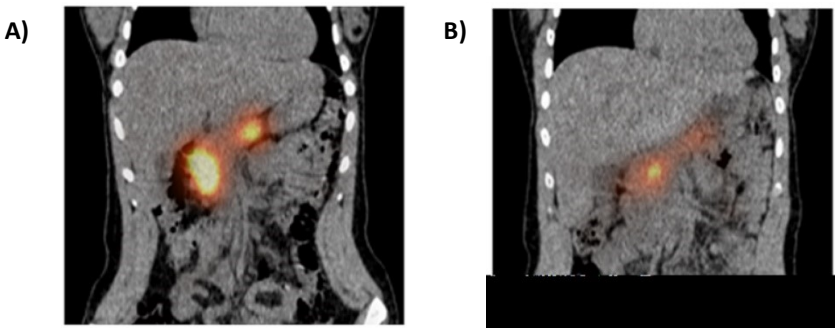

Figure 9 [^{111}In]-Exendin-4 SPECT/CTPET images of the abdomen of a healthy volunteer (A) and a patient with T1D (B). Pancreas uptake was clearly reduced in diabetic patient. (Adapted from Brom).[90]

Nevertheless, one limitation with GLP-1R targeting molecules could arise: some concerns exist whether potential downregulation of the receptor may influence uptake of the tracer.[91, 92] This downregulation may lead to an erroneously low quantification of β-cell number. Notably, it was shown that changes in Exendin-4 fluorescent probe signal intensity did not directly reflect changes in BCM in two T2D mouse models ($Lepr^{db/db}$ and Diet-Induced Obese), most likely due to receptor downregulation.[93] However, evidence indicating that mice are not a suitable model to follow β-cell evolution with GLP-1R targeting probes has recently come to light.[94] In contrast, in a model of T1D where rats were subjected to alloxan-induced beta cell depletion, a good correlation was observed between [^{111}In]-Exendin uptake and BCM.[90] Whether GLP-1R downregulation in the course of T1D and T2D also occurs in human – and if so, to which extent and under what circumstances – still has to be clarified. In summary, although imaging of VMAT2 or GLP-1R is promising, some shortcomings and challenges remain. Accordingly, the search for alternative targets and probes with ideal properties for accurate imaging of β-cell mass should continue.

The free fatty acid receptor 1 (FFAR1-GPR40)

The free fatty acid receptor 1 (FFAR1) belongs to the superfamily of the seven-transmembrane domain G protein-coupled receptors (GPCRs). These receptors induce biological responses via the activation of associated heterotrimeric G proteins (G_α, G_β and G_γ) and/or β-arrestins. GPCR signaling is involved in countless physiological processes and around 40% of all clinically prescribed drugs target GPCRs.[95]
FFAR1 (also called GPR40 for G protein-coupled receptor 40) was independently deorphanized by three different groups in 2003[96-98] who showed that a broad range of medium- to long-chain free fatty acids (C12–C22) serve as ligands for the receptor. The discovery that free fatty acids act as agonist for cell-surface receptors created a new paradigm: free fatty acids are not only nutrients and metabolic substrates but also behave as extracellular signaling molecules.[49] Insulin secretion in response to glucose occurs in two phases, and the FFAR1 activation triggers a glucose dependent insulin secretion, with a strong effect on the second phase as shown in Figure 10.

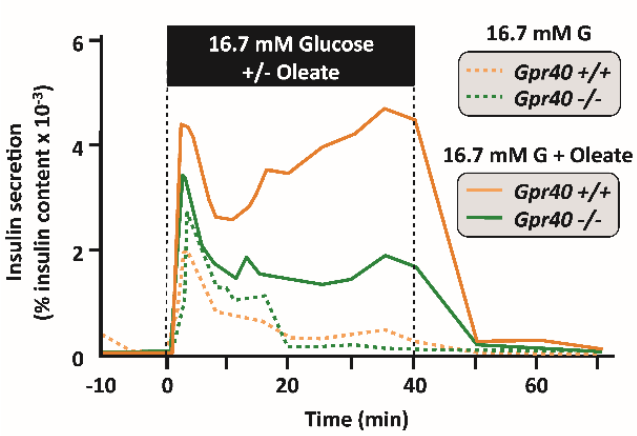

Figure 10 Perifusion experiment in mouse pancreatic islets demonstrating that free fatty acids (here a C18 free fatty acid: oleate) primarily potentiate second-phase glucose-stimulated insulin secretion. Islets derived from GPR40 knock out mice exhibited a ~50% reduction of this potentiating effect, but displayed no appreciable difference in first-phase glucose-induced insulin release. (Adapted from Mancini).[99]

Following FFAR1 stimulation, the α subunit of receptor-associated heterotrimeric G protein $G_{q/11}$ is activated upon GDP-for-GTP exchange and subsequently dissociates from the β/γ subunit. The GTP-bound (active) α-subunit activates phospholipase C (PLC), which cleaves phosphatidylinositol-4,5-bisphosphate (PIP2) to produce inositol-1,4,5-triphosphate (IP3) and diacylglycerol (DAG). IP3 triggers Ca^{2+} efflux from the endoplasmic reticulum (ER). DAG promotes the phosphorylation and activation of PKD1; in turn, PKD1 phosphorylates and activates targets implicated in filamentous (F)-actin remodeling, ultimately potentiating the 2nd phase of glucose-stimulated insulin granule exocytosis. The IP3 pathway also likely plays a role in the control of intracellular Ca^{2+} levels and insulin secretion in response to FFA activation of GPR40 (Figure 11).

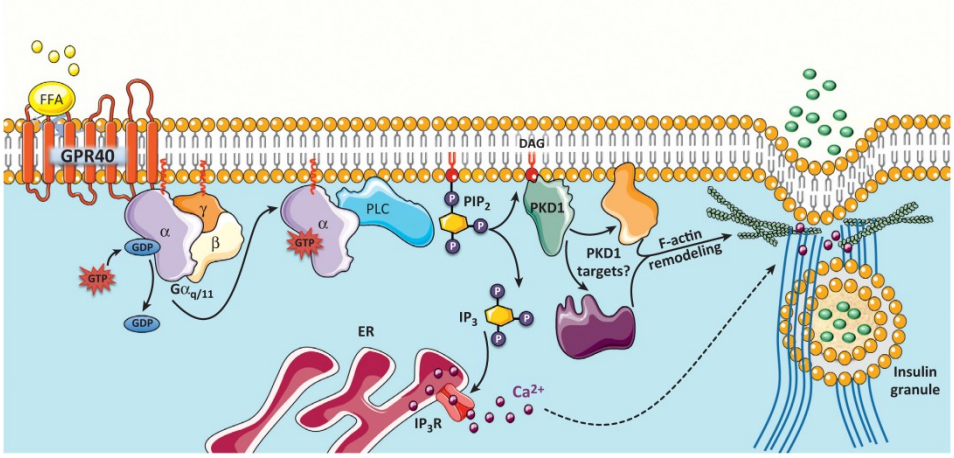

Figure 11 Free fatty acid trigger glucose-stimulated insulin secretion through FFAR1/GPR40 activation. (Adapted from Mancini).[49]

An interesting target for β-cell imaging?

When it was deorphanized, the corresponding mRNA receptor transcript levels were probed to characterize the tissue distribution of the GPR40. Although evidence of receptor expression was found in the human brain and in the enteroendocrine cells of the gastrointestinal tract,[96, 100] the receptor was found to be predominantly expressed in human and rodent β-cells of the pancreas (Figure 12).[96-98,101] Remarkably the estimated mRNA copy number for the GPR40 gene in human pancreatic islets was comparable to those for genes encoding SUR1, GLP-1R and somatostatin receptors, all of which are known to be expressed abundantly in the human pancreatic islet.[102] FFAR1 expression has also been detected in glucagon-producing α-cells within the pancreas[103] using a polyclonal antibody generated against the C-terminal part of the receptor. However, this result remains controversial: one research group failed to detect expression of GPR40 mRNA in α-cells using quantitative PCR on human glucagonomas;[104] another group who developed a monoclonal antibody directed to the extracellular domain of the GPR40 could not detect expression of the receptor in α-cells.[105] There is an ongoing discussion in recent literature on the effectiveness and particularly on specificity of antibody-mediated detection of FFAR1.[106]

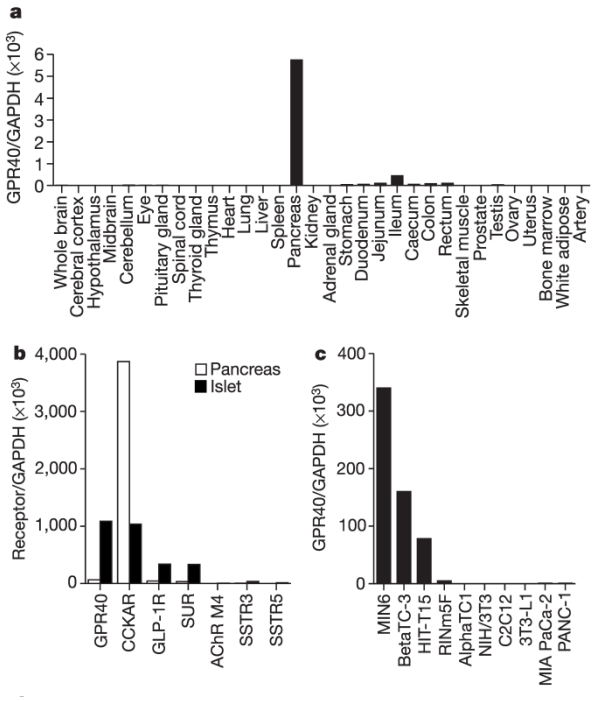

Figure 12 GPR40 mRNA is expressed abundantly in pancreatic β-cells. GPR40 mRNA in rat tissue measured by RT-PCR. Data represent the ratios of GPR40 and other mRNAs to GAPDH mRNA. a) Distribution of GPR40 mRNA in rat tissues. b) Specific expression of GPR40 mRNA in rat pancreatic islets compared to pancreas as a whole. c) Expression of GPR40 mRNA in pancreatic β-cell lines (MIN6 mouse pancreatic β-cells; betaTC-3 mouse pancreatic β-cells; HIT-T15 Syrian golden hamster pancreatic β-cells; RINm5F, rat pancreatic β-cells), α-cells (alphaTC1 mouse pancreatic α-cells), and other cell types (NIH/3T3 mouse embryonic cells; C2C12 mouse myoblasts; 3T3-L1 mouse embryonic fibroblasts; MIA PaCa-2 human pancreatic carcinoma cells; PANC-1 human pancreatic carcinoma cells). (Adapted from Itoh).[97]

Given that the free fatty acids only stimulate insulin release in the presence of glucose, it became immediately apparent that FFAR1 could be targeted to enhance insulin secretion in T2D patients while minimizing the risk of hypoglycemia events. Indeed, many synthetic FFAR1 agonists have been described in recent years, thus enabling a better understanding of the receptor signaling and pharmacology; many of them were or still are under development as T2D drugs.[107]

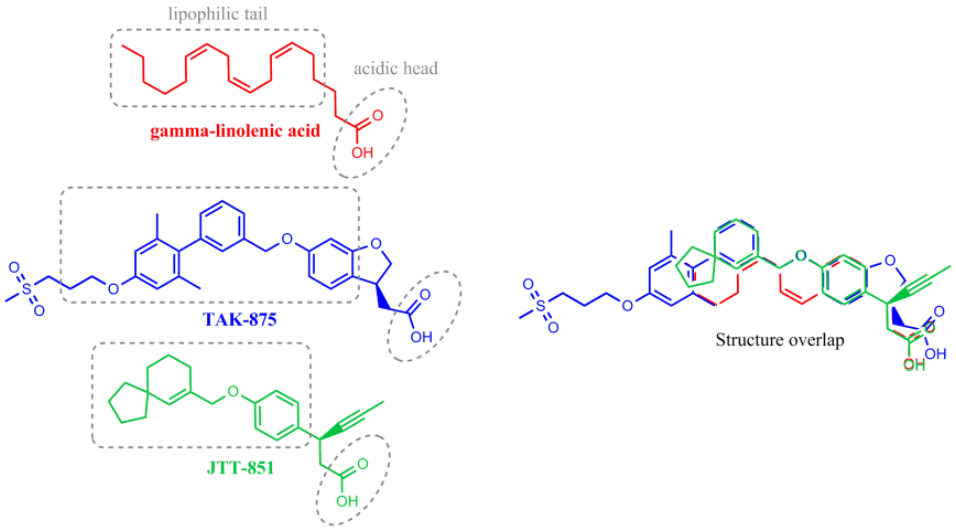

Figure 13 Examples of structures of endogenous (γ-linolenic acid) and synthetic (TAK-875 and JTT-851) FFAR1 agonists.

Typically, synthetic FFAR1 agonists mimic the free fatty acid structure with an acidic head group and a hydrophobic tail (Figure 13 and Table 1), based on this rationale the first small molecule FFAR1 agonist was reported in 2006 by Glaxo Smith Kline (GW-9508[108] - Table 1). The carboxylic acid function is of prime importance for the activity (but can be replaced by an acidic bioisosteric group as shown by Astella AS-2034178[109] - Table 1) and is typically attached via a two carbon atom linker to an aromatic ring. In more advanced compounds the β-position to the carboxylic function is substituted by small residues (AMG-1638/AMG-837/LY-2922470/JTT851/P-11187 - Table 1), which can be also cyclized to the aromatic ring (TAK-875), to reduce the potential for β-oxidation, which is the catabolic process by which fatty acid molecules are broken down. A second aromatic moiety, either a substituted monocyclic or bicyclic aryl or a biaryl residue, is linked to the first aromatic ring via a short spacer (2–4 atoms in length). This second aromatic moiety can be used to install further substituents in order to manipulate the overall physicochemical properties such as polarity and solubility.

Of the numerous FFAR1 agonists developed to date, the Takeda molecule TAK-875 (Fasiglifam) was the most clinically advanced by reaching the phase III. TAK-875 is an orally available and potent agonist of FFAR1 (EC_{50} in the low nanomolar range for human FFAR1) with marked selectivity for FFAR1 over other members of the FFA receptor family (i.e., FFAR2, FFAR3, GPR120)[110]. In isolated rat and human islets, TAK-875 stimulated insulin secretion in a glucose-dependent manner without affecting glucagon secretion.[111, 112] In Zucker diabetic fatty rats (a commonly used genetic rodent model of T2D), TAK-875 was found to promote glucose-stimulated insulin secretion and reduce fasting and postprandial hyperglycemia, as opposed to healthy normoglycemic rats where the compound did not induce hypoglycemia.

These therapeutic effects observed in animal models were then translated to humans in clinical trials. Initial pharmacokinetic studies in healthy volunteers receiving TAK-875 revealed good safety and tolerability, and a pharmacokinetic profile appropriate for once-daily oral dosage.[113] In two randomized, double-blind, placebo-controlled trials,[114] T2D patients on a 12 week TAK-875 treatment (>50 mg/day, once daily) exhibited improved fasting plasma glucose and insulin secretion with a 1.2–1.4% reduction in HbA1c levels. Improvements in HbA1c levels were comparable to those observed with the glimepiride, a sulfonylurea antidiabetic drug (sulphonylureas stimulate insulin secretion by selectively targeting ATP-regulated K^+ channels in the plasma membrane of pancreatic β-cells. This mechanism is independent of plasma glucose levels which consequently increases the risk of hypoglycaemia);[115] however, the occurrence of hypoglycemia was significantly lower in the TAK-875-treated groups relative to the glimepiride groups. Most importantly, the beneficial effects of TAK-875 were only observed in diabetic individuals, thus confirming that the molecule is active only when high levels of blood glucose are reached. Even if the clinical development of TAK-875 was terminated on phase III due to concerns on liver toxicity,[116] the encouraging initial results reported by Takeda provide strong evidence in support of the clinical utility of GPR40 agonists, and unsurprisingly multiple pharmaceutical companies still have active GPR40 agonist programs.

Company	Name	Structure
Endogenous ligand	Gamma-linolenic acid	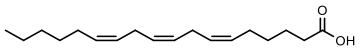
Glaxo Smith Kline	GW-9508	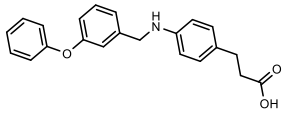
Takeda	TAK-875	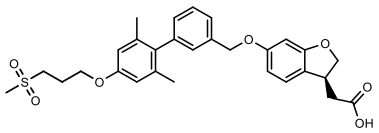
Amgen	AM-837	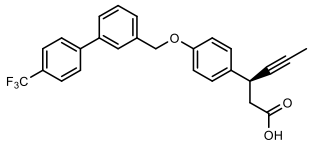
Amgen	AM-1638	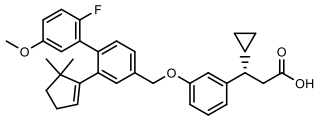
Eli Lilly	LY-2922470	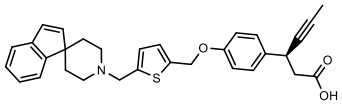
Japan Tobacco	JTT-851	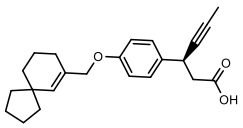
Astella	AS-2034178	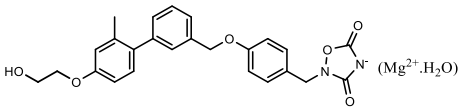
Piramal	P-11187	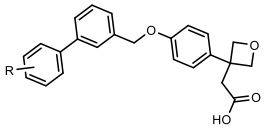
Hengrui	SHR-0534	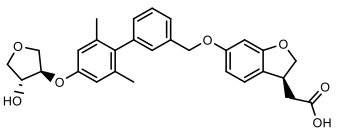

Table 1 Structures of relevant FFA1 receptor agonists.

Currently, the molecule most advanced in clinical trials is the FFAR1 agonist JTT-851 from Japan Tobacco which are conducting phase II clinical trials, followed by Piramal which began phase I clinical trials on their FFAR1 agonist P-11187 (Piramal clinical Trial), Eli Lilly LY-2922470 (completed phase I in 2014) and Hengrui SHR-0534 (phase I in China) (Table 1).[117]

As already mentioned above, GPR40 was found to be expressed in enteroendocrine cells and can also promote ligand-stimulated secretion of incretins such as glucagon-like peptide-1 and glucose-dependent insulinotropic polypeptide (GIP).[100] These two potent metabolic hormones induce a decrease in blood glucose levels by both stimulating insulin release and inhibiting glucagon release. Consequently, in addition to their direct action on pancreatic β-cells, GPR40 agonists may also indirectly promote insulin secretion by stimulating incretin release through the enteroendocrine intestinal L cells. With the attractive hypothesis that GRP40 full agonists would lead to greater therapeutic efficacy, Amgen scientists discovered AM-1638 the first reported synthetic GPR40 agonist to stimulate both GIP and GLP-1 secretion.[118] The glucose-lowering efficacy of AM-1638 was reduced in the presence of the GLP-1R antagonist Exendin(9–39)NH_2 highlighting the importance of the GLP-1 pathway to GPR40 full agonist pharmacology. These results provided a preclinical proof-of-mechanism for the therapeutic benefit and advantages of GPR40 full agonism (Figure 14). Synthetic GPR40 agonists developed before 2012 such as GW-9508 and TAK-875 which do not engage both the insulinogenic and incretinogenic axes are therefore regarded as partial agonists.

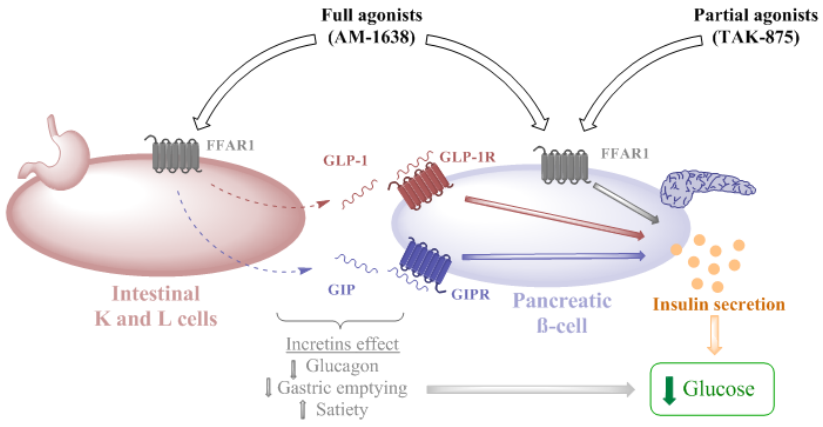

Figure 14 Stimulation of the enteroendocrine and insulin axes by GPR40 full agonists (such as AM-1638) promote enhanced glucose control and stimulate incretins such as GLP-1/GIP and insulin secretion, whereas partial agonists (such as TAK-875) stimulate insulin secretion from the pancreatic β-cells but not incretin secretion from enteroendocrine cells. (Adapted from Luo).[118]

When discovered, it was believed that GPR40 harbored one ligand-binding pocket called 'orthosteric' binding site which is used by both endogenous and synthetic ligands to induce their biological effects.[49] This binding site is defined by a cluster of hydrophilic residues in transmembrane regions 5, 6, and 7 (Arg183, Asn244, and Arg258 shown in red in Figure 15.A) that interact with the carboxyl group present in most GPR40 agonists.[119, 120]

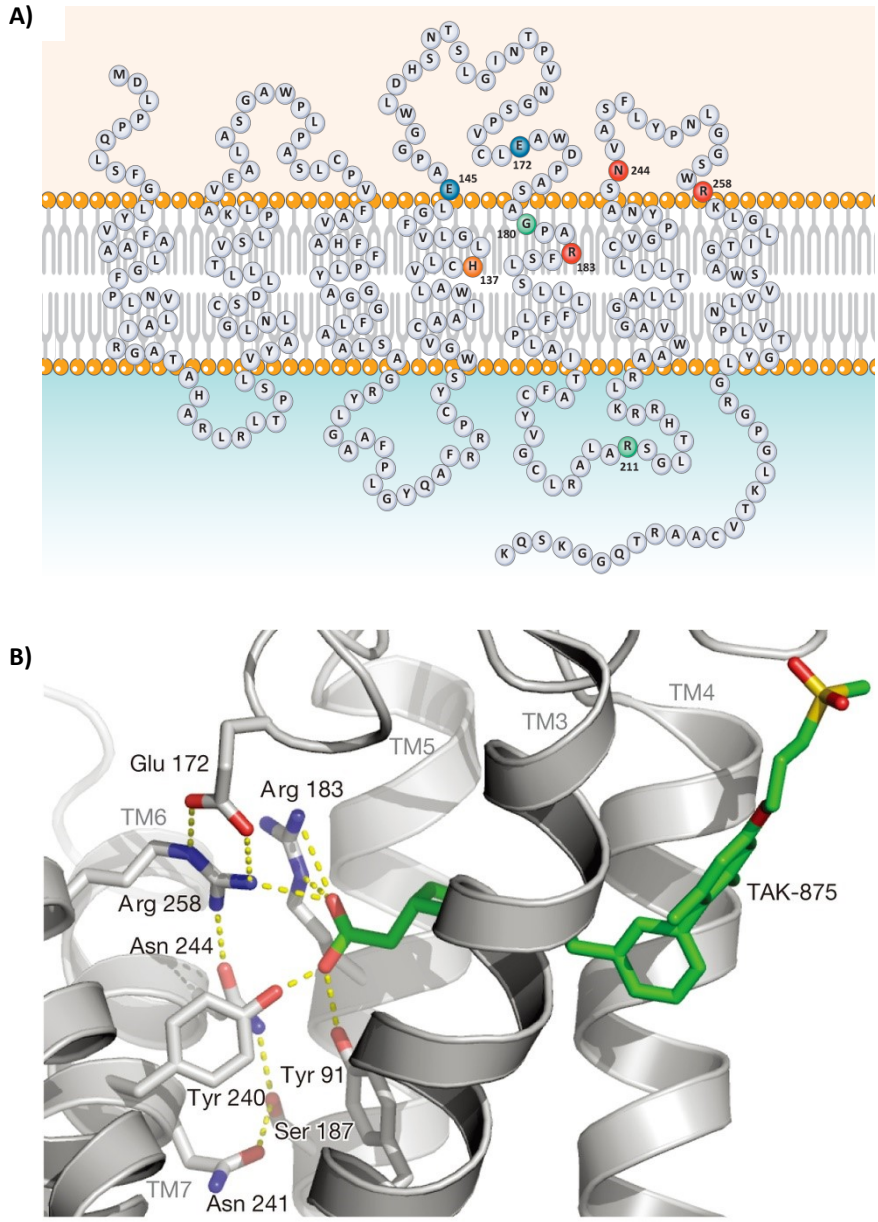

Figure 15 A) Predicted topology and functionally important residues of human GPR40. Amino acids implicated in ligand binding or receptor activation are shown in red (key residues in the GPR40 binding pocket, they interact with the carboxyl group present in various GPR40 ligands), orange (important for binding of synthetic agonist GW-9508 but not the endogenous ligand linoleic acid), and blue (form ionic locks with R183 and R258, maintaining GPR40 in an inactive conformation; ligand interaction with one or both arginine residues disrupts the lock and promotes receptor activation), whereas two known polymorphic residues are shown in green.(Adapted from Mancini).[49] B) Interaction of the carboxylate of TAK-875 with the charge cluster as seen in a lateral view. The carboxylate moiety is highly coordinated by several key residues, notably Arg183, Arg258, and Asn244.(Adapted from Srivastava).[121]

This interaction with the three amino acids Arg183, Asn244, and Arg258 was confirmed by the high-resolution crystal structure of the human GPR40 bound to TAK-875 at 2.3A˚ resolution[121] as depicted in Figure 15.B. However, mutation of these key residues differentially affected the functional activity of different agonists,[120, 122] thus suggesting the possible existence of additional, topographically distinct ligand-binding sites named 'allosteric'. This hypothesis was confirmed by the work of Lin, who discovered three novel GPR40 allosteric agonists that bind to separate sites and display complex binding and functional cooperativity with one another and with the endogenous GPR40 ligands docosahexaenoic.[123] Further research on the mode of action of TAK-875 revealed that the compound acts as an ago-allosteric modulator of FFAR1 that exerts its effects by acting cooperatively with endogenous plasma FFAs in human patients as well as diabetic animals (Figure 16).[124]

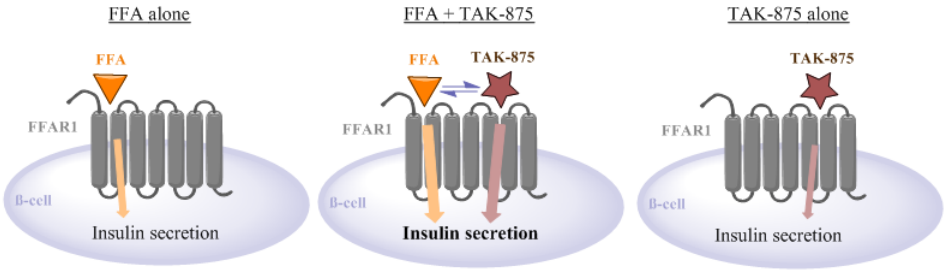

Figure 16 Schematic model of insulinotropic action of TAK-875 in cooperativity with endogenous FFAs in β-cells. FFAR1 activation by endogenous FFAs contributes to a moderate glucose-stimulated insulin secretion (GSIS) *in vivo* (left). TAK-875 treatment potentiates FFA induced boosted insulin secretion as an allosteric modulator, whereas FFAs also augment the activity of TAK-875, showing reciprocal positive cooperativity (middle). TAK-875 treatment in the absence of FFAs (nonphysiological) results in partial activation of FFAR1 and weak potentiation of GSIS (right) (Adapted from Yabuki).[124]

Conclusion

In conclusion, the evaluation of mRNA levels suggests FFAR1 is expressed highly and predominantly on pancreatic β-cells. Extensive work on structure-activity relationship was done by both academic and industrial research groups, in order to generate selective and potent ligands with optimized physicochemical properties. These compounds enabled research that has provided valuable insight into the pharmacology of the receptor, as well as precious information on ligand binding. Taken together, all these data paved the way for the design, synthesis and characterization of novel imaging probes targeting this relevant and attractive receptor, which had until now been unexplored for imaging based determination of β-cell mass. Additionally, as this receptor is highly conserved between species, it should allow good translation of binding efficacy between different animal models and human.

Gut peptides such as GLP-1, GIP and Glucagon, stabilized analogs thereof and even combination of them, have already proved valuable therapeutic effects, or are currently clinically evaluated for the treatment of diabetes. These metabolic hormones, which can be isolated from natural sources, or their derivatives are an interesting basis for the design of novel bio imaging probes. The development of new methods to label such peptides with fluorophores or chelators is of high interest for the scientific community.

References

[1] IDF Diabetes Atlas - Seventh Edition.
[2] Group, N. D. D. (1979) Classification and diagnosis of diabetes mellitus and other categories of glucose intolerance, *Diabetes 28*, 1039-1057.
[3] Definition and diagnosis of diabetes mellitus and intermediate hyperglycaemia - World Health Organization.
[4] Mellitus, D. (2005) Diagnosis and classification of diabetes mellitus, *Diabetes care 28*, S37.
[5] Tisch, R., and Wang, B. (2008) Dysregulation of T Cell Peripheral Tolerance in Type 1 Diabetes, *100*, 125-149.
[6] Zhao, Y. (2011) Autoimmunity and Therapeutic Challenges of Type 1 Diabetes, *Translational Medicine 01*.
[7] Cryer, P. E., Davis, S. N., and Shamoon, H. (2003) Hypoglycemia in diabetes, *Diabetes care 26*, 1902-1912.
[8] Soumya, D., and Srilatha, B. (2011) Late Stage Complications of Diabetes and Insulin Resistance, *Journal of Diabetes & Metabolism 02*.
[9] Evans, J., Newton, R. W., Ruta, D. A., MacDonald, T. M., and Morris, A. D. (2000) Socio-economic status, obesity and prevalence of Type 1 and Type 2 diabetes mellitus, *Diabetic Medicine 17*, 478-480.
[10] Holman, N., Young, B., and Gadsby, R. (2015) Current prevalence of Type 1 and Type 2 diabetes in adults and children in the UK, *Diabet Med 32*, 1119-1120.
[11] Boyle, J. P., Engelgau, M. M., Thompson, T. J., Goldschmid, M. G., Beckles, G. L., Timberlake, D. S., Herman, W. H., Ziemer, D. C., and Gallina, D. L. (1999) Estimating prevalence of type 1 and type 2 diabetes in a population of African Americans with diabetes mellitus, *American Journal of Epidemiology 149*, 55-63.
[12] Bruno, G., Runzo, C., Cavallo-Perin, P., Merletti, F., Rivetti, M., Pinach, S., Novelli, G., Trovati, M., Cerutti, F., and Pagano, G. (2005) Incidence of Type 1 and Type 2 Diabetes in Adults Aged 30–49 Years The population-based registry in the province of Turin, Italy, *Diabetes Care 28*, 2613-2619.
[13] Stern, M. P. (1991) Kelly West Lecture: primary prevention of type II diabetes mellitus, *Diabetes Care 14*, 399-410.
[14] Manson, J. E., Stampfer, M., Colditz, G., Willett, W., Rosner, B., Hennekens, C., Speizer, F., Rimm, E., and Krolewski, A. (1991) Physical activity and incidence of non-insulin-dependent diabetes mellitus in women, *The Lancet 338*, 774-778.
[15] Tuomilehto, J., and Wolf, E. (1987) Primary prevention of diabetes mellitus, *Diabetes Care 10*, 238-248.
[16] Zimmet, P. Z. (1988) Primary prevention of diabetes mellitus, *Diabetes Care 11*, 258-262.
[17] Ohlson, L. O., Larsson, B., Bjorntorp, P., Eriksson, H., Svardsudd, K., Welin, L., Tibblin, G., and Wilhelmsen, L. (1988) Risk factors for type 2 (non-insulin-dependent) diabetes mellitus. Thirteen and one-half years of follow-up of the participants in a study of Swedish men born in 1913, *Diabetologia 31*, 798-805.
[18] Gregg, E. W., Chen, H., Wagenknecht, L. E., Clark, J. M., Delahanty, L. M., Bantle, J., Pownall, H. J., Johnson, K. C., Safford, M. M., Kitabchi, A. E., Pi-Sunyer, F. X., Wing, R. R., Bertoni, A. G., and Look, A. R. G. (2012) Association of an intensive lifestyle intervention with remission of type 2 diabetes, *JAMA 308*, 2489-2496.
[19] Costa, T., Detsch, J., Nascimento, D., and Rea, R. (2011) Glycemic Variability and Mean Weekly Glucose in the Evaluation and Treatment of Blood Glucose in Gestational Diabetes Mellitus; Evidence for Lower Neonatal Complications, *Journal of Diabetes & Metabolism*.
[20] American-Diabetes-Association. (2004) Gestational diabetes mellitus, *Diabetes care 27*, S88.
[21] Buchanan, T. A., and Xiang, A. H. (2005) Gestational diabetes mellitus, *Journal of Clinical Investigation 115*, 485.

[22] Buchanan, T. A., Xiang, A., Kjos, S. L., and Watanabe, R. (2007) What is gestational diabetes?, *Diabetes care 30*, S105-S111.
[23] Kim, C., Newton, K. M., and Knopp, R. H. (2002) Gestational Diabetes and the Incidence of Type 2 Diabetes A systematic review, *Diabetes care 25*, 1862-1868.
[24] Sokup, A., Ruszkowska, B., Goralczyk, B., Goralczyk, K., Szymański, M., Grabiec, M., and Rość, D. (2012) Elevation of sE-Selectin Levels 2–24 Months following Gestational Diabetes Is Associated with Early Cardiometabolic Risk in Nondiabetic Women, *International journal of endocrinology 2012*.
[25] Fetita, L.-S., Sobngwi, E., Serradas, P., Calvo, F., and Gautier, J.-F. (2006) Consequences of fetal exposure to maternal diabetes in offspring, *The Journal of Clinical Endocrinology & Metabolism 91*, 3718-3724.
[26] Thomas, C., Celeste, Philipson, H. (2015) Update on Diabetes Classification, *Medical Clinics of North America*, 1-16
[27] Aguiree, F., Brown, A., Cho, N. H., Dahlquist, G., Dodd, S., Dunning, T., Hirst, M., Hwang, C., Magliano, D., and Patterson, C. (2013) IDF Diabetes atlas - Sixth Edition.
[28] Fact sheets 2014 - UNAIDS - World Health Organization.
[29] Global tuberculosis report 2014 - World Health Organization.
[30] World malaria report 2014 - World Health Organization.
[31] Zhuo, X., Zhang, P., and Hoerger, T. J. (2013) Lifetime direct medical costs of treating type 2 diabetes and diabetic complications, *Am J Prev Med 45*, 253-261.
[32] Köster, I., Von Ferber, L., Ihle, P., Schubert, I., and Hauner, H. (2006) The cost burden of diabetes mellitus: the evidence from Germany—the CoDiM Study, *Diabetologia 49*, 1498-1504.
[33] Javanbakht, M., Baradaran, H. R., Mashayekhi, A., Haghdoost, A. A., Khamseh, M. E., Kharazmi, E., and Sadeghi, A. (2011) Cost-of-illness analysis of type 2 diabetes mellitus in Iran, *PLoS One 6*, e26864.
[34] González, J. C., Walker, J. H., and Einarson, T. R. (2009) Cost-of-illness study of type 2 diabetes mellitus in Colombia, *Revista Panamericana de Salud Pública 26*, 55-63.
[35] Yang, W., Zhao, W., Xiao, J., Li, R., Zhang, P., Kissimova-Skarbek, K., Schneider, E., Jia, W., Ji, L., Guo, X., Shan, Z., Liu, J., Tian, H., Chen, L., Zhou, Z., Ji, Q., Ge, J., Chen, G., and Brown, J. (2012) Medical care and payment for diabetes in China: enormous threat and great opportunity, *PLoS One 7*, e39513.
[36] Kirigia, J. M., Sambo, H. B., Sambo, L. G., and Barry, S. P. (2009) Economic burden of diabetes mellitus in the WHO African region, *BMC Int Health Hum Rights 9*, 6.
[37] Association, A. D. (2013) Economic costs of diabetes in the US in 2012, *Diabetes care 36*, 1033-1046.
[38] Zhang, Y., Dall, T. M., Mann, S. E., Chen, Y., Martin, J., Moore, V., Baldwin, A., Reidel, V. A., and Quick, W. W. (2009) The economic costs of undiagnosed diabetes, *Population health management 12*, 95-101.
[39] DeFronzo, R. A., Ferrannini, E., Zimmet, P., and Alberti, G. (2015) *International textbook of diabetes mellitus*, John Wiley & Sons.
[40] Von Mering, J., and Minkowski, O. (1890) Diabetes mellitus nach Pankreasexstirpation, *Arch Exp Pathol Pharmakol 26*, 371-387.
[41] Hédon, E. (1893) Sur la consommation du sucre chez la chien apres l'extirpation du pancreas, *Arch Physiol Normal Pathol Vth Series 5*, 154-163.
[42] Langerhans, P. (1990) *Beiträge zur mikroskopischen Anatomie der Bauchspeicheldrüse: Inaugural-dissertation*, Farbwerke Hoechst.
[43] Opie, E. L. (1901) The relation Oe diabetes mellitus to lesions of the Pancreas. Hyaline degeneration of the Islands Oe Langerhans, *The Journal of experimental medicine 5*, 527-540.
[44] Hilgenfeld, R., Seipke, G., Berchtold, H., and Owens, D. R. (2014) The evolution of insulin glargine and its continuing contribution to diabetes care, *Drugs 74*, 911-927.
[45] Sjöström, L., Garellick, G., Krotkiewski, M., and Luyckx, A. (1980) Peripheral insulin in response to the sight and smell of food, *Metabolism 29*, 901-909.

[46] Floyd Jr, J. C., Fajans, S. S., Conn, J. W., Knopf, R. F., and Rull, J. (1966) Stimulation of insulin secretion by amino acids, *Journal of Clinical Investigation 45*, 1487.

[47] Sonksen, P., and Sonksen, J. (2000) Insulin: understanding its action in health and disease, *British journal of anaesthesia 85*, 69-79.

[48] Fu, Z., R Gilbert, E., and Liu, D. (2013) Regulation of insulin synthesis and secretion and pancreatic Beta-cell dysfunction in diabetes, *Current diabetes reviews 9*, 25-53.

[49] Mancini, A. D., and Poitout, V. (2013) The fatty acid receptor FFA1/GPR40 a decade later: how much do we know?, *Trends in Endocrinology & Metabolism 24*, 398-407.

[50] Feldman, M., Friedman, L. S., and Brandt, L. J. (2010) *Sleisenger and Fordtran's gastrointestinal and liver disease: pathophysiology, diagnosis, management, expert consult premium edition-enhanced online features*, Vol. 1, Elsevier Health Sciences.

[51] Brissova, M., Fowler, M. J., Nicholson, W. E., Chu, A., Hirshberg, B., Harlan, D. M., and Powers, A. C. (2005) Assessment of human pancreatic islet architecture and composition by laser scanning confocal microscopy, *Journal of Histochemistry & Cytochemistry 53*, 1087-1097.

[52] Halban, P. A., Polonsky, K. S., Bowden, D. W., Hawkins, M. A., Ling, C., Mather, K. J., Powers, A. C., Rhodes, C. J., Sussel, L., and Weir, G. C. (2014) β-cell failure in type 2 diabetes: postulated mechanisms and prospects for prevention and treatment, *Diabetes Care 37*, 1751-1758.

[53] Meier, J. J., Butler, A. E., Saisho, Y., Monchamp, T., Galasso, R., Bhushan, A., Rizza, R. A., and Butler, P. C. (2008) β-cell replication is the primary mechanism subserving the postnatal expansion of β-cell mass in humans, *Diabetes 57*, 1584-1594.

[54] Matveyenko, A., and Butler, P. (2008) Relationship between β-cell mass and diabetes onset, *Diabetes, Obesity and Metabolism 10*, 23-31.

[55] Gepts, W., and De Mey, J. (1978) Islet Cell Survival Determined by Morphology An Immunocytochemical Study of the Islets of Langerhans in Juvenile Diabetes Mellitus, *Diabetes 27*, 251-261.

[56] Scheen, A. (2005) Diabetes mellitus in the elderly: insulin resistance and/or impaired insulin secretion?, *Diabetes & metabolism 31*, 5S27-25S34.

[57] Neutzsky-Wulff, A. V., Andreassen, K. V., Hjuler, S. T., Feigh, M., Bay-Jensen, A.-C., Zheng, Q., Henriksen, K., and Karsdal, M. A. (2012) Future detection and monitoring of diabetes may entail analysis of both β-cell function and volume: How markers of β-cell loss may assist, *Journal of translational medicine 10*, 1.

[58] Butler, A. E., Janson, J., Bonner-Weir, S., Ritzel, R., Rizza, R. A., and Butler, P. C. (2003) β-cell deficit and increased β-cell apoptosis in humans with type 2 diabetes, *Diabetes 52*, 102-110.

[59] Sakuraba, H., Mizukami, H., Yagihashi, N., Wada, R., Hanyu, C., and Yagihashi, S. (2002) Reduced beta-cell mass and expression of oxidative stress-related DNA damage in the islet of Japanese Type II diabetic patients, *Diabetologia 45*, 85-96.

[60] Yoon, K. H., Ko, S. H., Cho, J. H., Lee, J. M., Ahn, Y. B., Song, K. H., Yoo, S. J., Kang, M. I., Cha, B. Y., and Lee, K. W. (2003) Selective β-cell loss and α-cell expansion in patients with type 2 diabetes mellitus in Korea, *The Journal of Clinical Endocrinology & Metabolism 88*, 2300-2308.

[61] Fakhfakh, R., (2011) Genetic Markers, Serological Auto Antibodies and Prediction of Type 1 Diabetes, *Type 1 Diabetes - Pathogenesis, Genetics and Immunotherapy*, Chap 27, 631-646

[62] Ritzel, R. A., Butler, A. E., Rizza, R. A., Veldhuis, J. D., and Butler, P. C. (2006) Relationship between β-cell mass and fasting blood glucose concentration in humans, *Diabetes care 29*, 717-718.

[63] Meier, J. J., Menge, B. A., Breuer, T. G., Müller, C. A., Tannapfel, A., Uhl, W., Schmidt, W. E., and Schrader, H. (2009) Functional assessment of pancreatic β-cell area in humans, *Diabetes 58*, 1595-1603.

[64] Donath, M., and Halban, P. A. (2004) Decreased beta-cell mass in diabetes: significance, mechanisms and therapeutic implications, *Diabetologia 47*, 581-589.

[65] Weir, G. C., and Bonner-Weir, S. (2004) Five stages of evolving beta-cell dysfunction during progression to diabetes, *Diabetes 53*, S16-S21.

[66] Goke, B. (2010) What are the Potential Benefits of Clinical β-Cell Imaging in Diabetes Mellitus?, *Current pharmaceutical design 16*, 1547-1549.

[67] Saudek, F., Brogren, C.-H., and Manohar, S. (2008) Imaging the beta-cell mass: why and how, *Rev Diabet Stud 5*, 6-12.

[68] Andralojc, K., Srinivas, M., Brom, M., Joosten, L., de Vries, I., Eizirik, D. L., Boerman, O., Meda, P., and Gotthardt, M. (2012) Obstacles on the way to the clinical visualisation of beta cells: looking for the Aeneas of molecular imaging to navigate between Scylla and Charybdis, *Diabetologia 55*, 1247-1257.

[69] Blomberg, B. A., Codreanu, I., Cheng, G., Werner, T. J., and Alavi, A. (2013) Beta-cell imaging: call for evidence-based and scientific approach, *Mol Imaging Biol 15*, 123-130.

[70] Schmitz, A., Shiue, C.-Y., Feng, Q., Shiue, G., Deng, S., Pourdehnad, M., Schirrmacher, R., Vatamaniuk, M., Doliba, N., and Matschinsky, F. (2004) Synthesis and evaluation of fluorine-18 labeled glyburide analogs as β-cell imaging agents, *Nuclear medicine and biology 31*, 483-491.

[71] Wängler, B., Schneider, S., Thews, O., Schirrmacher, E., Comagic, S., Feilen, P., Schwanstecher, C., Schwanstecher, M., Shiue, C.-Y., and Alavi, A. (2004) Synthesis and evaluation of (S)-2-(2-[18 F] fluoroethoxy)-4-([3-methyl-1-(2-piperidin-1-yl-phenyl)-butyl-carbamoyl]-methyl)-benzoic acid ([18 F] repaglinide): a promising radioligand for quantification of pancreatic β-cell mass with positron emission tomography (PET), *Nuclear medicine and biology 31*, 639-647.

[72] Brogren, C.-H., Hirsch, F., Wood, P., Druet, P., and Poussier, P. (1986) Production and characterization of a monoclonal islet cell surface autoantibody from the BB rat, *Diabetologia 29*, 330-333.

[73] Moore, A., Bonner-Weir, S., and Weissleder, R. (2001) Noninvasive in vivo measurement of β-cell mass in mouse model of diabetes, *Diabetes 50*, 2231-2236.

[74] Ahnfelt-Rønne, J., Hecksher-Sørensen, J., Schäffer, L., and Madsen, O. (2012) A new view of the beta cell, *Diabetologia*, 1-3.

[75] Vats, D., Wang, H., Esterhazy, D., Dikaiou, K., Danzer, C., Honer, M., Stuker, F., Matile, H., Migliorini, C., and Fischer, E. (2012) Multimodal imaging of pancreatic beta cells in vivo by targeting transmembrane protein 27 (TMEM27), *Diabetologia 55*, 2407-2416.

[76] Brom, M., Andraojc, K., JG Oyen, W., C Boerman, O., and Gotthardt, M. (2010) Development of radiotracers for the determination of the beta-cell mass in vivo, *Current pharmaceutical design 16*, 1561-1567.

[77] Eriksson, O., Selvaraju, R. K., Johansson, L., Eriksson, J. W., Sundin, A., Antoni, G., Sörensen, J., Eriksson B., Korsgren O. (2014) Quantitative Imaging of Serotonergic Biosynthesis and Degradation in the Endocrine Pancreas, *Journal of Nuclear Medicine 55,* 460-465.

[78] Eriksson, O., Espes, D., Selvaraju, R. K., Jansson E., Antoni, G., Sörensen, J., Lubberink, M., Biglarnia A., Eriksson, J. W., Sundin, A., Ahlström, H., Eriksson B., Johansson, L., Carlsson P., Korsgren O. (2014) Positron emission tomography ligand [^{11}C]5-hydroxy-tryptophan can be used as a surrogate marker for the human endocrine pancreas, *Diabetes 63*, 3428-3437.

[79] Anlauf, M., Eissele, R., Schäfer, M. K.-H., Eiden, L. E., Arnold, R., Pauser, U., Klöppel, G., and Weihe, E. (2003) Expression of the two isoforms of the vesicular monoamine transporter (VMAT1 and VMAT2) in the endocrine pancreas and pancreatic endocrine tumors, *Journal of Histochemistry & Cytochemistry 51*, 1027-1040.

[80] Kung, M.-P., Hou, C., Lieberman, B. P., Oya, S., Ponde, D. E., Blankemeyer, E., Skovronsky, D., Kilbourn, M. R., and Kung, H. F. (2008) In vivo imaging of β-cell mass in rats using 18F-FP-(+)-DTBZ: a potential PET ligand for studying diabetes mellitus, *Journal of Nuclear Medicine 49*, 1171-1176.

[81] Normandin, M. D., Petersen, K. F., Ding, Y.-S., Lin, S.-F., Naik, S., Fowles, K., Skovronsky, D. M., Herold, K. C., McCarthy, T. J., and Calle, R. A. (2012) In vivo imaging of endogenous pancreatic β-cell mass in healthy and type 1 diabetic subjects using 18F-fluoropropyl-dihydrotetrabenazine and PET, *Journal of Nuclear Medicine 53*, 908-916.

[82] Tsao, H.-H., Lin, K.-J., Juang, J.-H., Skovronsky, D. M., Yen, T.-C., Wey, S.-P., and Kung, M.-P. (2010) Binding characteristics of 9-fluoropropyl-(+)-dihydrotetrabenzazine (AV-133) to the vesicular monoamine transporter type 2 in rats, *Nuclear medicine and biology 37*, 413-419.

[83] Freeby, M., Ichise, M., Harris, E. P. (2012) Vesicular monoamine transporter, type 2 (VMAT2) expression as it compares to insulin and pancreatic polypeptide in the head, body and tail of the human pancreas, *Islets* 4:6, 393–397

[84] Richards, P., Parker, H. E., Adriaenssens, A. E., Hodgson, J. M., Cork, S. C., Trapp, S., Gribble, F. M., and Reimann, F. (2014) Identification and characterization of GLP-1 receptor–expressing cells using a new transgenic mouse model, *Diabetes 63*, 1224-1233.

[85] Reiner, T., Thurber, G., Gaglia, J., Vinegoni, C., Liew, C. W., Upadhyay, R., Kohler, R. H., Li, L., Kulkarni, R. N., and Benoist, C. (2011) Accurate measurement of pancreatic islet β-cell mass using a second-generation fluorescent exendin-4 analog, *Proceedings of the National Academy of Sciences 108*, 12815-12820.

[86] Vinet, L., Lamprianou, S., Babič, A., Lange, N., Thorel, F., Herrera, P. L., Montet, X., and Meda, P. (2015) Targeting GLP-1 receptors for repeated magnetic resonance imaging differentiates graded losses of pancreatic beta cells in mice, *Diabetologia 58*, 304-312.

[87] Selvaraju, R. K., Velikyan, I., Johansson, L., Wu, Z., Todorov, I., Shively, J., Kandeel, F., Korsgren, O., and Eriksson, O. (2013) In vivo imaging of the glucagonlike peptide 1 receptor in the pancreas with 68Ga-labeled DO3A-exendin-4, *Journal of Nuclear Medicine 54*, 1458-1463.

[88] Brom, M., Joosten, L., Frielink, C., Boerman, O., and Gotthardt, M. (2015) 111In-exendin Uptake in the Pancreas Correlates With the β-Cell Mass and Not With the α-Cell Mass, *Diabetes 64*, 1324-1328.

[89] Kirsi, M., Cheng-Bin, Y., Veronica, F., Tamiko, I., Viki-Veikko, E., Johan, R., Jori, J., Tiina, S., Tuula, T., and Marko, T. (2014) 64Cu-and 68Ga-labelled [Nle14, Lys40 (Ahx-NODAGA) NH2]-exendin-4 for pancreatic beta cell imaging in rats, *Molecular imaging and biology 16*, 255-263.

[90] Brom, M., Woliner-Van Der Weg, W., Joosten, L., Frielink, C., Bouckenooghe, T., Rijken, P., Andralojc, K., Göke, B. J., de Jong, M., and Eizirik, D. L. (2014) Non-invasive quantification of the beta cell mass by SPECT with 111In-labelled exendin, *Diabetologia 57*, 950-959.

[91] Xu, G., Kaneto, H., Laybutt, D. R., Duvivier-Kali, V. F., Trivedi, N., Suzuma, K., King, G. L., Weir, G. C., and Bonner-Weir, S. (2007) Downregulation of GLP-1 and GIP receptor expression by hyperglycemia possible contribution to impaired incretin effects in diabetes, *Diabetes 56*, 1551-1558.

[92] Shu, L., Matveyenko, A. V., Kerr-Conte, J., Cho, J.-H., McIntosh, C. H., and Maedler, K. (2009) Decreased TCF7L2 protein levels in type 2 diabetes mellitus correlate with downregulation of GIP-and GLP-1 receptors and impaired beta-cell function, *Human molecular genetics 18*, 2388-2399.

[93] Lehtonen, J., Schaffer, L., Rasch, M. G., Hecksher-Sorensen, J., and Ahnfelt-Ronne, J. (2015) Beta cell specific probing with fluorescent exendin-4 is progressively reduced in type 2 diabetic mouse models, *Islets 7*, e1137415.

[94] Willekens, S. M. A., Joosten L., Boerman C. O., Balhuizen A., Eizirik, D. L., Gotthardt, M., Brom, M. (2016) Strain Differences Determine the Suitability of Animal Models for Noninvasive In Vivo Beta Cell Mass Determination with Radiolabeled Exendin, *Molecular Imaging and Biology, 18*, 705-714

[95] Filmore, D. (2004) It'sa GPCR world, *Modern drug discovery 7*, 24-28.

[96] Briscoe, C. P., Tadayyon, M., Andrews, J. L., Benson, W. G., Chambers, J. K., Eilert, M. M., Ellis, C., Elshourbagy, N. A., Goetz, A. S., and Minnick, D. T. (2003) The orphan G protein-coupled receptor GPR40 is activated by medium and long chain fatty acids, *Journal of Biological chemistry 278*, 11303-11311.

[97] Itoh, Y., Kawamata, Y., Harada, M., Kobayashi, M., Fujii, R., Fukusumi, S., Ogi, K., Hosoya, M., Tanaka, Y., and Uejima, H. (2003) Free fatty acids regulate insulin secretion from pancreatic β cells through GPR40, *Nature 422*, 173-176.

[98] Kotarsky, K., Nilsson, N. E., Flodgren, E., Owman, C., and Olde, B. (2003) A human cell surface receptor activated by free fatty acids and thiazolidinedione drugs, *Biochemical and biophysical research communications 301*, 406-410.

[99] Mancini, A., and Poitout, V. (2015) GPR40 agonists for the treatment of type 2 diabetes: life after 'TAKing'a hit, *Diabetes, Obesity and Metabolism 17*, 622-629.

[100] Edfalk, S., Steneberg, P., and Edlund, H. (2008) Gpr40 is expressed in enteroendocrine cells and mediates free fatty acid stimulation of incretin secretion, *Diabetes 57*, 2280-2287.

[101] Del Guerra, S., Bugliani, M., D'Aleo, V., Del Prato, S., Boggi, U., Mosca, F., Filipponi, F., and Lupi, R. (2010) G-protein-coupled receptor 40 (GPR40) expression and its regulation in human pancreatic islets: the role of type 2 diabetes and fatty acids, *Nutrition, Metabolism and Cardiovascular Diseases 20*, 22-25.

[102] Tomita, T., Masuzaki, H., Iwakura, H., Fujikura, J., Noguchi, M., Tanaka, T., Ebihara, K., Kawamura, J., Komoto, I., and Kawaguchi, Y. (2006) Expression of the gene for a membrane-bound fatty acid receptor in the pancreas and islet cell tumours in humans: evidence for GPR40 expression in pancreatic beta cells and implications for insulin secretion, *Diabetologia 49*, 962-968.

[103] Flodgren, E., Olde, B., Meidute-Abaraviciene, S., Winzell, M. S., Ahrén, B., and Salehi, A. (2007) GPR40 is expressed in glucagon producing cells and affects glucagon secretion, *Biochemical and biophysical research communications 354*, 240-245.

[104] Tomita, T., Masuzaki, H., Noguchi, M., Iwakura, H., Fujikura, J., Tanaka, T., Ebihara, K., Kawamura, J., Komoto, I., and Kawaguchi, Y. (2005) GPR40 gene expression in human pancreas and insulinoma, *Biochemical and biophysical research communications 338*, 1788-1790.

[105] Hirasawa, A., Itsubo, C., Sadakane, K., Hara, T., Shinagawa, S., Koga, H., Nose, H., Koshimizu, T.-a., and Tsujimoto, G. (2008) Production and characterization of a monoclonal antibody against GPR40 (FFAR1; free fatty acid receptor 1), *Biochemical and biophysical research communications 365*, 22-28.

[106] Teutsch, C.-A., Panse, M., Grundmann, M., Kaiser, G., Kostenis, E., Häring, H.-U., and Ullrich, S. (2014) Detection of free fatty acid receptor 1 expression: the critical role of negative and positive controls, *Diabetologia 57*, 776-780.

[107] Defossa, E., and Wagner, M. (2014) Recent developments in the discovery of FFA1 receptor agonists as novel oral treatment for type 2 diabetes mellitus, *Bioorganic & medicinal chemistry letters 24*, 2991-3000.

[108] Garrido, D. M., Corbett, D. F., Dwornik, K. A., Goetz, A. S., Littleton, T. R., McKeown, S. C., Mills, W. Y., Smalley, T. L., Briscoe, C. P., and Peat, A. J. (2006) Synthesis and activity of small molecule GPR40 agonists, *Bioorganic & medicinal chemistry letters 16*, 1840-1845.

[109] Tanaka, H., Yoshida, S., Oshima, H., Minoura, H., Negoro, K., Yamazaki, T., Sakuda, S., Iwasaki, F., Matsui, T., and Shibasaki, M. (2013) Chronic treatment with novel GPR40 agonists improve whole-body glucose metabolism based on the glucose-dependent insulin secretion, *Journal of Pharmacology and Experimental Therapeutics 346*, 443-452.

[110] Negoro, N., Sasaki, S., Mikami, S., Ito, M., Suzuki, M., Tsujihata, Y., Ito, R., Harada, A., Takeuchi, K., and Suzuki, N. (2010) Discovery of TAK-875: a potent, selective, and orally bioavailable GPR40 agonist, *ACS medicinal chemistry letters 1*, 290-294.

[111] Tsujihata, Y., Ito, R., Suzuki, M., Harada, A., Negoro, N., Yasuma, T., Momose, Y., and Takeuchi, K. (2011) TAK-875, an orally available G protein-coupled receptor 40/free fatty acid receptor 1 agonist, enhances glucose-dependent insulin secretion and improves both postprandial and fasting hyperglycemia in type 2 diabetic rats, *Journal of Pharmacology and Experimental Therapeutics 339*, 228-237.

[112] Yashiro, H., Tsujihata, Y., Takeuchi, K., Hazama, M., Johnson, P. R., and Rorsman, P. (2012) The effects of TAK-875, a selective G protein-coupled receptor 40/free fatty acid 1 agonist, on insulin and glucagon secretion in isolated rat and human islets, *Journal of Pharmacology and Experimental Therapeutics 340*, 483-489.

[113] Naik, H., Vakilynejad, M., Wu, J., Viswanathan, P., Dote, N., Higuchi, T., and Leifke, E. (2012) Safety, Tolerability, Pharmacokinetics, and Pharmacodynamic Properties of the GPR40 Agonist TAK-875: Results From a Double-Blind, Placebo-Controlled Single Oral Dose Rising Study in Healthy Volunteers, *The Journal of Clinical Pharmacology 52*, 1007-1016.

[114] Burant, C. F., Viswanathan, P., Marcinak, J., Cao, C., Vakilynejad, M., Xie, B., and Leifke, E. (2012) TAK-875 versus placebo or glimepiride in type 2 diabetes mellitus: a phase 2, randomised, double-blind, placebo-controlled trial, *The Lancet 379*, 1403-1411.

[115] Leese, G. P., Wang, J., Broomhall, J., Kelly, P., Marsden, A., Morrison, W., Frier, B. M., and Morris, A. D. (2003) Frequency of Severe Hypoglycemia Requiring Emergency Treatment in Type 1 and Type 2 Diabetes A population-based study of health service resource use, *Diabetes care 26*, 1176-1180.

[116] Kaku, K., Enya, K., Nakaya, R., Ohira, T., and Matsuno, R. (2015) Efficacy and safety of fasiglifam (TAK-875), a G protein-coupled receptor 40 agonist, in Japanese patients with type 2 diabetes inadequately controlled by diet and exercise: a randomized, double-blind, placebo-controlled, phase III trial, *Diabetes, Obesity and Metabolism 17*, 675-681.

[117] Li, Z., Qiu, Q., Geng, X., Yang, J., Huang, W., and Qian, H. (2016) Free fatty acid receptor agonists for the treatment of type 2 diabetes: drugs in preclinical to phase II clinical development, *Expert opinion on investigational drugs*.

[118] Luo, J., Swaminath, G., Brown, S. P., Zhang, J., Guo, Q., Chen, M., Nguyen, K., Tran, T., Miao, L., and Dransfield, P. J. (2012) A potent class of GPR40 full agonists engages the enteroinsular axis to promote glucose control in rodents, *PLoS One 7*, e46300.

[119] Tikhonova, I. G., Sum, C. S., Neumann, S., Thomas, C. J., Raaka, B. M., Costanzi, S., and Gershengorn, M. C. (2007) Bidirectional, iterative approach to the structural delineation of the functional "chemoprint" in GPR40 for agonist recognition, *Journal of medicinal chemistry 50*, 2981-2989.

[120] Sum, C. S., Tikhonova, I. G., Neumann, S., Engel, S., Raaka, B. M., Costanzi, S., and Gershengorn, M. C. (2007) Identification of residues important for agonist recognition and activation in GPR40, *Journal of Biological Chemistry 282*, 29248-29255.

[121] Srivastava, A., Yano, J., Hirozane, Y., Kefala, G., Gruswitz, F., Snell, G., Lane, W., Ivetac, A., Aertgeerts, K., and Nguyen, J. (2014) High-resolution structure of the human GPR40 receptor bound to allosteric agonist TAK-875, *Nature 513*, 124-127.

[122] Smith, N. J., Stoddart, L. A., Devine, N. M., Jenkins, L., and Milligan, G. (2009) The action and mode of binding of thiazolidinedione ligands at free fatty acid receptor 1, *Journal of Biological Chemistry 284*, 17527-17539.

[123] Lin, D. C.-H., Guo, Q., Luo, J., Zhang, J., Nguyen, K., Chen, M., Tran, T., Dransfield, P. J., Brown, S. P., and Houze, J. (2012) Identification and pharmacological characterization of multiple allosteric binding sites on the free fatty acid 1 receptor, *Molecular pharmacology 82*, 843-859.

[124] Yabuki, C., Komatsu, H., Tsujihata, Y., Maeda, R., Ito, R., Matsuda-Nagasumi, K., Sakuma, K., Miyawaki, K., Kikuchi, N., and Takeuchi, K. (2013) A novel antidiabetic drug, fasiglifam/TAK-875, acts as an ago-allosteric modulator of FFAR1, *PloS one 8*, e76280.

Chapter 2

Synthesis and Characterization of a Promising Novel FFAR1-GPR40 targeting fluorescent probe for β-cell imaging

Romain Bertrand[1,2], Andrea Wolf[1], Yuri Ivashchenko[1], Matthias Löhn[1], Matthias Schäfer[1], Mark Brönstrup[3,4], Martin Gotthardt[2], Volker Derdau[4], and Oliver Plettenburg[1,5,6]

[1]Diabetes Division, Research & Translational Medicine, Sanofi GmbH, Frankfurt am Main 65926, Germany
[2]Department of Nuclear Medicine, Radboud UMC, Nijmegen 6525, The Netherlands
[3]Helmholtz Centre for Infection Research, Braunschweig 38124, Germany
[4]DSAR/Drug Disposition, Sanofi GmbH, Frankfurt am Main 65926, Germany
[5]Institute of Medicinal Chemistry, Helmholtz Zentrum München, Ingolstaedter Landstr. 1, Neuherberg 85764, Germany
[6]Leibniz University Hannover, Schneiderberg 1 B, Hannover 30167, Germany

Adapted from: ACS Chemical Biology, **2016**, *11* (6), pp 1745–1754, "*Synthesis and Characterization of a Promising Novel FFAR1/GPR40 Targeting Fluorescent Probe for* β*-Cell Imaging"*
DOI**:** 10.1021/acschembio.5b00791

Abstract

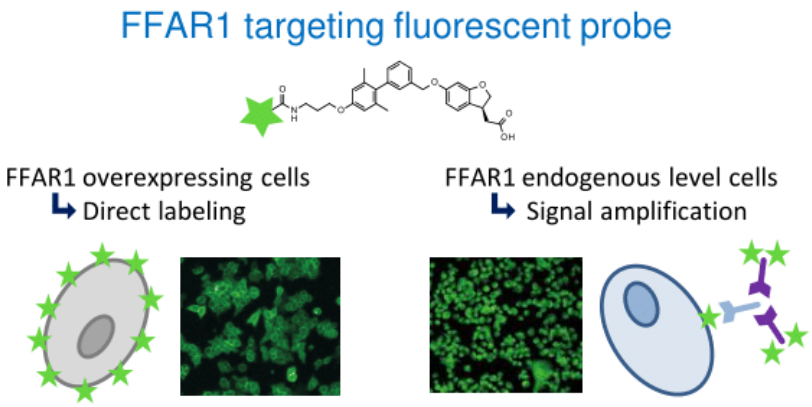

Diabetes affects an increasing number of patients worldwide and is responsible for a significant rise in healthcare expenses. Imaging of β-cells bears the potential to contribute to an improved understanding, diagnosis, and development of new treatment options for diabetes. Here, we describe the first small molecule fluorescent probe targeting the free fatty acid receptor 1 (FFAR1/GPR40). This receptor is highly expressed on β-cells, and was up to now unexplored for imaging purposes. We designed a novel probe by facile modification of the selective and potent FFAR1 agonist TAK-875. Effective and specific binding of the probe was demonstrated using FFAR1 overexpressing cells. We also successfully labeled FFAR1 on MIN6 and INS1E cells, two widely used β-cell models, by applying an effective amplification protocol. Finally, we showed that the probe is capable of inducing insulin secretion in a glucose-dependent manner, thus demonstrating that functional activity of the probe was maintained. These results suggest that our probe represents a first important step to successful β-cell imaging by targeting FFAR1. The developed probe may prove to be particularly useful for in vitro and ex vivo studies of diabetic cellular and animal models to gain new insights into disease pathogenesis.

Introduction

Diabetes is a chronic metabolic disease characterized by hyperglycemia resulting either from deficiency in insulin secretion due to β-cell loss or dysfunction, insulin resistance, or both. According to the International Diabetes Federation, around 390 million* of people are affected worldwide,[1] and treatment to date still is only symptomatic. It generates a massive and intensifying burden on healthcare systems by cost of direct disease management, as well as a consequence of complications caused by long-standing and not properly controlled diabetes, such as cardiovascular disease, diabetic foot ulcers, diabetic nephropathy or retinopathy. Yet, the precise molecular and cellular mechanisms that cause the decrease in mass of the insulin-producing cells remain to be further elucidated. Longitudinal studies aiming at in vivo quantification of β-cells in animal models, as well as in patients, would significantly improve the knowledge on the pathophysiology of the disease; it would allow monitoring of therapeutic efficacy and thus facilitate the discovery of new drugs for optimized diabetes treatment.[2] However, noninvasive β-cell imaging remains a significant challenge. First, in healthy pancreatic tissue, endogenous β-cells account for only 2−3% of the total cells and are dispersed throughout the whole organ. Second, the pancreas is surrounded by the gastrointestinal system and liver,[3, 4] and therefore, probe uptake in the latter organs obscures visualization of the pancreas.[5] Several receptors or proteins that are selectively expressed on β-cell membranes have been described as potentially useful targets for β-cell imaging, including sulfonylurea receptor 1 (SUR1),[6, 7] vesicular monoamine transporter 2 (VMAT2),[8–10] membrane protein IC2,[11–13] or transmembrane protein 27 (TMEM27).[14, 15] However, all these targets show limitations such as heterogeneous or non-β-cell specific expression, low absolute uptake, or even unspecific accumulation of the tracer.[16] To date, the most promising probes are based on agonists of the glucagon like peptide 1 receptor (GLP-1R)[17, 18] with proven high specificity for β-cells; however, some concerns exist whether potential downregulation of the receptor may influence uptake of the tracer.[19, 20] This downregulation may lead to an erroneously low quantification of β-cell number. In summary, although imaging of the GLP-1 receptor is promising, the search for alternative probes with ideal properties for accurate imaging of β-cell mass should continue.

The free fatty acid receptor 1 (FFAR1, also known as GPR40) belongs to the class of the seven-transmembrane domain G-protein-coupled receptors and was deorphanized in 2003.[21–23] Endogenous ligands of the receptor include medium to long-chain free fatty acids which enhance a glucose-dependent insulin secretion. Although evidence of FFAR1 expression was found in human brain and intestine,[21] the receptor is predominantly expressed in human and rodent β- cells.[22–24] Since expression in islets is high, FFAR1 appears to be an attractive receptor to target, which had up to now been unexplored for imaging based determination of functional β-cell mass. It also represents an interesting option to follow another β-cell specific receptor population in animal models, possibly providing new insights in the pathogenesis of diabetes. As this receptor is highly conserved between species (see Supporting Information for sequence homology), it should allow good translation of binding efficacy between different rodent and human cells.[25] As FFAR1 activation stimulates insulin release only at high glucose concentration, it became an attractive therapeutic target[26, 27] to enhance insulin secretion in T2D without the risk of hypoglycemia. Numerous synthetic FFAR1 agonists have been described in the last years and many of them are under development as T2D drugs.[28] Fasiglifam (TAK-875) is an orally

*When the paper was written, the last available report from the Internation Diabetes Federation dated from 2013. At that time, 390 million people were affected by diabetes worldwide. Updated numbers can be found in the introduction.

available and potent agonist of FFAR1 with good selectivity for the receptor over other members of the FFA receptor family (i.e., FFAR2, FFAR3, GPR120).[29] It reached clinical phase III and improved glucose-stimulated insulin secretion (GSIS) and blood glucose control in diabetic patients, with a low risk of hypoglycemia.[30, 31] We therefore envisioned that the TAK-875 scaffold would serve as a good starting point to develop FFAR1 targeting probes.

Material and Methods

Chemistry

See the Supporting Information for a detailed description of the syntheses.

Cell Culture

Human embryonic kidney (HEK293) cells stably expressing human GPR40/FFAR1 (HEK293 cells were transfected with hGPR40 using a pEAK8 vector system) were grown in high glucose DMEM (41965 Life Technologies) containing 10% (v/v) FCS gold PAA, 1% (v/v) NEAA and puromycin (1 μg/mL), in a humidified 5% CO2 atmosphere at 37 °C. Human embryonic kidney (HEK293) cells were cultured under the same conditions except for the absence of puromycin. Transgenic C57BL/6 mouse insulinoma cell line (MIN6) were grown in high-glucose DMEM (Life Technologies 31966) media supplemented with 15% FCS (Good Forte, Cat no. P40-47500), 100 units/mL penicillin and 100 μg/mL streptomycin antibiotics, 1× HEPES (Life Technologies) and 100 μM β-mercaptoethanol in a humidified 5% CO2 atmosphere at 37 °C. The rat insulinoma cell line (INS1E) was grown in RPMI-1640 medium supplemented with 10% FBS, 2 mM glutamine, 10 mM HEPES, 50 μM β-mercaptoethanol, 1 mM sodium pyruvate, 100 units/mL penicillin, and 100 μg/mL streptomycin in a humidified 5% CO2 atmosphere at 37 °C.

Fluorometric Imaging Plate Reader (FLIPR) Ca^{2+} Assays

HEK293 cells stably expressing human GPR40/FFAR1 were plated in a poly-D-Lys coated 96-well plate with 40 000 cells/well and incubated overnight in a humidified 5% CO2 atmosphere at 37 °C. Then, cells were incubated in Hank's buffer salt solution supplemented with HEPES (pH = 7.5) containing fluorescent calcium indicator Fluo 4 AM (Molecular Devices, final concentration 2 μM) + 20% (w/v) pluronic acid for 60 min at 37 °C. Cells were washed with a Tecan Ultra (Tecan Group Ltd.) device before the addition in the wells of tested compounds at various concentrations (previously dissolved in DMSO at 10 mM concentration and diluted with assay buffer). Increase of the intracellular Ca^{2+} concentration after addition was monitored by FLIPR Tetra system (Molecular Devices). Experiments were performed in triplicates.

In Vitro Live Cell Imaging

HEK293 cells overexpressing GPR40 were plated in a 96-well plate with 50 000 cells per well and incubated overnight in a humidified 5% CO2 atmosphere at 37 °C. Then culture media was removed and replaced by PBS buffer before the addition of varying concentrations of fluorescent probe. For the blocking experiment, unlabeled TAK-875 (200 nM) was added 3 min before the fluorescent probe (20 nM). After 30 min of incubation in a humidified 5% CO2 atmosphere at 37 °C, DRAQ5 was added (1/ 1000, nucleus staining, 10 min incubation) and cells were washed twice with PBS buffer before being imaged with the high content imaging system Operetta from PerkinElmer with a 20× long working distance objective and analyzed with Harmony Imaging software. With this software, first nuclei were identified using DRAQ5 staining and subsequently cytoplasm was identified using the fluorescence of probe 16. With this information, the software calculated the mean fluorescence for each cell.

In Vitro Live Cell Imaging−Confocal Microscopy

HEK293 cells overexpressing FFAR1/GPR40 were plated in a 96-well plate with 50 000 cells per well and incubated overnight in a humidified 5% CO2 atmosphere at 37 °C. Then, culture media was removed and replaced by fresh medium before the addition of probe 16 (2 μM). For the blocking experiment, a 10-fold excess of unlabeled TAK-875 was added 3 min before the fluorescent probe. After 30 min of incubation in a humidified 5% CO2 atmosphere at 37 °C, DRAQ5 was added (1/ 500, nucleus staining, 10 min incubation) and cells were washed once with HBSS buffer (supplemented with 5% FCS) before being imaged with the TCS SP8 confocal microscope from Leica Microsystems with a 40× objective. Then, cells were incubated in a humidified 5% CO2 atmosphere at 37 °C for another 2.5 h to enhance internalization before being imaged with a 40× objective (+ numerical zoom 4). Pictures and quantification of fluorescence were analyzed using the Leica Application Suite X (LAS X) imaging software.

RT-PCR mRNA Levels

Expression levels of FFAR1 in different cell lines were analyzed using real time, quantitative PCR. To this end, TaqMan Gene Expression Assays were used together with TaqMan Fast Virus 1-Step Master Mix and the StepOnePlus Real-Time PCR System (Applied Biosystems, Thermo Fisher Scientific, Inc.). The PCR preparation, as well as run, was performed according to the protocol provided by the manufacturer. The gene expression assays used can be found in Table 1. For analysis, the house keeping gene GAPDH was used as control and for normalization. 2ΔCt values were calculated for fold change and then displayed as difference to GAPDH expression.

Table 1. TaqMan probes for real time PCR analysis

GENE	ACCESSION NUMBER	EXPRESSION ASSAY
h*FFAR1*	NM_005303	Hs03045166_s1
r*FFAR1*	NM_153304	Rn00824686_s1
m*FFAR1*	NM_194057	Mm00809442_s1

Antibody Amplification

Cells were incubated in either PBS or PBS with 10 μM of probe 16 at RT. The incubation was carried out for either 15 min or 1 h. Subsequently, cells were fixed for 15 min in 3.5% formaldehyde in PBS, washed and blocked for 20 min in blocking buffer with 0.1% Tween (SuperBlock, Thermo Scientific). The antibody incubation with Anti-Alexa Fluor 488 Rabbit (Life Technologies) and with Anti-Rabbit Alexa Fluor 488 (Jackson Immuno Research) was done for 1 h each with a 1:100 dilution in blocking buffer (Figure 6). Hoechst 33342 was used to label nuclei. To evaluate the binding specificity of the probe, we performed a blocking experiment. Therefore, we added 1 mM of unlabeled TAK-875 (100-fold excess) before adding the probe 16. Immunostainings were analyzed using the Operetta System.

Staining of Dispersed Mouse Islets

Adult C57BL/6 (Jackson Laboratories, ME) were euthanized by cervical dislocation. An incision around the upper abdomen was performed to expose liver and intestines. Thereafter, the ampulla was located and clipped. Pancreas was perfused through the common bile duct with 5 mL of cold collagenase (1 mg mL−1 of collagenase P, Roche) saline solution. The pancreas was dissected and placed into a warm collagenase saline solution for 15 min. After enzymatic digestion of the pancreatic tissue, islets were picked and cultured overnight in an incubator at 37 °C. Thereafter, islets were incubated with Liberase (Roche) for approximately 20 min and mechanically dispersed and cultured overnight at 37 °C. Beta cells were placed into a physiological saline solution and incubated with the probe as indicated in the amplification section above. Thereafter, cells were stained for insulin. The investigation conforms to the Guide for the Care and Use of Laboratory Animals published by the United States National Institutes of Health (NIH publication no. 85-23, revised 1996).

Calcium Measurements

Cells were seeded on Ibidi culture dishes (µ-Dish, 35 mm high glass bottom) with 4 × 105 cells overnight. Medium was removed and the cells were loaded with Fura-2 (AM) (Invitrogen) (10 µL of a 2.87 µM solution) in HBSS (Hanks buffered-salt solution) for 1h at RT. The cells were washed with tyrode buffer and the dish was mounted on the microscope (Olympus IX81). Temperature was regulated to 37 °C and the dishes are filled with 2 mL of tyrode buffer. Equilibration of the system was allowed for 5 min; then the compound of interest was added and signal was recorded for 10 min. The effect was determined by calculation of the ratio of fluorescence at 340 nm/380 nm using the Olympus Xcellence Imaging software.

Glucose-Stimulated Insulin Secretion (GSIS)

The INS1E cells were preincubated in HEPES-buffered Krebs Ringer bicarbonate buffer with 2.5 mM glucose and 0.1% FAF-BSA for 1.5 h at 37 °C with 5% CO2. Subsequently, the buffer was replaced with the same buffer supplemented with either 2.5 mM or 8.3 mM glucose, 0.1% BSA and compounds with indicated concentrations. This incubation was carried out for 1.5 h at 37 °C with 5% CO2. At the end of the incubation, the supernatant was collected and the insulin secretion was measured using the RAT Ultrasensitive Insulin ELISA (Alpco).

Results and Discussion

Design of a New FFAR1 Targeting Optical Probe

We started the design of a FFAR1 targeting probe with the selection of an appropriate ligand, demonstrating high affinity and selectivity for the target receptor. TAK-875 as a potent and selective agonist of the FFAR1[29] fulfilled these requirements. The clinical development of TAK-875 was terminated due to concerns on liver toxicity after meta-analysis of the pursued clinical studies,[31] which involved extended treatment with moderate to high doses of TAK-875.[30] The mechanism of the observed alanine aminotransferase (ALT) increase in liver is unclear, but seemingly did not result from an acute drug effect. We thus believe that this will not be detrimental for future diagnostic work, as for imaging purposes only single applications of probe are required. By inspection of the structure activity relationship of the TAK-875 scaffold,[25] we concluded that the dihydrobenzofuran carboxylic acid is the key moiety for the interaction with the receptor and that modifications on the 4'-position of the terminal biphenyl ring were well tolerated in terms of agonistic activity and binding affinities. A docking model of FFAR1 supported this assumption by showing that tail substituents pointed toward the exit of the binding pocket.[25] Accordingly, we used the 4'-position to synthesize TAK-875 derivatives **1**–**8** containing various linker systems. During the course of our work, a high-resolution structure of the TAK-875 bound FFAR1 was published, confirming that the position we used should be suitable to modify the compound with minimal effects on potency.[32] We envisioned incorporation of a functional group allowing facile conjugation with a fluorophore,[33] such as an alkyne/azide for click reactions or an amine for peptide coupling. To evaluate the functional activity of the synthesized derivatives, we performed a FLIPR Ca^{2+} assay (Figure 1), measuring the increase in cytosolic Ca^{2+} concentration caused by stimulation of the $G_{\alpha q}$–phospholipase C signaling pathway by FFAR1.[34, 35] A short lipophilic linker chain seemed to be favorable since increasing number of PEG units led to a significant drop in agonistic potency (compounds **6**–**8**). We decided to select the short-size amine containing linker of compound **4**, because its acylation was well tolerated as shown by **5**, displaying low nanomolar potency in the order of the original ligand TAK-875. Furthermore, the amino group enabled convenient conjugation with dyes, most of them being commercially available as amine-reactive N-hydroxysuccinimide (NHS) esters.

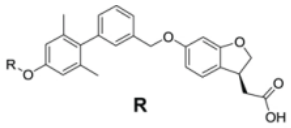

Compound	R	hFFAR1 EC_{50} (nM)
1	H	7
2		3
3		52
4		115
5		6
6	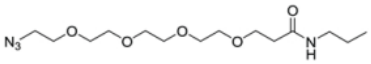	66
7	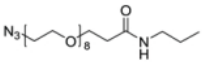	106
8	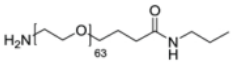	694
TAK-875		8

Figure 1 In vitro activity of TAK-875 derivatives Structures and activity of TAK-875 derivatives with different linkers compared to the original ligand TAK-875. Activities were measured by FLIPR Ca^{2+} assay. All values are mean of triplicates. See also Supporting Information for detailed description of the syntheses.

The Charge of the Fluorophore Influences the Specificity of Binding

To evaluate the influence of the incorporated fluorophore on cellular binding, we synthesized several fluorescent probes in a few steps, starting from the building blocks **9** and **11** whose preparations were previously published[25] (Figure 2). The amine function of compound **13** allowed quick attachment of a wide variety of dyes with different optical and physical properties. We selected small molecule fluorophores among representative cores used in biomolecular labeling including coumarin, fluorescein, BODIPY, rhodamine and cyanine.[36] In the FLIPR assay described above, a drop of agonistic activity was observed compared to TAK-875 (EC_{50} = 1.72 µM (**13**), 2.37 µM (**19**)). Unfortunately, several other probes could not be characterized in this system due to interference with the Fluo-4AM dye used for detection. It was interesting to note that the near-infrared Bodipy derivative did not show agonistic activity up to 20 µM. However, the functional activity of a ligand may not reflect its binding properties, and therefore, it was difficult to assess, if attachment of the dye may reduce the agonistic properties of the compound, but still would allow binding. Thus, transgenic HEK293 cells overexpressing human FFAR1 (hFFAR1-HEK) were used to further evaluate the synthesized fluorescent probes. To assess specificity of the binding, regular HEK293 cells, lacking expression of FFAR1, were used as control. We observed that fluorophore charge strongly influenced the binding specificity of the probe. Probes with neutral (Bodipy 650, tetramethylrhodamine TAMRA)37 or positively charged (Cyanine Cy5.5) dyes exhibited medium to high unspecific membrane staining, whereas probes with negatively charged dyes (carboxyfluorescein CF, fluorescein isothiocyanate FITC, Alexa Fluor 488) were less prone to this phenomenon (Figure 3 and Supplementary Figure S1). These results are in agreement with a recent publication describing the strong interaction of many commonly used fluorophores with lipid bilayers.

The resulting unspecific signals can easily be misinterpreted as binding to targets located on the cell surface.[38] This highlights that a careful choice of fluorophore is essential for designing a new probe, in particular if nonpeptidic small molecule probes are concerned.

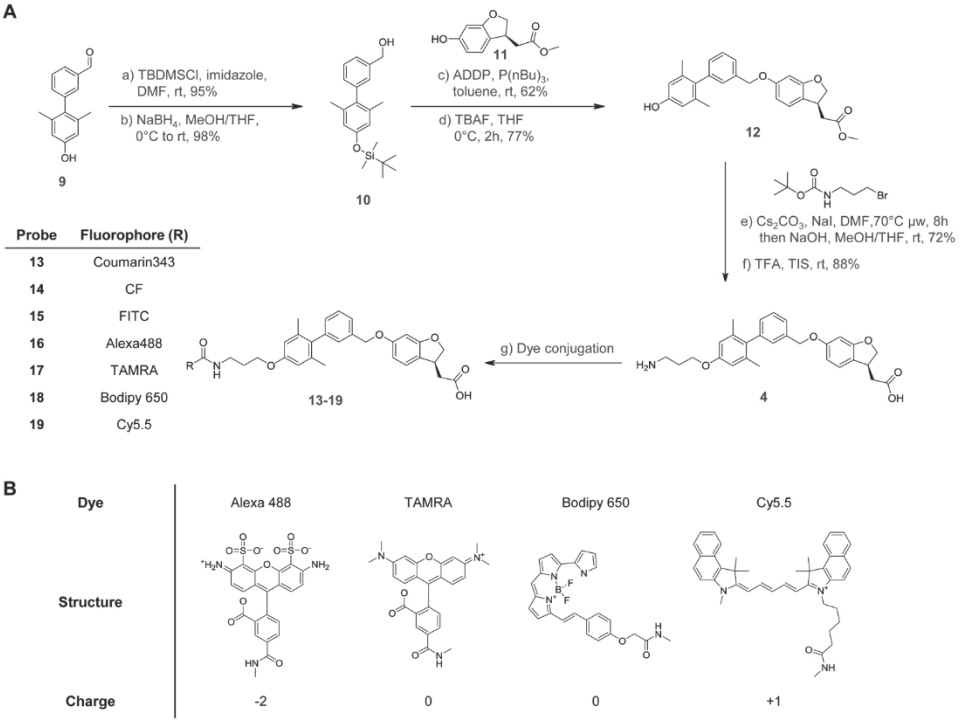

Figure 2 Structures of the fluorescent probes. (A) Synthetic scheme of hFFAR1-targeting fluorescent probes. CF, carboxyfluorescein; FITC, fluorescein isothiocyanate; TAMRA, tetramethylrhodamine; Cy, cyanine. (B) Structure and overall net charge of the dyes Alexa488, TAMRA, Bodipy 650, and Cy5.5 at physiological pH. Detailed description of the syntheses is provided in the Supporting Information.

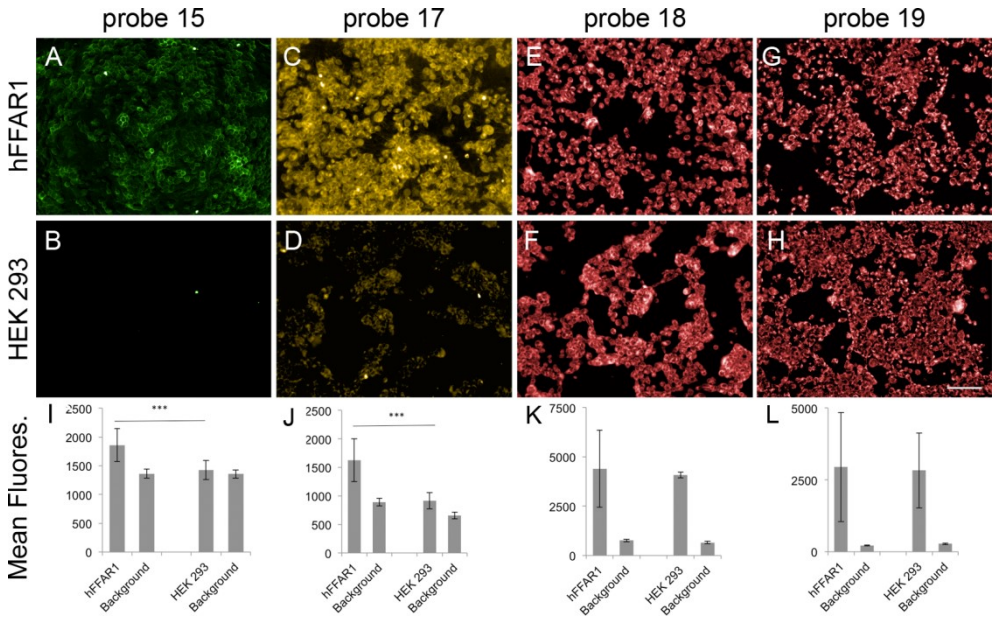

Figure 3 Influence of fluorophore charge on unspecific binding. HEK293 cells overexpressing hFFAR1 show a distinct signal on the cell membrane when incubated with the probe **15** containing the negatively charged dye FITC (A and B), while HEK293 expressing no FFAR1 show no fluorescence. In contrast, probes **17** and **18** with the neutral fluorophores TAMRA (C and D) and Bodipy 650 (E and F) as well as probe **19** containing the positively charged fluorophore Cy5.5 (G and H) showed a clear signal both in hFFAR1 overexpressing and HEK293 control cells. Scale bar is 100 µm. (I–L) Quantification of the signal in mean fluorescence per cell versus background. Student's test, *P < 0.05, **P < 0.01, ***P < 0.001; error bars indicate SD.

Labeling in Live HEK293 Cells Overexpressing hFFAR1

We thus focused on probe **16** to gain more insight into the probe binding properties, as in this case signal to background seemed favorable. This probe is conjugated with Alexa488 which was reported to be superior to other fluorescein equivalents such as fluorescein thioisocyanate and carboxyfluorescein.[39] Live cell imaging of hFFAR1-HEK293 cells demonstrated that the receptor could be visualized using probe **16** (Supplementary Figure S1). As expected, membrane staining was concentration dependent (Supplementary Figure S2). Fluorescent signals were detectable at probe concentrations as low as 20 nM. To confirm whether the observed signal is specific to the receptor ligand interaction, a blocking experiment was performed. By co-incubation of the fluorescent probe with a 10-fold excess of unlabeled agonist (TAK-875), we were able to effectively prevent the binding of **16** to hFFAR1 (Figure 4). These results show that **16** is a specific FFAR1 targeting probe. The applied image analysis software (Harmony) is, in this setup, not capable of distinguishing between membrane and cytoplasm, thus the determined mean fluorescence graphs underestimate the levels of bound probe. For this reason, we performed another set of experiments to obtain confocal images, allowing a more detailed analysis (Supplementary Figure S3. We could determine membrane to background ratio to be 13.0 ± 3.7 that could be effectively blocked with only 10× excess of TAK-875 (signal-to-noise ratio for the blocking experiment: 1.5 ± 0.3). It is noteworthy that a concentration of 2 µM of **16** was used to properly assess potential nonspecific binding properties. We also investigated the tendency of FFAR1 to internalize upon binding of probe **16**. Internalization was observed from 90 min incubation time. White arrows indicate strong enrichment of the probe in intracellular vesicles that were largely clustered in the perinuclear region (Supplementary Figure S4, 3 h incubation time). This data is in good

agreement with results described in two recent publications, (40,41) examining Myc and FLAG-tagged FFAR1/GPR40 overexpressing cells. Localization and distribution supports receptor mediated uptake of probe.

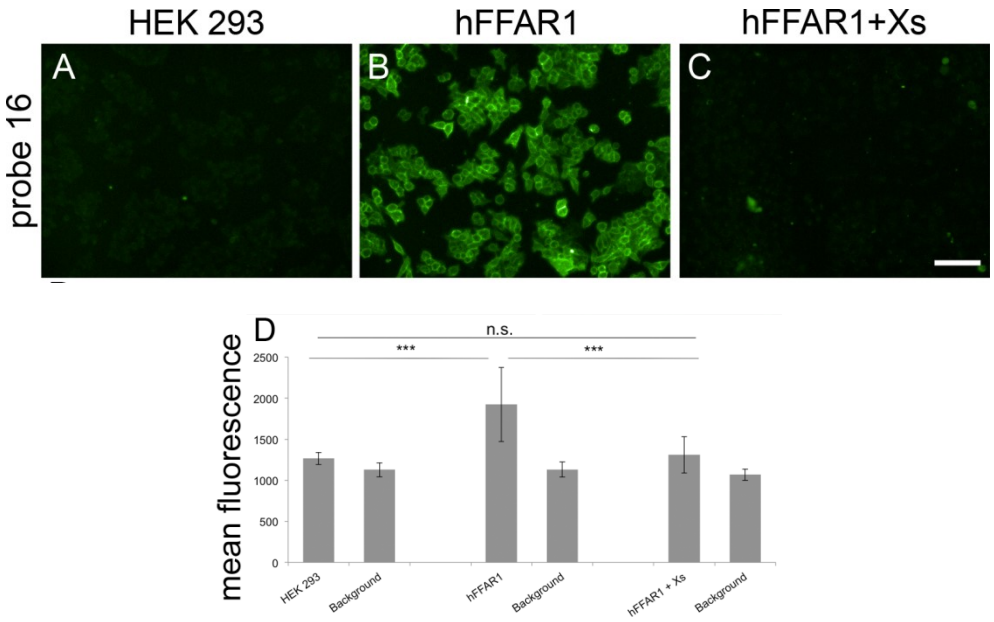

Figure 4 Probe **16** specifically binds the hFFAR1. HEK293 cells incubated with probe **16** at a concentration of 20 nM showed low fluorescence (A), while HEK293 overexpressing hFFAR1 showed strong fluorescence on cell membranes (B). This effect was no longer visible in cells treated with a 10-fold excess of unlabeled TAK-875 prior to incubation with probe **16** (C). Scale bar is 100 µm. (D) Quantification of the mean fluorescence per cell with Student's test. *P < 0.05, **P < 0.01, ***P < 0.001; error bars indicate SD.

Imaging of FFAR1 in Immortalized β-Cells with Endogenous Levels of FFAR1 Expression

Having established that probe **16** can specifically detect FFAR1 in an overexpression system, we set out to determine whether it can be effective to label FFAR1 on cells expressing biological relevant levels of the targeted receptor. We chose MIN6 and INS1E as two commonly used pancreatic β-cell lines;(42) however, the attempt to label FFAR1 with different concentrations of probe **16** on these two cell lines resulted in no detectable fluorescence. We were not able to examine FFAR1 expression by staining with commercially available antibodies; thus, we compared the mRNA expression levels for FFAR1 in the used cell lines (Figure 5). The overexpressing FFAR1-HEK cells show drastically higher mRNA expression levels of hFFAR1 compared to MIN6 and INS1E cells, suggesting that the obtainable signal is too weak due to low abundance of receptors available for ligand binding on the cell surface.

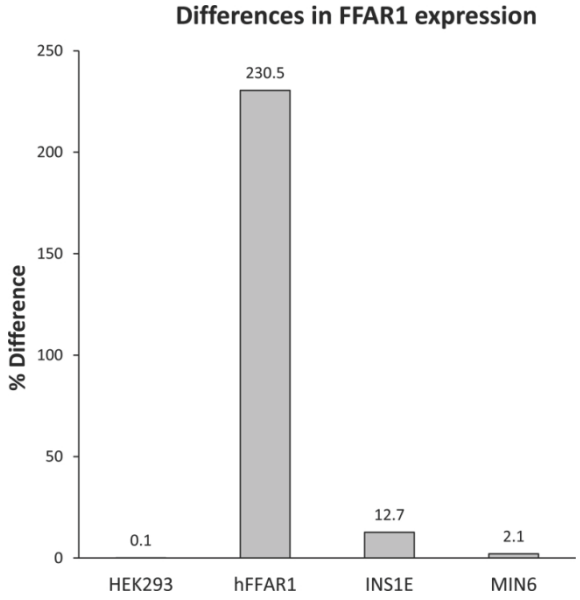

Figure 5 Differences of FFAR1 mRNA expression levels between HEK293 overexpressing FFAR1 and β-cells lines. hFFAR1 mRNA expression has been determined by three independent real time PCR experiments. The control cell line HEK293 expressed hFFAR1 at marginal levels, while the hFFAR1 overexpressing HEK293 cell line showed a 230% difference in expression of hFFAR1. Both β-cell lines INS1E and MIN6 showed a significant expression of FFAR1. Shown data are from one representative experiment.

To improve sensitivity of detection, we developed an efficient protocol for signal amplification using an anti-Alexa 488 antibody (Figure 6). In brief, cells were fixed after incubation with probe **16** and treated with Anti-Alexa Fluor 488 Rabbit and Anti-Rabbit Alexa Fluor 488 goat-antibodies, successively, which led to a significant increase on signal strength. With this amplification strategy, we were able to achieve receptor detection in the applied experimental setup. We observed that this effect increased with longer incubation times. Interestingly, incubation of **16** under high glucose conditions also resulted in an increase of fluorescence (Figure 6A–E and Supplementary Figure S5). Whether this effect is due to a higher abundance of receptor molecules on the cell surface or an increase in receptor accessibility remains to be elucidated. To rule out unspecific binding of probe **16** in MIN6 cells or of the Alexa488 labeled secondary antibody used in this experiment, we performed additional control experiments (Figure 6I–J'). Fluorescence could be efficiently blocked by coincubation with excess of unlabeled ligand. Incubation with secondary antibody alone also did not result in any detectable signal. These experiments demonstrate that we specifically label FFAR1 (Figure 6E–J'). Notably, this effect was also visible with INS1E cells shown in Supplementary Figure S6. Unfortunately, incubation with **16** after fixation was unsuccessful, likely due to alterations of the FFAR1 ligand binding site during fixation. Although the developed signal amplification strategy adds a layer of complexity and limits the probe applicability for the moment to *in vitro* and *ex vivo* work, further investigations will be carried out to translate these results to an in vivo environment. A possible sensitive alternative to the amplification protocol may be utilization of flow cytometry (FACS) for the detection of cells expressing FFAR1. With the help of this much more sensitive method, we were able to demonstrate that probe **16** shows detectable binding to FFAR1 not only to overexpressing HEK 293 cells, but also to MIN6 cells representing cells with endogenous expression levels of FFAR1 (Supplementary Figures S7 and S8). Lastly, we examined specificity of binding of probe **16** using dispersed mouse islets isolated from C57BL/6J mice. Beta cells were stained with anti-insulin antibodies, labeled with Alexa 594. A

satisfactory overlap could be observed after thorough optimization of assay conditions. It has to be stated that insulin content of cells may vary and may be influenced by the isolation and, moreover, by the dispersion and culture protocol, as well as by incubation protocol and washing conditions. Also, little is known on the number of FFAR-1 receptor copies presented on the surface and how this would be influenced by the above-mentioned factors. However, we could confirm good correlation of the two signals at 488 and 594 nm, underlining the binding preference of **16** to β-cells (Supplementary Figure S9). In recent literature, there is an ongoing discussion on the effectiveness and specificity of antibody-mediated detection of FFAR1.[43–45] In our own hands, we have not been able to achieve reliable and specific staining of FFAR1 using six commercially available antibodies, as well as four custom-made anti-hGPR40 antibodies. Thus, FFAR1 detection in living cells is so far difficult to obtain with the available antibodies, while probe **16** can be effectively used to detect FFAR1 on cells. To this end, we propose that a further developed fluorescent FFAR1-specific probe will prove to be useful to study this receptor in the course of diabetes.

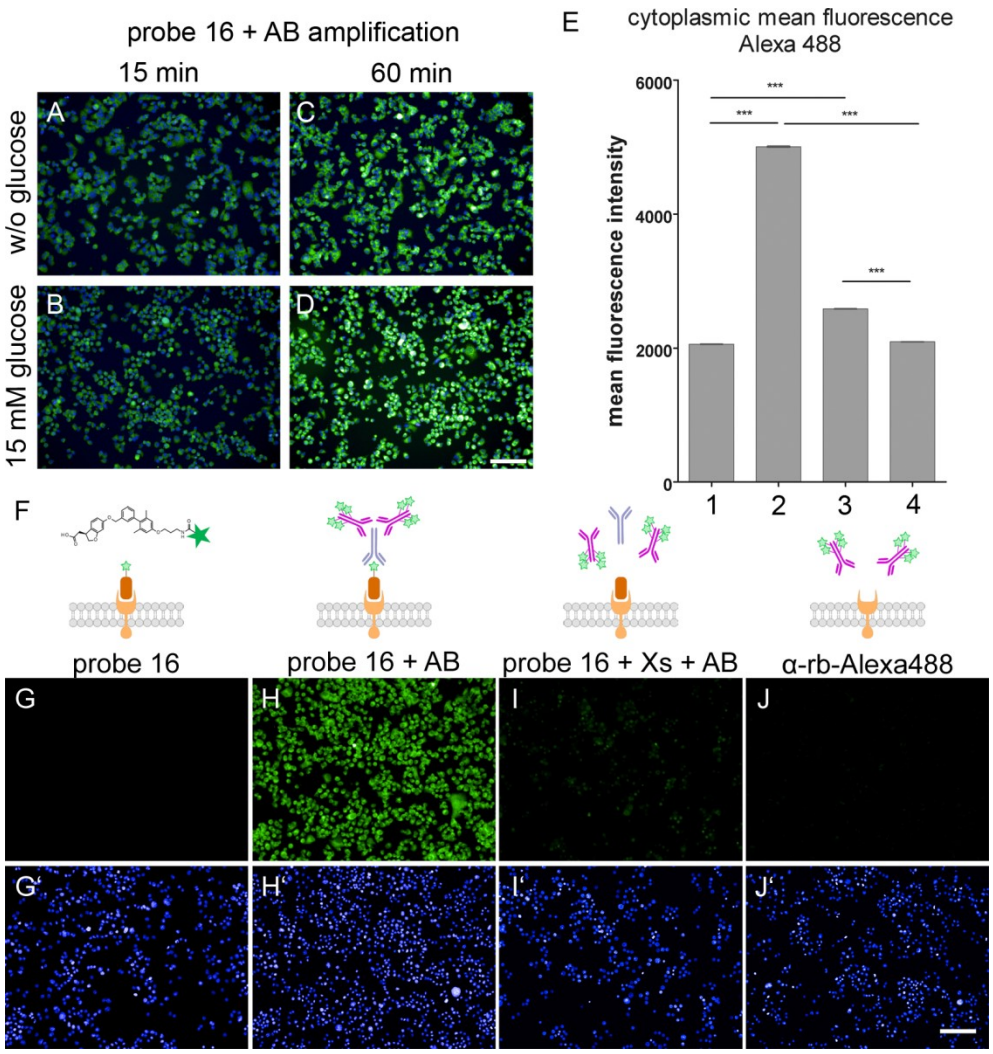

Figure 6 Probe **16** stains MIN6 cells after antibody signal amplification. MIN6 live cells incubated with probe **16** at a 10 µM concentration showed fluorescence after signal amplification (A–D). This effect was strengthened with longer incubation time (C and D) or high glucose concentration (B and D). The mean intensity of Alexa488 was measured in all MIN6 cells after 60 min incubation under high glucose condition and analyzed using Kruskal–Wallis test together with Dunn's post hoc test (E). This measurement shows the increase in fluorescence with antibody amplification and the mean intensity of Alexa488 in the necessary controls. The blocking with excess of unlabeled TAK-875 shows a slight increase in fluorescence. 1, probe **16**; 2, probe **16** and antibody amplification; 3, excess TAK-875, probe **16**, and antibody amplification; 4, anti-rabbit-Alexa488 antibody control; *P < 0.05, **P < 0.01, ***P < 0.001; error bars indicate SEM. Schematic illustration of the antibody signal amplification as shown in (G– J'). Probe **16** (brown) containing the dye Alexa488 (green star) binds hFFAR1 (light orange). The first antibody Anti-Alexa488 Rabbit (blue) allows multiple attachment of the second antibody Anti-Rabbit Alexa488 (purple) resulting in an amplification of the fluorescent signal. No antibody amplification in the presence of an excess of unlabeled TAK-875 and no unspecific binding of the secondary antibody (F). MIN6 cells incubated only with 10 µM of probe **16** showed no detectable fluorescence (G and G'), while after antibody amplification (H and H'), a high fluorescence signal was detected. Cells treated with an excess of unlabeled TAK-875 prior to incubation with probe **16** and signal amplification showed no fluorescence (I and I'). Incubation with secondary antibody only showed no fluorescence (J and J'). Green: Alexa488. Blue: Hoechst 33342. Scale bar is 100 µm. AB, antibody; α-rb-Alexa488, second antibody Anti-Rabbit Alexa488.

*Probe **16** Is an Agonist, Stimulating Glucose-Dependent Insulin Secretion*

To gain more insight into the nature of binding of the probe to FFAR1, we checked whether **16** still effectively activates the receptor. Since probe **16** contains a green-range fluorophore and thus is not compatible with the Fluo-4AM dye used in a standard FLIPR Ca^{2+} assay, we performed a calcium assay using the dye Fura-2 which allows ratiometric detection of intracellular calcium levels. At concentrations of 1 µM of probe **16**, we observed similar calcium response as detected when incubating cells with 10 nM of TAK-875 (ratio 1.45 ± 0.14 vs 1.07 ± 0.01 see Supplementary Figure S10). As these experiments were performed in an overexpressing cell line, we furthermore carried out a glucose-stimulated insulin secretion assay to confirm functional activity in a β-cell line with endogenous FFAR1/GPR40 levels. In agreement with previously published results, TAK-875 showed an insulinotropic effect in INS1E cells in a glucose-dependent manner.[46] We observed similar effects with conjugate **16**, which also enhanced insulin secretion at elevated glucose concentration (Figure 7). As expected, conjugation of the dye results in a certain loss of potency. Endogenous FFAR1 ligands like γ-linolenic acid or oleic acid display functional activities in micromolar concentrations (1− 10 µM),[22] which is in the same concentration range as observed for probe **16**. Accordingly, while coupling a fluorophore to the TAK-875 scaffold results in a drop of potency, we showed that the probe still behaves as a FFAR1 agonist, capable of inducing an insulin secretion upon receptor activation.

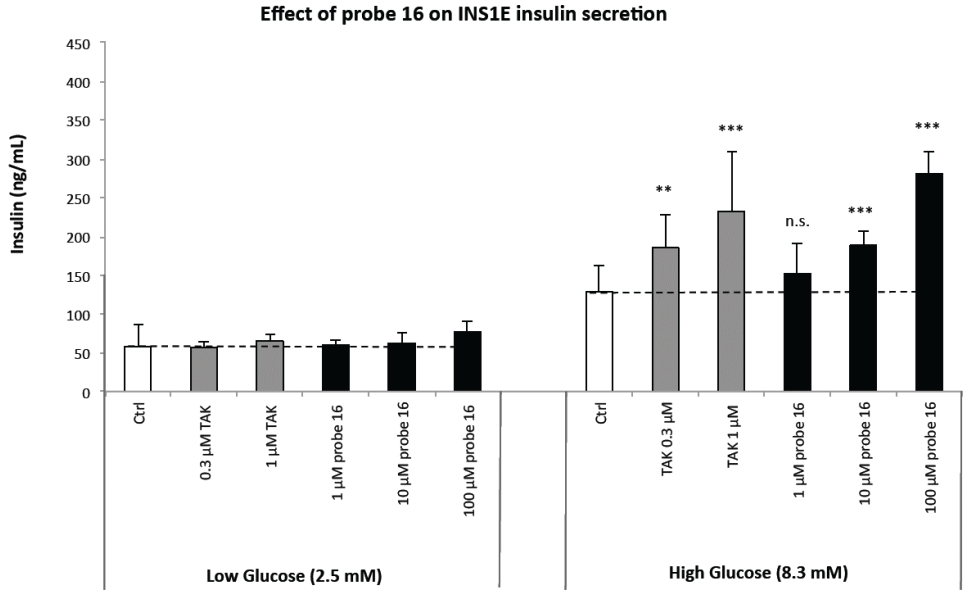

Figure 7 Glucose stimulated insulin secretion of probe 16 in INS1E cells. Probe 16 induced a concentration-dependent increase in insulin secretion only at high glucose concentrations. TAK: unlabeled ligand TAK-875. For each condition, N = 4, data is represented in means and error bars indicate SD, *P < 0.05, **P < 0.01, ***P < 0.001. The whole experiment was repeated six times.

Conclusion

The accurate assessment of the number and viability of remaining β-cells within the pancreas of the diseased animal or patient remains a veritable challenge in the development of new treatment options for diabetes. Imaging of β-cells is a key tool to provide insights into disease development and therapy status. In this study, we present the development and characterization of the first fluorescent probe that specifically binds the FFAR1, a G-protein coupled receptor that is specifically expressed on β- cells. We designed it by modification of TAK-875, a selective and potent FFAR1 agonist. Careful choice of linker and fluorophore proved to be essential to reduce unspecific binding. The probe is well tolerated at tested concentrations up to 10 µM, displaying no signs of cytotoxicity even at extended incubation times. Using this novel probe, we were able to successfully detect FFAR1 in INS1E and MIN6 cells, which could not be achieved before.[45] Also, we have been able to demonstrate staining of primary β-cells isolated from dispersed mouse islets with probe **16**. Albeit utilization of probe **16** to date is limited to in vitro imaging, it represents a new option to detect an important functional marker of β-cells. This opens up new opportunities to study β-cell fate over the course of disease and can help unravel underlying pathological processes, e.g., related to changes in its receptor population or β-cell dysfunction in different disease or nutritional conditions. We believe that this approach may in the future provide a valuable tool to detect and track pancreatic β-cell mass changes in the progress of diabetes using ex vivo models. It may thus also help to determine efficacy of newly explored treatment options to preserve β-cell mass or to quantify number of FFAR1 copies presented on β-cells in longitudinal studies. With increasing availability of highly specific small molecules for different classes of β-cell specific targets (e.g., FFAR1, GLP-1, ion channels, etc.), the reported approach can become an important addition to the growing arsenal of imaging tools for diabetes. Being able to follow another β-cell specific receptor type besides GLP-1, which is well established, will complement available information and may provide new insights in disease pathogenesis, particularly by studying animal models. Last but not least, providing a specific small molecule FFAR1/GPR40 probe may help to overcome issues arising from lack of specific antibodies and complement studies performed with tagged receptors, thus possibly shedding more light on binding events and receptor kinetics. However, more work will have to be invested to turn this into a probe suitable for in vivo examinations.

Acknowledgements

The research leading to these results has received funding from the People Program (Marie Curie Actions) of the European Union's Seventh Framework Program FP7/2007-2013/under REA Grant Agreement No. 289932. We are grateful to M. de Hoop for helpful advice on antibody amplification and to M. Lohmann and D. Crowther for critically reading the manuscript. We also acknowledge U. Messinger and J. Schubert for their help with providing analytical data, A. Sabel for the calcium measurements and J. Dedio and B. Herzog for performing the FLIPR Ca^{2+} assay.

References

[1] Federation, I. D. (2013) in IDF Diabetes Atlas (Guariguata, L., Nolan, T., Beagley, J., Linnenkamp, U., and Jacqmain, O., Eds.) 6 ed. Update 2014.pdf, International Diabetes Federation.
[2] Gotthardt, M., Eizirik, D. L., Cnop, M., and Brom, M. (2014) Beta cell imaging - a key tool in optimized diabetes prevention and treatment. Trends Endocrinol. Metab. 25, 375−377.
[3] Bonner-Weir, S. (1994) Regulation of pancreatic beta-cell mass in vivo. Recent Prog. Horm Res. 49, 91−104.
[4] Weir, G. C., Bonner-Weir, S., and Leahy, J. L. (1990) Islet mass and function in diabetes and transplantation. Diabetes 39, 401−405.
[5] Arifin, D. R., and Bulte, J. W. (2011) Imaging of pancreatic islet cells. Diabetes/Metab. Res. Rev. 27, 761−766.
[6] Schmitz, A., Shiue, C. Y., Feng, Q., Shiue, G. G., Deng, S., Pourdehnad, M. T., Schirrmacher, R., Vatamaniuk, M., Doliba, N., Matschinsky, F., Wolf, B., Rosch, F., Naji, A., and Alavi, A. A. (2004) Synthesis and evaluation of fluorine-18 labeled glyburide analogs as beta-cell imaging agents. Nucl. Med. Biol. 31, 483−491.
[7] Wangler, B., Schneider, S., Thews, O., Schirrmacher, E., Comagic, S., Feilen, P., Schwanstecher, C., Schwanstecher, M., Shiue, C. Y., Alavi, A., Hohnemann, S., Piel, M., Rosch, F., and Schirrmacher, R. (2004) Synthesis and evaluation of (S)-2-(2-[18F]fluoroethoxy)-4- ([3-methyl-1-(2-piperidin-1-yl-phenyl)-butyl-carbam oyl]-methyl)- benzoic acid ([18F]repaglinide): a promising radioligand for quantification of pancreatic beta-cell mass with positron emission tomography (PET). Nucl. Med. Biol. 31, 639−647.
[8] Eriksson, O., Jahan, M., Johnstrom, P., Korsgren, O., Sundin, A., Halldin, C., and Johansson, L. (2010) In vivo and in vitro characterization of [18F]-FE-(+)-DTBZ. as a tracer for beta-cell mass. Nucl. Med. Biol. 37, 357−363.
[9] Kung, M. P., Hou, C., Lieberman, B. P., Oya, S., Ponde, D. E., Blankemeyer, E., Skovronsky, D., Kilbourn, M. R., and Kung, H. F. (2008) In vivo imaging of beta-cell mass in rats using 18F-FP- (+)-DTBZ: a potential PET ligand for studying diabetes mellitus. J. Nucl. Med. 49, 1171−1176.
[10] Virostko, J., Henske, J., Vinet, L., Lamprianou, S., Dai, C., Radhika, A., Baldwin, R. M., Ansari, M. S., Hefti, F., Skovronsky, D., Kung, H. F., Herrera, P. L., Peterson, T. E., Meda, P., and Powers, A. C. (2011) Multimodal image coregistration and inducible selective cell ablation to evaluate imaging ligands. Proc. Natl. Acad. Sci. U. S. A. 108, 20719−20724.
[11] Andralojc, K., Srinivas, M., Brom, M., Joosten, L., de Vries, I. J., Eizirik, D. L., Boerman, O. C., Meda, P., and Gotthardt, M. (2012) Obstacles on the way to the clinical visualisation of beta cells: looking for the Aeneas of molecular imaging to navigate between Scylla and Charybdis. Diabetologia 55, 1247−1257.
[12] Brogren, C. H., Hirsch, F., Wood, P., Druet, P., and Poussier, P. (1986) Production and characterization of a monoclonal islet cell surface autoantibody from the BB rat. Diabetologia 29, 330−333.
[13] Moore, A., Bonner-Weir, S., and Weissleder, R. (2001) Noninvasive in vivo measurement of beta-cell mass in mouse model of diabetes. Diabetes 50, 2231−2236.
[14] Ahnfelt-Ronne, J., Hecksher-Sorensen, J., Schaffer, L., and Madsen, O. D. (2012) A new view of the beta cell. Diabetologia 55, 2316−2318.
[15] Vats, D., Wang, H., Esterhazy, D., Dikaiou, K., Danzer, C., Honer, M., Stuker, F., Matile, H., Migliorini, C., Fischer, E., Ripoll, J., Keist, R., Krek, W., Schibli, R., Stoffel, M., and Rudin, M. (2012)

Multimodal imaging of pancreatic beta cells in vivo by targeting transmembrane protein 27 (TMEM27). Diabetologia 55, 2407−2416.
[16] Brom, M., Andralojc, K., Oyen, W. J., Boerman, O. C., and Gotthardt, M. (2010) Development of radiotracers for the determination of the beta-cell mass in vivo. Curr. Pharm. Des. 16, 1561−1567.
[17] Reiner, T., Thurber, G., Gaglia, J., Vinegoni, C., Liew, C. W., Upadhyay, R., Kohler, R. H., Li, L., Kulkarni, R. N., Benoist, C., Mathis, D., and Weissleder, R. (2011) Accurate measurement of pancreatic islet beta-cell mass using a second-generation fluorescent exendin-4 analog. Proc. Natl. Acad. Sci. U. S. A. 108, 12815−12820.
[18] Brom, M., Woliner-van der Weg, W., Joosten, L., Frielink, C., Bouckenooghe, T., Rijken, P., Andralojc, K., Goke, B. J., de Jong, M., Eizirik, D. L., Behe, M., Lahoutte, T., Oyen, W. J., Tack, C. J., Janssen, M., Boerman, O. C., and Gotthardt, M. (2014) Non-invasive quantification of the beta cell mass by SPECT with (1)(1)(1)Inlabelled exendin. Diabetologia 57, 950−959.
[19] Shu, L., Matveyenko, A. V., Kerr-Conte, J., Cho, J. H., McIntosh, C. H., and Maedler, K. (2009) Decreased TCF7L2 protein levels in type 2 diabetes mellitus correlate with downregulation of GIP- and GLP-1 receptors and impaired beta-cell function. Hum. Mol. Genet. 18, 2388−2399.
[20] Xu, G., Kaneto, H., Laybutt, D. R., Duvivier-Kali, V. F., Trivedi, N., Suzuma, K., King, G. L., Weir, G. C., and Bonner-Weir, S. (2007) Downregulation of GLP-1 and GIP receptor expression by hyperglycemia: possible contribution to impaired incretin effects in diabetes. Diabetes 56, 1551−1558.
[21] Briscoe, C. P., Tadayyon, M., Andrews, J. L., Benson, W. G., Chambers, J. K., Eilert, M. M., Ellis, C., Elshourbagy, N. A., Goetz, A. S., Minnick, D. T., Murdock, P. R., Sauls, H. R., Jr., Shabon, U., Spinage, L. D., Strum, J. C., Szekeres, P. G., Tan, K. B., Way, J. M., Ignar, D. M., Wilson, S., and Muir, A. I. (2003) The orphan G proteincoupled receptor GPR40 is activated by medium and long chain fatty acids. J. Biol. Chem. 278, 11303−11311.
[22] Itoh, Y., Kawamata, Y., Harada, M., Kobayashi, M., Fujii, R., Fukusumi, S., Ogi, K., Hosoya, M., Tanaka, Y., Uejima, H., Tanaka, H., Maruyama, M., Satoh, R., Okubo, S., Kizawa, H., Komatsu, H., Matsumura, F., Noguchi, Y., Shinohara, T., Hinuma, S., Fujisawa, Y., and Fujino, M. (2003) Free fatty acids regulate insulin secretion from pancreatic beta cells through GPR40. Nature 422, 173−176.
[23] Kotarsky, K., Nilsson, N. E., Flodgren, E., Owman, C., and Olde, B. (2003) A human cell surface receptor activated by free fatty acids and thiazolidinedione drugs. Biochem. Biophys. Res. Commun. 301, 406−410.
[24] Tomita, T., Masuzaki, H., Noguchi, M., Iwakura, H., Fujikura, J., Tanaka, T., Ebihara, K., Kawamura, J., Komoto, I., Kawaguchi, Y., Fujimoto, K., Doi, R., Shimada, Y., Hosoda, K., Imamura, M., and Nakao, K. (2005) GPR40 gene expression in human pancreas and insulinoma. Biochem. Biophys. Res. Commun. 338, 1788−1790.
[25] Negoro, N., Sasaki, S., Mikami, S., Ito, M., Tsujihata, Y., Ito, R., Suzuki, M., Takeuchi, K., Suzuki, N., Miyazaki, J., Santou, T., Odani, T., Kanzaki, N., Funami, M., Morohashi, A., Nonaka, M., Matsunaga, S., Yasuma, T., and Momose, Y. (2012) Optimization of (2,3-dihydro- 1-benzofuran-3-yl)acetic acids: discovery of a non-free fatty acid-like, highly bioavailable G protein-coupled receptor 40/free fatty acid receptor 1 agonist as a glucose-dependent insulinotropic agent. J. Med. Chem. 55, 3960−3974.
[26] Ferdaoussi, M., Bergeron, V., Kebede, M., Mancini, A., Alquier, T., and Poitout, V. (2012) Free Fatty Acid Receptor 1- A New Drug Target for Type 2 Diabetes. Can. J. Diabetes 36, 275−280.
[27] Feng, X. T., Leng, J., Xie, Z., Li, S. L., Zhao, W., and Tang, Q. L. (2012) GPR40: a therapeutic target for mediating insulin secretion (review). Int. J. Mol. Med. 30, 1261−1266.

[28] Defossa, E., and Wagner, M. (2014) Recent developments in the discovery of FFA1 receptor agonists as novel oral treatment for type 2 diabetes mellitus. Bioorg. Med. Chem. Lett. 24, 2991−3000.
[29] Negoro, N., Sasaki, S., Mikami, S., Ito, M., Suzuki, M., Tsujihata, Y., Ito, R., Harada, A., Takeuchi, K., Suzuki, N., Miyazaki, J., Santou, T., Odani, T., Kanzaki, N., Funami, M., Tanaka, T., Kogame, A., Matsunaga, S., Yasuma, T., and Momose, Y. (2010) Discovery of TAK-875: A Potent, Selective, and Orally Bioavailable GPR40 Agonist. ACS Med. Chem. Lett. 1, 290−294.
[30] Burant, C. F., Viswanathan, P., Marcinak, J., Cao, C., Vakilynejad, M., Xie, B., and Leifke, E. (2012) TAK-875 versus placebo or glimepiride in type 2 diabetes mellitus: a phase 2, randomised, double-blind, placebo-controlled trial. Lancet 379, 1403− 1411.
[31] Kaku, K., Enya, K., Nakaya, R., Ohira, T., and Matsuno, R. (2015) Efficacy and safety of fasiglifam (TAK-875), a G proteincoupled receptor 40 agonist, in Japanese patients with type 2 diabetes inadequately controlled by diet and exercise: a randomized, doubleblind, placebo-controlled, phase III trial. Diabetes, Obes. Metab. 17, 675−681.
[32] Srivastava, A., Yano, J., Hirozane, Y., Kefala, G., Gruswitz, F., Snell, G., Lane, W., Ivetac, A., Aertgeerts, K., Nguyen, J., Jennings, A., and Okada, K. (2014) High-resolution structure of the human GPR40 receptor bound to allosteric agonist TAK-875. Nature 513, 124−127.
[33] Suckow, A. T., Polidori, D., Yan, W., Chon, S., Ma, J. Y., Leonard, J., and Briscoe, C. P. (2014) Alteration of the glucagon axis in GPR120 (FFAR4) knockout mice: a role for GPR120 in glucagon secretion. J. Biol. Chem. 289, 15751−15763.
[34] Fujiwara, K., Maekawa, F., and Yada, T. (2005) Oleic acid interacts with GPR40 to induce Ca2+ signaling in rat islet beta-cells: mediation by PLC and L-type Ca2+ channel and link to insulin release. AJP: Endocrinology and Metabolism 289, E670−677.
[35] Shapiro, H., Shachar, S., Sekler, I., Hershfinkel, M., and Walker, M. D. (2005) Role of GPR40 in fatty acid action on the beta cell line INS-1E. Biochem. Biophys. Res. Commun. 335, 97−104.
[36] Goncalves, M. S. (2009) Fluorescent labeling of biomolecules with organic probes. Chem. Rev. 109, 190−212.
[37] Schrum, K. F., Lancaster, J. M., 3rd, Johnston, S. E., and Gilman, S. D. (2000) Monitoring electroosmotic flow by periodic photobleaching of a dilute, neutral fluorophore. Anal. Chem. 72, 4317−4321.
[38] Hughes, L. D., Rawle, R. J., and Boxer, S. G. (2014) Choose your label wisely: water-soluble fluorophores often interact with lipid bilayers. PLoS One 9, e87649.
[39] Panchuk-Voloshina, N., Haugland, R. P., Bishop-Stewart, J., Bhalgat, M. K., Millard, P. J., Mao, F., Leung, W. Y., and Haugland, R. P. (1999) Alexa dyes, a series of new fluorescent dyes that yield exceptionally bright, photostable conjugates. J. Histochem. Cytochem. 47, 1179−1188.
[40] Guo, S., Zhang, J., Zhang, S., and Li, J. (2015) A Single Amino Acid Mutation (R104P) in the E/DRY Motif of GPR40 Impairs Receptor Function. PLoS One 10, e0141303.
[41] Qian, J., Wu, C., Chen, X., Li, X., Ying, G., Jin, L., Ma, Q., Li, G., Shi, Y., Zhang, G., and Zhou, N. (2014) Differential requirements of arrestin-3 and clathrin for ligand-dependent and -independent internalization of human G protein-coupled receptor 40. Cell. Signalling 26, 2412−2423.
[42] Hohmeier, H. E., and Newgard, C. B. (2004) Cell lines derived from pancreatic islets. Mol. Cell. Endocrinol. 228, 121−128.
[43] Nakamoto, K., Nishinaka, T., Matsumoto, K., Kasuya, F., Mankura, M., Koyama, Y., and Tokuyama, S. (2012) Involvement of the long-chain fatty acid receptor GPR40 as a novel pain regulatory system. Brain Res. 1432, 74−83.

[44] Natalicchio, A., Labarbuta, R., Tortosa, F., Biondi, G., Marrano, N., Peschechera, A., Carchia, E., Orlando, M. R., Leonardini, A., Cignarelli, A., Marchetti, P., Perrini, S., Laviola, L., and Giorgino, F. (2013) Exendin-4 protects pancreatic beta cells from palmitateinduced apoptosis by interfering with GPR40 and the MKK4/7 stress kinase signalling pathway. Diabetologia 56, 2456−2466.
[45] Teutsch, C. A., Panse, M., Grundmann, M., Kaiser, G., Kostenis, E., Haring, H. U., and Ullrich, S. (2014) Detection of free fatty acid receptor 1 expression: the critical role of negative and positive controls. Diabetologia 57, 776−780.
[46] Tsujihata, Y., Ito, R., Suzuki, M., Harada, A., Negoro, N., Yasuma, T., Momose, Y., and Takeuchi, K. (2011) TAK-875, an orally available G protein-coupled receptor 40/free fatty acid receptor 1 agonist, enhances glucose-dependent insulin secretion and improves both postprandial and fasting hyperglycemia in type 2 diabetic rats. J. Pharmacol. Exp. Ther. 339, 228−237.

Supporting Information

Supplementary Figure S1 related to Figure 3 Probe **14**, **15** and **16** with negatively charged fluorophores show no unspecific binding on hFFAR1- HEK293 overexpressing cells.
Supplementary Figure S2 related to Figure 4: Probe **16** binding to hFFAR1 is concentration dependent.
Supplementary Figure S3: Cytoplasmic mean fluorescence of probe **16** (confocal microscopy).
Supplementary Figure S4: Internalization of Probe **16** upon hFFAR1 binding
Supplementary Figure S5 rel. to Figure 6: Cytoplasmic mean fluorescence of probe **16** in picture A-D.
Supplementary Figure S6: Cytoplasmic mean fluorescence of INS1E cells after incubation with **16**
Supplementary Figure S7: FACS-based quantification of probe **16**-fluorescence of GPR40-HEK293 and MIN6 cells.
Supplementary Figure S8: Summary of GPR40-HEK293 and MIN6 cells mean fluorescence.
Supplementary Figure S9: Staining of dispersed mouse islets
Supplementary Figure S10: Representative calcium traces for TAK 875 and probe **16**.
Chemical synthesis: Molecules presented in Figure 1.
Chemical synthesis: Fluorescent probes 13-19 presented in Figure 2.
Sequence Homology of mouse, rat and human FFAR1.

Supplementary Figure S1 related to Figure 3

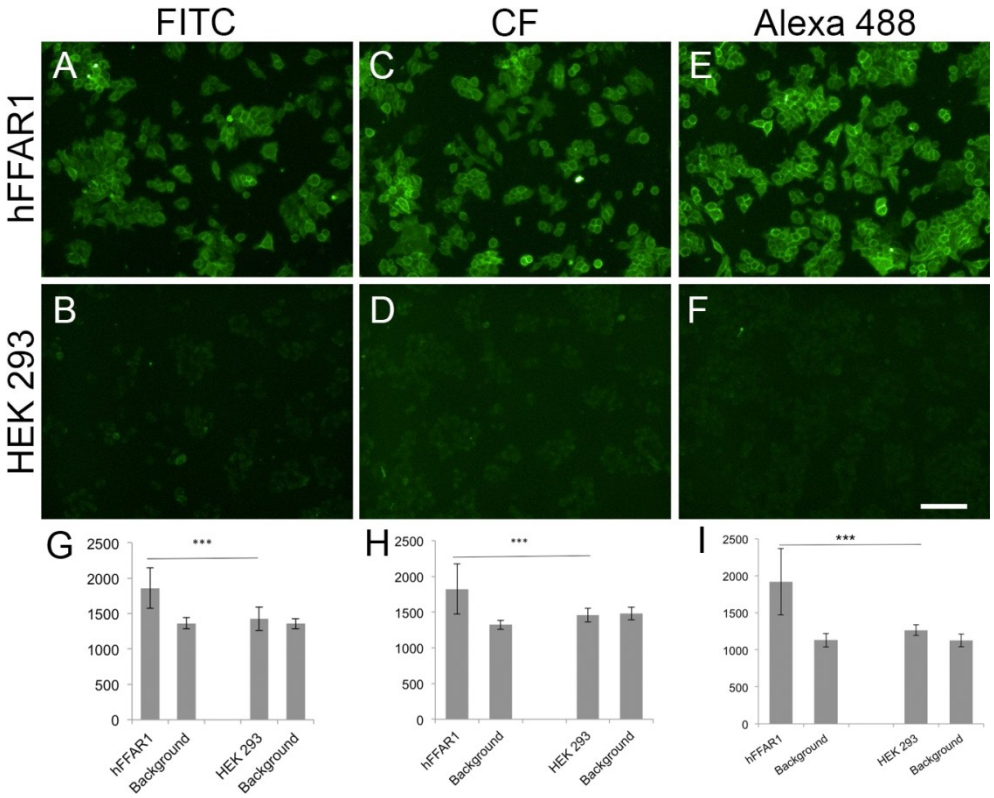

Probe **14**, **15** and **16** with negatively charged fluorophores show low unspecific binding on hFFAR1-HEK293 overexpressing cells. hFFAR1-HEK293 overexpressing cells incubated with probe **15** (FITC), **14** (CF) and **16** (Alexa 488) showed a clear signal on the membrane (A,C,E), while HEK293 cells expressing no FFAR1 incubated with the same probes show no fluorescence (B,D,F). Scale bar is 100 µm. (G-I) show the quantification of A-F in mean fluorescence per cell. Student's Test, *P<0.05, **P<0.01, ***P<0.001; error bars indicate s.e.m.

Supplementary Figure S2 related to Figure 4

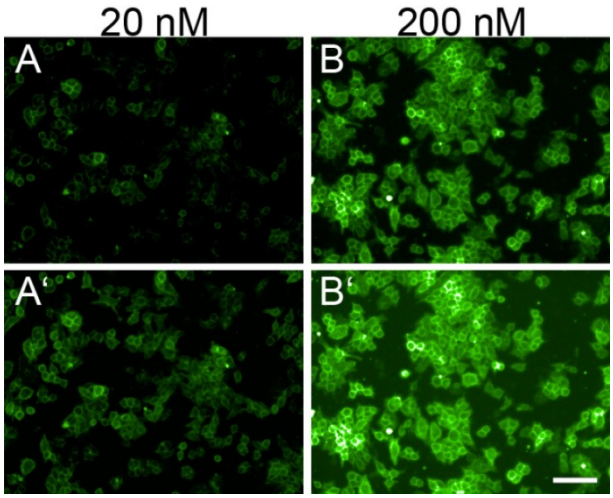

Probe **16** binding to hFFAR1 is concentration dependent. hFFAR1-HEK293 overexpressing cells incubated with probe **16** at a concentration of 200 nM (B, B') showed a more intense fluorescent signal than the same probe at a concentration of 20 nM (A, A'). A and A' show the same image with different intensities to allow improved optical comparison, the intensity was adjusted for optimal signal intensity at 200 nM in the top lane (A and B), while it was adjusted to optimal signal intensity for cells treated with 20 nM in the lower lane (A' and B'). Scale bar is 100 µm.

Supplementary Figure S3

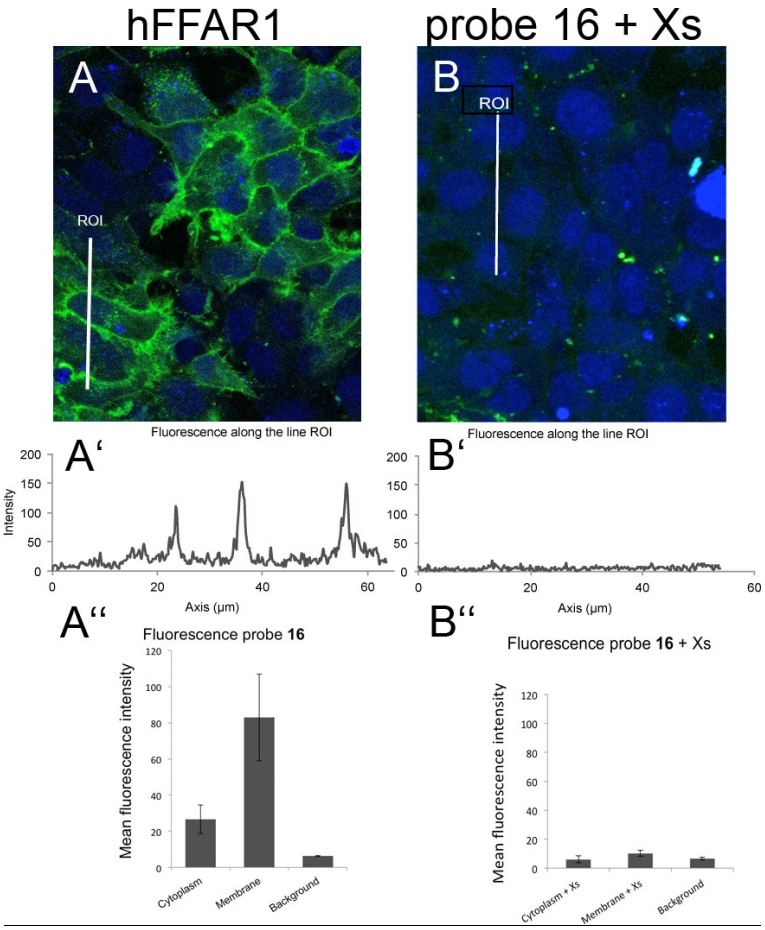

Probe **16** specifically binds the hFFAR. Confocal microscopy high-resolution pictures of hFFAR1-HEK29 overexpressing cells labeled with probe **16** at a concentration of 2 µM (A) or cells treated with a tenfold excess of unlabeled TAK-875 (Xs) prior to incubation with probe **16** at a concentration of 2 µM (B). Fluorescence along an exemplary linear region of interest (ROI) shows a clear membrane labeling on cells (A'). This effect was no longer visible in the blocking experiment (B). Quantification of fluorescence for cells treated with probe **16** (A'') or cells treated with probe **16** and a tenfold excess of unlabeled TAK-875 (B'') (complete analysis). Green: Alexa488. Blue: DRAQ5 (nuclei).

Supplementary Figure S4

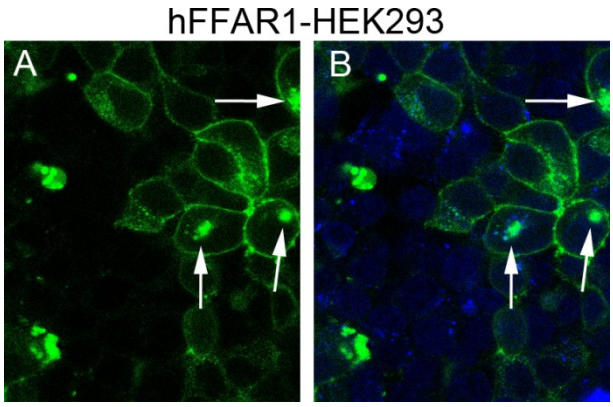

Internalization of Probe **16** upon hFFAR1 binding. Confocal microscopy high-resolution pictures of hFFAR1-HEK293 overexpressing cells labeled with probe **16** at a concentration of 2 µM show internalization of probe **16** in vesicles clustered in the perinuclear region indicated by white arrows. (A) Green: Alexa488. (B) Merged Green: Alexa488 and Blue: DRAQ5 (nuclei).

Supplementary Figure S5 rel. to Figure 6

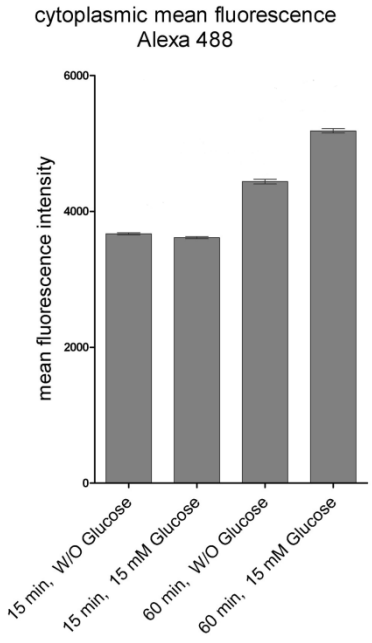

Measurements of cytoplasmic mean fluorescence of probe **16** in picture A-D of Figure 6. The mean intensity of Alexa488 was measured in all MIN6 cells. This analysis showed the increase in fluorescence with longer incubation time but only after 60 min incubation a glucose-dependent increase in fluorescence can be shown. Error bars indicate s.e.m.

Supplementary Figure S6

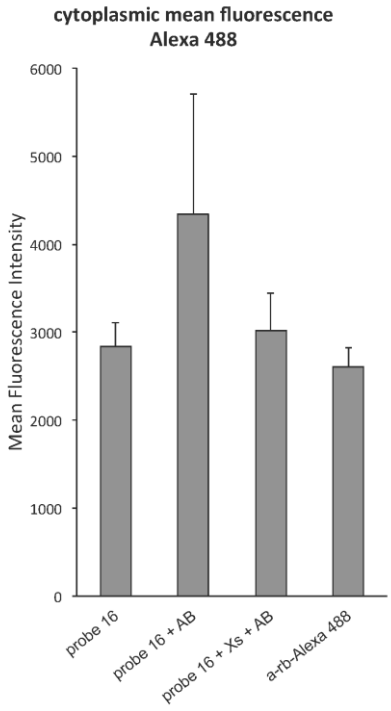

Cytoplasmic mean fluorescence of INS1E cells after incubation with probe **16**. Measurements of cytoplasmic mean fluorescence of probe **16** of Ins1E cells analogous to Figure 6 for MIN6. The mean intensity of Alexa488 was measured in all INS1E cells; error bars indicate s.e.m.

Supplementary Figure S7

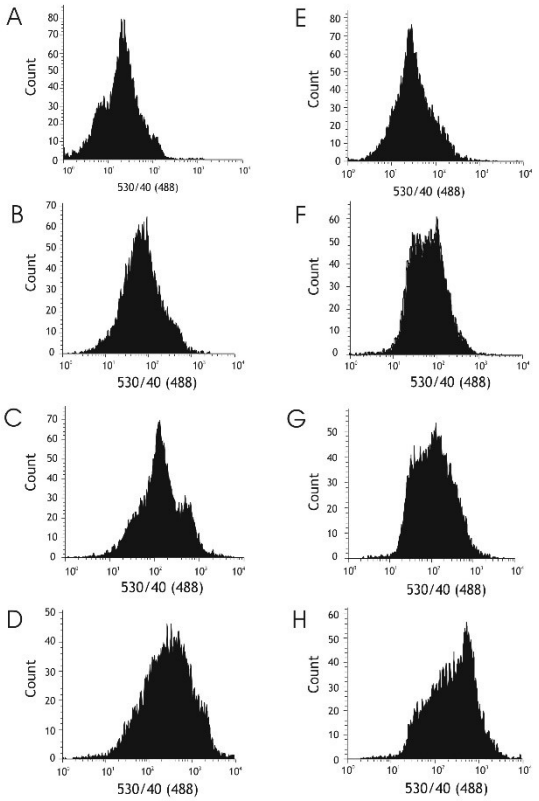

FACS-based quantification of probe **16** fluorescence of GPR40-HEK293 and MIN6 cells. The cells were stained with probe **16** at different concentrations: A,E: no treatment, B,F: 1 µM, C,G: 3 µM, and D,H: 10 µM of probe **16**. To distinguish non-viable cells or debris from viable cells, cells have been additionally incubated with propidium iodide at 1 µM and have been excluded form the analysis by appropriate gating. Mean of fluorescence increased upon increasing concentration of probe **16**. GPR-HEK293 overexpressing cells showed stronger fluorescence intensity in comparison to MIN6.

Supplementary Figure S8

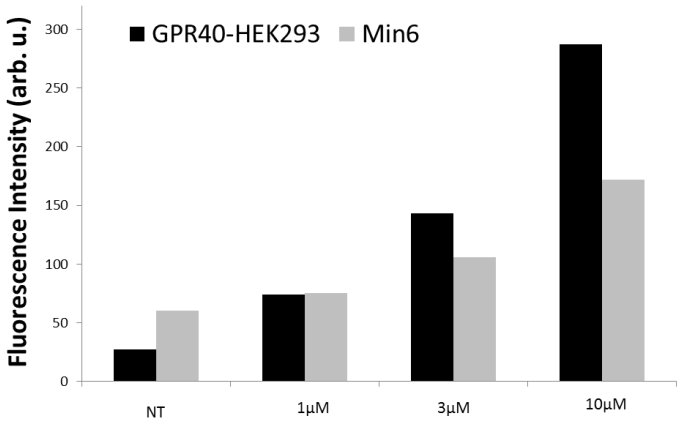

Summary of GPR40-HEK293 and MIN6 cells mean fluorescence. FACS analysis of GPR40-HEK293 (A-D) and MIN6 (E-H) cells using probe **16** at different concentrations (A,E: no treatment, B,F: 1 μM, C,G: 3 μM, and D,H: 10 μM of probe **16**. A dose dependent increase of fluorescence has been observed for both cell lines.

Supplementary Figure S9

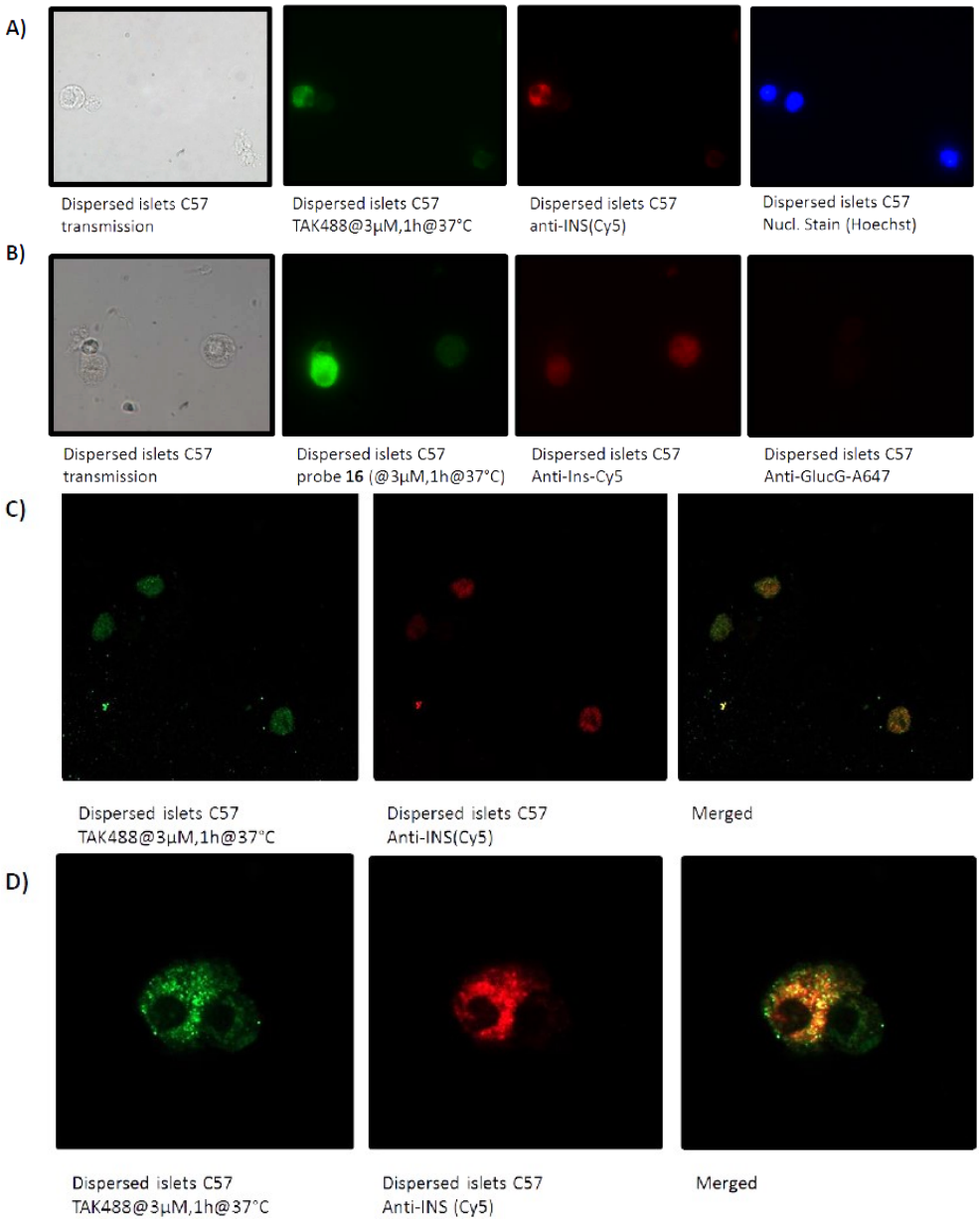

Staining of dispersed mouse islets. Dispersed islets of C57 mice, stained with anti-INS (labelled with Cy5) and compound **16** (Alexa488). A with Hoechst control for detection of nuclei, B with glucagon staining as control against alpha cells), C and D confocal images with merged staining of insulin and probe **16**.

Supplementary Figure S10

A) Probe **16** (1 µM) (ratio 340 nm/380) = 1.07 ± 0.01)

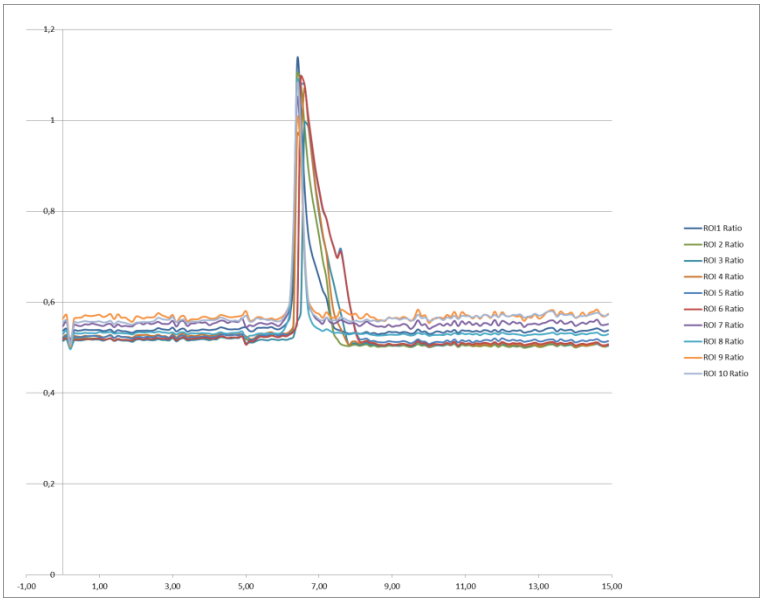

B) TAK 875 (10 nM) (ratio 340 nm/380) = 1.45 ± 0.14)

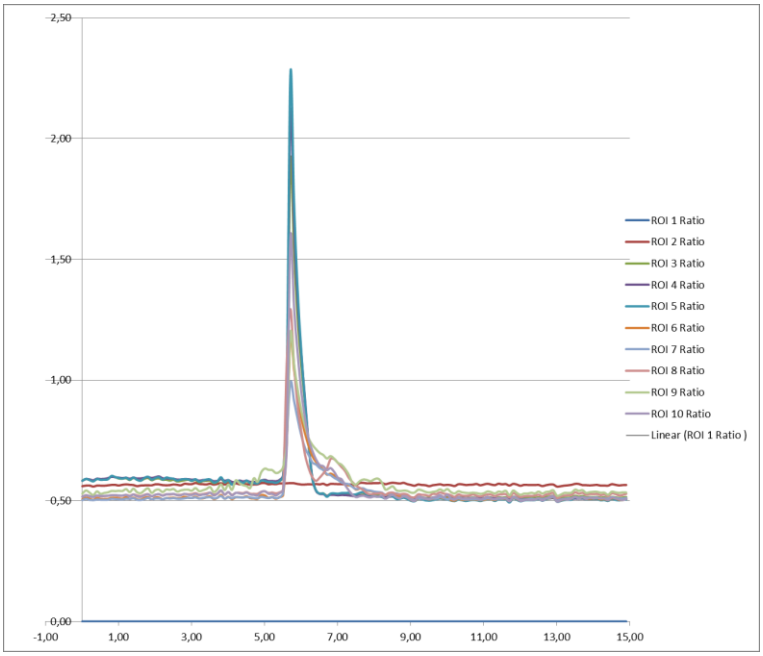

Representative calcium traces for TAK 875 and probe **16**.

Supplemental experimental procedures - chemical synthesis

General methods

Unless otherwise noted, all reagents were purchased from commercial suppliers (Sigma Aldrich, Fisher) and used without further purification. Alexa 488 and Bodipy 650 were purchased from Life Technologies as NHS ester, Fluorescein isothiocyanate (FITC), carboxyfluorescein (CF) NHS ester, carboxytetramethylrhodamine (TAMRA) NHS ester and Coumarin 343 were purchased from Sigma Aldrich, Cy5.5 NHS ester was purchased from InterChim. Boc-NH-PEG_{63}-NHS ester was purchased from Rapp Polymer GmbH. N_3-PEG_4-NHS ester and N_3-PEG_8-NHS ester were purchased from Iris Biotech GmbH. All solvents used were of HPLC grade. Microwave assisted reactions were performed with a Biotage Initiator device. Reactions were monitored by LC-MS or by thin-layer chromatography on Merck 50x100 mm silica gel 60 aluminum sheets with fluorescent indicator. LC-MS data were acquired using the HP-Agilent 1100 MSD system with a Phenomenex Luna column Luna (C-18, 100 Å pore size, 3 µm particle size, 10x2.0 mm) (METHOD 1: 0 min - 93%H_2O (0.05%TFA) to 1.2min - 95%ACN; 95%ACN until 1.4min; 7%ACN 1.50min; flow: 1 1ml/min; MS: 110-1000MW. METHOD 2: 0 min 80%H_2O (0.05%TFA) to 0.8min-95%ACN; 95%ACN until 1.4min; 20%ACN 1.45min; flow: 1.1ml/min; MS: 110-1000MW). Final fluorescent probes were analyzed with a LC-MS Agilent Technologies 1200 Series system equipped with a Waters Xbridge (C-18, 130 Å pore size, 2.5 µm particle size, 50x2.1 mm) (METHOD 3: 0 min 85%H2O(0.05%TFA) to 6 min-95%ACN; 8.5 min 95%ACN; 10 min 15 %ACN; flow: 0.6 ml/min; MS: 400-1500MW). Silica-gel column chromatography was carried out on a CombiFlash Rf - Isco Teledyne. Reverse-phase preparative HPLC was performed on the HP-Agilent 1100 with either a column from Agilent Zorbax Rx C-18 250x9.4mm, 5 µm (4 mL/min) or with a column from Waters Xbridge OBD C-18-250x19mm, 5 µm (16 mL/min) (Gradient: 0 min – 5 min 25% ACN/H_2O(0.1%TFA) to 30 min - 95%ACN; 95%ACN until 35 min). ^1H and ^{13}C NMR spectra were recorded on a Bruker DRX-400 or 600 systems in d_6-DMSO or $CDCl_3$. Chemical shifts are given in parts per million (ppm) with tetramethylsilane as an internal standard. Abbreviations are used as follows: s = singlet, d = doublet, t = triplet, q = quartet, p = pentet, m = multiplet, dd = doublets of doublet, br = broad. Coupling constants (*J* values) are given in hertz (Hz). Absorption and Emission spectra were acquired with a Thermo Varioskan using the SkanIt 2.4.3 software.

Abbreviations

ACN = acetonitrile
ADDP = 1,1'-(azodicarbonyl)dipiperidine
Boc = *tert*-butyloxycarbonyl
DCM = dichloromethane
DIEA = diisopropylethyl amine
DMF = dimethylformamide
ESI-TOF = electrospray ionization mass spectrometry – time of flight
EtOAc = ethylacetate
HATU = 2-(7-Aza-1H-benzotriazole-1-yl)-1,1,3,3-tetramethyluronium hexafluorophosphate
Hept = heptane
HPLC = high performance liquid chromatography
HRMS = high resolution mass spectrometry
LC-MS = liquid chromatography - mass spectrometry
MeOH = methanol

NMR = nuclear magnetic resonance
TBAF = Tetra-*n*-butylammonium fluoride
TFA = trifluoroacetic acid
THF = tetrahydrofuran
TIS = triisopropylsilane
TLC = thin layer chromatography
TBDMS-Cl = tert-butyldimethylsilyl chloride

Supplemental experimental procedure Figure 1 – molecules measured by FLIPR Ca^{2+} assay

Synthesis of compound **1**

Compound **12** methyl 2-[(3S)-6-[[3-(4-hydroxy-2,6-dimethyl-phenyl)phenyl]methoxy]-2,3-dihydrobenzofuran-3-yl]acetate was dissolved in 80 µL of THF and 40 µL of MeOH before 80 µL of 1N aqueous NaOH (800 µmol) were added. The mixture was allowed to stir at 50°C for 45 minutes. The mixture was then concentrated, diluted with water, acidified with 1M HCl aqueous solution and extracted with EtOAc. The organic layer was washed with brine and evaporated under reduced pressure. The crude was purified via silica gel chromatography (0-65% EtOAc/Hept) to afford desired product **1** 2-[(3S)-6-[[3-(4-hydroxy-2,6-dimethyl-phenyl)phenyl]methoxy]-2,3-dihydrobenzofuran-3-yl]acetic acid as a white powder (m = 44 mg, 109 µmol, yield 73%).
^{1}H NMR (600 MHz, $CDCl_3$) δ: 1.94 (s, 6H), 2.61 (dd, 1H, J = 16.6, 9.0 Hz), 2.82 (dd, 1H, J = 16.6, 5.6 Hz), 3.79 (m, 1H, 9.1, 9.0, 6.4, 5.6 Hz), 4.28 (dd, 1H, J = 9.1, 6.4 Hz), 4.74 (t, 1H, J = 9.1 Hz), 5.05 (s, 2H), 6.45 (s, 1H), 6.48 (d, 1H, J_{ortho} = 8.0 Hz), 6.58 (s, 2 H), 7.01 (d, 1H, J_{ortho} = 8.0 Hz), 7.06 (d, 1H, J_{ortho} = 7.5 Hz), 7.15 (s, 1H), 7.38 (d, 1H, J_{ortho} = 7.5 Hz), 7.42 (t, 1H, J_{ortho} = 7.5 Hz).
^{13}C NMR (150 MHz, $CDCl_3$) δ: 20.9, 37.5, 39.1, 70.3, 97.5, 107.4, 114.2, 121.2, 124.3, 125.5, 128.6, 128.7, 129.3, 134.4, 137.1, 137.7, 141.0, 154.2, 160.4, 161.1, 175.9
Retention time R_t = 0.93 min (METHOD 1)
HRMS (ESI-TOF) m/z: $[M-H]^-$: Calcd for $C_{25}H_{23}O_5$: 403.1551; Found: 403.1586

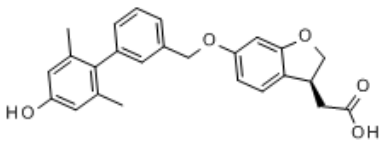

Synthesis of compound **2** methyl ester

Compound **12** methyl 2-[(3S)-6-[[3-(4-hydroxy-2,6-dimethyl-phenyl)phenyl]methoxy]-2,3-dihydrobenzofuran-3-yl]acetate (250 mg, 597 µmol), propargyl bromide - 80% in toluene (650 µL, 5.97 mmol), potassium carbonate (115 mg, 836 µmol) and potassium iodide (19.8 mg, 0.2 eq) were dissolved in 10 mL of DMF, and the mixture was allowed to stir under argon at 60°C for 24 hours. The volatiles were removed under reduced pressure and the crude was purified through silica gel chromatography (0-20% EtOAc-Hept) to afford methyl 2-[(3S)-6-[[3-(2,6-dimethyl-4-prop-2-ynoxy-phenyl)phenyl]methoxy]-2,3-dihydrobenzofuran-3-yl]acetate as a colorless oil (m = 241 mg, 528 µmol, yield 88%).

^{1}H NMR (600 MHz, $CDCl_3$) δ: 2.01 (s, 6H), 2.55 (t, 1H, J = 2,0 Hz), 2.57 (dd, 1H, J = 16.6,9.2 Hz), 2.74 (dd, 1H, J = 16.6, 5.4 Hz), 3.73 (s, 3H), 3.81 (m, 1H, 9.2, 9.1, 6.2, 5.4 Hz), 4.27 (dd, 1H, J = 9.1, 6.2 Hz), 4.71 (d, 2H, J = 2.0 Hz), 4.76 (t, 1H, J = 9.1 Hz), 5.07 (s, 2H), 6.47 (d, 1H, J_{meta} = 2.0 Hz), 6.48 (dd, 1H, J_{ortho} = 8.2 Hz, J_{meta} = 2.2 Hz), 6.74 (s, 2 H), 7.02 (d, 1H, J_{ortho} = 8.2 Hz), 7.08 (d, 1H, J_{ortho} = 7.5 Hz), 7.18 (s, 1H), 7.38 (d, 1H, J_{ortho} = 7.5 Hz), 7.43 (t, 1H, J_{ortho} = 7.5 Hz).
^{13}C NMR (150 MHz, $CDCl_3$) δ: 21.2, 37.8, 39.5, 51.8, 55.7, 70.3, 75.4, 78.8, 97.5, 107.3, 113.5, 121.5, 124.3, 125.6, 128.58, 128.65, 129.1, 135.1, 137.1, 137.6, 140.9, 156.3, 159.9, 161.1, 172.3
Retention time R_t = 0.90 min (METHOD 2)
HRMS (ESI-TOF) m/z: $[M-H]^-$: Calcd for $C_{29}H_{27}O_5$: 455.1864; Found: 455.1918

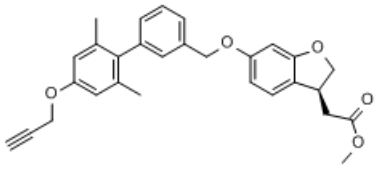

Synthesis of compound **2**

Methyl 2-[(3S)-6-[[3-(2,6-dimethyl-4-prop-2-ynoxy-phenyl)phenyl]methoxy]-2,3-dihydrobenzofuran-3-yl]acetate (220 mg, 472 µmol) synthesized previously was dissolved in 1.9 mL of THF and 950 µL of MeOH before 965 µL of 1N aqueous NaOH (965 µmol) were added. The mixture was allowed to stir at room temperature for 30 minutes. The mixture was concentrated, diluted with water, acidified with 1M HCl aqueous solution and extracted with EtOAc. The organic layer was washed with brine and evaporated under reduced pressure to afford compound **2** 2-[(3S)-6-[[3-(2,6-dimethyl-4-prop-2-ynoxy-phenyl)phenyl]methoxy]-2,3-dihydrobenzofuran-3-yl]acetic acid as a white powder (m = 201 mg, 454 µmol, yield 96%).
^{1}H NMR (600 MHz, $CDCl_3$) δ: 2.02 (s, 6H), 2.55 (t, 1H, J = 2,4 Hz), 2.63 (dd, 1H, J = 16.8, 9.2 Hz), 2.82 (dd, 1H, J = 16.8, 5.4 Hz), 3.83 (m, 1H, 9.2, 9.1, 6.2, 5.4 Hz), 4.30 (dd, 1H, J = 9.1, 6.2 Hz), 4.72 (d, 2H, J = 2.4 Hz), 4.78 (t, 1H, J = 9.1 Hz), 5.08 (s, 2H), 6.48 (d, 1H, J_{meta} = 2.2 Hz), 6.52 (dd, 1H, J_{ortho} = 8.2 Hz, J_{meta} = 2.2 Hz), 6.75 (s, 2 H), 7.06 (d, 1H, J_{ortho} = 8.2 Hz), 7.10 (d, 1H, J_{ortho} = 7.5 Hz), 7.19 (s, 1H), 7.39 (d, 1H, J_{ortho} = 7.5 Hz), 7.42 (t, 1H, J_{ortho} = 7.5 Hz).
^{13}C NMR (150 MHz, $CDCl_3$) δ: 20.6, 37.1, 38.7, 55.2, 69.9, 74.8, 78.4, 97.1, 107.0, 113.1, 120.7, 123.8, 125.1, 128.08, 128.14, 128.7, 134.6, 136.6, 137.0, 140.5, 155.9, 159.6, 160.6, 176.1
Retention time R_t = 0.83 min (METHOD 2)
HRMS (ESI-TOF) m/z: $[M-H]^-$: Calcd for $C_{28}H_{25}O_5$: 441.1707; Found: 441.1738

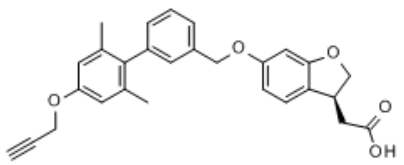

Synthesis of compound **3** methyl ester

Compound **12** methyl 2-[(3S)-6-[[3-(4-hydroxy-2,6-dimethyl-phenyl)phenyl]methoxy]-2,3-dihydrobenzofuran-3-yl]acetate (762 mg, 1.82 mmol) and cesium carbonate (705 mg, 2.16 mmol) were dissolved in 9 mL of ACN under argon. Allyl bromide (740 µL, 8.42 mmol) was added to the solution and the mixture was allowed to stir under microwave heating (40 min, 110°C microwave

assisted, 30 sec. pre-stirring). Insolubles were removed by filtration and the mixture was evaporated under reduced pressure. The crude was then diluted in Et_2O and filtered again to remove the last traces of cesium carbonate and evaporated to afford methyl 2-[(3S)-6-[[3-(4-allyloxy-2,6-dimethyl-phenyl)phenyl]methoxy]-2,3-dihydrobenzofuran-3-yl]acetate as a yellowish oil (m = 765 mg, 1.67 mmol, yield 92 %).

^{1}H NMR (500 MHz, $CDCl_3$) δ: 1.99 (s, 6H), 2.55 (dd, 1H, J = 16.6, 9.0 Hz), 2.75 (dd, 1H, J = 16.6, 5.6 Hz), 3.71 (s, 3H), 3.79 (m, 1H, 9.4, 9.0, 6.1, 5.6 Hz), 4.25 (dd, 1H, J = 9.4, 6.1 Hz), 4.54 (dd, 2H, J = 5.2 Hz), 4.74 (t, 1H, J = 9.0 Hz), 5.05 (s, 2H), 5.28 (dd, 1H, J_{cis} = 10.4 Hz and J_{gem} = 1.4 Hz), 5.41 (dd, 1H, J_{trans} = 17.3 Hz and J_{gem} = 1.4 Hz), 6.07 (ddd, 1H, J_{trans} = 17.3, J_{cis} = 10.4, J = 5.2 Hz), 6.46 (d, 1H, J_{meta} = 2.2 Hz), 6.49 (dd, 1H, J_{ortho} = 8.2 Hz, J_{meta} = 2.2 Hz), 6.67 (s, 2 H), 7.02 (d, 1H, J_{ortho} = 8.2 Hz), 7.09 (d, 1H, J_{ortho} = 7.4 Hz), 7.17 (s, 1H), 7.38 (d, 1H, J_{ortho} = 7.7 Hz), 7.41 (t, 1H, J_{ortho} = 7.4 Hz).

^{13}C NMR (125 MHz, $CDCl_3$) δ: 21.1, 37.8, 39.5, 51.8, 68.7, 70.3, 97.5, 107.3, 113.4, 117.5, 121.5, 124.3, 125.5, 128.6, 128.7, 129.2, 133.6, 134.4, 137.1, 137.4, 141.1, 157.4, 159.4, 161.1, 172.4

Retention time R_t = 0.99 min (METHOD 2)

HRMS (ESI-TOF) m/z: $[M-H]^-$: Calcd for $C_{29}H_{29}O_5$: 457.2020; Found: 457.2056

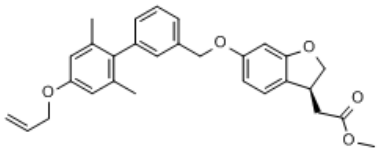

Synthesis of compound **3**

Methyl 2-[(3S)-6-[[3-(4-allyloxy-2,6-dimethyl-phenyl)phenyl]methoxy]-2,3-dihydrobenzofuran-3-yl]acetate previously synthesized (15 mg, 32.7 µmol, 1eq) was dissolved in 250 µL of THF and 100 µL of MeOH before 65 µL of 1N aqueous NaOH (65 µmol) were added. The mixture was allowed to stir at room temperature for 45 minutes.

The mixture was concentrated, diluted with water, acidified with 1M HCl aqueous solution down to pH = 2 and extracted with EtOAc three times. The organic layer was evaporated under reduced pressure to afford compound **3** 2-[(3S)-6-[[3-(4-allyloxy-2,6-dimethyl-phenyl)phenyl]methoxy]-2,3-dihydrobenzofuran-3-yl]acetic acid as a white powder (m = 11.8 mg, 26.5 µmol, yield 81%).

^{1}H NMR (600 MHz, $CDCl_3$) δ: 2.01 (s, 6H), 2.63 (dd, 1H, J = 16.8, 9.2 Hz), 2.82 (dd, 1H, J = 16.8, 5.3 Hz), 3.83 (m, 1H, 9.2, 9.0, 6.2, 5.3 Hz), 4.30 (dd, 1H, J = 9.0, 6.2 Hz), 4.56 (d, 2H, J = 5.2 Hz), 4.78 (t, 1H, J = 9.0 Hz), 5.08 (s, 2H), 5.30 (dd, 1H, J_{cis} = 10.4 Hz and J_{gem} = 1.0 Hz), 5.44 (dd, 1H, J_{trans} = 17.3 Hz and J_{gem} = 1.0 Hz), 6.10 (ddd, 1H, J_{trans} = 17.3, J_{cis} = 10.4, J = 5.2 Hz), 6.48 (s, 1H), 6.52 (dd, 1H, J_{ortho} = 8.2 Hz), 6.70 (s, 2 H), 7.06 (d, 1H, J_{ortho} = 8.2 Hz), 7.10 (d, 1H, J_{ortho} = 7.4 Hz), 7.19 (s, 1H), 7.39 (d, 1H, J_{ortho} = 7.4 Hz), 7.43 (t, 1H, J_{ortho} = 7.4 Hz).

^{13}C NMR (150 MHz, $CDCl_3$) δ: 20.6, 37.1, 38.6, 68.3, 69.9, 97.1, 107.0, 113.0, 116.9, 120.7, 123.8, 125.0, 128.1, 128.2, 128.7, 133.1, 133.9, 136.6, 136.9, 140.7, 156.9, 159.6, 160.6, 175.5

Retention time R_t = 0.87 min (METHOD 2)

HRMS (ESI-TOF) m/z: $[M-H]^-$: Calcd for $C_{28}H_{27}O_5$: 443.1863; Found: 443.1935

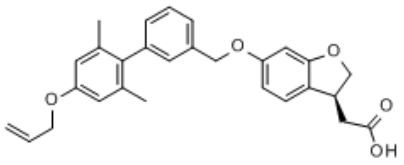

Synthesis of compound **4**

See synthesis below in section "Supplemental experimental procedure Figure 2"

Synthesis of compound **5**

Compound **4** 2-[(3S)-6-[[3-[4-(3-aminopropoxy)-2,6-dimethyl-phenyl]phenyl]methoxy]-2,3-dihydrobenzofuran-3-yl]acetic acid (2.9 mg, 6.28 µmol) was dissolved in 250 µL of DMF, before DIEA (3 µl, 17.18 µmol) and acetic anhydride (0.650 µl, 6.92 µmol) were added to the reaction mixture. The reaction was allowed to stir at room temperature for 15 minutes. Then 50 µL of a 1M NaOH aqueous solution (50 µl, 50.00 µmol) were added to the mixture. The crude was directly submitted to preparative HPLC (25% to 95% ACN/water) to afford, after lyophilization, compound **5** 2-[(3S)-6-[[3-[4-(3-acetamidopropoxy)-2,6-dimethyl-phenyl]phenyl] methoxy]-2,3-dihydrobenzofuran-3-yl]acetic acid as a lyophilized powder (m = 3.1 mg, 6.16 µmol, yield 98%).

^{1}H NMR (500 MHz, d_6-DMSO) δ: 1.81 (s, 3H), 1.84 (p, 2H, J = 6.2 Hz), 1.92 (s, 6H), 2,47 (dd, 1H, J = 16.8, 9.0 Hz), 2,68 (dd, 1H, J = 16.8, 5.6 Hz), 3.19 (q, 2H, J = 6.2 Hz), 3.68 (m, 1H), 3.98 (t, 2H, J = 6.2 Hz), 4.19 (dd, 1H, J = 9.0, 6.9 Hz), 4.68 (t, 1H, J = 9.0 Hz), 5.10 (s, 2H), 6.46 (s, 1H), 6.49 (d, 1H, J_{ortho} = 8.1 Hz), 6.69 (s, 2 H), 7.05 (d, 1H, J_{ortho} = 7.5 Hz), 7.09 (d, 1H, J_{ortho} = 8.1 Hz), 7.14 (s, 1H), 7.39 (d, 1H, J_{ortho} = 7.5 Hz), 7.45 (t, 1H, J_{ortho} = 7.5 Hz), 7.92 (s, 1H), 12.32 (s, 1H)

^{13}C NMR (125 MHz, d_6-DMSO) δ: 20.7, 22.6, 28.9, 35.5, 37.1, 64.9, 69.3, 77.1, 97.0, 107.0, 113.3, 122.0, 124.5, 125.8, 128.6, 128.8, 128.8, 133.9, 136.5, 137.4, 140.3, 157.0, 159.1, 160.7,169.1, 173.0

Retention time R_t = 0.88 min (METHOD 1)

HRMS (ESI-TOF) m/z: $[M-H]^-$: Calcd for $C_{30}H_{32}NO_6$: 502.2235; Found: 502.2295

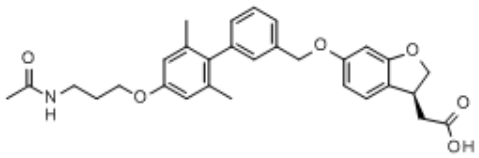

Synthesis of compound **6**

Compound **4** 2-[(3S)-6-[[3-[4-(3-aminopropoxy)-2,6-dimethyl-phenyl]phenyl]methoxy]-2,3-dihydrobenzofuran-3-yl]acetic acid previously synthesized (5.0 mg, 10.83 µmol) was dissolved in 400 µL of DMF before DIEA (5.68 µl, 32.50 µmol) was added followed by N_3-PEG_4-NHS ester (2,5-dioxopyrrolidin-1-yl 1-azido-3,6,9,12-tetraoxapentadecan-15-oate, 5 mg, 12.87 µmol). The reaction was allowed to stir at room temperature for 15 minutes. The crude was directly purified through preparative HPLC (25% to 95% ACN/water) to afford, after lyophilization, compound **6** 2-[(3S)-6-[[3-[4-[3-[3-[2-[2-[2-(2-azidoethoxy)ethoxy]ethoxy]ethoxy]propanoylamino]propoxy]-2,6-dimethyl-phenyl]phenyl] methoxy]-2,3-dihydrobenzofuran-3-yl]acetic acid as a lyophilized powder (m = 3.7 mg, 5.04 µmol, 46% yield).

^{1}H NMR (500 MHz, d_6-DMSO) δ: 1.85 (p, 2H, J = 6.2 Hz), 1.92 (s, 6H), 2.32 (t, 2H, J = 6.4 Hz), 2.48 (dd, 1H, J = 16.8, 9.0 Hz), 2,68 (dd, 1H, J = 16.5, 5.6 Hz), 3.21 (q, 2H, J = 6.0 Hz), 3.39 (t, 2H, J = 5.2 Hz), 3.48-3.62 (m, 16H, PEG), 3.68 (m, 1H), 3.98 (t, 2H, J = 6.2 Hz), 4.18 (dd, 1H, J = 9.0, 6.9 Hz), 4.68 (t, 1H,

J = 9.0 Hz), 5.10 (s, 2H), 6.46 (s, 1H), 6.49 (d, 1H, J_{ortho} = 8.0 Hz), 6.69 (s, 2 H), 7.05 (d, 1H, J_{ortho} = 7.5 Hz), 7.09 (d, 1H, J_{ortho} = 8.0 Hz), 7.14 (s, 1H), 7.39 (d, 1H, J_{ortho} = 7.5 Hz), 7.45 (t, 1H, J_{ortho} = 7.5 Hz), 7.92 (t, 1H, J = 5.4 Hz), 12.32 (s, 1H)

^{13}C NMR (125 MHz, d_6-DMSO) δ: 20.7, 28.9, 35.5, 36.2, 37.1, 49.9, 64.9, 66.9, 69.2, 69.3, 69.5, 69.7, 69.7, 69.8, 69.8, 77.1, 96.9, 106.9, 113.2, 121.9, 124.5, 125.8, 128.6, 128.8, 128.8, 133.7, 136.5, 137.4, 140.3, 157.2, 159.1, 160.7, 170.0, 173.0

Retention time R_t = 0.93 min (METHOD 1)

HRMS (ESI-TOF) m/z: $[M-H]^-$: Calcd for $C_{39}H_{49}N_4O_{10}$: 733.3454; Found: 733.3558

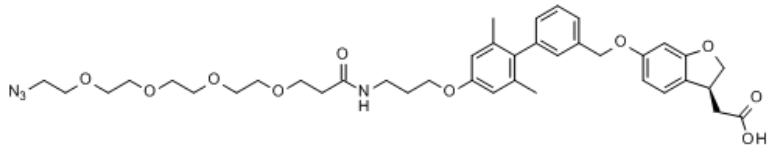

Synthesis of compound **7**

Compound **4** 2-[(3S)-6-[[3-[4-(3-aminopropoxy)-2,6-dimethyl-phenyl]phenyl]methoxy]-2,3-dihydrobenzofuran-3-yl]acetic acid previously synthesized (4.4 mg, 9.53 µmol) was dissolved in 300 µL of DMF before DIEA (5.0 µl, 28.63 µmol) was added followed by N_3-PEG_8-NHS ester (2,5-dioxopyrrolidin-1-yl 1-azido-3,6,9,12,15,18,21,24-octaoxaheptacosan-27-oate, 5.92 mg, 10.49 µmol). The reaction was allowed to stir at room temperature for 15 minutes. The crude was directly purified through preparative HPLC (25% to 95% ACN/water) to afford, after lyophilization, compound **7** 2-[(3S)-6-[[3-[4-[3-[3-[2-[2-[2-[2-[2-[2-[2-(2- azidoethoxy) ethoxy]ethoxy]ethoxy]ethoxy]ethoxy] ethoxy]ethoxy] propanoylamino]propoxy]-2,6-dimethyl-phenyl]phenyl]methoxy]-2,3-dihydrobenzofuran-3-yl]acetic acid as a lyophilized powder (m = 4.1 mg, 4.50 µmol, 47% yield).

^{1}H NMR (500 MHz, d_6-DMSO) δ: 1.85 (p, 2H, J = 6.2 Hz), 1.92 (s, 6H), 2.32 (t, 2H, J = 6.4 Hz), 2.48 (dd, 1H, J = 16.8, 9.0 Hz), 2,68 (dd, 1H, J = 16.5, 5.6 Hz), 3.21 (q, 2H, J = 6.2 Hz), 3.39 (t, 2H, J = 5.2 Hz), 3.48-3.62 (m, 32H, PEG), 3.68 (m, 1H), 3.98 (t, 2H, J = 6.2 Hz), 4.18 (dd, 1H, J = 9.0, 6.9 Hz), 4.68 (t, 1H, J = 9.0 Hz), 5.09 (s, 2H), 6.46 (s, 1H), 6.49 (d, 1H, J_{ortho} = 8.0 Hz), 6.69 (s, 2 H), 7.05 (d, 1H, J_{ortho} = 7.5 Hz), 7.09 (d, 1H, J_{ortho} = 8.0 Hz), 7.14 (s, 1H), 7.39 (d, 1H, J_{ortho} = 7.5 Hz), 7.45 (t, 1H, J_{ortho} = 7.5 Hz), 7.92 (t, 1H, J = 5.2 Hz), 12.32 (s, 1H)

^{13}C NMR (125 MHz, d_6-DMSO) δ: 20.7, 28.9, 35.5, 36.2, 37.1, 49.9, 64.9, 66.9, 69.2, 69.3, 69.5, 69.7, 69.7, 69.8, 69.8, 77.1, 96.9, 106.9, 113.2, 121.9, 124.5, 125.8, 128.6, 128.8, 128.8, 133.7, 136.5, 137.4, 140.3, 157.2, 159.1, 160.7, 170.0, 173.0

Retention time R_t = 0.92 min (METHOD 1)

HRMS (ESI-TOF) m/z: $[M-H]^-$: Calcd for $C_{47}H_{65}N_4O_{14}$: 909.4503; Found: 909.4621

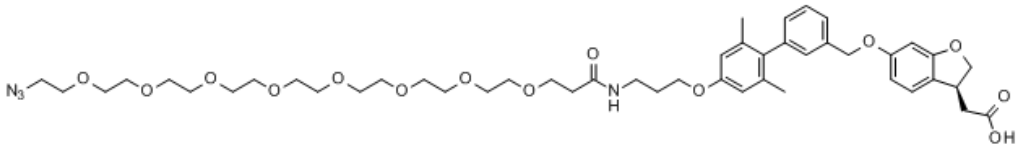

Synthesis of compound **8**

Compound **4** 2-[(3S)-6-[[3-[4-(3-aminopropoxy)-2,6-dimethyl-phenyl]phenyl]methoxy]-2,3-dihydrobenzofuran-3-yl]acetic acid previously synthesized (9.8 mg, 16.99 µmol) was dissolved in 500

µL of DMF before DIEA (6 µl, 34.35 µmol) was added followed by Boc-NH-PEG_{63}-NHS ester (55,4 mg, 15,31 µmol) (5.9 mg, 10.49 µmol). The reaction was allowed to stir at room temperature for 15 minutes, the solvent was evaporated under reduced pressure and the crude was redissolved in 1 mL of DCM. Then 250 µL of TFA/TIS/water (95:2.5:2.5) were added, and the reaction ran for 45 min. The crude was directly purified through preparative HPLC (25% to 95% ACN/water) to afford, after lyophilization, compound **8** 2-[(3S)-6-[[3-[4-[3-[3-(2-aminoethoxy)PEG-63-propanoylamino]propoxy] -2,6-dimethyl-phenyl]phenyl]methoxy]-2,3-dihydrobenzofuran-3-yl]acetic acid as a colorless oil (m = 29.7 mg, 8.94 µmol, 53% yield).

^{1}H NMR (500 MHz, d_6-DMSO) δ: 1.72 (p, 2H, J = 6.4 Hz), 1.85 (p, 2H, J = 6.4 Hz), 1.92 (s, 6H), 2.32 (t, 2H, J = 7.2 Hz), 2.48 (dd, 1H, J = 16.8, 9.0 Hz), 2,68 (dd, 1H, J = 16.5, 5.6 Hz), 2.97 (t, 2H, J = 5.2 Hz), 3.21 (q, 2H, J = 6.2 Hz), 3.36 (t, 2H, J = 6.4 Hz), 3.40-3.75 (m, PEG), 3.98 (t, 2H, J = 6.2 Hz), 4.18 (dd, 1H, J = 9.0, 6.8 Hz), 4.68 (t, 1H, J = 9.0 Hz), 5.09 (s, 2H), 6.46 (s, 1H), 6.49 (d, 1H, J_{ortho} = 8.0 Hz), 6.69 (s, 2 H), 7.05 (d, 1H, J_{ortho} = 7.5 Hz), 7.09 (d, 1H, J_{ortho} = 8.0 Hz), 7.14 (s, 1H), 7.39 (d, 1H, J_{ortho} = 7.5 Hz), 7.45 (t, 1H, J_{ortho} = 7.5 Hz), 7.86 (t, 1H, J = 5.2 Hz)

^{13}C NMR (125 MHz, d_6-DMSO) δ: 20.7, 25.4, 28.9, 32.1, 35.5, 37.1, 38.8, 64.9, 66.9, 69.3, 69.4, 69.6, 69.7, 69.8, 77.1, 96.9, 106.9, 113.2, 121.9, 124.5, 125.8, 128.6, 128.7, 133.7, 136.5, 137.4, 140.3, 157.2, 159.1, 160.7, 171.7, 173.1

Retention time R_t = 0.81 min (METHOD 1)

HRMS (ESI-TOF) m/z: No mass

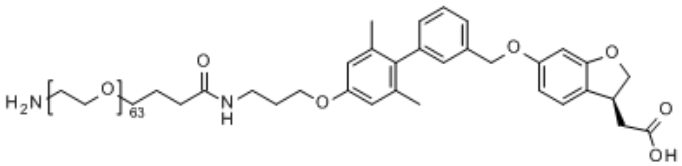

Supplemental experimental procedure Figure 2 – Syntheses of the fluorescent probes 13-19

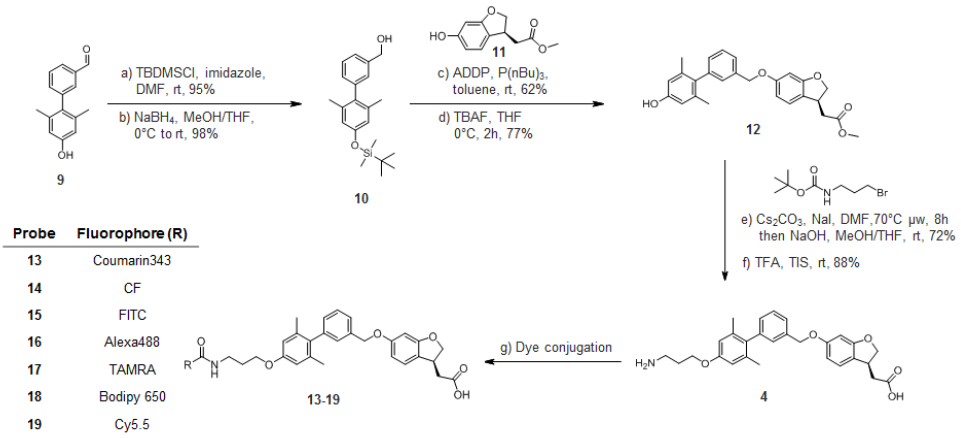

Probe	Fluorophore (R)
13	Coumarin343
14	CF
15	FITC
16	Alexa488
17	TAMRA
18	Bodipy 650
19	Cy5.5

Compound **9** and **11** were synthesized as described by Negoro et al., 2012

Synthesis of compound **10** – step (a)

Hydroxy-dimethylbiphenyl carbaldehyde **9** (5.40 g, 23.74 mmol), TBDMS-Cl (4.30 g, 28.50 mmol) and imidazole (4.85 g, 71.20 mmol) were dissolved in 35 mL of DMF. The mixture was allowed to stir at room temperature for 1 hour. The reaction was followed by LCMS and TLC (25% EtOAc/Hept). After 60 minutes of reaction, the mixture was diluted with 100 mL of EtOAc and 50 mL of brine and the organic phase was washed with brine (3 x 50 mL) and water (1 x 50 mL), before being dried over $MgSO_4$, filtered and evaporated under reduced pressure. Purification was performed via silica gel chromatography (0->5% EtOAc/Hept), affording the desired product 3-[4-[tert-butyl(dimethyl)silyl]oxy-2,6-dimethyl-phenyl]benzaldehyde as an oil (m = 7.68 g, 22.55 mmol, yield 95%).

^{1}H NMR (600 MHz, $CDCl_3$) δ: 0.23 (s, 6H), 1.00 (s, 9H), 1.96 (s, 6H), 6.60 (s, 2H), 7.41 (d, 1H, J_{ortho}= 7.6 Hz), 7.57 (t,1H, J_{ortho}= 7.6 Hz), 7.67 (s, 1H), 7.84 (d, 1H, J_{ortho}= 7.6 Hz), 10.04 (s, 1H).

^{13}C NMR (150 MHz, $CDCl_3$) δ: -4.28, 18.2, 20.9, 25.7, 118.9, 127.8, 129.1, 131.2, 133.5, 136.0, 136.7, 137.1, 142.2, 154.7, 192.4

Retention time Rt = 1.08 min (METHOD 2)

HRMS (ESI-TOF) m/z: $[M-H]^-$: Calcd for $C_{21}H_{27}O_2Si$: 339.1786; Found: 339.2366

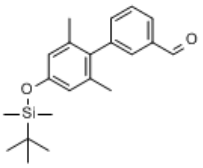

Synthesis of compound **10** – step (b)

3-[4-[tert-butyl(dimethyl)silyl]oxy-2,6-dimethyl-phenyl]benzaldehyde synthesized in the previous step (7.68 g, 22.55 mmol) was dissolved in MeOH(15 mL)/THF(30 mL) at 0°C, and sodium borohydride $NaBH_4$ (0.98 g, 25.93 mmol) was added. The mixture was allowed to stir under argon at 0°C for 1h30. Volatiles were evaporated and the mixture was diluted with a pH=5 water solution (50 mL) and EtOAc (100 mL). The organic phase was washed successively with brine (50 mL) and water (50 mL), dried over $MgSO_4$ and concentrated to give the desired product **10** [3-[4-[tert-butyl(dimethyl)silyl]oxy-2,6-dimethyl-phenyl]phenyl]methanol as a white powder (m = 7.69 g, 22.44 mmol, quant.)

^{1}H NMR (600 MHz, $CDCl_3$) δ: 0.26 (s, 6H), 1.03 (s, 9H), 1.99 (s, 6H), 4.75 (s, 2H), 6.60 (s, 2H), 7.08 (d, 1H, J_{ortho}= 7.6 Hz), 7.15 (s, 1H), 7.35 (d, 1H, J_{ortho}= 7.6 Hz), 7.42 (t, 1H, J_{ortho}= 7.6 Hz).

^{13}C NMR (150 MHz, $CDCl_3$) δ: -4.28, 18.2, 21.0, 25.8, 65.5, 118.6, 125.1, 128.2, 128.6, 129.1, 134.8, 137.1, 140.9, 141.5, 154.3

Retention time R_t = 0.98 min (METHOD 2)

HRMS (ESI-TOF) m/z: $[M-H]^-$: Calcd for $C_{21}H_{29}O_2Si$: 341.1942; Found: 341.2454

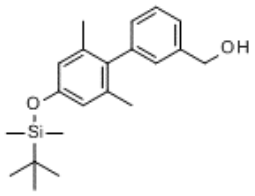

Synthesis of compound **12 –** step (c)

Compound **10** [3-[4-[tert-butyl(dimethyl)silyl]oxy-2,6-dimethyl-phenyl]phenyl]methanol (3 g, 8.32 mmol, 1eq), (S)-methyl-(6-hydroxy-2,3-dihydrobenzofuran-3-yl)acetate **11** (1.77 g, 8.32 mmol) and tributylphosphine $P(nBu)_3$ (3 mL, 11.55 mmol) were dissolved in 150 mL of toluene before a solution of 1,1'-(azodicarbonyl)dipiperidine ADDP (3 g, 11.55 mmol, dissolved in 50 mL of toluene) was added dropwise during 20 minutes under argon. The mixture was then put in an ultrasound bath for 10 minutes at room temperature. The reaction was followed by LCMS which showed appearance of the desired mass and TLC (25% EtOAc/Hept) which indicated total consumption of the phenol starting material. Then 100 mL of hexane were added and the insoluble material was removed by filtration. The filtrate was concentrated and the residue was purified through silica gel chromatography (0->15% EtOAc-Hept) to afford the desired product methyl 2-[(3S)-6-[[3-[4-[tert-butyl(dimethyl)silyl]oxy-2,6-dimethyl-phenyl]phenyl]methoxy]-2,3-dihydrobenzofuran-3-yl]acetate as a pale oil (m= 2.75 g, 5.16 mmol, yield 62%)

^{1}H NMR (600 MHz, $CDCl_3$) δ: 0.22 (s, 6H), 1.00 (s, 9H), 1.95 (s, 6H), 2.55 (dd, 1H, J = 16.5, 9.0 Hz), 2.75 (dd, 1H, J = 16.5, 5.6 Hz), 3.71 (s, 3H), 3.79 (m, 1H, J = 9.1, 9.0, 6.4, 5.6 Hz), 4.25 (dd, 1H, J = 9.1, 6.4 Hz), 4.75 (t, 1H, J = 9.1 Hz), 5.05 (s, 2H), 6.45 (d, 1H, J_{meta} = 2.0 Hz), 6.49 (dd, 1H, J_{ortho} = 8.2 Hz, J_{meta} = 2.0 Hz), 6.58 (s, 2H), 7.00 (d, 1H, J_{ortho} = 8.2 Hz), 7.08 (d, 1H, J_{ortho} = 7.5 Hz), 7.17 (s, 1H), 7.35 (d, 1H, J_{ortho} = 7.5 Hz), 7.40 (t, 1H, J_{ortho} = 7.5 Hz).

^{13}C NMR (150 MHz, $CDCl_3$) δ: -4.28, 18.2, 21.0, 25.8, 37.8, 39.5, 51.8, 70.4, 97.5, 107.4, 118.6, 121.5,

124.3, 125.5, 128.6, 128.7, 129.3, 134.7, 137.1, 137.2, 141.4, 154.3, 160.0, 161.2, 172.
Retention time R_t = 1.18 min (METHOD 2)
HRMS (ESI-TOF) m/z: $[M-H]^-$: Calcd for $C_{32}H_{39}O_5Si$: 531.25722; Found: 531.2634

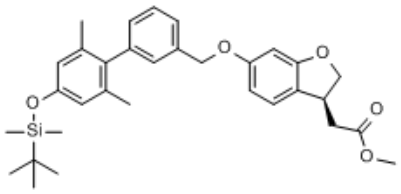

Synthesis of compound **12 –** step (d)
Methyl 2-[(3S)-6-[[3-[4-[tert-butyl(dimethyl)silyl]oxy-2,6-dimethyl-phenyl]phenyl]methoxy]-2,3-dihydrobenzofuran-3-yl]acetate synthesized in the previous step (2.5 g, 4.55 mmol, 1eq) was dissolved in 20 mL of THF and the solution was cooled to 0°C before TBAF (5.5 mL, 5.5 mmol, 1M solution in THF) was added. The mixture was allowed to stir at 0°C for 1 hour. Solvent was removed by evaporation under reduced pressure. Purification was performed through silica gel chromatography (0-40% EtOAc-Hept) to afford desired product **12** methyl 2-[(3S)-6-[[3-(4-hydroxy-2,6-dimethyl-phenyl)phenyl]methoxy]-2,3-dihydrobenzofuran-3-yl]acetate as a white powder (m = 1.47g, 3.51 mmol, yield 77%)
^{1}H NMR (600 MHz, $CDCl_3$) δ: 1.96 (s, 6H), 2.55 (dd, 1H, J = 16.6, 9.0 Hz), 2.75 (dd, 1H, J = 16.6, 5.6 Hz), 3.71 (s, 3H), 3.79 (m, 1H, 9.1, 9.0, 6.4, 5.6 Hz), 4.25 (dd, 1H, J = 9.1, 6.4 Hz), 4.75 (t, 1H, J = 9.1 Hz), 5.05 (s, 2H), 6.45 (d, 1H, J_{meta} = 2.0 Hz), 6.48 (dd, 1H, J_{ortho} = 8.2 Hz, J_{meta} = 2.0 Hz), 6.58 (s, 2 H), 7.01 (d, 1H, J_{ortho} = 8.2 Hz), 7.06 (d, 1H, J_{ortho} = 7.5 Hz), 7.15 (s, 1H), 7.36 (d, 1H, J_{ortho} = 7.5 Hz), 7.41 (t, 1H, J_{ortho} = 7.5 Hz).
^{13}C NMR (150 MHz, $CDCl_3$) δ: 20.4, 37.3, 39.0, 51.3, 69.9, 97.0, 106.9, 113.5, 121.0, 123.8, 125.0, 128.1, 128.2, 128.8, 133.8, 136.6, 137.2, 140.5, 153.8, 159.5, 160.6, 171.9
Retention time R_t = 0.78 min (METHOD 2)
HRMS (ESI-TOF) m/z: $[M-H]^-$: Calcd for $C_{26}H_{25}O_5$: 417.1707; Found: 417.1750

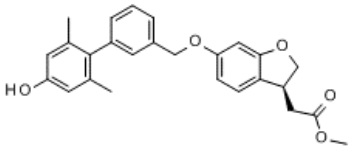

Synthesis of compound **4** – step (e)
Compound **12** (250 mg, 597.4 µmol), tert-butyl (3-bromopropyl)carbamate (223 mg, 936.5 µmol), potassium carbonate (99.1 mg, 716.9 µmol) and sodium iodide (17.9 mg, 119.5 µmol) were dissolved in 3 mL of DMF under argon. The reaction mixture was microwaved at 70°C for 8 hours. Then, another 1,5 equivalent of bromide and 1,1 equivalent of potassium carbonate were added to the

reaction mixture, and a second run of microwave heating (1 hours, 70°C) was needed to reach completion of reaction. The reaction was diluted with 10 mL of brine and 20 mL of EtOAc. The organic phase was then washed with brine (3 x 15 mL) and then with 5% NH_4Cl solution (2 x 15 mL), dried over sodium sulfate, filtered, and evaporated under reduced pressure.
The crude was then dissolved in 2 mL of THF and 0,6 mL of methanol before 800 µL of a 2,5M sodium hydroxide aqueous solution (2 mmol) were added. The mixture was allowed to stir at room temperature for 30 minutes.
The mixture was concentrated under reduced pressure, diluted with 15 mL of water, acidified with 1 HCl until pH = 2 and extracted with DCM (3 x 15 mL). The organic phase was then dried over sodium sulfate, filtered and evaporated under reduced pressure before being purified via silica gel chromatography (0-10% MeOH/DCM) to afford 2-[(3S)-6-[[3-[4-[3-(tert-butoxycarbonylamino)propoxy]-2,6-dimethyl-phenyl]phenyl]methoxy]-2,3-dihydrobenzofuran-3-yl]acetic acid as a pale yellow oil (m = 241 mg, 429.1 µmol, 72% yield).
^{1}H NMR (600 MHz, d_6-DMSO) δ: 1.37 (s, 9H), 1.81 (quint, 2H, J = 6.5 Hz), 1.90 (s, 6H), 2.46 (dd, 1H, J = 16.6, 8.9 Hz), 2.68 (dd, 1 H, J = 16.6, 5.6 Hz), 3.08 (q, 2 H, J = 6.5 Hz), 3.66 (m, 1 H, J = 9.1, 8.9, 6.6, 5.6 Hz), 3. 95 (t, 2 H, J = 6.5 Hz), 4.17 (dd, 1 H, J = 9.1, 6.6 Hz), 4.66 (t, 1 H, J = 9.1 Hz), 5.08 (s, 2 H), 6.44 (d, 1H, J_{meta} = 2.1 Hz), 6.46 (dd, 1H, J_{ortho} =8.2 Hz, J_{meta} = 2.1 Hz), 6.66 (s, 2 H), 6.87 (t, 1H, J = 6.5 Hz), 7.04 (d, 1H, J_{ortho} = 7.5 Hz), 7.08 (d, 1H, J_{ortho} = 8.2 Hz), 7.12 (s, 1H), 7.36 (d, 1H, J_{ortho} = 7.5 Hz), 7.43 (t, 1H, J_{ortho} = 7.5 Hz).
^{13}C NMR (150 MHz, d_6-DMSO) δ: 20.7, 28.2, 29.3, 37.0, 37.1, 65.0, 69.3, 77.1, 77.5, 96.9, 107.0, 113.2, 121.9, 124.5, 125.8, 128.5, 128.5, 128.7, 133.6, 136.5, 137.3, 140.3, 155.6, 157.2, 159.0, 160.6, 173.0
Retention time R_t = 0.75 min (METHOD 2)
HRMS (ESI-TOF) m/z: $[M-H]^-$: Calcd for $C_{33}H_{38}NO_7$: 560.2654; Found: 560.2760

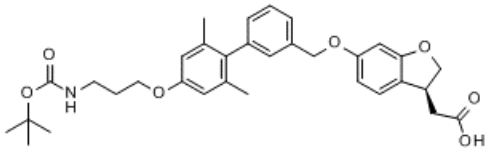

Synthesis of **4** – step (f)
2-[(3S)-6-[[3-[4-[3-(tert-butoxycarbonylamino)propoxy]-2,6-dimethyl-phenyl]phenyl]methoxy]-2,3-dihydrobenzofuran-3-yl]acetic acid synthesized in the previous step (120 mg, 213,7 µmol) was dissolved in 2,5 mL of dichloromethane before TFA (500 µl, 6.5 mmol) + 1% triisopropylsilane (25 µl, 213,65 µmol) were added. The mixture was allowed to stir at room temperature for 10 minutes. The reaction mixture was diluted with 3 mL of water. The organic phase was washed with brine (3 x 3 mL). During the last washing step with brine, product precipitated as a slightly brown solid. It was filtered, redissolved in a mixture of acetonitrile and water, and lyophilized to afford desired product **4** 2-[(3S)-6-[[3-[4-(3-aminopropoxy)-2,6-dimethyl-phenyl]phenyl]methoxy]-2,3-dihydrobenzofuran-3-yl]acetic acid as an off-white lyophilized powder (m = 86.6 mg, 187.6 µmol, 88 % yield).
^{1}H NMR (400 MHz, d_6-DMSO) δ: 1.91 (s, 6H), 2.04 (dd, 2H, J = 7.5, 6.2 Hz), 2.46 (dd, 1H, J = 16.4, 9.0 Hz), 2.70 (dd, 1 H, J = 16.4, 5.6 Hz), 2.94 (t, 2 H, J = 7.5 Hz), 3.67 (m, 1 H, 9.1, 9.0, 6.8, 5.6), 4.07 (t, 2 H, J = 6.2 Hz), 4.18 (dd, 1 H, J = 9.1, 6.8 Hz), 4.67 (t, 1H, J = 9.1 Hz), 5.09 (s, 2 H), 6.44 (d, 1H, J_{meta} = 2.3 Hz), 6.46 (dd, 1H, J_{ortho} = 8.0, J_{meta} = 2.3 Hz), 6.71 (s, 2H), 7.04 (d, 1H, J_{ortho} = 7.7 Hz), 7.10 (d, 1H, J_{ortho} =

8.0 Hz), 7.12 (s, 1H), 7.38 (d, 1H, J_{ortho} = 7.7 Hz), 7.44 (t, 1H, J_{ortho} = 7.7 Hz), 8.21 (s, 3H), 12.36 (s, 1H)
^{13}C NMR (150 MHz, d_6-DMSO) δ: 20.7, 26.9, 37.2, 37.1, 64.5, 69.4, 77.1, 97.0, 107.0, 113.3, 122.0, 124.5, 125.8, 128.5, 128.5, 128.7, 133.9, 136.5, 137.4, 140.3, 157.0, 159.1, 160.7, 173.0
Retention time R_t = 0.52 min (METHOD 2)
HRMS (ESI-TOF) m/z: $[M-H]^-$: Calcd for $C_{28}H_{30}NO_5$: 460.2129; Found: 460.2131

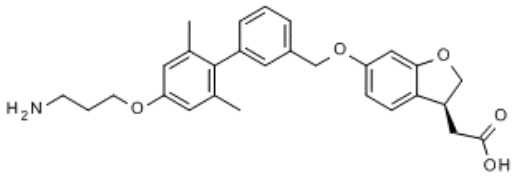

Synthesis of probe **13** (TAK-Coumarin343)
Coumarin 343 (5.2 mg, 18.2 µmol), HATU (6.9 mg, 18.2 µmol) and DIEA (8.4 µL, 48.3 µmol) were dissolved in 200 µL of DMF and 200 µL of DCM in a small Eppendorf vial protected from light with aluminum foil, and were mixed for 5 minutes at room temperature before the addition of compound **4** (8.1 mg, 16.3 µmol). The reaction mixture was allowed to stir for one hour. The crude was directly purified by preparative HPLC (25->95% ACN) to afford, after lyophilization, the desired product **13** TAK-Coumarin343 conjugate as a yellow powder (m = 1.7 mg, 2.3 µmol, yield 14%).
Retention time R_t = 5.172 min (METHOD 3)
HRMS (ESI-TOF) m/z: $[M-H]^-$: Calcd for $C_{44}H_{43}N_2O_8$: 727.3025; Found: 727.3092
Max Abs/Em 438/482 nm

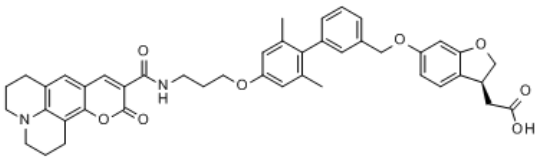

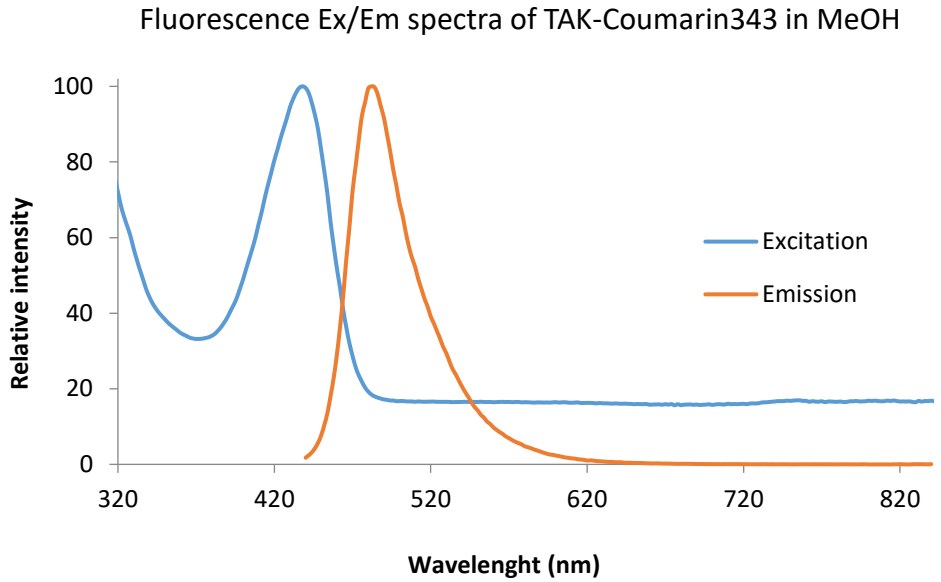

Data File	C:\Daten\2015\NOVEMBER\16NOV0001124.D	Sample Name	RBE-138 TAK-Coumarin		
Injection Date	26-Nov-2015 19:11:26	Vial	5	Replicate	1
LCMS Method	XBR_SHORT_15_95.M	Sequence Line	7	Injection Volume	2
0 min 85%H2O(0.05%TFA) 6 min-95%ACN; 8.5 min 95%ACN; 10 min 15 %ACN; 0.6 ml/min; 400-1500MW; 2 µL; 50X2.1; 2.5µ; XBridge OST C18; Autosampler					
Sample Info	729				

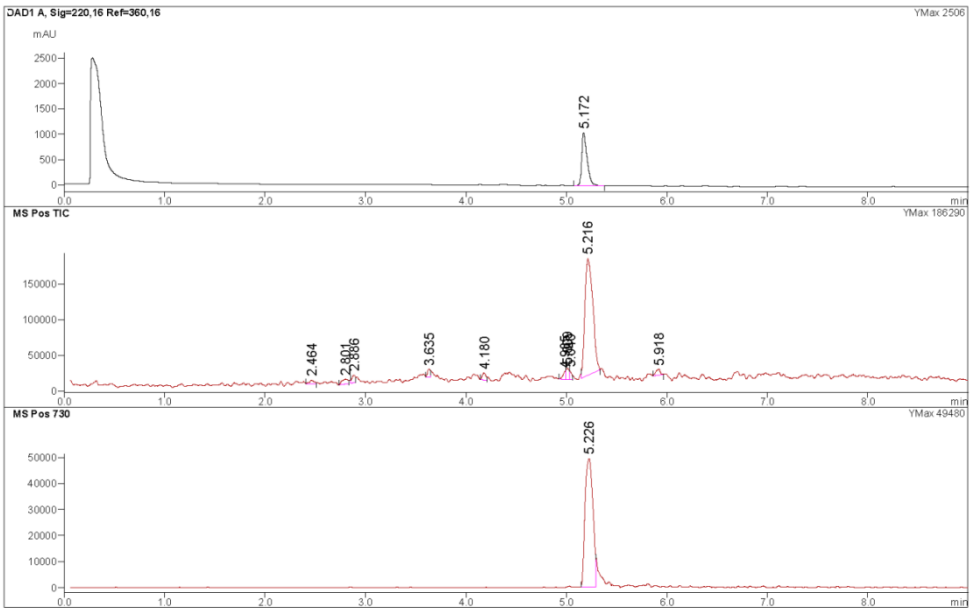

Data File	C:\Daten\2015\NOVEMBER\16NOV0001124.D	Sample Name	RBE-138 TAK-Coumarin		
Injection Date	26-Nov-2015 19:11:26	Vial	5	Replicate	1
LCMS Method	XBR_SHORT_15_95.M	Sequence Line	7	Injection Volume	2
0 min 85%H2O(0.05%TFA) 6 min-95%ACN; 8.5 min 95%ACN; 10 min 15 %ACN; 0.6 ml/min; 400-1500MW; 2 µL; 50X2.1; 2.5µ; XBridge OST C18; Autosampler					
Sample Info	729				

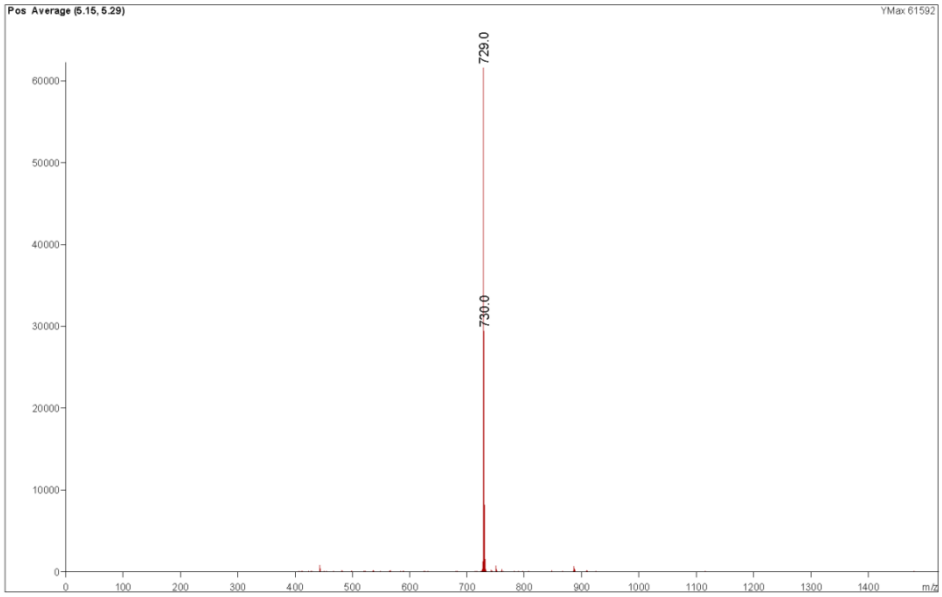

Synthesis of probe **14** (TAK-CF)

Compound **4** (6.5 mg, 13.1 µmol) was dissolved in 500 µL of DMF in a small Eppendorf vial protected from light with aluminum foil, followed by DIEA (9.1 µL, 52.2 µmol) and carboxyfluorescein NHS ester (5.1 mg, 10.7 µmol). The reaction was allowed to stir for 30 minutes at room temperature, in the dark. The crude was directly purified through preparative HPLC (25->95% ACN) to afford, after lyophilization, the desired product **14** TAK-CF conjugate as a yellow powder (m = 4.7 mg, 5.7 µmol, yield 53%).

Retention time R_t = 4.099 min (METHOD 3)

HRMS (ESI-TOF) m/z: $[M-H]^-$: Calcd for $C_{49}H_{40}NO_{11}$: 818.2607; Found: 818.2663

Max Abs/Em 496/520 nm

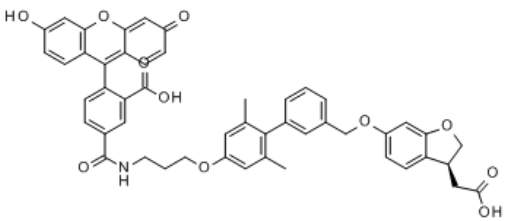

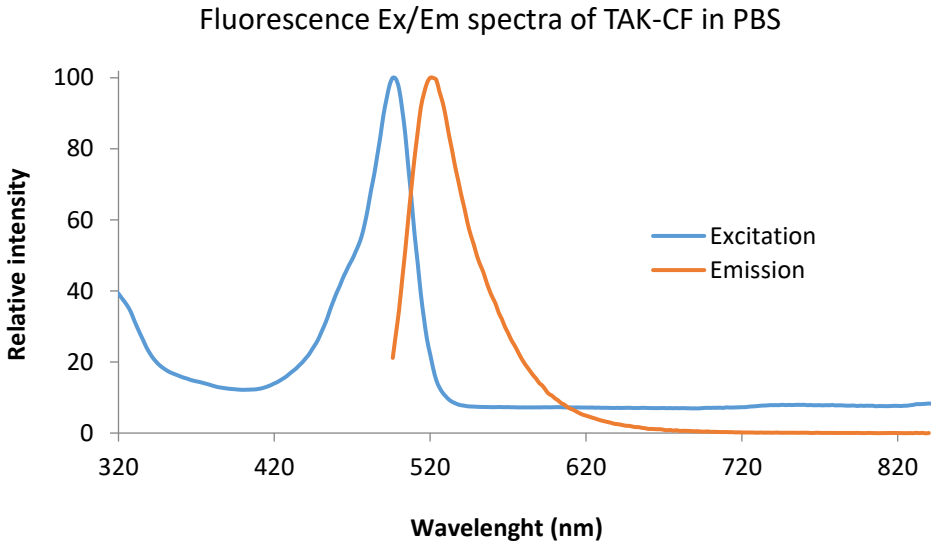

Data File	C:\Daten\2015\NOVEMBER\16NOV0001199.D	Sample Name	RBE-249- TAK-CF		
Injection Date	27-Nov-2015 17:09:28	Vial	13	Replicate	1
LCMS Method	XBR_SHORT_15_95.M	Sequence Line	1	Injection Volume	2
0 min 85%H2O(0.05%TFA) 6 min-95%ACN; 8.5 min 95%ACN; 10 min 15 %ACN; 0.6 ml/min; 400-1500MW; 2 µL; 50X2.1; 2.5µ; XBridge OST C18; Autosampler					
Sample Info	819				

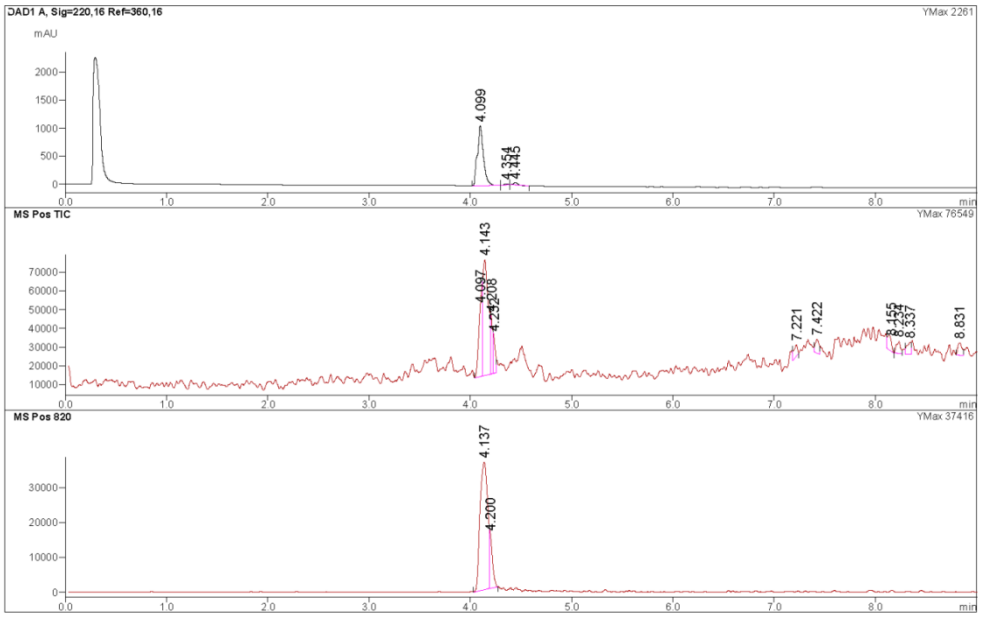

Data File	C:\Daten\2015\NOVEMBER\16NOV0001199.D	Sample Name	RBE-249- TAK-CF		
Injection Date	27-Nov-2015 17:09:28	Vial	13	Replicate	1
LCMS Method	XBR_SHORT_15_95.M	Sequence Line	1	Injection Volume	2
0 min 85%H2O(0.05%TFA) 6 min-95%ACN; 8.5 min 95%ACN; 10 min 15 %ACN; 0.6 ml/min; 400-1500MW; 2 µL; 50X2.1; 2.5µ; XBridge OST C18; Autosampler					
Sample Info	819				

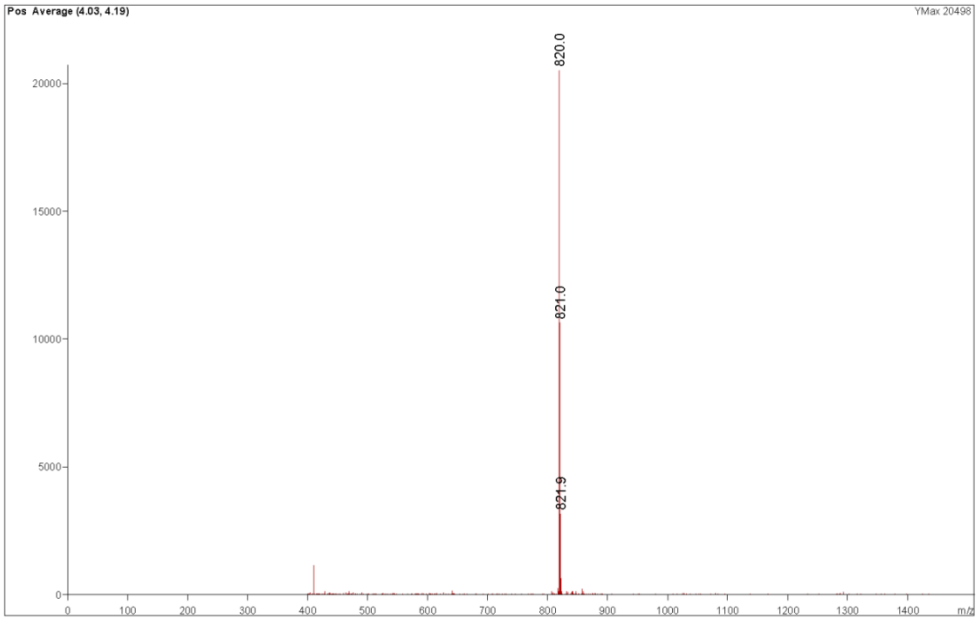

Synthesis of probe **15** (TAK-FITC)

Compound **4** (10.7 mg, 21.53 µmol) was dissolved in 300 µL of DMF in a small Eppendorf vial protected from light with aluminum foil, followed by DIEA (10.3 µL, 59.13 µmol). Then was added fluorescein thioisocyanate (9.8 mg, 25.04 µmol) to the mixture. Reaction was allowed to run for 1 hour in the dark.

The crude was directly purified through preparative HPLC (25->95% ACN) to afford, after lyophilization, the desired product **15** TAK-FITC conjugate as a dark orange powder (m = 6.5 mg, 7.62 µmol, 35% yield).

Retention time R_t = 4.172 min (METHOD 3)

HRMS (ESI-TOF) m/z: $[M-H]^-$: Calcd for $C_{49}H_{41}N_2O_{10}S$: 849.2487; Found: 849.2480

Max Abs/Em 496/520 nm

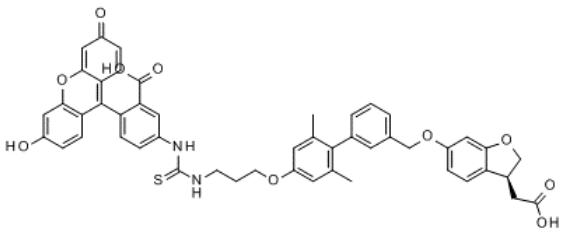

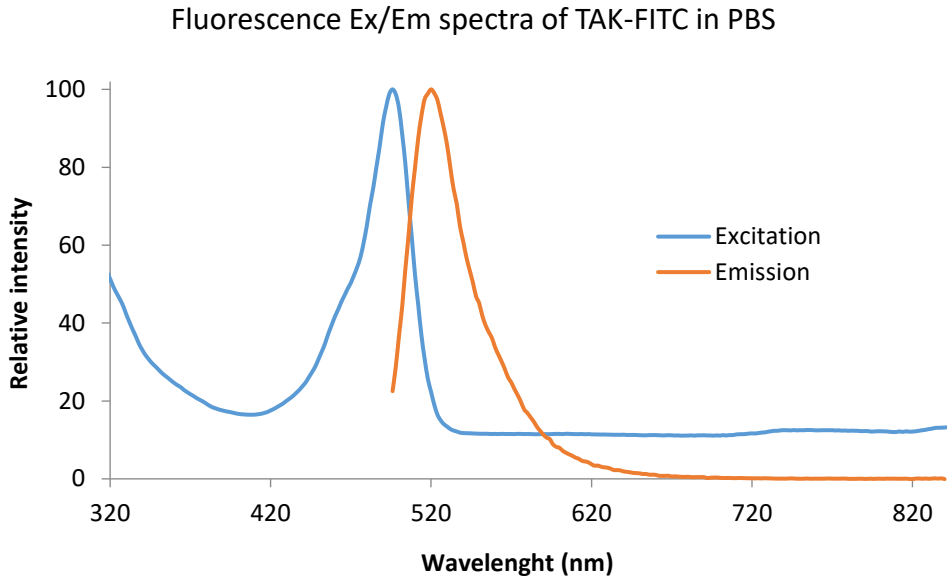
Fluorescence Ex/Em spectra of TAK-FITC in PBS
Relative intensity
100
80
60
40
20
0
320
420
520
620
720
820
Wavelenght (nm)
Excitation
Emission

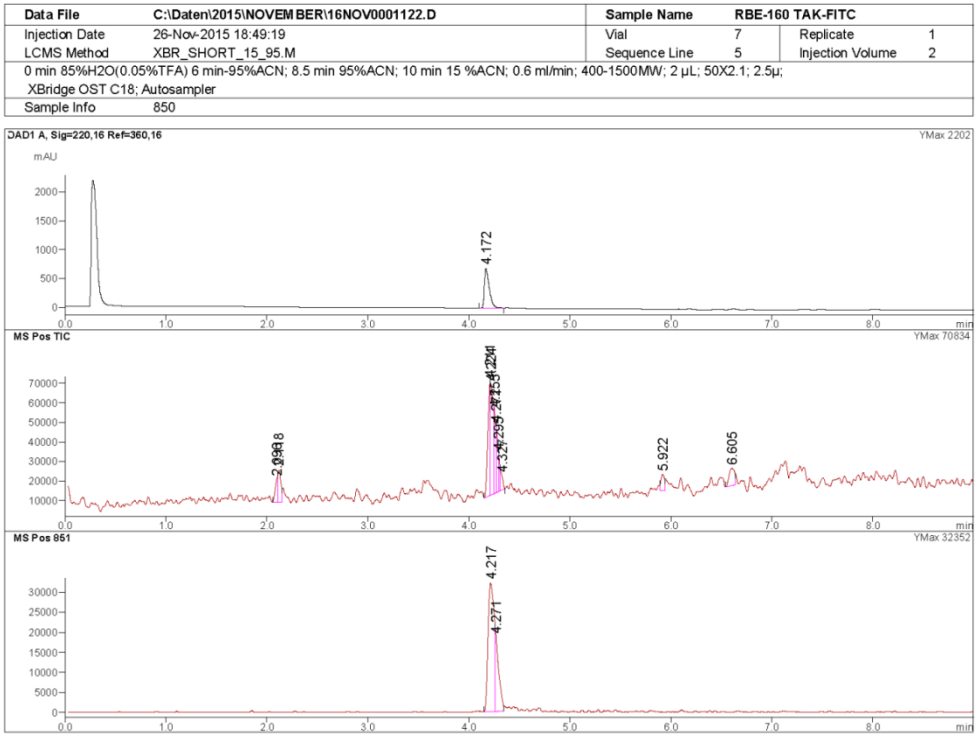
Data File C:\Daten\2015\NOVEMBER\16NOV0001122.D
Sample Name RBE-160 TAK-FITC
Injection Date 26-Nov-2015 18:49:19
Vial 7
Replicate 1
LCMS Method XBR_SHORT_15_95.M
Sequence Line 5
Injection Volume 2
0 min 85%H2O(0.05%TFA) 6 min-95%ACN; 8.5 min 95%ACN; 10 min 15 %ACN; 0.6 ml/min; 400-1500MW; 2 µL; 50X2.1; 2.5µ; XBridge OST C18; Autosampler
Sample Info 850
DAD1 A, Sig=220,16 Ref=360,16
mAU
4.172
MS Pos TIC
5.922
6.605
MS Pos 851
4.217
4.271
min

Data File	C:\Daten\2015\NOVEMBER\16NOV0001122.D	Sample Name	RBE-160 TAK-FITC		
Injection Date	26-Nov-2015 18:49:19	Vial	7	Replicate	1
LCMS Method	XBR_SHORT_15_95.M	Sequence Line	5	Injection Volume	2
0 min 85%H2O(0.05%TFA) 6 min-95%ACN; 8.5 min 95%ACN; 10 min 15 %ACN; 0.6 ml/min; 400-1500MW; 2 µL; 50X2.1; 2.5µ; XBridge OST C18; Autosampler					
Sample Info	850				

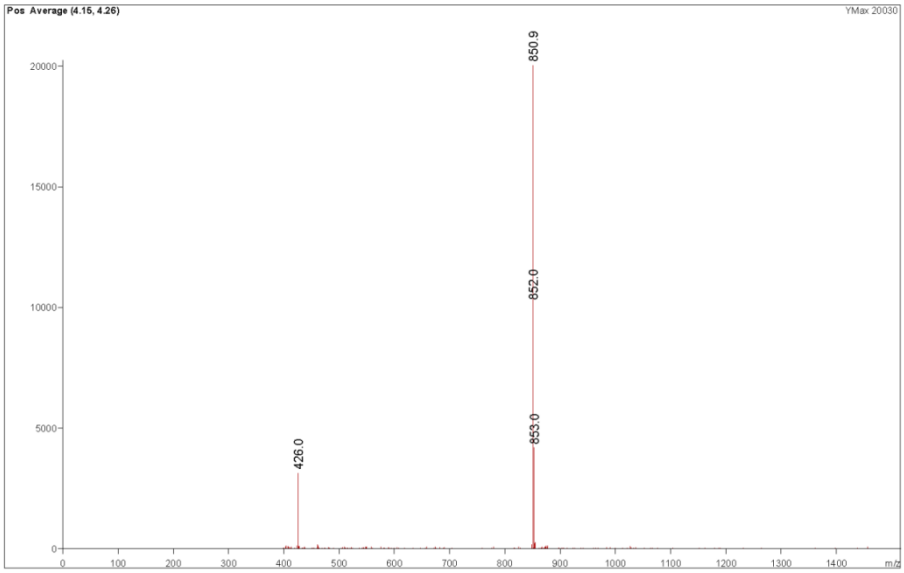

Synthesis of probe **16** (TAK-Alexa488)

Compound **4** (2.0 mg, 4.33 µmol) was dissolved in 300 µL of water in a small Eppendorf vial protected from light with aluminum foil, followed by DIEA (3 µl, 17.18 µmol). Then was added Alexa-488 NHS ester (3.36 mg, 5.20 µmol) to the mixture and pH was adjusted to pH = 9 with DIEA. The reaction was allowed to run for 10 minutes in the dark.

The crude was directly submitted to preparative HPLC (25->95% ACN) to afford, after lyophilization, the desired product **16** TAK-Alexa488 conjugate as a dark orange powder (m = 2.8 mg, 2.86 µmol, 66% yield).

Retention time R_t = 3.185 min (METHOD 3)

HRMS (ESI-TOF) m/z: $[M-H]^-$: Calcd for $C_{49}H_{43}N_3O_{15}S_2$: 977.2136; Found: 977.2130

^{1}H NMR (600 MHz, d_6-DMSO) δ: 1.89 (s, 3H), 1.92 (s, 3H), 1.99-1.94 (m, 1H), 2.07-2.01 (m, 1H), 2.46 (t, 1H, *J* = 8.9 Hz), 2.68 (dd, 1H, *J* = 16.7, 5.5 Hz), 3.53-3.50 (m, 2H), 3.70-3.63 (m, 2H), 4.01 (t, 2H, *J* = 6.07 Hz), 4.08 (t, 1H, *J* = 6.07 Hz), 4.18 (dd, 1H, *J* = 8.9, 6.7 Hz), 4.67 (t, 1H, *J* = 9.15 Hz), 5.09 (s, 2H), 6.44 (t, 1H, *J* = 2.0 Hz), 6.46 (dd, 0.5H, *J* = 2.4, 1.4 Hz), 6.48 (dd, 0.5H, *J* = 2.4, 1.4 Hz), 6.67 (s, 1H), 6.72 (s, 1H), 6.99 (s, 3H), 7.04 (dd, 1,3 Hz, *J* = 11.1, 7.6 Hz), 7.09 (d, 1H, *J* = 8.2 Hz), 7.12 (d, 1H, *J* = 10.4 Hz), 7.39-7.35 (m, 1H), 7.46-7.41 (m, 1H), 7.54 (s, 0.4 H, *J* = 7.8 Hz), 7.85 (s, 0.5H), 8.22 (dd, 0.5H, *J* = 8.2, 1.7 Hz), 8.31-8.27 (m, 1H), 8.71 (s, 0.7H), 8.76 (t, 0.7H, *J* = 5.6 Hz), 8.95 (t, 0.6H, *J* = 5.5 Hz) (mixture of isomers)

Max Abs/Em 496/518 nm

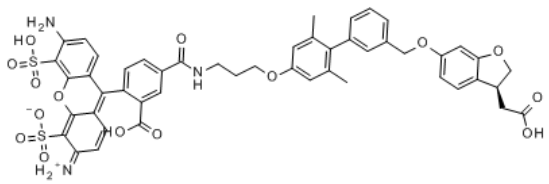

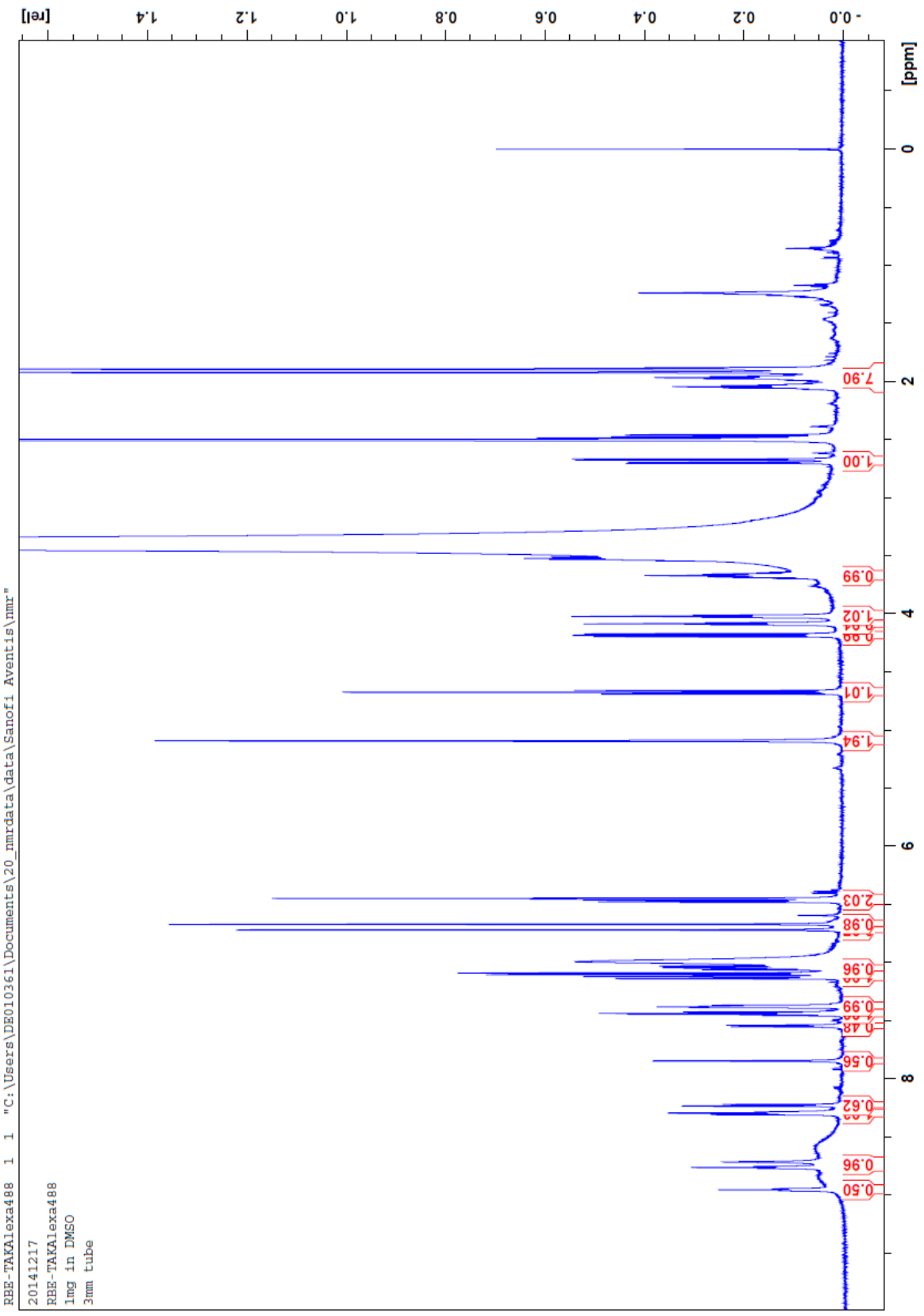
RBE-TAKAlexa488 1 1 "C:\Users\DE01036l\Documents\20_nmrdata\data\Sanofi Aventis\nmr"
20141217
RBE-TAKAlexa488
1mg in DMSO
3mm tube
[rel]
[ppm]
7.90
1.00
0.99
1.02
1.01
1.94
2.03
0.98
0.96
0.99
0.56
0.62
0.96
0.50

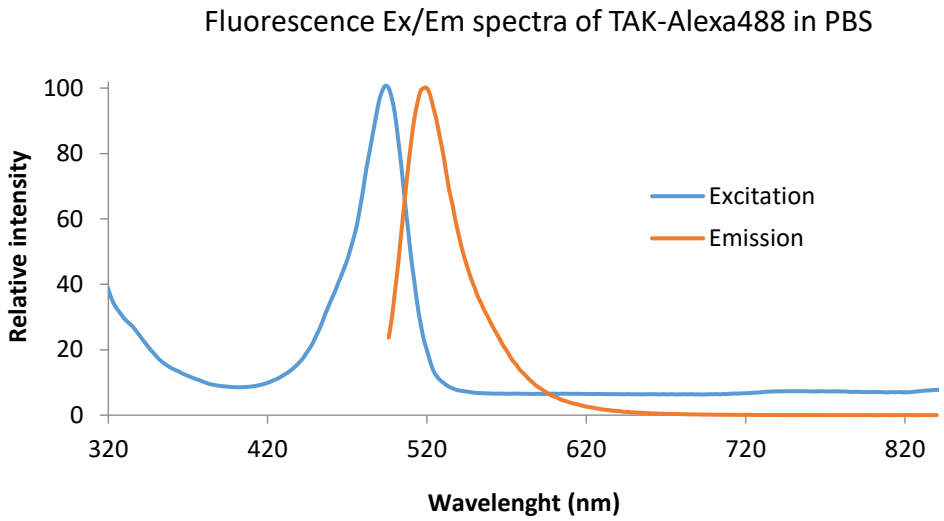

Data File	C:\Daten\2015\NOVEMBER\16NOV0001200.D	Sample Name	RBE-2-098 TAK-A488		
Injection Date	27-Nov-2015 17:53:52	Vial	12	Replicate	1
LCMS Method	XBR_SHORT_15_95.M	Sequence Line	1	Injection Volume	4
0 min 85%H2O(0.05%TFA) 6 min-95%ACN; 8.5 min 95%ACN; 10 min 15 %ACN; 0.6 ml/min; 400-1500MW; 2 µL; 50X2.1; 2.5µ; XBridge OST C18; Autosampler					
Sample Info	977				

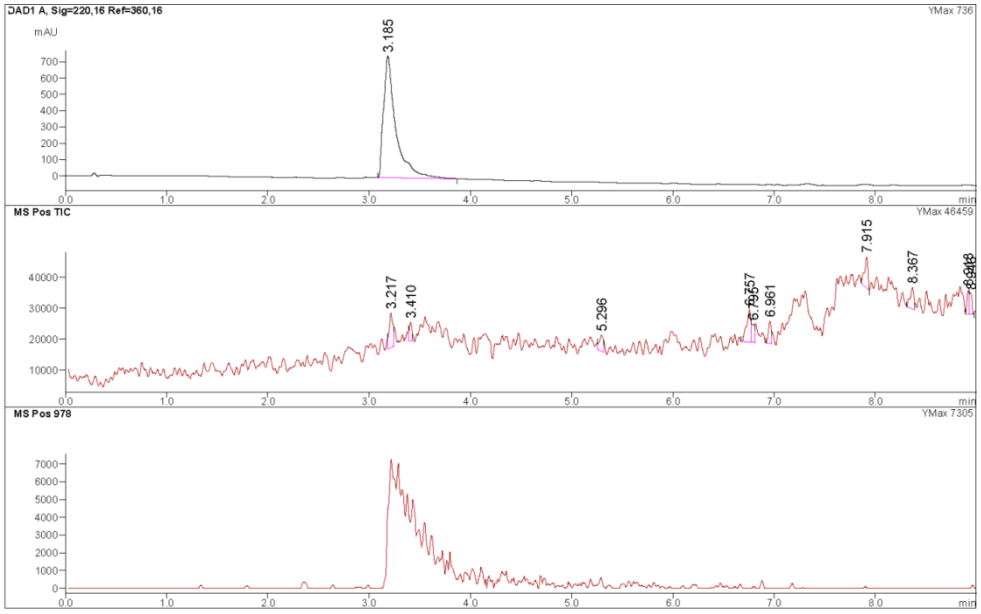

Data File	C:\Daten\2015\NOVEMBER\16NOV0001200.D	Sample Name	RBE-2-098 TAK-A488		
Injection Date	27-Nov-2015 17:53:52	Vial	12	Replicate	1
LCMS Method	XBR_SHORT_15_95.M	Sequence Line	1	Injection Volume	4
0 min 85%H2O(0.05%TFA) 6 min-95%ACN; 8.5 min 95%ACN; 10 min 15 %ACN; 0.6 ml/min; 400-1500MW; 2 µL; 50X2.1; 2.5µ; XBridge OST C18; Autosampler					
Sample Info	977				

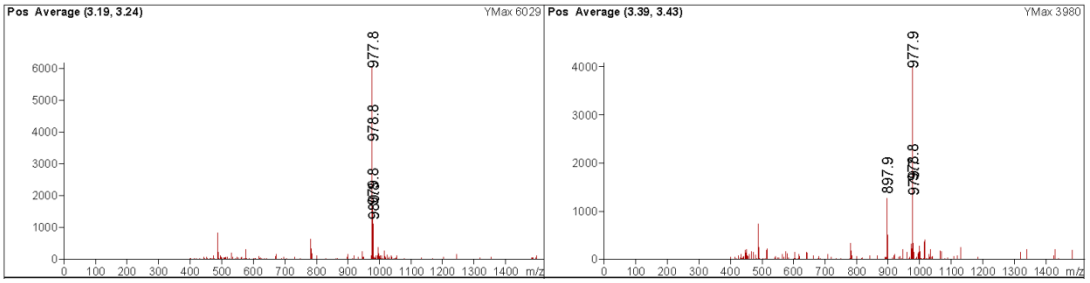

Synthesis of probe **17** (TAK-TAMRA)

Compound **4** (4.8 mg, 9.7 µmol) was dissolved in 400 µL of DMF in a small Eppendorf vial protected from light with aluminum foil, followed by DIEA (3.5 µL, 20.1 µL) and TAMRA NHS-ester (7.4 mg, 9.8 µmol). The reaction was allowed to stir for 30 minutes at room temperature, in the dark. The crude was directly purified through preparative HPLC (25->95% ACN) to afford, after lyophilization, the desired product **17** TAK-TAMRA conjugate as a dark orange powder (m = 5.5 mg, 6.3 µmol, yield 65%).

Retention time Rt = 4.172 (METHOD 3)

HRMS (ESI-TOF) m/z: $[M-H]^-$: Calcd for $C_{53}H_{50}N_3O_9$: 872.3552; Found: 872.3592

Max Abs/Em 544/574 nm

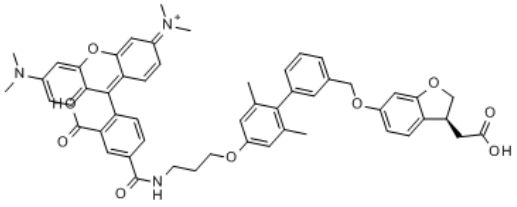

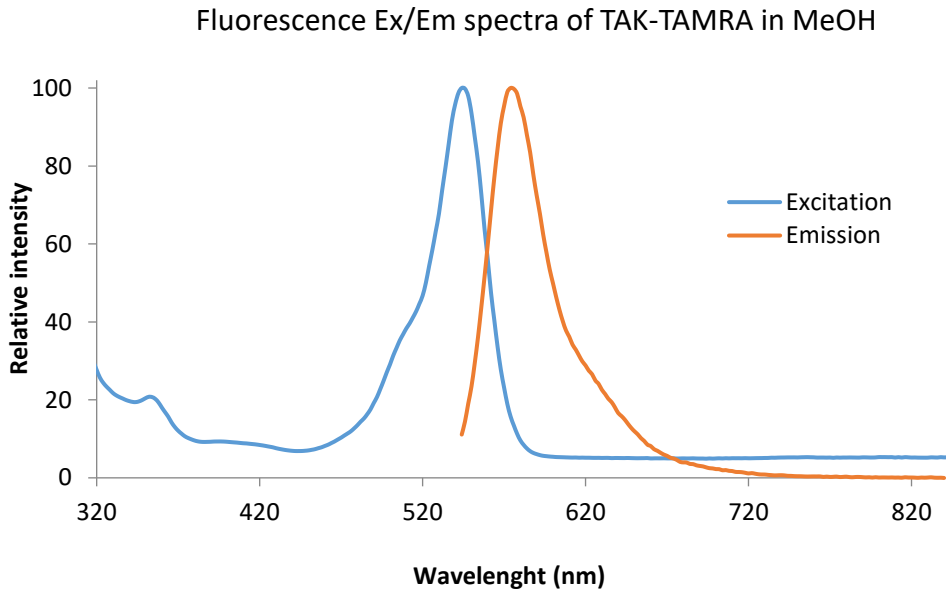

Data File	C:\Daten\2015\NOVEMBER\16NOV0001126.D	Sample Name	RBE-246 TAK-TAMRA		
Injection Date	26-Nov-2015 19:33:34	Vial	8	Replicate	1
LCMS Method	XBR_SHORT_15_95.M	Sequence Line	9	Injection Volume	2
0 min 85%H2O(0.05%TFA) 6 min-95%ACN; 8.5 min 95%ACN; 10 min 15 %ACN; 0.6 ml/min; 400-1500MW; 2 µL; 50X2.1; 2.5µ; XBridge OST C18; Autosampler					
Sample Info	874				

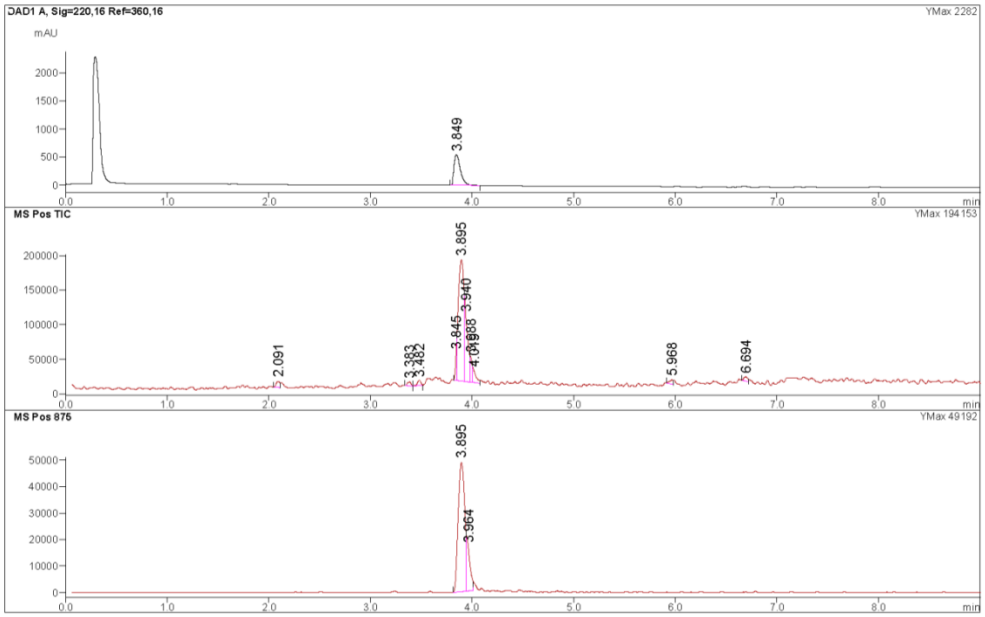

Data File	C:\Daten\2015\NOVEMBER\16NOV0001126.D	Sample Name	RBE-246 TAK-TAMRA		
Injection Date	26-Nov-2015 19:33:34	Vial	8	Replicate	1
LCMS Method	XBR_SHORT_15_95.M	Sequence Line	9	Injection Volume	2
0 min 85%H2O(0.05%TFA) 6 min-95%ACN; 8.5 min 95%ACN; 10 min 15 %ACN; 0.6 ml/min; 400-1500MW; 2 µL; 50X2.1; 2.5µ; XBridge OST C18; Autosampler					
Sample Info	874				

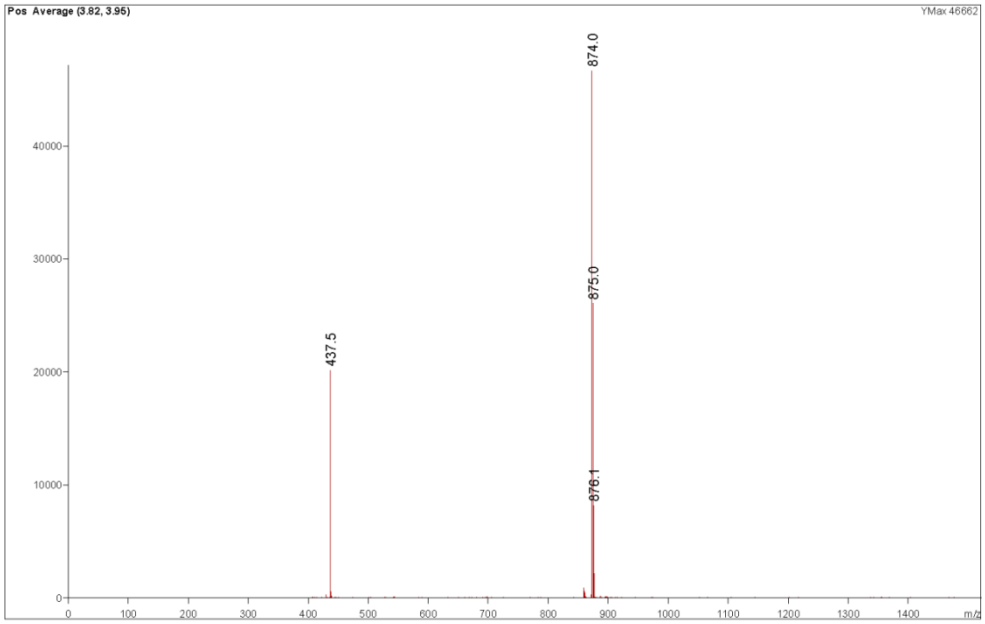

Synthesis of probe **18** (TAK-Bodipy 650)

Compound **4** (2.6 mg, 3.92 µmol) was dissolved in 500 µL of DMF in a small Eppendorf vial protected from light with aluminum foil, followed by DIEA (2.6 µL, 14.89 µmol). Then Bodipy 650/665-X NHS ester (2.1 mg, 3.26 µmol) was added to the mixture. Reaction was allowed to run overnight in the dark.

The crude was directly purified through preparative HPLC (25->95% ACN) to afford, after lyophilization, the desired product **18** TAK-Bodipy650 conjugate a dark blue powder (m = 2.0 mg, 2.02 µmol, 62% yield).

Retention time Rt = 4.925 min (METHOD 3)

HRMS (ESI-TOF) m/z: $[M-H]^-$: Calcd for $C_{57}H_{58}BF_2N_5O_8$: 988.4383; Found: 988.4457

Max Abs/Em 646/666 nm

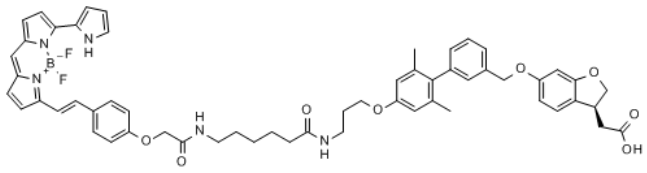

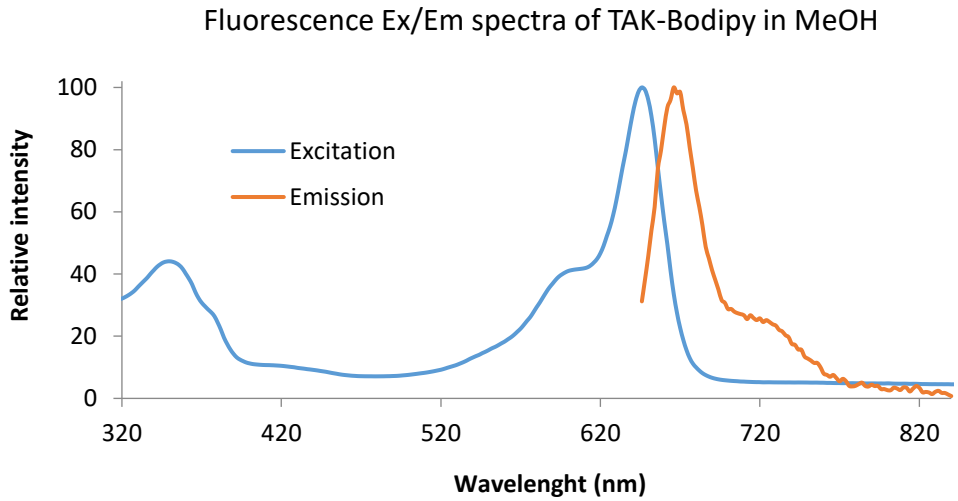
Fluorescence Ex/Em spectra of TAK-Bodipy in MeOH
Relative intensity
100
80
60
40
20
0
Excitation
Emission
320
420
520
620
720
820
Wavelenght (nm)

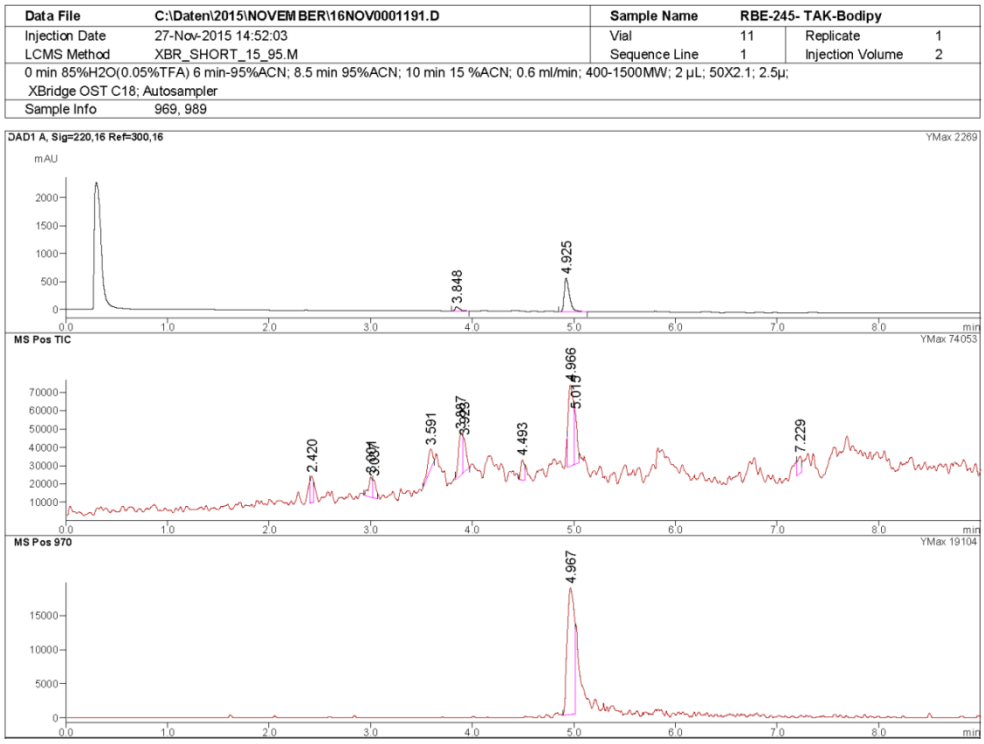
Data File C:\Daten\2015\NOVEMBER\16NOV0001191.D
Sample Name RBE-245- TAK-Bodipy
Injection Date 27-Nov-2015 14:52:03
Vial 11
Replicate 1
LCMS Method XBR_SHORT_15_95.M
Sequence Line 1
Injection Volume 2
0 min 85%H2O(0.05%TFA) 6 min-95%ACN; 8.5 min 95%ACN; 10 min 15 %ACN; 0.6 ml/min; 400-1500MW; 2 µL; 50X2.1; 2.5µ; XBridge OST C18; Autosampler
Sample Info 969, 989
DAD1 A, Sig=220,16 Ref=300,16
mAU
3.848
4.925
MS Pos TIC
2.420
3.591
4.493
4.966
7.229
MS Pos 970
4.967
min

Data File	C:\Daten\2015\NOVEMBER\16NOV0001191.D	Sample Name	RBE-245- TAK-Bodipy		
Injection Date	27-Nov-2015 14:52:03	Vial	11	Replicate	1
LCMS Method	XBR_SHORT_15_95.M	Sequence Line	1	Injection Volume	2
0 min 85%H2O(0.05%TFA) 6 min-95%ACN; 8.5 min 95%ACN; 10 min 15 %ACN; 0.6 ml/min; 400-1500MW; 2 µL; 50X2.1; 2.5µ; XBridge OST C18; Autosampler					
Sample Info	969, 989				

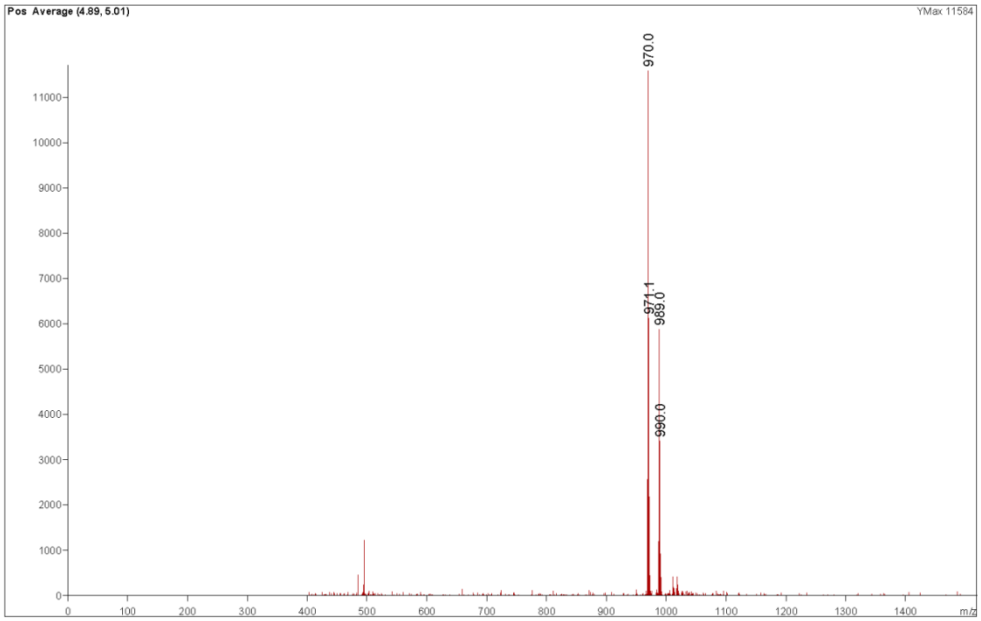

Synthesis of probe **19** (TAK-Cy5.5)

Compound **4** (10.2 mg, 20.52 µmol) was dissolved in 400 µL of DMF in a small Eppendorf vial protected from light with aluminum foil, followed by DIEA (10 µL, 57.41 µmol). Cy5.5 NHS ester (17 mg, 23.72 µmol) was then added to the mixture. Reaction was allowed to run for 10 minutes in the dark. The crude was directly purified through preparative HPLC (25->95% ACN) to afford, after lyophilization, the desired product **19** TAK-Cy5.5 conjugate as a dark blue powder (m = 10.0 mg, 9.73 µmol, 47% yield).

Retention time Rt = 5.096 min (METHOD 3)

HRMS (ESI-TOF) m/z: $[M-H]^-$: Calcd for $C_{68}H_{72}N_3O_6$: 1026.5421; Found: 1026.5445

Max Abs/Em 680/710 nm

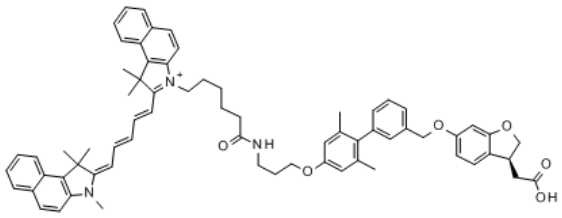

Species homology of FFAR1

According to database searches in http://www.expasy.org, the homology of FFAR 1 between the different species is as follows:

Homology FFAR1 Human // FFAR1 Mouse: 83%
Homology FFAR1 Human // FFAR1 Rat: 81.7%
Homology FFAR1 Rat // FFAR1 Mouse: 95.7%

http://www.uniprot.org/uniprot/O14842

Chapter 3

Synthesis of FFAR1-GPR40 targeting ^{3}H- and ^{18}F probes towards selective β-cell imaging

Romain Bertrand[1,2], Isabel Hamp[1,6], Mark Brönstrup[3,4], Remo Weck[4], Mario Lukacevic[7], Andras Polyak[7], Tobias L. Ross[7], Martin Gotthardt[2], Oliver Plettenburg[1,5,6] and Volker Derdau[4]

[1]Diabetes Division, Research & Translational Medicine, Sanofi GmbH, Frankfurt am Main 65926, Germany
[2]Department of Nuclear Medicine, Radboud UMC, Nijmegen 6525, The Netherlands
[3]Helmholtz Centre for Infection Research, Braunschweig 38124, Germany
[4]DSAR/Drug Disposition, Sanofi GmbH, Frankfurt am Main 65926, Germany
[5]Institute of Medicinal Chemistry, Helmholtz Zentrum München, Ingolstaedter Landstr. 1, Neuherberg 85764, Germany
[6]Leibniz University Hannover, Schneiderberg 1 B, Hannover 30167, Germany
[7]Department of Nuclear Medicine, Hannover Medical School, Hannover, Germany

Adapted from: Journal of Labelled Compounds and Radiopharmaceuticals, **2016**, "*Synthesis of GPR40 targeting ^{3}H- and ^{18}F probes towards selective beta cell imaging*"

Abstract

Diabetes affects an increasing number of patients worldwide and is responsible for a significant rise in healthcare expenses. Imaging of β-cells in vivo is expected to contribute to an improved understanding of the underlying pathophysiology, improved diagnosis, and development of new treatment options for diabetes. Here, we describe the first radiosyntheses of [^{3}H]-TAK875 and [^{18}F]-TAK875 derivatives to be used as β-cell imaging probes addressing the free fatty acid receptor 1 (FFAR1/GPR40). The fluorine-labeled derivative showed similar agonistic activity as TAK875 in a functional assay. The radiosynthesis of the ^{18}F-labelled tracer 2a was achieved with 16.7 ± 5.7% radiochemical yield in a total synthesis time of 60–70 min.

Introduction

Diabetes is a chronic metabolic disease characterized by hyperglycemia resulting either from deficiency in insulin secretion, insulin resistance, or both. Around 387 million people are affected worldwide, and the burden on healthcare costs imposed by the disease is dramatically increasing.[1] However, the precise molecular and cellular mechanisms that cause the decrease in mass and function of the insulin-producing β-cells remain to be elucidated. Longitudinal studies on quantification of β-cells in animal models as well as in patients would significantly improve the knowledge on the pathophysiology of the disease.[2] One approach to provide new tools for efficient noninvasive β-cell imaging is the development of chemical probes with high selectivity to provide transferable and reliable information on mass of the insulin-producing β-cells.[3] Positron-emission tomography (PET) imaging is an attractive imaging modality to determine the variation in β-cell mass because of its high sensitivity and the possibility to quantitatively analyze the images.[4] Several positron emitting isotopes can be used in PET imaging.[5] Because of its favorable physical and nuclear characteristics, [^{18}F] is often regarded as the "radionuclide of choice", as the 110 min half-life allows sufficient time for the synthetic labeling reaction and purification. Furthermore, the short positron linear range in tissue (2.3 mm) gives the highest resolution PET images of all the available positron emitters.[6–8] Therefore, we investigated the development of a new [^{18}F]-labeled PET tracer with high β-cell affinity for selective β-cell imaging. Because the G protein–coupled receptor 40 (GPR40 – also known as free fatty-acid receptor 1 FFAR1) is highly and predominantly expressed in human and rodents islets β-cells,[9–11] it attracted our attention as a β-cell specific receptor for imaging. Moreover, many GPR40 agonists are described in the literature.[12] TAK875 is an orally available, selective, and potent agonist of GPR40,[13] which reached clinical phase III: administration of the compound to diabetic patients resulted in improvements in blood glucose control.[14] We envisioned that the TAK875 **1** scaffold would serve as a good starting point to develop a GPR40-targeting [^{18}F]-labeled PET tracer and specifically selected compound **2a**, as favorable pharmacokinetic and pharmacodynamics data were reported for **2**[15] (Scheme 1).

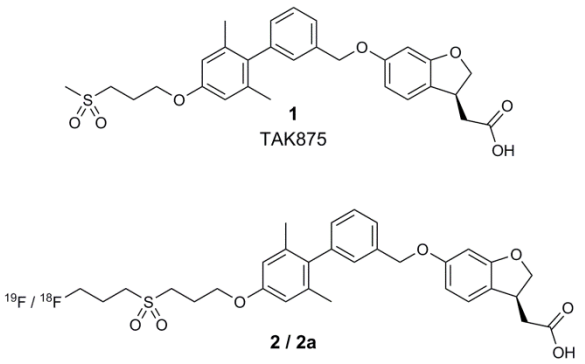

Scheme 1 Structure of TAK875 **1** and envisioned [^{19}F/^{18}F] tracer **2**/**2a**

Material and Methods

Chemistry

See the Supporting Information for a detailed description of the syntheses.

Cell Culture

Human embryonic kidney (HEK293) cells stably expressing human GPR40/FFAR1 (HEK293 cells were transfected with hGPR40 using a pEAK8 vector system) were grown in highglucose DMEM (41965 Life Technologies) containing 10% (v/v) FCS gold PAA, 1% (v/v) NEAA and puromycin (1 µg/mL), in a humidified 5% CO_2 atmosphere at 37 °C. Human embryonic kidney (HEK293) cells were cultured under the same conditions except for the absence of puromycin.

Fluorometric Imaging Plate Reader (FLIPR) Ca^{2+} Assays

HEK293 cells stably expressing human GPR40/FFAR1 were plated in a poly-D-Lys coated 96-well plate with 40 000 cells/well and incubated overnight in a humidified 5% CO_2 atmosphere at 37 °C. Then, cells were incubated in Hank's buffer salt solution supplemented with HEPES (pH = 7.5) containing fluorescent calcium indicator Fluo 4 AM (Molecular Devices, final concentration 2 µM) + 20% (w/v) pluronic acid for 60 min at 37 °C. Cells were washed with a Tecan Ultra (Tecan Group Ltd.) device before the addition in the wells of tested compounds at various concentrations (previously dissolved in DMSO at 10 mM concentration and diluted with assay buffer). Increase of the intracellular Ca^{2+} concentration after addition was monitored by FLIPR Tetra system (Molecular Devices). Experiments were performed in triplicates.

Binding experiments with [3H]-TAK875 on GPR-HEK and HEK cells

Twenty-four hours before the experiment 400 × 105 cells/well of either GPR40-HEK cells or HEK cells (control) were plated on a 48 well plate (well volume 1 mL) and incubated overnight in a humidified 5% CO_2 atmosphere at 37°C. The day of the experiment, the culture media were removed from the cells, and they were washed once with Roswell Park Memorial Institute (RPMI) medium supplemented with 0.5% albumin (Gibco LifeTechnologies, ThermoFisher, Gibco, MA, USA). Then was added the tritiated compound to all the wells (100 µL of 2.05 × 103 Bq/ mL solution), and the cells were incubated in a humidified 5% CO_2 atmosphere at 37°C. The same amount of hot compound (100 µL) was also added to wells without any cells as a standard. After 1 hour of incubation, were extracted out from the supernatant 75 µL and mixed with 225 µL of a scintillation cocktail before being measured on a TopCounter NXT (PerkinElmer, MA, USA). All the experiments were carried out as quadruplicates. P-value was determined with a t-test performed with Excel ($p = 0.0017$).

Results and discussion

We first synthesized [^{3}H]-TAK875 1a to obtain a model compound for in vitro binding evaluation studies. To our knowledge, a [^{3}H]-synthesis of TAK875 has not been reported. Briefly, **1** was mono-brominated with one equivalent of N-bromosuccinimide (NBS). The tritiation was performed with dry 5% Pd/C catalyst and 98 MBq/2.61 Ci tritium gas[16] using a tritium manifold at room temperature to afford **1a** in 4 h with 5.3% radiochemical yield (RCY) (Scheme 2).

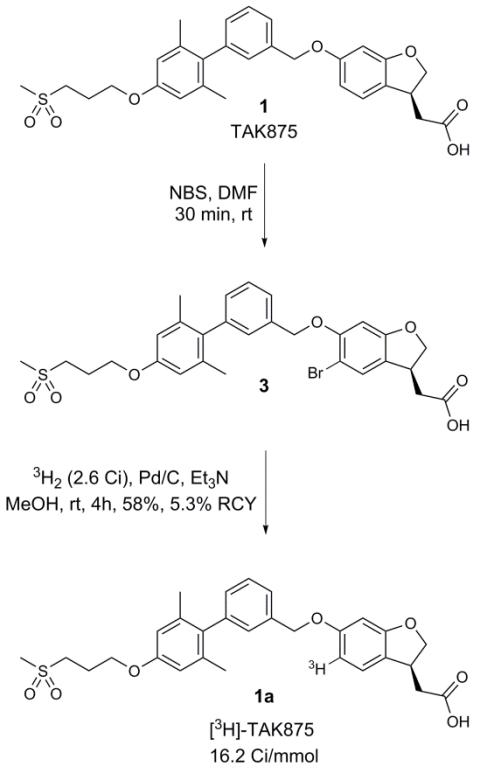

Scheme 2 Synthesis of [^{3}H]-TAK875 **1a**

In the next step, the receptor binding of **1a** on HEK293-cells (Human Embryonic Kidney 293 cells) transfected to overexpress the GPR40 receptor (GPR40-HEK) was evaluated. In order to assess the specificity of the binding, wild type HEK293-cells (HEK) lacking expression of GPR40 were used as control

(Figure 1). After 1 hour of incubation, we observed binding of **1a** in HEK cells at levels above background. However, specifically bound signal was at least sevenfold higher in the GPR40-transfected cells preparation. These results indicate that **1a** bound to the targeted receptor in vitro and therefore encouraged us to investigate this structure for the design and synthesis of a [^{18}F]-labeled tracer.

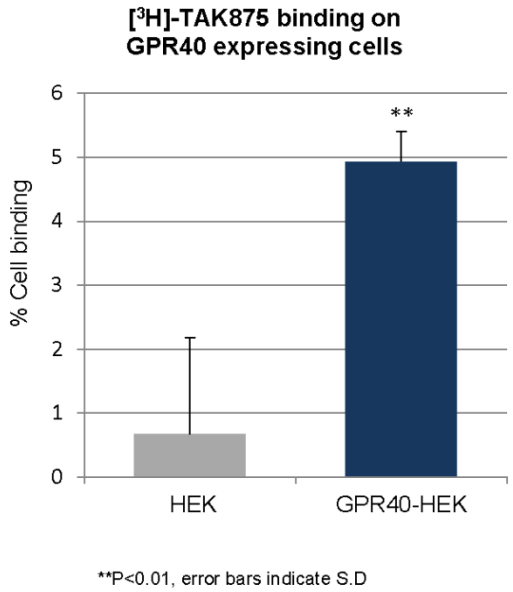

Figure 1 [^{3}H]-TAK875 **1a** binds preferably HEK-cells expressing GPR40

The design of a new [18F]-tracer started with the selection of a suitable labeling position. It was reported that modifications on the 4'-position of the terminal biphenyl ring of **1** were well tolerated in terms of agonistic activities and binding affinities.[13, 15] Consequently, we envisioned to use the phenol side chain to introduce a tosylate leaving group as precursor for [^{18}F]-introduction. Starting from phenol **4**, alkylation with a fivefold excess of allyl bromide under microwave irradiation afforded compound **5** in 94% yield. The sulfone function was introduced by using a thiol-ene click approach[17] with thiopropanol. This reaction was reported not only with several Michael acceptors such as maleimide or acrylates[18] but also with non-conjugated alkenes.[19] We then performed a selective oxidation of the sulfur with meta-chloroperbenzoic acid (mCPBA), affording compound **6** in 88% yield over two steps.

Finally, alcohol **6** was tosylated to provide the fluorination precursor **7** (Scheme 3).

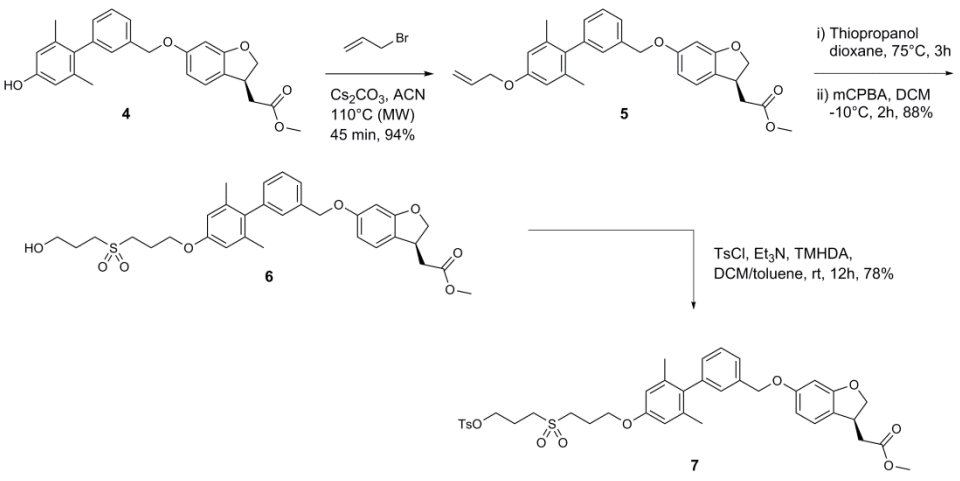

Scheme 3 Synthesis of the fluorination precursor **7**

To evaluate the impact of structural modification in the phenol side chain of TAK875 building block **4** we measured compounds **2**, **4**, **5**, **6** (as the active free carboxylic acid form) in a Fluorometric Imaging Plate Reader (FLIPR, Molecular Devices, Sunnyvale, CA, USA) Ca^{2+} assay (molecular functional assay of agonistic receptor activity). The agonistic activities of the acid compounds of **6** and **2** were 1.5 and 2.4-fold more potent than parent ligand TAK875 **1**, confirming that introduction of fluorine was well tolerated (Table 1).

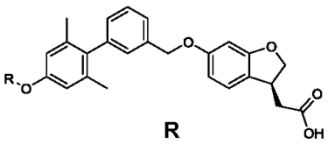

Cpd[1]	R	Relative GPR40 activity[2]
TAK875	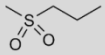	1.0
2	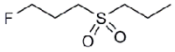	2.4
4	H	1.1
5		0.1
6	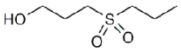	1.5

[1]Measured as free acids.
[2]Values based on TAK875 normalized EC_{50} data (FLIPR-Ca^{2+} assay in triplicates)

Table 1 *In Vitro* activities of TAK875 derivatives

To establish the reaction conditions for the PET radiochemistry laboratory under non-radioactive conditions, we decided to use KF as ^{19}F-source, potassium carbonate, acetonitrile and Kryptofix 2.2.2 (K2.2.2) as standard parameters in our labeling optimization approach. We studied the SN2 substitution reaction of the tosylate **7** under various temperatures and reaction times (Table 2). At room temperature we observed only limited conversion (Entry 1). We increased the temperature to 40°C, which led to a moderate conversion to the desired product (Entry 2–5). At a temperature of 100°C or 130°C (Entry 6–10) we reached full conversion of the starting material. However, we also observed formation of hydrolyzed and elimination side products. This was accentuated at higher temperature, resulting in reduced yields (Entry 9–10). Furthermore, extended reaction times were also detrimental for the yields (Entry 6–8 and 9–10). Based on these results, we concluded that the preferred conditions to implement the [^{18}F] radiolabeling are 2 min reaction time at 100°C (Entry 6).

Entry	Temp. (°C)	Time (min)	Yield (%)*
1	RT	10	15
2	40	2	29
3	40	5	39
4	40	10	47
5	40	15	48
6	100	2	86
7	100	5	83
8	100	10	74
9	130	5	39
10	130	10	28

*Determined by LCMS.

Table 2 Screening of conditions for ^{19}F-labeling of tosylate **7** with potassium fluoride

[^{18}F]-labeling of the tosylate **7** was performed using azeotropically dried n.c.a. [^{18}F] fluoride, activated by the potassium carbonate/K2.2.2-system. The conditions of entry 6 from the non-radioactive optimization were directly transferable to the n.c.a. radiosynthesis. The radiolabeling (n = 10) showed very fast kinetics with 30–35% RCY within only 1 min (Scheme 4). However, the excellent yields (83-86%) from the cold optimization could not be reached under n.c.a. condition, which is presumably due to the inverse stoichiometry in both situations. Already within the first minutes of the labeling reaction, the strong basic conditions cause partly deprotection of the intermediate labeling product to the final radiotracer **2a**. Prolonged reaction times did not result in higher RCY, but further deprotection (Scheme 4). The sum of both products, protected intermediate and **2a**, stays constant over 15 min. A complete deprotection after 5 min at room temperature was achieved by adding a 1/1 solution of methanol/2.5M aqueous sodium hydroxide solution. During the deprotection step, product losses were observed, which we assume to be due to hydrolysis and elimination as shown by the cold ^{19}F-optimization study. Optimization studies of the deprotection step resulted either in full degradation of the product or incomplete deprotection. Still the deprotection step gives room for improvement.

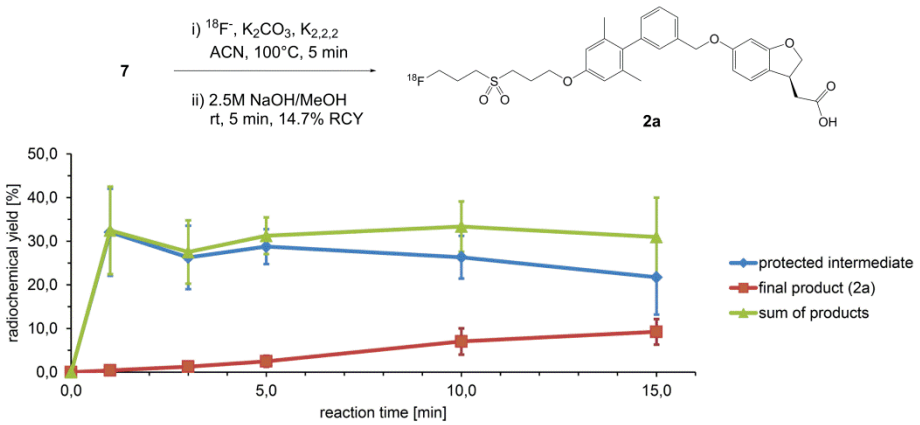

Scheme 4 Radiosynthesis of ^{18}F-radiotracer **2a**. The diagram shows the course of the radiolabeling over 15 min for the protected intermediate (blue line) product and the final product (red line). In addition, the green graph represents the sum of both products. Radiochemical yield (RCY) were determined by radio-TLC.

The final radiotracer **2a** was obtained in 16.7% ± 5.7% RCY (n = 6) and with only a low specific activity of ≥0.6 GBq/µmol. So far, only low specific activities could be obtained, which is a crucial issue in imaging targets of low density such as the GPR40. The low specific activities are mainly due to low starting activities. We expect good to high specific activities after automation of the radiosynthesis and the use of high starting activities. The identity **2a** was confirmed by coinjection with the cold reference compound **2** on analytical radio-HPLC and co-spotting on radio-TLC. For upscaling and potential translation, the first steps of the radiosynthesis of **2a** were successfully transferred to an automated, cassette-based radiosynthesis module (selfdesigned, custom-made cassettes, and materials are available from ABX) giving identical good results in labeling and deprotection. The automated HPLC-purification with subsequent SPE-isolation and formulation are currently under optimization. The tracer is currently evaluated in in-vitro and in-vivo studies, whose outcome will be reported in due course.

Conclusion

We described the radiosyntheses of two potent GPR40 ligands for selective β-cell imaging. The tritiated [^{3}H]-TAK875 analog **1a** was successfully synthesized and evaluated on HEK293-cells transfected to overexpress the GPR40 receptor. Based on these positive results, we investigated the development of a potential new [^{18}F]-PET tracer **2a**. The fluoride labeled derivative **2** showed similar agonistic activity as TAK875 **1** in a functional assay. The synthesis of ^{18}F-tracer **2a** was achieved in reasonable RCY and is already transferred to an automated, cassette-based radiosynthesis module.

Ackowledgements

The research leading to these results has received funding from the People Program (Marie Curie Actions) of the European Union's Seventh Framework Program FP7/2007-2013/under REA Grant Agreement No. 289932. We acknowledge Ute Messinger and Jenny Schubert for their help with providing analytical data, Juergen Dedio, Birgit Herzog, Inge Kress-Fischer, and Matthias Lohmann for performing the FLIPR Ca2+ assay. We would also like to thank Future Chemistry (Nijmegen, NL) for initial experiments on 18F-PET labeling.

References

[1] I. D. Federation. IDF DIABETES ATLAS Sixth edition - Update 2014. pdf, (Guariguata, L., Tim nolan, Jessica beagley, Ute Linnenkamp, and Jacqmain, o., Eds.), International Diabetes Federation, 2013.
[2] M. Gotthardt, D. L. Eizirik, M. Cnop, M. Brom, Trends Endocrinol. Metab. 2014, 25, 375–377.
[3] B. Goke, Curr. Pharm. Des. 2010, 16, 1547–1549.
[4] M. Brom, K. Andralojc, W. J. Oyen, O. C. Boerman, M. Gotthardt, Curr. Pharm. Des. 2010, 16, 1561–1567.
[5] S. M. Ametamey, M. Honer, P. A. Schubiger, Chem. Rev. 2008, 108, 1501–1516.
[6] P. W. Miller, N. J. Long, R. Vilar, A. D. Gee, Angew. Chem. Int. Ed. Engl. 2008, 47, 8998–9033.
[7] M. M. Alauddin, Am. J. Nucl. Med. Mol. Imaging 2012, 2, 55–76.
[8] H. Schieferstein, T. L. Ross, J. Labelled Comp. Radiopharm. 2013, 56, 432–440.
[9] C. P. Briscoe, M. Tadayyon, J. L. Andrews, W. G. Benson, J. K. Chambers, M. M. Eilert, C. Ellis, N. A. Elshourbagy, A. S. Goetz, D. T. Minnick, P. R. Murdock, H. R. Sauls, Jr., U. Shabon, L. D. Spinage, J. C. Strum, P. G. Szekeres, K. B. Tan, J. M. Way, D. M. Ignar, S. Wilson, A. I. Muir, J. Biol. Chem. 2003, 278, 11303–11311.
[10] Y. Itoh, Y. Kawamata,M. Harada,M. Kobayashi, R. Fujii, S. Fukusumi, K. Ogi, M. Hosoya, Y. Tanaka, H. Uejima, H. Tanaka, M. Maruyama, R. Satoh, S. Okubo, H. Kizawa, H. Komatsu, F. Matsumura, Y. Noguchi, T. Shinohara, S. Hinuma, Y. Fujisawa, M. Fujino, Nature 2003, 422, 173–176.
[11] K. Kotarsky, N. E. Nilsson, E. Flodgren, C. Owman, B. Olde, Biochem. Biophys. Res. Commun. 2003, 301, 406–410.
[12] E. Defossa, M. Wagner, Bioorg. Med. Chem. Lett. 2014, 24, 2991–3000.
[13] N. Negoro, S. Sasaki, S. Mikami, M. Ito, M. Suzuki, Y. Tsujihata, R. Ito, A. Harada, K. Takeuchi, N. Suzuki, J. Miyazaki, T. Santou, T. Odani, N. Kanzaki, M. Funami, T. Tanaka, A. Kogame, S. Matsunaga, T. Yasuma,Y. Momose, ACS Med. Chem. Lett. 2010, 1, 290–294.
[14] C. F. Burant, P. Viswanathan, J. Marcinak, C. Cao, M. Vakilynejad, B. Xie, E. Leifke, Lancet 2012, 379, 1403–1411.
[15] N. Negoro, S. Sasaki, S. Mikami, M. Ito, Y. Tsujihata, R. Ito, M. Suzuki, K. Takeuchi, N. Suzuki, J. Miyazaki, T. Santou, T. Odani, N. Kanzaki, M. Funami, A. Morohashi, M. Nonaka, S. Matsunaga, T. Yasuma, Y. Momose, J. Med. Chem. 2012, 55, 3960–3974.
[16] J. R. Heys, R. Voges, T. Moenius, Preparation of Compounds Labeled with Tritium and Carbon-14, Wiley, Chichester, UK, 2009.
[17] C. E. Hoyle, C. N. Bowman, Angew. Chem. Int. Ed. Engl. 2010, 49, 1540–1573.
[18] D. Nair, M. Podgorski, S. Chatani, T. Gong, W. Xi, C. Fenoli, C. Bowman, Chem. Mater. 2013, 26, 724–744.
[19] K. L. Killops, L. M. Campos, C. J. Hawker, J. Am. Chem. Soc. 2008, 130, 5062–5064.

Supporting Information

General Methods

^{1}H, ^{19}F and ^{13}C NMR spectra were obtained on Bruker spectrometers in the indicated solvents. Silica-gel column chromatography was carried out on a CombiFlash Rf - Isco Teledyne. Microwave assisted reactions were performed with a Biotage Initiator device. The purity of the products was determined by an LC-MS system with a Symmetry Shield RP18 column, 3.9x150 mm with a gradient program under the following conditions: mobile phase A: water (900 mL), acetonitrile (100 mL), TFA (1 mL); mobile phase B: water (100 mL), acetonitrile (900 mL), TFA (0.75 mL); flow 1.5 mL/min; detection UV 254 nm and UV 210 nm. Commercially available chemicals and solvents were used as received. Analytical radio-HPLC was performed on a Varian ProStar HPLC system (pump model 240, UV/Vis detector model 335) equipped with a radiodetector (Berthold LB500) using a monolithic RP 18 column, Chromolith® High Resolution RP-18e (Merck), 100 x 4.6 mm, with a solvent system and gradient as follows: Eluent A was 100% water; Eluent B was 100% acetonitrile. The gradient was from 100% eluent A to 95% eluent A in 0–4 min, 0% eluent A in 4–16 min, 0% eluent A in 16-21 min, from 0% eluent A to 100% eluent A in 21–23 min and 100% eluent A in 23-28 min. The flow was 1 mL/min. RadioTLC was performed on silica gel coated aluminium sheets using ethyl acetate with 0.5% acetic acid as mobile phase. The radioTLC were analysed on a autoradiography system (Instant Imager, Canberra).

*2-[5-bromo-6-[[3-[2,6-dimethyl-4-(3-methylsulfonylpropoxy)phenyl]phenyl]methoxy]2,3-dihydrobenzofuran-3-yl]acetic acid (**3**)*

2-[6-[[3-[2,6-dimethyl-4-(3-methylsulfonylpropoxy)phenyl]phenyl]methoxy]2,3-dihydro-benzofuran-3-yl]acetic acid (**1**) (30 mg, 57.2 µmol) was dissolved in 3 ml DCM and N-bromsuccinimide (10.2 mg, 57.2 µmol) was added at room temperature. The solution was stirred for 30 min and the mixture was evaporated to dryness to afford 39 mg of (**3**). The product was used in the next step without further purification. MS (ESI-) m/z: 601/603 $[M-H]^-$

*2-[6-[[3-[2,6-dimethyl-4-(3-methylsulfonylpropoxy)phenyl]phenyl]methoxy]5-tritio-2,3-dihydrobenzofuran-3-yl]acetic acid (**1a**)*

2-[5-bromo-6-[[3-[2,6-dimethyl-4-(3-methylsulfonylpropoxy)phenyl]phenyl]methoxy]2,3-dihydrobenzofuran-3-yl]acetic acid (**3**) (9 mg, 14.9 µmol), methanol (0.7 mL), Et_3N (20.7 µL, 0.3 mmol) and Pd/C (2 mg, Pd dry 5% Heraeus K02102) were placed in a 1 mL reaction vessel. The vessel was connected to a tritium manifold, cooled with liquid nitrogen and $[^3H_2]$ (0.27 mg, 44.7 µmol, 96 GBq, 2.6 Ci) was added. The reaction mixture was allowed to reach room temperature (pressure inside 220 mbar) and stirred for 4 hours. After three times removal of all the volatiles by addition and removal of methanol, the residue was purified by HPLC to afford [^3H] compound (**1a**) (4.5 mg, 8.55 µmol, 5146 MBq, 139 mCi, 57.5% chemical yield; 5.3 % RCY). ^1H NMR (500 MHz, DMSO-d_6) δ: 1.91 (s, 6H), 2.14-2.25 (m, 4H), 3.05 (s, 3H), 3.62-3.71 (m, 3H), 4.21 (t, *J* = 6 Hz, 1H), 4.35 (t, *J* = 5 Hz, 2H), 4.65 (t, *J* = 6 Hz, 1H), 5.12 (s, 2H), 6.45 (s, 1H), 6.7 (s, 2H), 7.05 (d, *J* = 7.5 Hz, 1H), 7.1 (d, *J* = 8.5 Hz, 1H), 7.15 (s, 1H), 7.38 (d, *J* = 8 Hz, 1H), 7.45 (t, *J* = 7.5 Hz, 1H); ^3H NMR (533 MHz, DMSO-d_6) δ: 6.47 (s, 1H) ppm; HPLC RD purity: 99.3%; 1143 MBq/mg, 599 GBq/mmol, 16.2 Ci/mmol; MS (ESI+)(%) m/z: 465 $[M-HCO2H]^+$ (27); 525 $[M+H]^+$(100); 549 $[M+Na]^+$ (12); 565 $[M+K]^+$(6).

*Methyl-2-[(3S)-6-[[3-(4-allyloxy-2,6-dimethyl-phenyl)phenyl]methoxy]2,3-dihydrobenzo-furan-3-yl]acetate(**5**)*

Methyl-2-[(3S)-6-[[3-(4-hydroxy-2,6-dimethyl-phenyl)phenyl]methoxy]2,3-dihydrobenzo-furan-3-yl]acetate (**4**) (762 mg, 1.8 mmol) and cesium carbonate (705 mg, 2.2 mmol) were dissolved in 9 mL of acetonitrile under argon. Allyl bromide (740 µL, 8.4 mmol) was added to the solution and the mixture was allowed to stir under microwave heating (45 min, 110°C microwave assisted, 30 sec pre-stirring). Insolubles were removed by filtration and the mixture was evaporated under reduced pressure. The crude product was then diluted in Et_2O and filtered again to remove the last traces of cesium carbonate and evaporated to afford (**5**) methyl 2-[(3S)-6-[[3-(4-allyloxy-2,6-dimethyl-phenyl)phenyl]methoxy]2,3-dihydrobenzo-furan-3-yl]acetate as a yellowish oil (765 mg, 1.7 mmol, yield 94%). ^1H NMR (500 MHz, $CDCl_3$) δ: 1.99 (s, 6H), 2.55 (dd, 1H, *J* = 16.6, 9.0 Hz), 2.75 (dd, 1H, *J* = 16.6, 5.6 Hz), 3.71 (s, 3H), 3.79 (m, 1H, *J* = 9.4, 9.0, 6.1, 5.6 Hz), 4.25 (dd, 1H, *J* = 9.4, 6.1 Hz), 4.54 (dd, 2H, *J* = 5.2 Hz), 4.74 (t, 1H, *J* = 9.0 Hz), 5.05 (s, 2H), 5.28 (dd, 1H, *J* = 10.4, 1.4 Hz), 5.41 (dd, 1H, *J* = 17.3, 1.4 Hz), 6.07 (ddd, 1H, *J* = 17.3, 10.4, 5.2 Hz), 6.46 (d, 1H, *J* = 2.2 Hz), 6.49 (dd, 1H, *J* = 8.2, 2.2 Hz), 6.67 (s, 2 H), 7.02 (d, 1H, *J* = 8.2 Hz), 7.09 (d, 1H, *J* = 7.4 Hz), 7.17 (s, 1H), 7.38 (d, 1H, *J* = 7.7 Hz), 7.41 (t, 1H, *J* = 7.4 Hz); ^{13}C NMR (125 MHz, $CDCl_3$) δ: 21.1, 37.8, 39.5, 51.8, 68.7, 70.3, 97.5, 107.3, 113.4, 117.5, 121.5, 124.3, 125.5, 128.6, 128.7, 129.2, 133.6, 134.4, 137.1, 137.4, 141.1, 157.4, 159.4, 161.1, 172.4 ppm; HRMS(ESI-TOF) m/z: [M-H]: Calcd for $C_{29}H_{29}O_5$: 457.2020; Found: 457.2056.

*2-[(3S)-6-[[3-(4-allyloxy-2,6-dimethyl-phenyl)phenyl]methoxy]2,3-dihydrobenzofuran-3-yl] acetic acid (free acid of **5**)*

Methyl ester (**5**) (15 mg, 32.7 µmol) was dissolved in 250 µL of THF and 100 µL of methanol before 65 µL of 1N aqueous NaOH (65 µmol) were added. The mixture was allowed to stir at room temperature for 45 minutes. The mixture was concentrated, diluted with water, acidified with 1M HCl aqueous solution down to pH = 2 and extracted with ethyl acetate three times. The organic layer was evaporated under reduced pressure to afford compound (**5a**) 2-[(3S)-6-[[3-(4-allyloxy-2,6-dimethyl-phenyl)phenyl]methoxy]2,3-dihydrobenzofuran-3-yl]acetic acid as a white powder (m = 11.8 mg, 26.5 µmol, yield 81%). ^1H NMR (600 MHz, $CDCl_3$) δ: 2.01 (s, 6H), 2.63 (dd, 1H, *J* = 16.8, 9.2 Hz), 2.82 (dd, 1H, *J* = 16.8, 5.3 Hz), 3.83 (m, 1H, *J* = 9.2, 9.0, 6.2, 5.3 Hz), 4.30 (dd, 1H, *J* = 9.0, 6.2 Hz), 4.56 (d, 2H, *J* = 5.2 Hz), 4.78 (t, 1H, *J* = 9.0 Hz), 5.08 (s, 2H), 5.30 (dd, 1H, *J* = 10.4, 1.0 Hz), 5.44 (dd, 1H, *J* = 17.3, 1.0 Hz), 6.10 (ddd, 1H, *J* = 17.3, 10.4, 5.2 Hz), 6.48 (s, 1H), 6.52 (dd, 1H, *J* = 8.2 Hz), 6.70 (s, 2 H), 7.06 (d, 1H, *J* = 8.2 Hz), 7.10 (d, 1H, *J* = 7.4 Hz), 7.19 (s, 1H), 7.39 (d, 1H, *J* = 7.4 Hz), 7.43 (t, 1H, *J* = 7.4 Hz); ^{13}C NMR (150 MHz, $CDCl_3$) δ: 20.6, 37.1, 38.6, 68.3, 69.9, 97.1, 107.0, 113.0, 116.9, 120.7, 123.8, 125.0, 128.1, 128.2, 128.7, 133.1, 133.9, 136.6, 136.9, 140.7, 156.9, 159.6, 160.6, 175.5 ppm; HRMS (ESI-TOF) m/z: [M-H]: Calcd for $C_{28}H_{27}O_5$: 443.1863; Found: 443.1935.

*(S)-methyl-2-(6-((4'-(3-((3-hydroxypropyl)sulfonyl)propoxy)-2',6'-dimethyl-[1,1'-biphenyl]3-yl)methoxy)-2,3-dihydrobenzofuran-3-yl)acetate (**6**)*

A mixture of thio-propanol (150 µL, d= 1.07, 1.83 mmol) and alkene **5** (158 mg, 345 µmol) were dissolved in dry dioxane (1 mL) under argon. The mixture was allowed to stir under argon at 75°C for 3 hours. The mixture was evaporated and then diluted in 500 µL of acetonitrile and 4500 µL of water were added which resulted in precipitation of the product. The product was washed once with 250 µL acetonitrile/4750 µL water, and finally once with 4000 µL of water, before being redissolved in acetonitrile and evaporated. The crude was subsequently dissolved in 2.5 mL of DCM and the mixture was cooled down to -10°C with an ice/NaCl bath. Then mCPBA (200 mg, 862 µmol) previously dissolved in 500 µL of DCM was added and the mixture was allowed to stir from -10°C to room temperature for 2 hours. Then, the reaction was quenched with 3 mL of a saturated $NaHCO_3$ solution to get rid of the excess of mCPBA and diluted with DCM and water. The organic phase was washed three times with water, dried over magnesium sulfate and evaporated under reduced pressure to afford compound **6** as yellowish oil. (S)-methyl 2-(6-((4'-(3-((3-hydroxypropyl)sulfonyl) propoxy)-2',6'-dimethyl-[1,1'-biphenyl]3-yl)methoxy)-2,3-dihydrobenzofuran-3-yl)acetate (177.6 mg, 304.8 µmol, 88 % yield). ^{1}H NMR (500 MHz, $CDCl_3$) δ: 1.99 (s, 6H), 2.13 (m, 2H), 2.35 (m, 2H), 2.56 (dd, 1H, *J* = 16.2, 9.2 Hz), 2.75 (dd, 1H, *J* = 16.2, 5.5 Hz), 3.17 (t, 2H, *J* = 7.5 Hz), 3.25 (t, 2H, *J* = 7.5 Hz), 3.72 (s, 3H), 3.79 (m, 1H), 3.83 (t, 2H, *J* = 5.9 Hz), 4.12 (t, 2H, *J* = 5.7 Hz), 4.25 (dd, 1H, *J* = 9.2, 6.1 Hz), 4.75 (t, 1H, *J* = 9.0 Hz), 5.05 (s, 2H), 6.44 (d, 1H, *J* = 2.1 Hz), 6.47 (dd, 1H, *J* = 8.1, 2.1 Hz), 6.64 (s, 2 H), 7.00 (d, 1H, *J* = 8.1 Hz), 7.07 (d, 1H, *J* = 7.5 Hz), 7.15 (s, 1H), 7.36 (d, 1H, *J* = 7.5 Hz), 7.41 (t, 1H, *J* = 7.5 Hz); ^{13}C NMR (125 MHz, $CDCl_3$) δ: 21.2, 22.4, 25.0, 29.7, 37.8, 39.5, 50.0, 50.1, 51.8, 60.6, 65.4, 70.3, 77.6, 97.5, 107.3, 113.2, 121.5, 124.3, 125.6, 128.6, 128.7, 129.1, 134.8, 137.2, 137.7, 140.9, 157.1, 159.9, 161.1, 172.4 ppm**;** HRMS (ESI-TOF) m/z: [M-H]: Calcd for $C_{32}H_{37}O_8S$: 581.2215; Found: 581.2241.

*(S)-2-(6-((4'-(3-((3-hydroxypropyl)sulfonyl)propoxy)-2',6'-dimethyl-[1,1'-biphenyl]3-yl)meth-oxy)-2,3-dihydrobenzofuran-3-yl)acetic acid (free acid of **6**)*

Methyl ester **6** (8 mg, 13.7 µmol) was dissolved in 150 µL of THF and 50 µL of methanol before the addition of 1M aqueous NaOH (28 µL, 28 µmol). The mixture was allowed to stir at room temperature for 60 minutes. Then, the reaction was neutralized with 28 µL of a 1M HCl aqueous solution and diluted with acetonitrile/water (1/1) before being submitted to HPLC purification to afford compound **6a** as a white powder after lyophilization.

(S)-2-(6-((4'-(3-((3-hydroxypropyl)sulfonyl)propoxy)-2',6'-dimethyl-[1,1'-biphenyl]3-yl) methoxy)-2,3-dihydrobenzofuran-3-yl)acetic acid (3.4 mg, 6.0 µmol, 44 % yield). ^{1}H NMR (600 MHz, d_6-DMSO) δ: 1.83 (m, 2H), 1.85 (s, 1H), 1.91 (s, 6H), 2.12 (m, 2H), 2.47 (dd, 1H, *J* = 16.4, 9.0 Hz), 2.66 (dd, 1H, *J* = 16.4, 5.5 Hz), 3.15 (t, 2H, *J* = 7.8 Hz), 3.24 (t, 2H, *J* = 7.8 Hz), 3.49 (t, 2H, *J* = 6.0 Hz), 3.66 (m, 1H), 4.09 (t, 2H, *J* = 6.2 Hz), 4.17 (dd, 1H, *J* = 9.2, 6.8 Hz), 4.66 (t, 1H, *J* = 9.0 Hz), 5.09 (s, 2H), 6.44 (s, 1H), 6.48 (dd, 1H, *J* = 8.2 Hz), 6.70 (s, 2 H), 7.05 (d, 1H, *J* = 7.5 Hz), 7.08 (d, 1H, *J* = 8.2 Hz), 7.13 (s, 1H), 7.37 (d, 1H, *J* = 7.5 Hz), 7.43 (t, 1H, *J* = 7.5 Hz); ^{13}C NMR (150 MHz, d_6-DMSO) δ: 20.7, 21.7, 24.8, 37.1, 48.7, 49.1, 58.9, 65.4, 69.3, 77.1, 96.9, 106.9, 113.3, 121.9, 124.5, 125.8, 128.4, 128.5, 128.7, 133.9, 136.6, 137.3, 140.2, 156.9, 159.1, 160.6, 173.0 ppm; HRMS (ESI-TOF) m/z: [M-H]: Calcd for $C_{31}H_{35}O_8S$: 567.2058; Found: 567.2136.

(S)-methyl-2-(6-((2',6'-dimethyl-4'-(3-((3-(tosyloxy)propyl)sulfonyl)propoxy)-[1,1'-biphenyl] 3-yl)methoxy)-2,3-dihydrobenzofuran-3-yl)acetate *(**7**)*

Alcohol **6** (42.4 mg, 76.7 µmol), triethylamine (15 µl, 109 µmol), and tetramethylhexane-1,6-diamine (1.5 µl, 7.3 µmol) were dissolved in 500 µL of toluene and 500 µL of DCM, before the addition of a solution of tosyl-chloride (21.1 mg, 110.7 µmol) previously dissolved in 200 µL of DCM. The reaction was allowed to stir overnight at room temperature. Complete conversion of the starting material was reached after three successive additions of 0.5 eq triethylamine, 0.1 eq tetramethylhexane-1,6-diamine and 0.5 eq tosyl-chloride (dissolved in DCM). The mixture was directly purified via silica gel chromatography (4 g silica column, 0-50% EtOAc/Hept over 20 min). Collected fractions were evaporated under reduced pressure to afford compound **7** as a colorless oil. (S)-methyl 2-(6-((2',6'-dimethyl-4'-(3-((3-(tosyloxy)propyl)sulfonyl)propoxy)-[1,1'-biphenyl]3-yl)methoxy)-2,3-dihydrobenzofuran-3-yl)acetate (42.7 mg, 60.0 µmol, 78 % yield). ^{1}H NMR (500 MHz, $CDCl_3$) δ: 1.99 (s, 6H), 2.25 (m, 2H), 2.32 (m, 2H), 2.45 (s, 3H), 2.54 (dd, 1H, *J* = 16.2, 9.2 Hz), 2.75 (dd, 1H, *J* = 16.2, 5.5 Hz), 3.09 (t, 2H, *J* = 7.5 Hz), 3.20 (t, 2H, *J* = 7.5 Hz), 3.72 (s, 3H), 3.80 (m, 1H), 4.10 (t, 2H, *J* = 5.9 Hz), 4.19 (t, 2H, *J* = 5.7 Hz), 4.25 (dd, 1H, *J* = 9.2, 6.1 Hz), 4.74 (t, 1H, *J* = 9.0 Hz), 5.05 (s, 2H), 6.45 (d, 1H, *J* = 2.1 Hz), 6.47 (dd, 1H, *J* = 8.1, 2.1 Hz), 6.64 (s, 2 H), 7.00 (d, 1H, *J* = 8.1 Hz), 7.07 (d, 1H, *J* = 7.5 Hz), 7.15 (s, 1H), 7.36 (m, 3H, *J* = 8.2, 7.5 Hz), 7.41 (t, 1H, *J* = 7.5 Hz), 7.78 (d, 2H, *J* = 8.2 Hz); ^{13}C NMR (125 MHz, $CDCl_3$) δ: 14.1, 21.1, 21.7, 21.9, 22.3, 22.7, 31.9, 37.8, 39.5, 49.1, 50.4, 51.8, 65.3, 68.0, 70.3, 77.6, 97.4, 107.3, 113.2, 121.5, 124.3, 125.6, 127.9, 128.6, 128.7, 129.1, 130.1, 132.5, 134.9, 137.1, 137.7, 140.9, 145.3, 157.1, 159.9, 161.1, 172.3 ppm; HRMS (ESI-TOF) m/z: $[M+H+Na]^+$: Calcd for $C_{39}H_{44}NaO_{10}S_2$: 759.2268; Found: 759.2089.

*(S)-2-(6-((4'-(3-((3-fluoropropyl)sulfonyl)propoxy)-2',6'-dimethyl-[1,1'-biphenyl]3-yl)methoxy)-2,3-dihydrobenzofuran-3-yl)acetic acid (**2**)*

Alcohol **6** (30.2 mg, 49.2 µmol) was dissolved in 3 mL of DCM and cooled down at 0°C before the addition of deoxofluor (30 µL, 81.4 µmol). The reaction was allowed to warm up from 0°C to room temperature under agitation for 90 min. Volatiles were removed under reduced pressure and the crude was taken up into 750 µL of THF and 250 µL of methanol. Then 125 µL of 1N aqueous NaOH (125 µl, 125 µmol) were added to the mixture and the reaction was allowed to stir at room temperature for 2 hours. Finally, the reaction was neutralized with 125 µL of a 1M HCl aqueous solution and diluted with acetonitrile/water before being submitted to hplc purification to afford compound **2a** as a white powder after lyophilization. (S)-2-(6-((4'-(3-((3-fluoropropyl)sulfonyl)propoxy)-2',6'-dimethyl-[1,1'-bi-phenyl]3-yl)methoxy)-2,3-dihydrobenzofuran-3-yl)acetic acid (8.5 mg, 14.9 µmol, 30 % yield). ^{1}H NMR (600 MHz, d_6-DMSO) δ: 1.91 (s, 6H), 2.05-2.20 (m, 4H), 2.47 (dd, 1H, *J* = 16.5, 9.1 Hz), 2.66 (dd, 1H, *J* = 16.5, 5.5 Hz), 3.24-3.32 (m, 4H), 3.66 (m, 1H), 4.09 (t, 2H, *J* = 6.2 Hz), 4.17 (dd, 1H, *J* = 9.2, 6.8 Hz), 4.50-4.62 (dt, 2H, $^{2}J(F-H)$ = 47.0 Hz, *J* = 5.9 Hz), 4.67 (t, 1H, *J* = 9.0 Hz), 5.09 (s, 2H), 6.44 (s, 1H), 6.46 (dd, 1H, *J* = 8.2 Hz), 6.70 (s, 2 H), 7.04 (d, 1H, *J* = 7.5 Hz), 7.08 (d, 1H, *J* = 8.2Hz), 7.13 (s, 1H), 7.36 (d, 1H, *J* = 7.5 Hz), 7.43 (t, 1H, *J* = 7.5 Hz); ^{13}C NMR (150 MHz, d_6-DMSO) δ: 20.4, 21.3, 22.4, 22.5, 36.8, 38.6, 47.7, 47.8, 48.5, 65.1, 69.1, 76.8, 81.2, 82.3, 96.7, 106.7, 113.0, 121.7, 124.2, 125.6, 128.2, 128.3, 128.5, 133.6, 136.3, 137.1, 139.9, 156.6, 158.8, 160.4, 172.8; ^{19}F NMR (400 MHz, d_6-DMSO) δ: -217.02 ppm (septet); HRMS (ESI-TOF) m/z: [M-H]: Calcd for $C_{31}H_{34}FO_7S$: 569.2015; Found: 569.2071.

*Condition screening for the displacement of tosylate **7** with KF*

In a microwave tube were dissolved tosylate (**7**) (1 eq, 7.5 µmol), KF (2 eq), K_2CO_3 (0.8 eq) and Kryptofix $K_{2,2,2}$ (1.5 eq) in 200 µL of anhydrous acetonitrile. The tube was sealed under argon and the sample was stirred at room temperature for 10 min or was heated under microwaves irradiations at 40°C, 100°C and 130°C for either 2, 5, 10 or 15 min. Indicated yields were determined from LC-MS profile by integration of the UV signal at 220 nm. No purifications were performed. No internal standard was used.

*(S)-2-(6-((4'-(3-((3-[^{18}F]fluoropropyl)sulfonyl)propoxy)-2',6'-dimethyl-[1,1'-biphenyl]3-yl)methoxy)-2,3-dihydrobenzofuran-3-yl)acetic acid (**2a**)*

N.c.a. [^{18}F]fluoride was produced via the ^{18}O(p,n)^{18}F nuclear reaction at a Scanditronix MC35 cyclotron using ≥97% enriched ^{18}O-water in a 2.5 mL liquid target. N.c.a. [^{18}F]fluoride (~2-5 GBq) was trapped on a preconditioned SepPak® light accell plus QMA-cartridge (Waters AG / ABX). The [^{18}F]fluoride was eluted directly into a 5 mL sealed glass reaction vessel using a solution of 300 µL of an aqueous solution of potassium carbonate (1.65 mg, 12 µmol) and 850 µL of Kryptofix $K_{2,2,2}$ (10 mg, 26.5 µmol) in ACN. The reaction vessel was placed in a heating block and the solution was dried azeotropically under reduced pressure and a stream of argon for 10-15 min at 100°C. The argon was removed and the reaction vessel was further dried under full vacuum for at least 5 min at 100°C. Subsequently, the tosylate precursor (**7**) (5.0 mg, 6.8 µmol) previously dissolved in 1 mL of anhydrous acetonitrile was added to the dry ^{18}F-cryptate-complex and heated at 100°C. Over a period of 15 min, aliquots of 10 µL were taken and analyzed by radioTLC. The reaction mixture was allowed to cool to room temperature, and 1 mL of a mixture of 250 µL of methanol and 250 µL of a 2.5M NaOH aqueous solution was added, and the reaction was kept at room temprerature for 5 min. For neutralization, the mixture was quenched with 500 µL of a 1.25M aqueous HCl solution, and filled with water (1.5 mL). The product was obtained in 16.7% ± 5.7% RCY with a specific activity of ≥0.6 GBq/µmol. Total time of synthesis was 60–70 min.

R_f-values were as follows: [^{18}F]fluoride: 0.0, ^{18}F-labelled protected intermediate: 0.9, product **2** and **2a**: 0.8. Analytical radioHPLC retention time of product **2** and **2a** was 14.7 min.

Chapter 4

Mild and selective mono-iodination of unprotected peptides as initial step for the synthesis of bioimaging probes

Romain Bertrand[1,2], Michael Wagner[1], Volker Derdau[3], and Oliver Plettenburg[1,4,5]

[1]Diabetes Division, Research & Translational Medicine, Sanofi GmbH, Frankfurt am Main 65926, Germany
[2]Department of Nuclear Medicine, Radboud UMC, Nijmegen 6525, The Netherlands
[3]DSAR/Drug Disposition, Sanofi GmbH, Frankfurt am Main 65926, Germany
[4]Institute of Medicinal Chemistry, Helmholtz Zentrum München, Ingolstaedter Landstr. 1, Neuherberg 85764, Germany
[5]Leibniz University Hannover, Schneiderberg 1 B, Hannover 30167, Germany

Adapted from: ACS Bioconjugate Chemistry, **2016**, *27* (10), pp 2281–2286, "*Mild and Selective Mono-Iodination of Unprotected Peptides as Initial Step for the Synthesis of Bioimaging Probes"*.
DOI: 10.1021/acs.bioconjchem.6b00461

Abstract

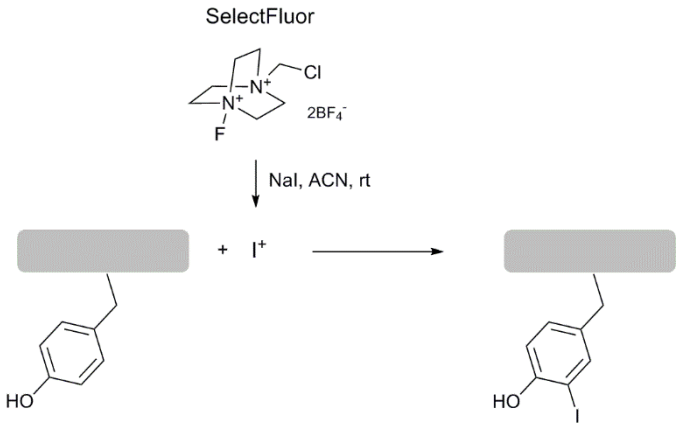

Chemoselective functionalization of peptides and proteins to selectively introduce residues for detection, capturing or specific derivatization is of high interest to the synthetic community. Here we report a new method for the mild and effective mono-iodination of tyrosine residues within fully unprotected peptides. This method is highly chemoselective and compatible with a wide variety of functional groups. The introduced iodine can subsequently serve as a handle for further functionalization such as introduction of fluorescent dyes and thus be used for chemoselective labeling of isolated peptides.

Introduction

While incorporation of conjugation sites into small peptides can be easily achieved at will by selection of appropriately functionalized amino acid building blocks for solid phase peptide synthesis, selective functionalization of isolated peptides and proteins not containing protecting groups still remains a challenging task. Among the 20 naturally occurring amino acids, the most relevant ones for bioconjugation purposes are cysteine and lysine as they can act as potent nucleophiles.[1] However, the high abundance of lysine on protein surfaces makes specific acylation challenging and non-oxidized cysteines are less frequently displayed on protein surfaces. As they are most often involved in disulfide bridges in their natural environment, reduction of the target disulfide is a prerequisite before labeling, which may also alter the overall structure of the target protein. Therefore the development of additional modification techniques targeting alternative amino acids remains of high significance.

Tyrosine offers a wide range of reactivities: the phenolate ring may be O-alkylated;[2] it can undergo electrophilic addition using diazonium derivaties[3] or can be involved in Mannich-type condensations[4] and reactions with ene-type electrophiles.[5] Owing to the electron-rich aromatic ring, tyrosine residues can also be a target for halogenation. Notably, iodination is of particular importance due to its utility for further transformations. It has been used to label biomolecules for a wide variety of purposes, such as mass spectrometry,[6] to help in the elucidation of foldamer structures[7] or to improve the self-assembly properties of peptides.[8] Moreover, tyrosine iodination with ^{125}I for the radiolabeling of compounds of medical and biological interest is the method of choice owing to its high specific radioactivity and convenience in counting γ-emissions.[9] Iodinations are carried out either enzymatically, for example by the enzyme thyroid peroxidase,[10] or by direct electrophilic aromatic substitution using an iodinating agent such as N-iodosuccinimide[11] or Barluenga's reagent.[12] Other alternatives involve the combination of sodium iodide with strong oxidizing agents like Iodogen[13,14] or Chloramin-T.[13,15] However, existing methods display limitations as iodination frequently results in a mixture of unreacted starting material, mono- and di-iodinated peptides,[9,11,13-30] which reduce yields and may also impose challenges in product purification. Formation of oxidized peptides[9,16,19] and histidine labeling[9,20,21] have also been described as limiting factors. For most applications a mono-iodinated version of the compound of interest would be highly desirable in order to minimize the negative influence of the added substituents on the activity of the target biomolecule. Indeed, examples were reported where the di-iodinated peptide exhibited a 3 to 10-fold lower receptor binding activity whereas the binding of the mono-iodinated was maintained.[17,18] Accordingly, further investigations towards a selective iodination method yielding selectively a mono-iodinated tyrosine are of high interest.

Here we present a new and efficient iodinating agent allowing highly controlled mono-iodination reactions and demonstrate its utility in the preparation of a wide range of fully unprotected and complex biologically active peptides.

Results and Discussion

We explored the combination of sodium iodide and Selectfluor in the search of a mild and selective iodinating reagent for tyrosine (Scheme 1, Supp Info 1).

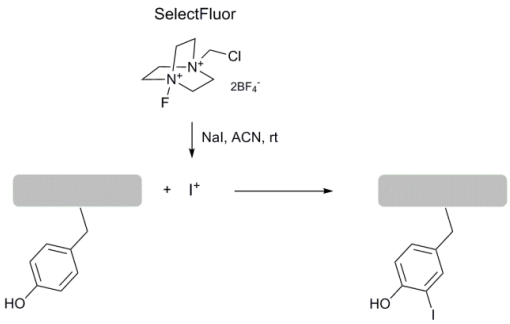

Scheme 1 Iodination of tyrosine with sodium iodide activated by Selectfluor

We first examined the iodination reaction in different solvents on the protected tyrosine Ac-Tyr-NH-Me as a model system to mimic the reactivity of a tyrosine incorporated in a peptide sequence. The reaction employing a slight excess (1.1 eq) of Selectfluor and NaI proceeded instantly at room temperature, affording a mixture of unreacted starting material (SM), mono-iodinated product (MI) and di-iodinated product (DI). Extending the reaction time to 120 min did not have an impact on the conversion rate (Supp Info 2). A strong influence of the solvent and pH was observed (Table 1). Aprotic polar solvents (entries 1, 2) or aqueous systems (entries 3 to 6) favored the formation of the di-iodinated product. Dichloromethane supplemented with TFA (entries 7 to 11) proved to be the optimal conditions to achieve a controlled mono-iodination. Addition of TFA allowed proper dissolution of the starting material but, more importantly, positively modulated the iodination reactivity. Besides, most peptides are soluble on 1%-20% TFA/DCM, these conditions are commonly used for cleavage of resins with hyperacid labile linker systems like SASRIN, HAL or chlorotrityl. We assume that, after conversion of the iodide of NaI to an electrophilic iodonium species I^+ by Selecfluor, the reaction proceeds via an electrophilic substitution mechanism as previously postulated by Syvret *et al.*[22]

We further applied the iodination reaction to other amino acids containing aromatic residues, phenylalanine, tryptophane, and histidine, that are prone to undergo electrophilic aromatic substitutions. Under these conditions, no formation of iodinated product was observed (Supp info 3).

We started to investigate the optimised iodination conditions on multifunctional, fully unprotected peptides. A total of eight biologically relevant peptides, either commercially available or prepared in our laboratory, were surveyed: Leucine-Enkephalinamide (agonist of μ and δ opioid receptors), Angiotensin III (agonist of AT_1 and AT_2 receptors), Cyclo(RGDyK) (high affinity αvβ3 integrin ligand), ACP fragment (65-74) (fragment of the acyl carrier protein), Goserelin (superagonist of LH- releasing hormone), Tocinoic acid (agonist of the oxytocin receptor), AcMeYVAD-CHO (reversible inhibitor of caspase-1), [Tyr^0]-Bradykinin (ligand of the kinin B_1 and B_2 receptors) (Table 2, entries 1-8).

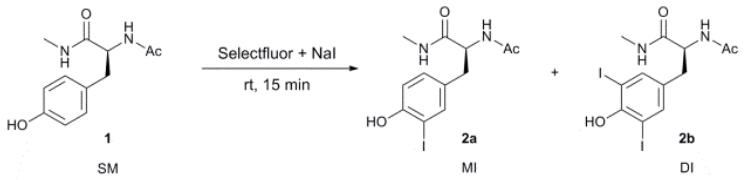

Entry	Solvent	TFA	SM **1** (%)[a]	MI **2a** (%)	DI **2b** (%)
1	DMSO	-	49	7	44
2	DMF	-	45	24	31
3	tBuOH/H_2O (5/1)	-	17	57	26
4	MeOH/DCM	-	23	54	23
5	H_2O/ACN (1/1)	-	22	44	33
6	H_2O/ACN (1/1)	10% TFA	27	57	16
7	DCM	1% TFA	46	48	6
8	DCM	5% TFA	46	53	1
9	DCM	10% TFA	47	53	-
10	DCM	20% TFA	54	46	-
11[b]	DCM	20% TFA	6	86	8

[a] SM=Starting material, MI=Mono-iodinated product, DI=Di-iodinated product. Relative ratio dertermined by LC/MS at 215 nm. [b] After extra addition of 2x0.25 eq of iodinating reagent.

Table 1 Solvent screening for the mono-iodination of Ac-Tyr-NH-Me **1**

The peptides studied were structurally diverse and collectively included i) other aromatic amino acids, ii) a free acid at the C-terminus, iii) a disulfide bridge between two cysteines, iv) cyclic structures, v) non-natural amino acid, and vi) an aldehyde function. Since the typical protein absorbance at 280 nm can shift to a maximum around 315 nm due to the iodination of the tyrosine phenolate ring,[23] we decided to carry out the analysis via LC-MS at 215 nm absorbance to quantify the relative amounts of starting material (SM), mono-iodinated product (MI) and di-iodinated product (DI). In all cases, the mono-iodinated product was the most predominant with a relative ratio of 88% to 97% as outlined in Table 2. The position of the tyrosine in the sequence did not seem to have an influence on the mono-iodination efficacy. An example is shown on Scheme 2, the mild mono-iodination reaction proceeded cleanly in the presence of a tryptophane residue, an aza-peptide moeity, and a tert-butyl protected serine which remained untouched. Interestingly, this method delivered superior results compared to a previously reported approach using N-iodosuccinimide in the case of Cyclo(RGDyK).[11]

Entry	Peptide	Sequence	Results[a]	Yield[b]
1	AcMeYVAD-CHO	Ac-(NMe)**Tyr**-Val-Ala-Asp-CHO	SM: 8.3% / **MI: 91.7%** / DI: - %	[c]
2	Tocinoic acid	H-Cys-**Tyr**-Ile-Gln-Asn-Cys-OH	SM: 5.5% / **MI: 93.1%** / DI: 1.4%	[c]
3	Goserelin	Glp-His-Trp-Ser-**Tyr**-Ser(tBu)-Leu-Arg-Pro-azaGly-NH_2	SM: - % / **MI: 97.4%** / DI: 2.6%	[c]
4	Leu-Enkephalinamide	H-**Tyr**-Gly-Gly-Phe-Leu-NH_2	SM: 1.0% / **MI: 88.2%** / DI: 10.8%	62%
5	Angiotensin III	H-Arg-Val-**Tyr**-Ile-His-Pro-Phe-NH_2	SM: 6.2% / **MI: 91.3%** / DI: 2.5%	74%
6	ACP fragment (65-74)	H-Val-Gln-Ala-Ala-Ile-Asp-**Tyr**-Ile-Asn-Gly-NH_2	SM: 2.3% / **MI: 93.7%** / DI: 4.0%	63%
7	Cyclo(RGDyK)	Cyclo(Arg-Gly-Asp-D-Tyr-Lys)	SM: 5.5% / **MI: 88.3%** / DI: 6.2%	77%
8	[Tyr^0]-Bradykinin	H-**Tyr**-Arg-Pro-Pro-Gly-Phe-Ser-Pro-Phe-Arg-OH	SM: 1.9% / **MI: 92.7%** / DI: 5.4%	72%
9	[Tyr^1]-Substance P	H-Arg-Pro-Lys-Pro-Gln-Gln-Phe-**Tyr**-Gly-Leu-Met-NH_2[d]	SM: 5.9% / **MI: 93.6%** / DI: 0.5%	72%
10	GLP-1 (7-37)	H-His-Ala-Glu-Gly-Thr-Phe-Thr-Ser-Asp-Val-Ser-Ser-**Tyr**-Leu-Glu-Gly-Gln-Ala-Ala-Lys-Glu-Phe-Ile-Ala-Trp-Leu-Val-lys-Gly-Arg-Gly-NH_2	SM: 4.5% / **MI: 91.3%** / DI: 4.1%	52%

[a] Reactions were monitored using LC-MS and the relative amounts of starting material (SM), monoiodinated product (MI) and the diiodination product (DI) were quantified using area under the curve integration (absorbance at 215 nm). [b] Isolated yields after HPLC purification. [c] Not isolated. [d] Methionine oxidation was detected as described in Fig. 3.

Table 2 Mono-iodination of multifunctional, fully unprotected peptides with Selecfluor and NaI

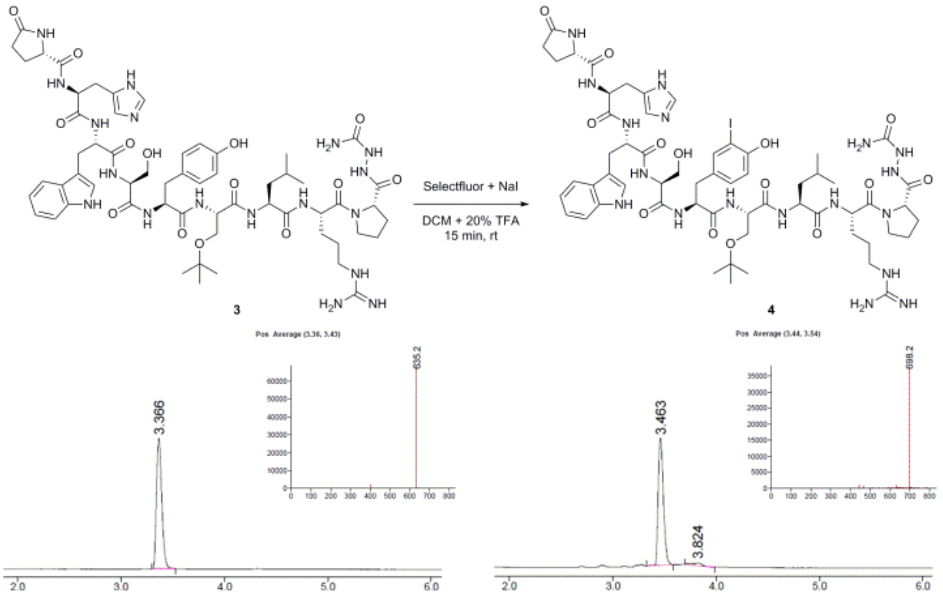

Scheme 2 Mono-iodination of Goserelin with Selecfluor and NaI

Next, we applied our method on a peptide containing a methionine residue: [Tyr[8]]-Substance P (ligand of the neurokinin-1 receptor) (entry 9). The ability of sulfur to react with halonium in acidic conditions is known and widely exploited e.g. in glycosylation chemistry where thioglycosides can serve as glycoside donors[143]. As expected, when reacting the peptide with the first equivalent of iodination reagent, we observed oxidation at the methionine residue, but also formation of the desired mono-iodinated product (around 25%). However, total consumption of both starting material and oxidized starting material was reached by careful addition of excess iodination reagent (2x0.35 eq) to afford an almost exclusive mixture of the mono-iodinated product and its oxidized methionine analog (Supp. info 4).

We then searched for a strategy to effectively reduce the oxidized mono-iodinated product, while keeping the reduced version intact. Several reagents have been reported for the reduction of methionine sulfoxide residue in peptides: trimethylsilyl bromide with 1,2-ethanedithiol, N-methyl mercapto-acetamide, tetrabutylammonium bromide or ammonium iodide with dimethylsulfide. Treatment of the peptide reaction mixture with either Bu_4NBr or NH_4I–Me_2S in TFA were successful in reducing the oxidized methionine but led to formation of byproducts, rendering these conditions ineffective. Finally, the use of potassium iodide and ascorbic acid in TFA[24] offered a very clean conversion of the methionine sulfoxide to the desired reduced peptide (Scheme 3, Supp. Info 4). Nicolas *et al.*[25] reports this reduction to proceeding via nucleophilic iodide attack on the protonated sulfoxide leading to the methionine sulfide and elemental iodine. The latter directly reacts with the ascorbic acid, with the consumption of the generated iodine driving further the reduction forward.[24]

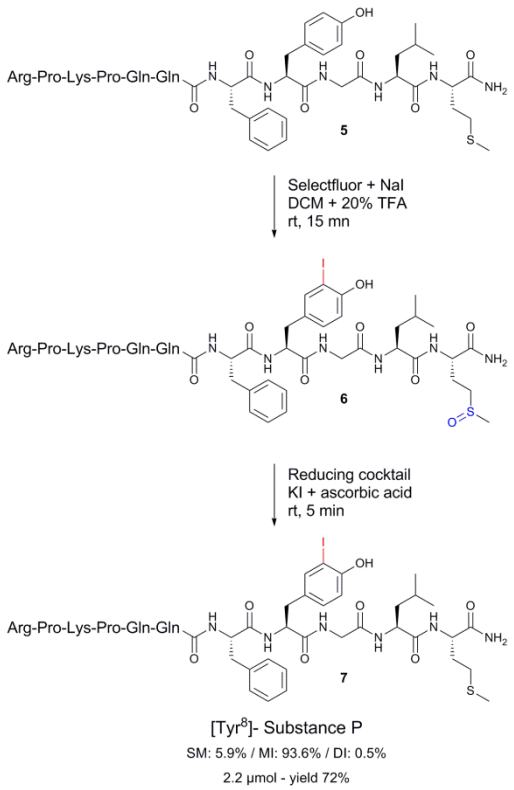

Scheme 3 Mono-iodination strategy for a methionine-containing peptide [Tyr^{8}]-Substance P

To verify the relevance of the method, mono-iodinations of Cyclo(RGDyK), Leucin-Enkephalinamide, [Tyr^{0}]-Bradykinin, Angiotensin III, ACP-fragment 65-74 and [Tyr^{8}]-Substance P were performed on different scales varying from 1 mg up to 35 mg (1 to 65 µmol). After isolation by HPLC, yields of between 61% and 77% were obtained. Characterization by UPLC, HRMS and ^{1}H-^{13}C NMR confirmed the identity of the desired mono-iodinated products, including the desired insertion of the iodine atom at the *ortho* position of the –OH group, as expected. Additionally, no trace of iodination was observed on Phe, ormost importantly, on His - the second most reactive amino acid toward iodination[26] - confirming the high chemoselectivity of the reagent for Tyr. Furthermore, careful UPLC and NMR analysis did not reveal any evidence of racemization.

A recent peptide drug class for the treatment of type 2 diabetes mellitus is the group of glucagon-like peptide-1 (GLP-1) agonists which includes GLP-1 itself, but also modified analogues such as Victoza (Liraglutide) and others. We therefore sought to demonstrate the wide and general applicability of the strategy by examining the mono-iodination of GLP-1(7-37), a native hormone which binds to the GLP-1 receptor and triggers insulin secretion glucose dependently. Single incorporation of an iodine atom on the tyrosine residue of the human GLP-1 (7-37) was achived with high selectivity (ratio of mono-iodinated compound > 91%) and the desired mono-iodinated peptide was isolated with a 52% yield after HPLC purification, confirming the success of the approach on a challenging 31-mer peptides (Table 2, entry 10).

Taking profit of the high reactivity of the newly formed aryl-iodo peptides, we applied a Suzuki-Miyaura cross-coupling as a final step in the preparation of bio-imaging probes, as examplified by [mono-Iodo]-Leucin Enkephalinamide **8** (Scheme 4, A). Carboxylphenyl boronic acid pinacol ester functionnalized

with a dansyl fluorophore **9** was directly attached to the iodo-peptides using a water soluble complex of $Pd(OAc)_2$ with the dihydroxypyrimidine ligand developed by Chalker *et al.*[27] To circumvent prior chemical modification of expensive fluorophores, the cross coupling with a boronic acid pinacol ester functionnalized with an azide (such as **12**) offers an alternative which enables subsequent copper-catalyzed azide-alkyne cycloaddition (CuAAC) to connect the peptide to the dye - most of them being commercially available as alkyne derivatives (Scheme 4, B). In both cases, cross-couplings proceeded smoothly at 38°C in 12 hours and addition of glycerol was found to improve solubility of the coupling partners and to increase yields as previously reported.[28]

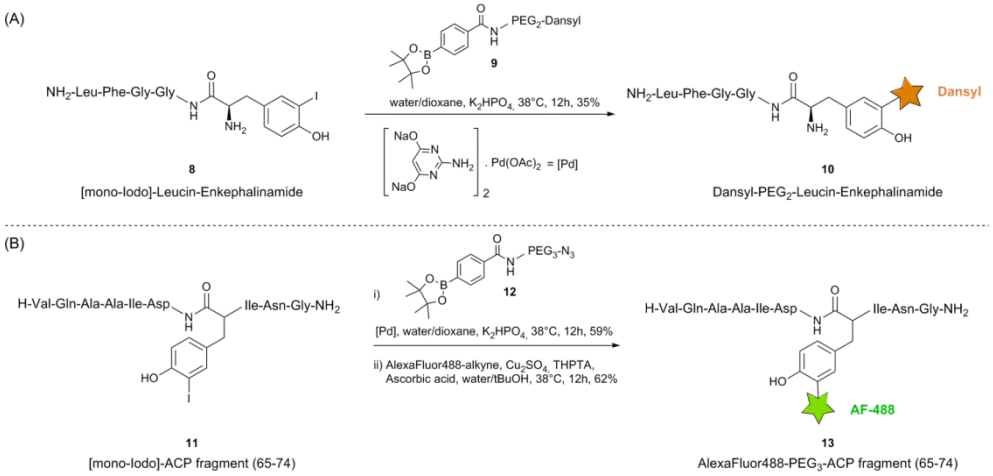

Scheme 4 Conjugation of fluorophores to mono-iodinated peptides Leucin-Enkephalinamide and ACP fragment

Conclusion

In summary, we have developed a new method enabling the efficient, specific and highly controled mono-iodination of tyrosine within fully unprotected peptides. Successful application of the approach was demonstrated on peptides with various sizes and complexity, including peptides containing other aromatic amino acids such as tryptophane and histidine, but also sulfur containing amino acids like methionine or cysteine. By exploiting the reactivity of the mono-iodo peptides we performed conjugation with fluorophore building blocks via Suzuki-Miyaura cross-coupling, as an example of bio-imaging probe synthesis. We believe our findings will prove to be a useful additional tool in the arsenal of bioconjugation chemistry, notably for peptides obtained by isolation from natural sources in which incorporation of particular conjugation sites is not possible and lysine or free cysteine are not available for labeling.

Acknowledgements

All authors acknowledge funding by Beta Train. The research leading to these results has received funding from the People Program (Marie Curie Actions) of the European Union's Seventh Framework Program FP7/2007-2013/ under REA grant agreement n° 289932. We are also grateful to Dr. Michael Kurz and Ute Messinger for the help in NMR characterization of peptides, to Jenny Schubert, Christian Ehrmann and Ana Villar Garea for the HRMS, to Richarda Hennig, Thorsten Zeisberg and Steffen Kohlitz for the help in purification of peptides, to Dr. Wolfgang Holla and Dr. Jens Atzrodt for the help and fruitful discussions; and to Dr. Seth Jones for critically reading the manuscript.

References

[1] Hermanson, G. T. (2013) Bioconjugate Techniques, 3rd ed., Academic Press.
[2] Chen, S., Li, X., and Ma, H. (2009) New Approach for Local Structure Analysis of the Tyrosine Domain in Proteins by Using a SiteSpecific and Polarity-Sensitive Fluorescent Probe. ChemBioChem 10, 1200−1207.
[3] Gavrilyuk, J., Ban, H., Uehara, H., Sirk, S. J., Saye-Francisco, K., Cuevas, A., Zablowsky, E., Oza, A., Seaman, M. S., Burton, D. R., and Barbas, C. F., 3rd (2013) Antibody conjugation approach enhances breadth and potency of neutralization of anti-HIV-1 antibodies and CD4-IgG. J. Virol. 87, 4985−4993.
[4] Joshi, N., Whitaker, L., and Francis, M. (2004) A threecomponent Mannich-type reaction for selective tyrosine bioconjugation. J. Am. Chem. Soc. 126, 15942−15943.
[5] Ban, H., Gavrilyuk, J., and Barbas, C. F., III (2010) Tyrosine bioconjugation through aqueous ene-type reactions: a click-like reaction for tyrosine. J. Am. Chem. Soc. 132, 1523−1525.
[6] Ly, T., and Julian, R. R. (2008) Residue-specific radical-directed dissociation of whole proteins in the gas phase. J. Am. Chem. Soc. 130, 351−358.
[7] Collie, G. W., Pulka-Ziach, K., and Guichard, G. (2016) In situ iodination and X-ray crystal structure of a foldamer helix bundle. Chem. Commun. 52, 1202−1205.
[8] Bertolani, A., Pirrie, L., Stefan, L., Houbenov, N., Haataja, J. S., Catalano, L., Terraneo, G., Giancane, G., Valli, L., Milani, R., Ikkala, O., Resnati, G., and Metrangolo, P. (2015) Supramolecular amplification of amyloid self-assembly by iodination. Nat. Commun. 6, 7574.
[9] Cruz, L. J., McIntosh, J. M., Imperial, J. S., and Gray, W. R. (2000) Conus Peptides and Their Iodinated Derivatives as Probes for Ion Channels and Receptors, In Animal Toxins, pp 74−89, Springer.
[10] Ruf, J., and Carayon, P. (2006) Structural and functional aspects of thyroid peroxidase. Arch. Biochem. Biophys. 445, 269−277.
[11] Schottelius, M., Konrad, M., Osl, T., Poschenrieder, A., and Wester, H.-J. (2015) An optimized strategy for the mild and efficient solution phase iodination of tyrosine residues in bioactive peptides. Tetrahedron Lett. 56, 6602−6605.
[12] Espuñ a, G., Arsequell, G., Valencia, G., Barluenga, J., Perez, M.,́ and Gonzalez, J. M. (2000) Control of the iodination reaction oń activated aromatic residues in peptides. Chem. Commun., 1307−1308.
[13] Vergote, V., Bode, S., Peremans, K., Vanbree, H., Baert, B., Slegers, G., Burvenich, C., and De Spiegeleer, B. (2007) Analysis of iodinated peptides by LC-DAD/ESI ion trap mass spectrometry. J. Chromatogr. B: Anal. Technol. Biomed. Life Sci. 850, 213−220.
[14] Lelesz, B., Toth, G. K., Peitl, B., Hegedus, C., Drimba, L., Sari,́ R., Szilvassy, Z., and Né meth, J. (2014) Description and application of a novel glucagon-like peptide-1 (GLP-1) radioimmunoassay. J. Radioanal. Nucl. Chem. 299, 157−164.
[15] Clerico, A., Iervasi, G., Manfredi, C., Salvadori, S., Marastoni, M., Del Chicca, M. G., Giannessi, D., Del Ry, S., Andreassi, M. G., Sabatinor, L., et al. (1995) Preparation of mono-radioiodinated tracers for study of the in vivo metabolism of atrial natriuretic peptide in humans. Eur. J. Nucl. Med. 22, 997−1004.
[16] Fu, Y., Letourneau, M., Chatenet, D., Dupuis, J., and Fournier, A. (2011) Characterization of iodinated adrenomedullin derivatives suitable for lung nuclear medicine. Nucl. Med. Biol. 38, 867−874.
[17] Murthy, K. K., Thibault, G., Schiffrin, E. L., Garcia, R., Chartier, L., Gutkowska, J., Genest, J., and Cantin, M. (1986) Disappearance of atrial natriuretic factor from circulation in the rat. Peptides 7, 241−246.

[18] Loot, A. E., van Buiten, A., Roks, A. J., and Henning, R. H. (2005) The suitability of iodinated Angiotensin-(1−7) peptides as pharmacological tools. J. Pharmacol. Toxicol. Methods 51, 51−55.
[19] Kozlowski, E., Johnson, G., Dischino, D., Dworetzky, S., Boissard, C., and Gribkoff, V. (1996) Synthesis and biological evaluation of an iodinated iberiotoxin analogue,[mono-iodo-Tyr5, Phe36]-iberiotoxin. Int. J. Pept. Protein Res. 48, 194−199.
[20] Vergote, V., Baert, B., Vandermeulen, E., Peremans, K., van Bree, H., Slegers, G., Burvenich, C., and De Spiegeleer, B. (2008) LCUV/MS characterization and DOE optimization of the iodinated peptide obestatin. J. Pharm. Biomed. Anal. 46, 127−136.
[21] Tsomides, T. J., and Eisen, H. N. (1993) Stoichiometric labeling of peptides by iodination on tyrosyl or histidyl residues. Anal. Biochem. 210, 129−135.
[22] Syvret, R. G., Butt, K. M., Nguyen, T. P., Bulleck, V. L., and Rieth, R. D. (2002) Novel process for generating useful electrophiles from common anions using Selectfluor® fluorination agent. J. Org. Chem. 67, 4487−4493.
[23] Hughes, W., Jr, and Straessle, R. (1950) Preparation and Properties of Serum and Plasma Proteins. XXIV. Iodination of Human Serum Albumin1a, b. J. Am. Chem. Soc. 72, 452−457.
[24] Jin, Y., Huang, Y., Xie, Y., Hu, W., Wang, F., Liu, G., and Zhao, R. (2012) Cyclic interconversion of methionine containing peptide between oxidized and reduced phases monitored by reversed-phase HPLC and ESI-MS/MS. Talanta 89, 531−536.
[25] Nicolas, E., Vilaseca, M., and Giralt, E. (1995) A study of the use´ of NH 4 I for the reduction of methionine sulfoxide in peptides containing cysteine and cystine. Tetrahedron 51, 5701−5710.
[26] Liu, Z., and Julian, R. R. (2009) Deciphering the peptide iodination code: influence on subsequent gas-phase radical generation with photodissociation ESI-MS. J. Am. Soc. Mass Spectrom. 20, 965− 971.
[27] Chalker, J. M., Wood, C. S., and Davis, B. G. (2009) A convenient catalyst for aqueous and protein Suzuki-Miyaura crosscoupling. J. Am. Chem. Soc. 131, 16346−16347.
[28] Ojida, A., Tsutsumi, H., Kasagi, N., and Hamachi, I. (2005) Suzuki coupling for protein modification. Tetrahedron Lett. 46, 3301− 3305.

Supporting Information

Table of Contents

Figure S1 – Iodination stock solution preparation

Iodination stock solution 50 mM in acetonitrile was prepared freshly. Selectfluor (15 mg, 42.3 µmol) was dissolved in 840 µL of acetonitrile by vigorous vortexing (solution **A**) followed by NaI (6.8 mg, 45.3 µmol). The addition of sodium iodide was easily visible by change in color: the transparent Selectfluor solution turned into a brown caramel mixture after 10 seconds (solution **B**).
Upon addition of the iodination stock solution to Tyr-peptides dissolved in DCM + 20% TFA (solution **C**), the reaction mixture turned light pink (solution **D**).

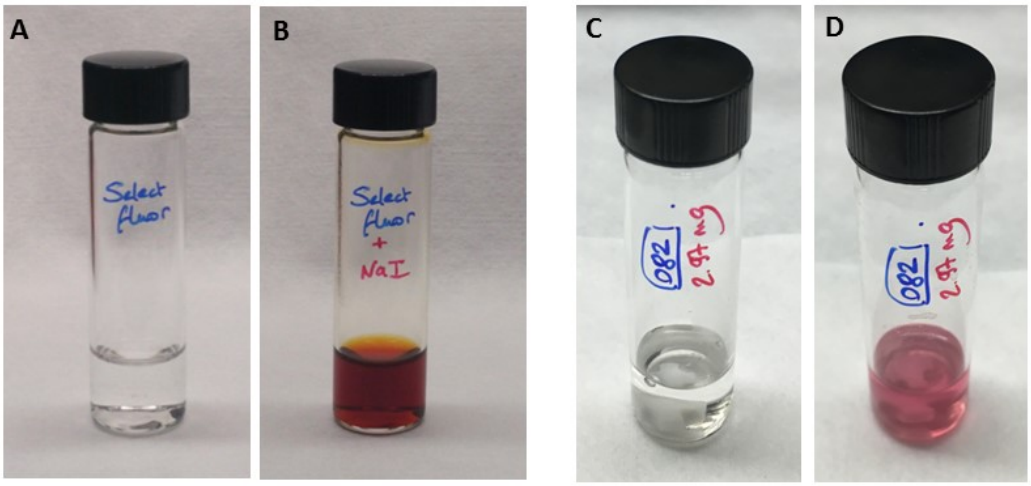

Figure S2 – Iodination reaction occurs quickly at room temperature

Ac-Tyr-NH-Me (2.0 mg, 8.5 µmol) was dissolved in 1 mL of DCM + 10% TFA. Then was added dropwise 1.1 eq of a 50 mM freshly prepared iodination stock solution. Reaction was allowed to stir at room temperature and monitored by LC-MS after 15 minutes and after 2 hours. No difference was observed. Analytical LC-MS chromatograms are shown below:

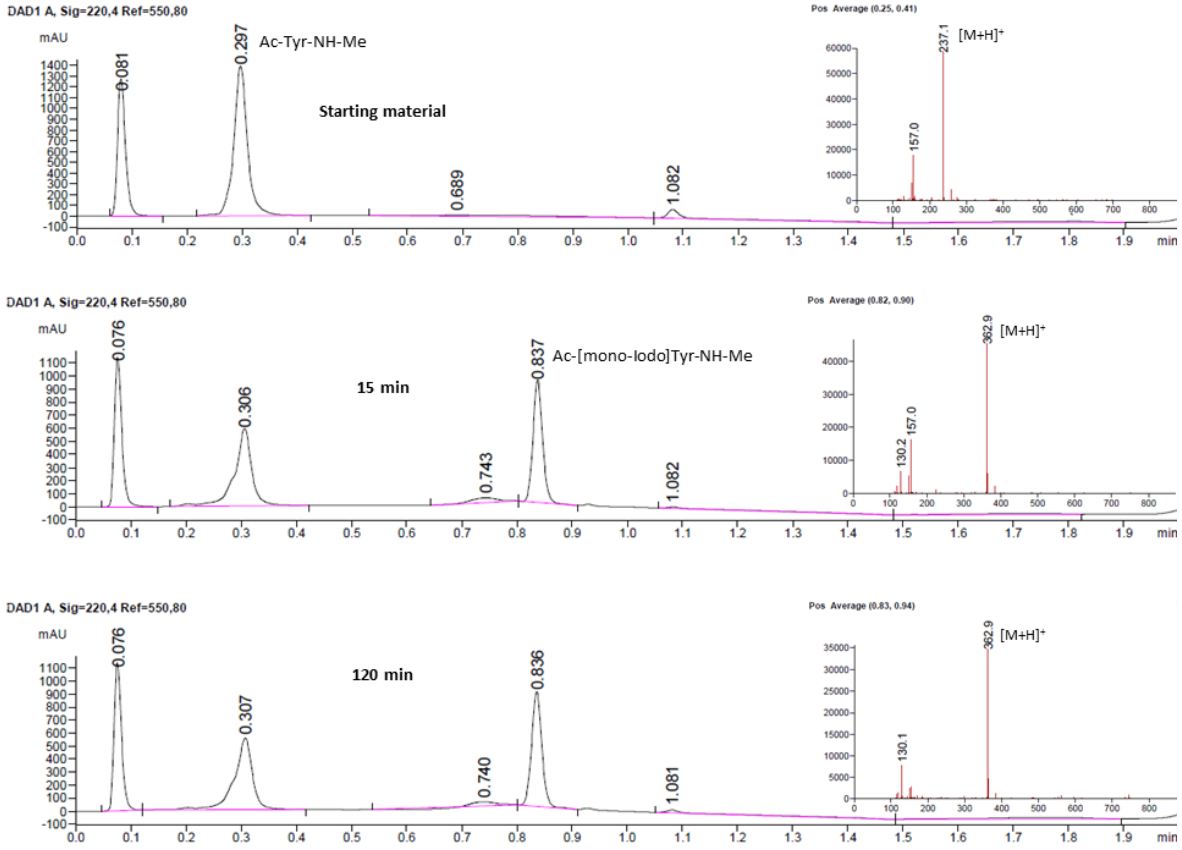

Figure S3 – Iodination is specific to Tyr residue

Ac-Tyr-NH-Me (2.0 mg, 8.5 µmol), Ac-Phe-Tyr-NH-Me, Ac-Phe-His-NH-Me and Ac-Phe-Trp-NH-Me were respectively dissolved in 1 mL of DCM + 10% TFA. Then was added dropwise 1.1 eq of a 50 mM freshly prepared iodination stock solution. Reaction was allowed to stir at room temperature and monitored by LC-MS after 2 minutes and after 15 minutes. Under these conditions, iodination proceeded only on Tyr residues. Analytical LC-MS chromatograms are shown below:

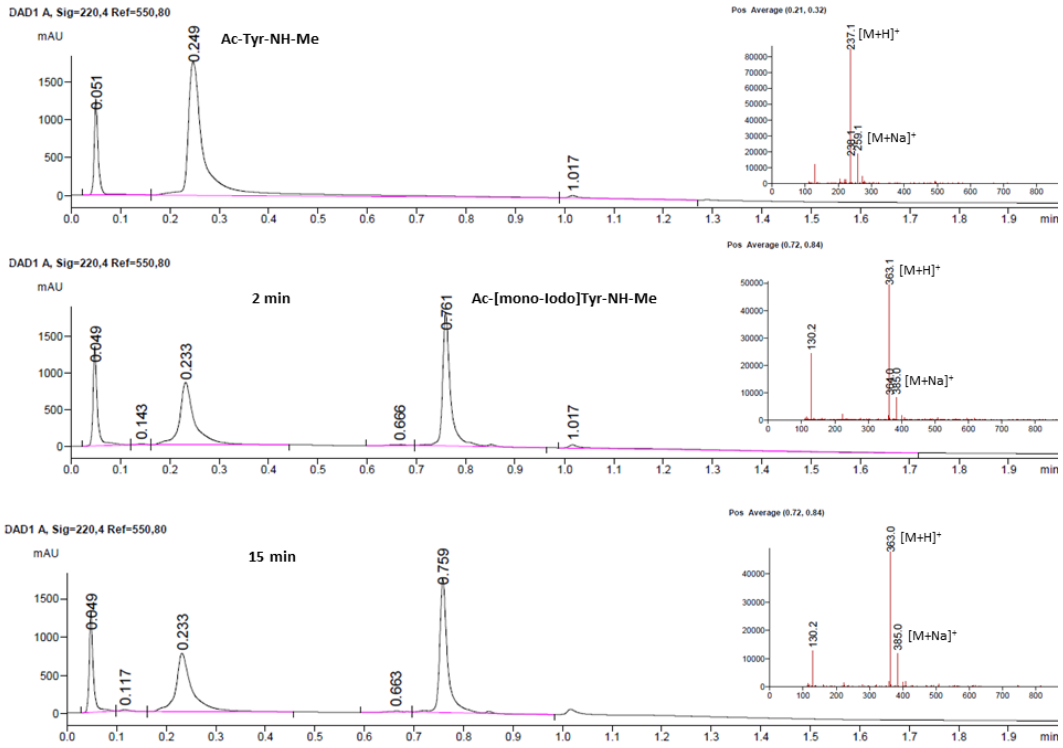

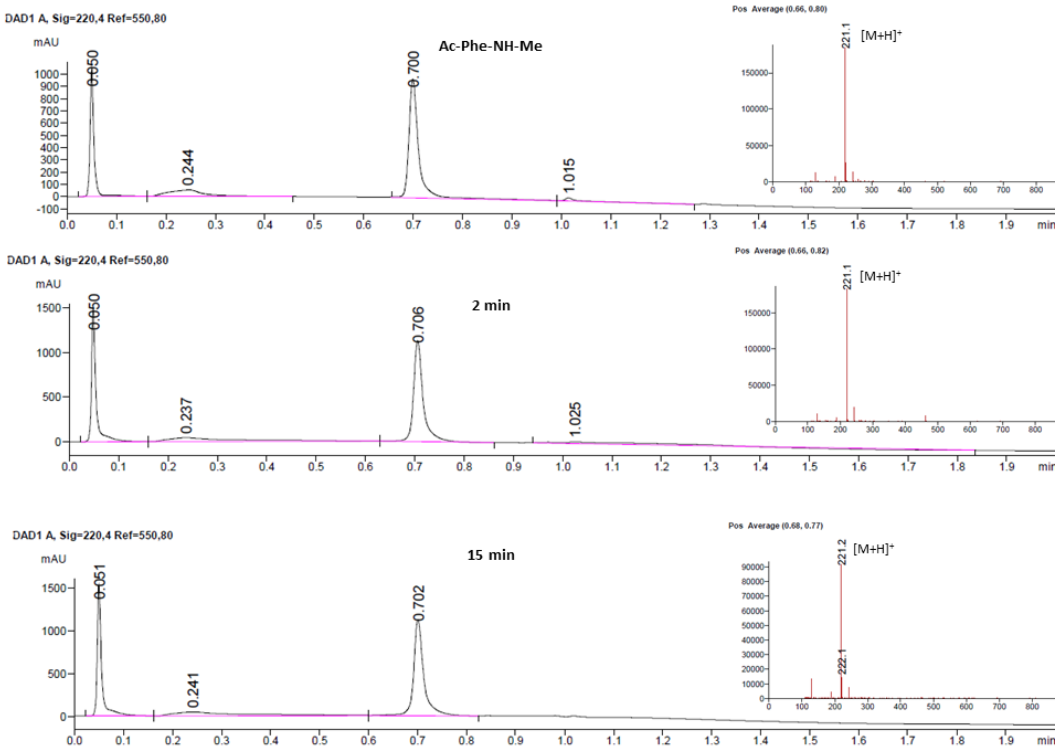
DAD1 A, Sig=220,4 Ref=550,80
mAU
Ac-Phe-NH-Me
0.650
0.244
0.700
1.015
Pos Average (0.66, 0.80)
221.1
[M+H]+
DAD1 A, Sig=220,4 Ref=550,80
mAU
2 min
0.650
0.237
0.706
1.025
Pos Average (0.66, 0.82)
221.1
[M+H]+
DAD1 A, Sig=220,4 Ref=550,80
mAU
15 min
0.651
0.241
0.702
Pos Average (0.68, 0.77)
221.2
222.1
[M+H]+
min

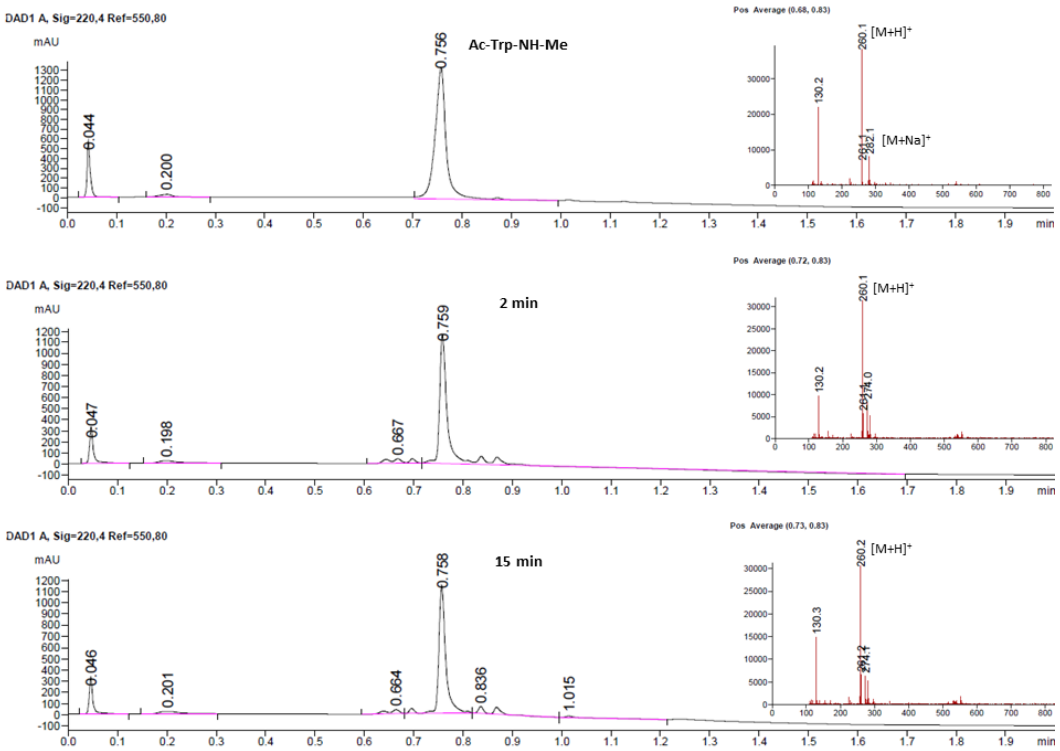
DAD1 A, Sig=220,4 Ref=550,80
mAU
Ac-Trp-NH-Me
0.044
0.200
0.756
Pos Average (0.68, 0.83)
260.1
130.2
261.1
282.1
[M+H]+
[M+Na]+
DAD1 A, Sig=220,4 Ref=550,80
mAU
2 min
0.047
0.198
0.667
0.759
Pos Average (0.72, 0.83)
260.1
130.2
261.1
274.0
[M+H]+
DAD1 A, Sig=220,4 Ref=550,80
mAU
15 min
0.046
0.201
0.664
0.758
0.836
1.015
Pos Average (0.73, 0.83)
260.2
130.3
261.2
274.1
[M+H]+
min

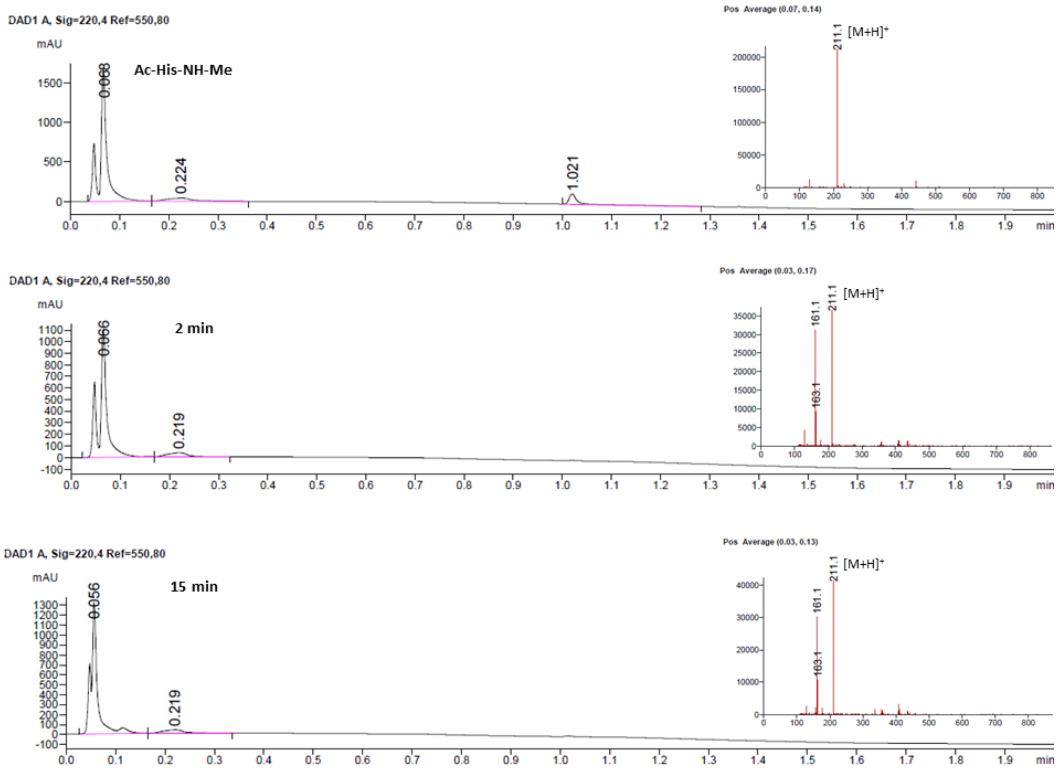
DAD1 A, Sig=220,4 Ref=550,80
mAU
Ac-His-NH-Me
0.068
0.224
1.021
Pos Average (0.07, 0.14)
211.1
[M+H]+
min

DAD1 A, Sig=220,4 Ref=550,80
mAU
2 min
0.066
0.219
Pos Average (0.03, 0.17)
211.1
161.1
163.1
[M+H]+
min

DAD1 A, Sig=220,4 Ref=550,80
mAU
15 min
0.056
0.219
Pos Average (0.03, 0.13)
211.1
161.1
163.1
[M+H]+
min

Figure S4 – Mono-iodination of a Met-containing peptide: [Tyr^{8}]-Substance P

[Tyr^{8}]-Substance P (0.81 mg, 0.59 µmol) was dissolved in 340 µL of DCM and 80 µL of TFA. Then were added dropwise 16 µL (1.4 eq.) of a 50 mM freshly prepared iodination stock solution. Reaction was allowed to stir at room temperature and monitored by LC-MS. A mixture containing the SM, the starting material with the oxidized methionine SM[Ox], and the MI. Addition of 4 µL (0.35 eq.) of a 50 mM iodination stock solution generated the oxidized methionine mono-iodinated compound MI[Ox]. Two other successive additions of 4 µL (3x 0.35 eq.) of a 50 mM iodination stock solution afforded MI and MI[Ox] as the major product. Finally, addition of 100 µL of the reducing cocktail (freshly prepared: potassium iodide KI (10 mg) and ascorbic acid (10 mg) were sonicated in 500 µL of TFA for 10 minutes) enabled reduction of MI[Ox] towards MI. Analytical LC-MS chromatograms are shown below:

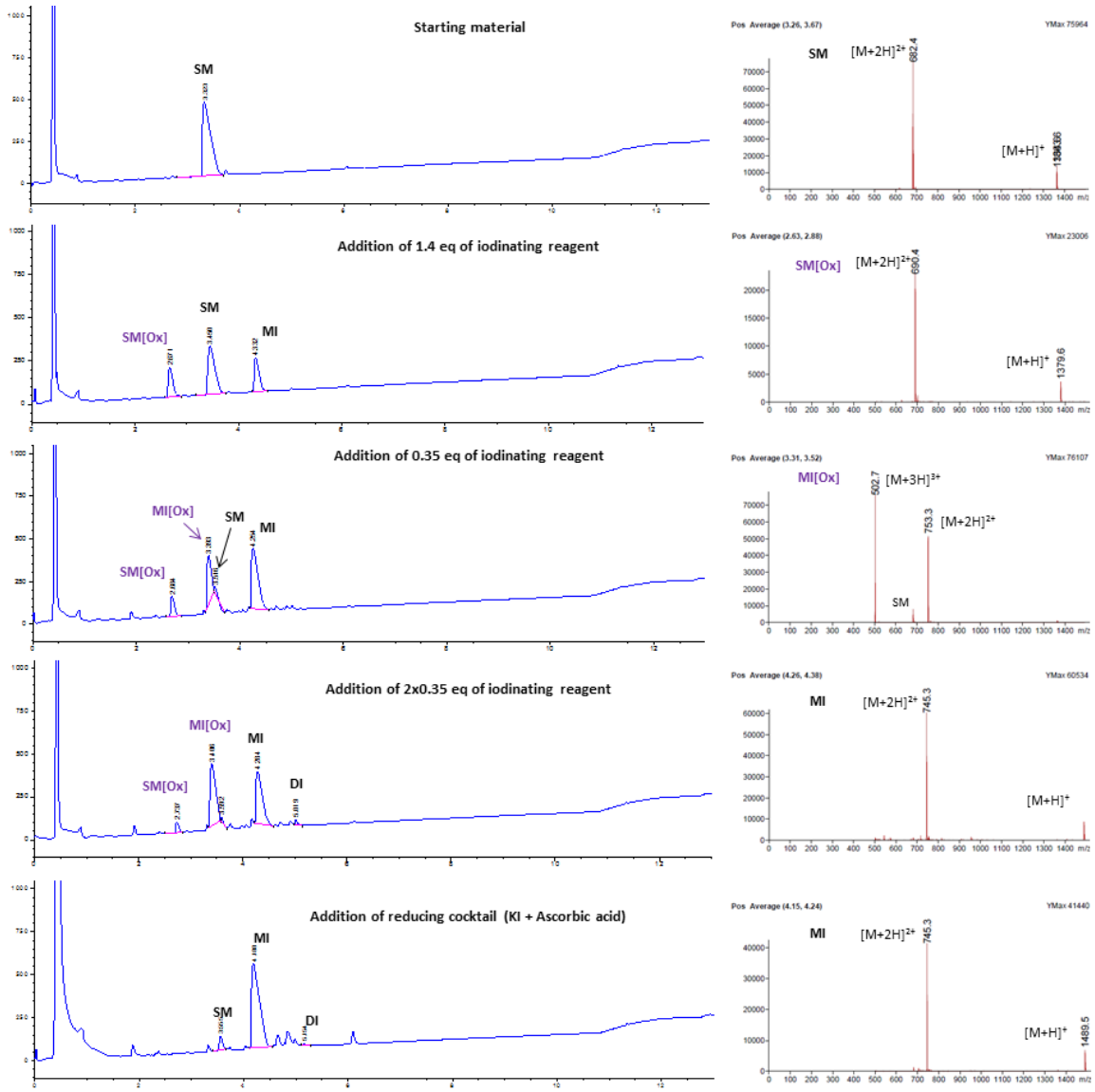

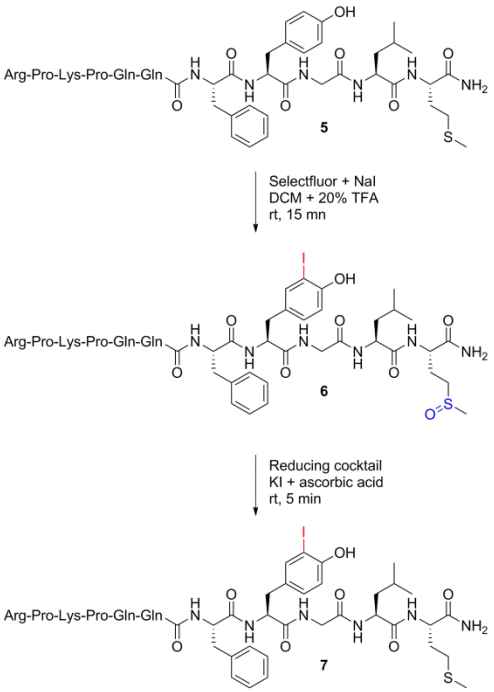

[Tyr^8]-Substance P
SM: 5.9% / MI: 93.6% / DI: 0.5%
2.2 µmol - yield 72%

General methods

Unless otherwise noted, all reagents and solvents were purchased from commercial suppliers (Sigma Aldrich, ThermoFisher, Merck Millipore) and used without further purification.

Reactions were monitored by LC-MS. For small molecules: data were acquired using the Agilent 1100 MSD system with a Phenomenex Luna column (C-18, 100Å pore size, 3 µm particle size, 10x2.0 mm, flow: 1.1 mL/min). Gradient: 0 min 1% ACN (+0.05% TFA) / 99% H_2O (+0.05% TFA); 0.3 min % ACN (+0.05% TFA); 1.3 min 95% ACN (+0.05% TFA); 1.75 min 1% ACN (+0.05% TFA); 1.80 min 1% ACN (+0.05% TFA). Mass detection range: 110-1000MW. Temperature: 30 °C. For peptides: data were acquired using the Agilent 1100 MSD system with a Phenomenex Aeris Widepore column (XB-C18, 200Å pore size, 3.6 µm particle size, 100x2.1 mm, flow: 0.5 mL/min). Gradient: 0 min 5% ACN (+0.1% formic acid) / 95% H_2O (+0.1% formic acid) to 10 min - 50% ACN (+0.1% formic acid); 11 min 90% ACN (+0.1% formic acid) to 12.5 min; 12.5 min to 13.5 min 5% ACN (+0.1% formic acid). Mass detection range: 500-1500MW. Temperature: 38°C.

Purifications on reverse-phase preparative HPLC were performed on the HP-Agilent 1100 with either i) a column from Agilent (Zorbax Rx C18, 5 µm particle size, 250x9.4mm, flow: 4 mL/min). Gradient: 0 min to 5 min 10% ACN (+0.1% TFA) / 90% H_2O (+0.1% TFA); 5 min to 30 min 95% ACN (+0.1% TFA) / 5% H_2O (+0.1% TFA); 30 min to 32 min 95% ACN (+0.1% TFA) / 5% H_2O (+0.1% TFA); 32 min to 35 min 10% ACN (+0.1% TFA) / 90% H_2O (+0.1% TFA) or ii) a column from Waters (Xbridge Prep C18 OBD, 5 µm particle size, 250x19mm, flow: 16 mL/min). Gradient: 0 min to 5 min 10% ACN (+0.1% TFA) / 90% H_2O (+0.1% TFA); 5 min to 30 min 95% ACN (+0.1% TFA) / 5% H_2O (+0.1% TFA); 30 min to 32 min 95% ACN (+0.1% TFA) / 5% H_2O (+0.1% TFA); 32 min to 35 min 10% ACN (+0.1% TFA) / 90% H_2O (+0.1% TFA) or iii) a column from Waters (Acquity UPLC CSH C18, 130Å pore size, 1.7 µm particle size, 2.1x150mm, flow: 0.5 mL/min). Gradient: 0 min to 3 min 20% ACN (+0.05% TFA) / 80% H_2O (+0.05% TFA); 3 min to 23 min 75% ACN (+0.05% TFA) / 25% H_2O (+0.05% TFA); 23 min to 23.5 min 95% ACN (+0.05% TFA) / 5% H_2O (+0.05% TFA). 23.5 min to 25.5 min 95% ACN (+0.05% TFA) / 5% H_2O (+0.05% TFA). Temperature: 50 °C.

Purification on silica gel chromatography was performed on CombiFlash Rf-Isco Teledyne.

Final peptides were analyzed by UPLC-MS Waters Acquity (C-18 CSH column - 130Å pore size, 1.7 µm particle size, 150x2.1 mm, flow: 0.5 mL/min – Gradient 1: 0 min 10% ACN (+0.1% formic acid) / 90% H_2O (+0.1% formic acid) to 19.2 min - 90% ACN (+0.1% formic acid); 20 min 90% ACN (+0.1% formic acid). Gradient 2: 0 min 2% ACN (+0.1% formic acid) / 98% H_2O (+0.1% formic acid) to 9.12 min - 40% ACN (+0.1% formic acid); 12 min 40% ACN (+0.1% formic acid). Mass detection range: 500-2000MW. Temperature: 40 °C. High resolution mass HRMS were recorded on the Agilent 6200 Series Accurate-Mass Time-of-flight (TOF). ^{1}H and ^{13}C NMR spectra were recorded on a Bruker DRX-400 or 600 systems in d_6-DMSO or $CDCl_3$. Chemical shifts are given in parts per million (ppm) with tetramethylsilane as an internal standard. Abbreviations are used as follows: s = singlet, d = doublet, t = triplet, q = quartet, p = pentet, m = multiplet or unresolved, dd = doublets of doublet, br = broad. Coupling constants (*J* values) are given in Hertz (Hz). Absorption and Emission spectra were acquired with a Thermo Varioskan using the SkanIt 2.4.3 software.

Abbreviations

ACN = acetonitrile
AUC = area under the curve
Boc = *tert*-butyloxycarbonyl
DCM = dichloromethane
DI = di-iodinated product
DIEA = N,N-diisopropylethylamine
DMF = dimethylformamide
DODT = 3,6-Dioxa-1,8-octane-dithiol
ESI-TOF = electrospray ionization mass spectrometry – time of flight
EtOAc = ethyl acetate
HE-SPPS = high-efficiency solid phase peptide synthesis
HPLC = high performance liquid chromatography
HRMS = high resolution mass spectrometry
LC-MS = liquid chromatography - mass spectrometry
MI = mono-iodinated product
NMR = nuclear magnetic resonance
PEG = poly-ethylene glycol
SM = starting material
tBuOH = tert-butanol
TFA = trifluoroacetic acid
THPTA = tris(3-hydroxypropyltriazolylmethyl)amine
TIS = triisopropylsilane
UPLC-MS = ultra-performance liquid chromatography - mass spectrometry

Peptides

Tocinoic acid, Goserelin acetate and [Tyr^8]-Substance P were purchased from Sigma Aldrich. Cyclo(RGGyK) was purchased from Selleckchem. AcMeYVAD-CHO, [Tyr^0]-Bradykinin, and human GLP-1 (7-37) were purchased from Bachem.

HE-SPPS

Leucin-Enkephalinamide, Angiotensin III and ACP fragment (65-74) were synthesized by High-Efficiency Solid Phase Peptide Synthesis[1] using a CEM Liberty Blue system on a 0.1 mmol scale with a Rink Amide AM resin low loading (0.29 mmol/g) 100-200 mesh from Novabiochem using 5-fold excess of reagents [0.2 M Fmoc amino acid solution (in DMF) with 0.5 M DIC (in DMF) and 1.0 M Oxyma (in DMF)] and 20% pipieridine in DMF for the Fmoc-deprotection cycles. Immediately after synthesis, the peptide resin was washed three times with 10 mL of DMF and then three times with 10 mL of DCM. Cleavage was then performed in all cases with 10 mL of a freshly prepared King's cocktail (TFA 82.5% / Phenol 5% / Thioanisol 5% / H_2O 5% / DODT 2.5%) for 3 hours before being precipitated in 70 mL of ice cold diisopropyl ether. Precipitate was centrifuged (4 min, 4000 rpm, 4 °C) and washed with ice cold diisopropyl ether three times. Finally, the resin was filtered off and the peptide precipitate was dissolved in H_2O + 25% ACN + 0.5% AcOH and lyophilized. Crude purity was > 95% for Leucin-Enkephalinamide. Angiotensin III and ACP fragment (65-74) were purified with reverse-phase preparative HPLC.

Solvent screening for Ac-Tyr-NH-Me mono-iodination

Ac-Tyr-NH-Me (2.0 mg, 8.5 µmol) was dissolved in 1 mL of different solvents (indicated in Table 1). Then was added dropwise 1.1 eq of a 50 mM freshly prepared iodination stock solution. Reaction was allowed to stir at room temperature and monitored by LC-MS instantly after addition of iodination solution, and after 15 minutes. Relative amounts of SM, MI, and DI shown in Table 1 were quantified using AUC integration (absorbance at 220 nm). Analytical LC-MS chromatograms are shown below:

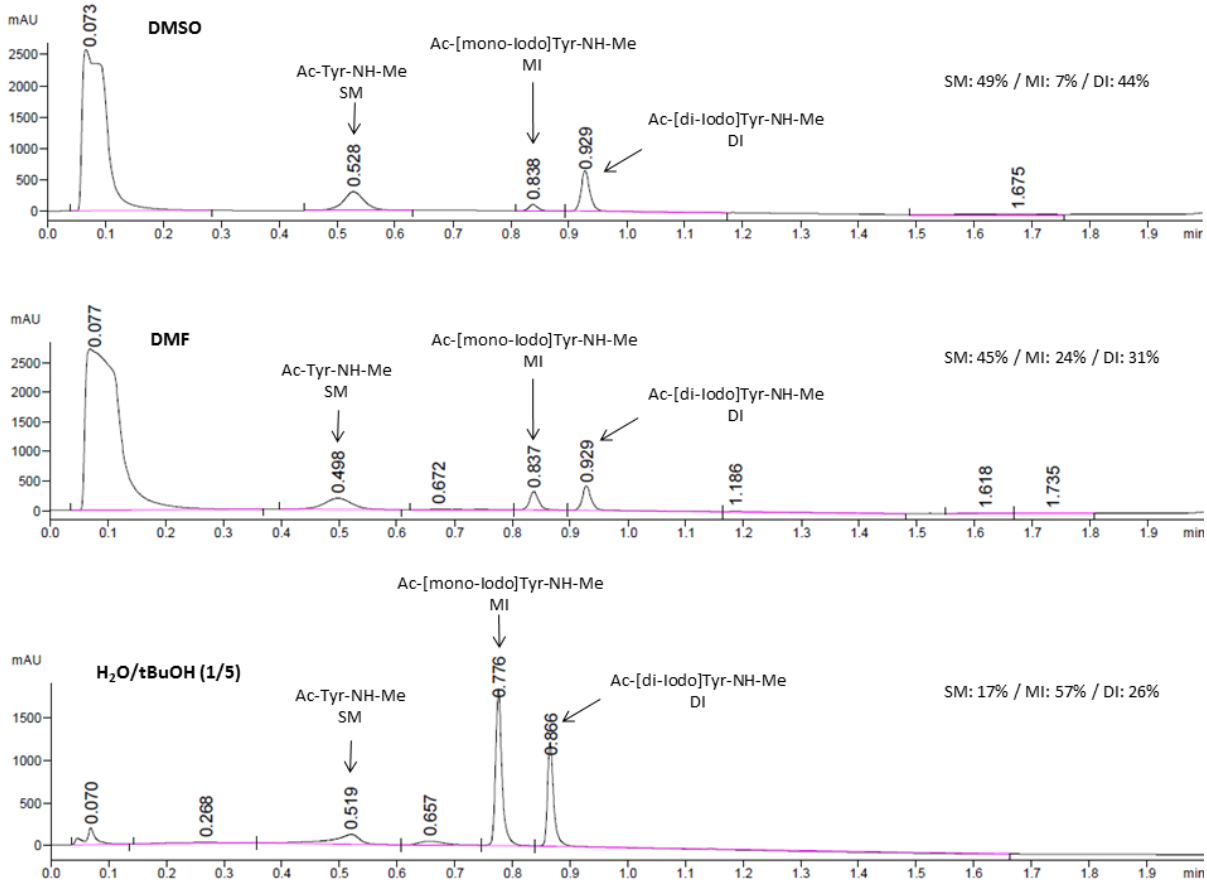

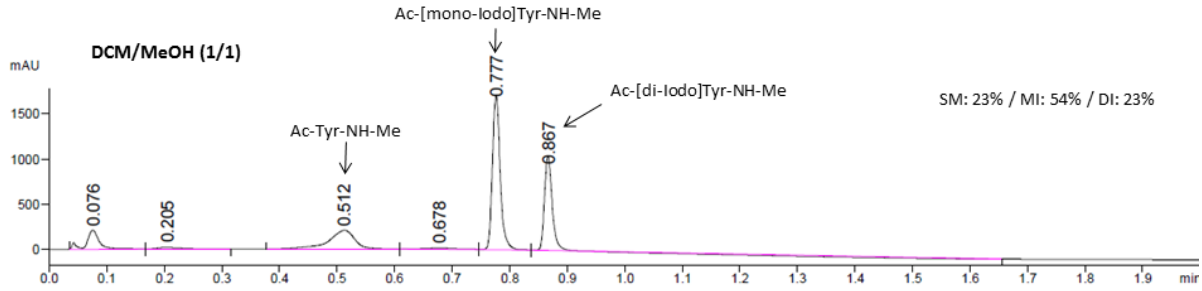
DCM/MeOH (1/1)
mAU
Ac-[mono-Iodo]Tyr-NH-Me
Ac-[di-Iodo]Tyr-NH-Me
Ac-Tyr-NH-Me
0.076
0.205
0.512
0.678
0.777
0.867
SM: 23% / MI: 54% / DI: 23%
min

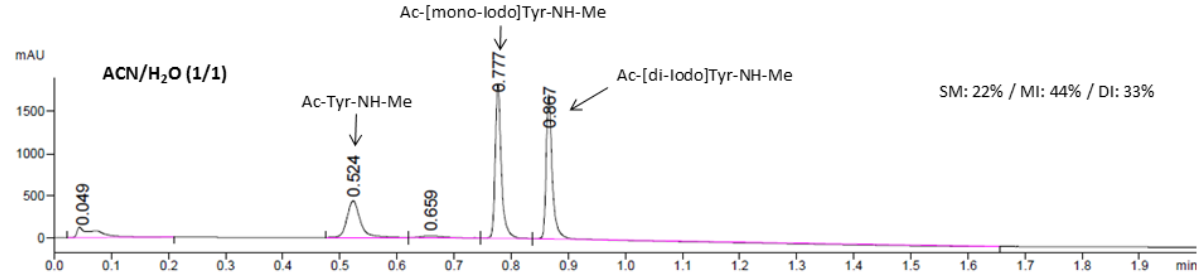
ACN/H2O (1/1)
mAU
Ac-[mono-Iodo]Tyr-NH-Me
Ac-[di-Iodo]Tyr-NH-Me
Ac-Tyr-NH-Me
0.049
0.524
0.659
0.777
0.867
SM: 22% / MI: 44% / DI: 33%
min

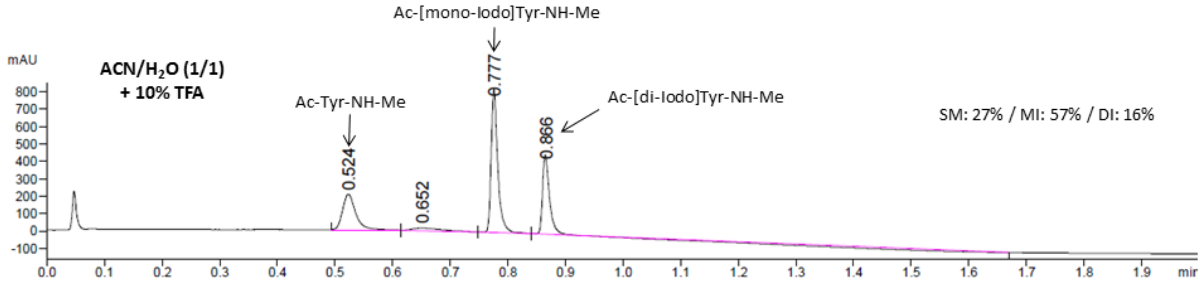
ACN/H2O (1/1)
+ 10% TFA
mAU
Ac-[mono-Iodo]Tyr-NH-Me
Ac-[di-Iodo]Tyr-NH-Me
Ac-Tyr-NH-Me
0.524
0.652
0.777
0.866
SM: 27% / MI: 57% / DI: 16%
min

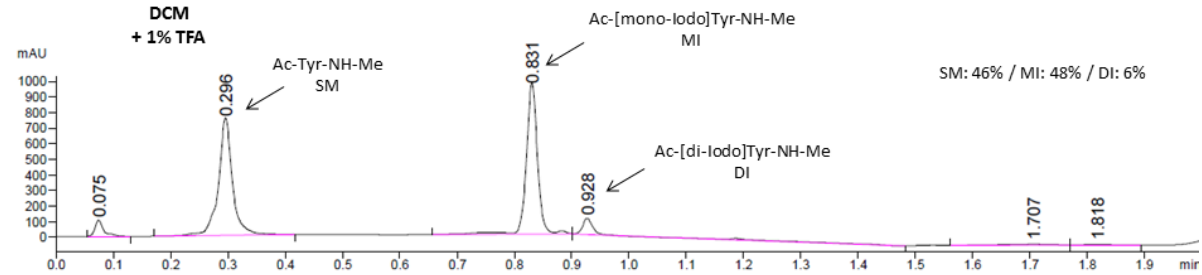
DCM
+ 1% TFA
mAU
Ac-Tyr-NH-Me
SM
Ac-[mono-Iodo]Tyr-NH-Me
MI
Ac-[di-Iodo]Tyr-NH-Me
DI
0.075
0.296
0.831
0.928
1.707
1.818
SM: 46% / MI: 48% / DI: 6%
min

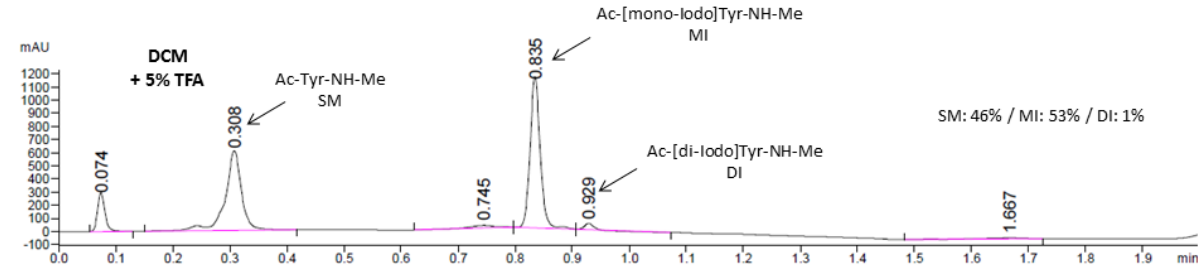
DCM
+ 5% TFA
mAU
Ac-Tyr-NH-Me
SM
Ac-[mono-Iodo]Tyr-NH-Me
MI
Ac-[di-Iodo]Tyr-NH-Me
DI
0.074
0.308
0.745
0.835
0.929
1.667
SM: 46% / MI: 53% / DI: 1%
min

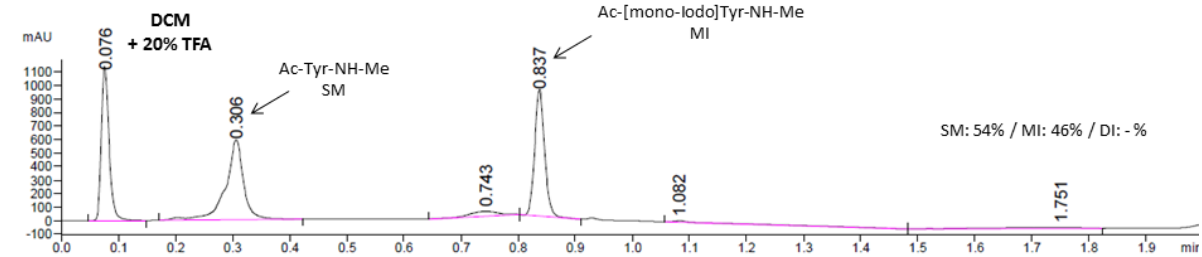
DCM
+ 20% TFA
mAU
Ac-Tyr-NH-Me
SM
Ac-[mono-Iodo]Tyr-NH-Me
MI
0.076
0.306
0.743
0.837
1.082
1.751
SM: 54% / MI: 46% / DI: - %
min

General Mono-iodination procedure

Tyr-containing peptide was dissolved in DCM+ 20% TFA at a concentration of 1-2 mM. Then were added dropwise 1.4 eq of a 50 mM freshly prepared iodination stock solution. Reaction was allowed to stir at room temperature for 15 minutes and was monitored by LC-MS as followed: 10 µL of the reaction mixture were quenched with 20 µL of distilled water which were submitted to analysis. Depending on the conversion, extra 0.25 eq of iodination stock solution were added sequentially to reach the described ratio of starting material (SM), mono-iodinated product (MI) and di-iodinated product (DI) in Scheme 2. Relative amounts of SM, MI and DI were quantified using AUC integration (absorbance at 215 nm) corresponding to their respective masses. Analytical LC-MS chromatograms are shown below:

<u>Cyclo(RGD[mono-iodo]yK)</u>

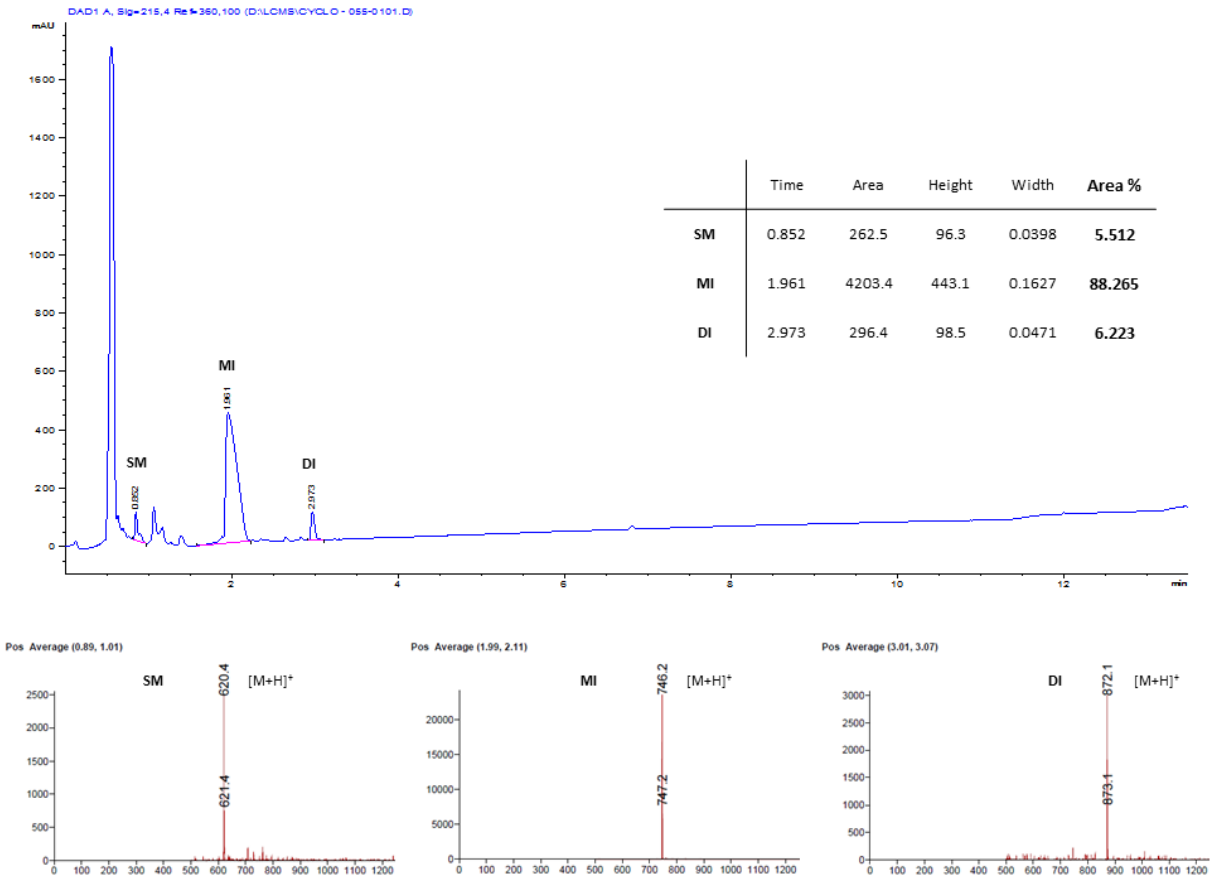

	Time	Area	Height	Width	Area %
SM	0.852	262.5	96.3	0.0398	**5.512**
MI	1.961	4203.4	443.1	0.1627	**88.265**
DI	2.973	296.4	98.5	0.0471	**6.223**

Leucin-Enkephalinamide

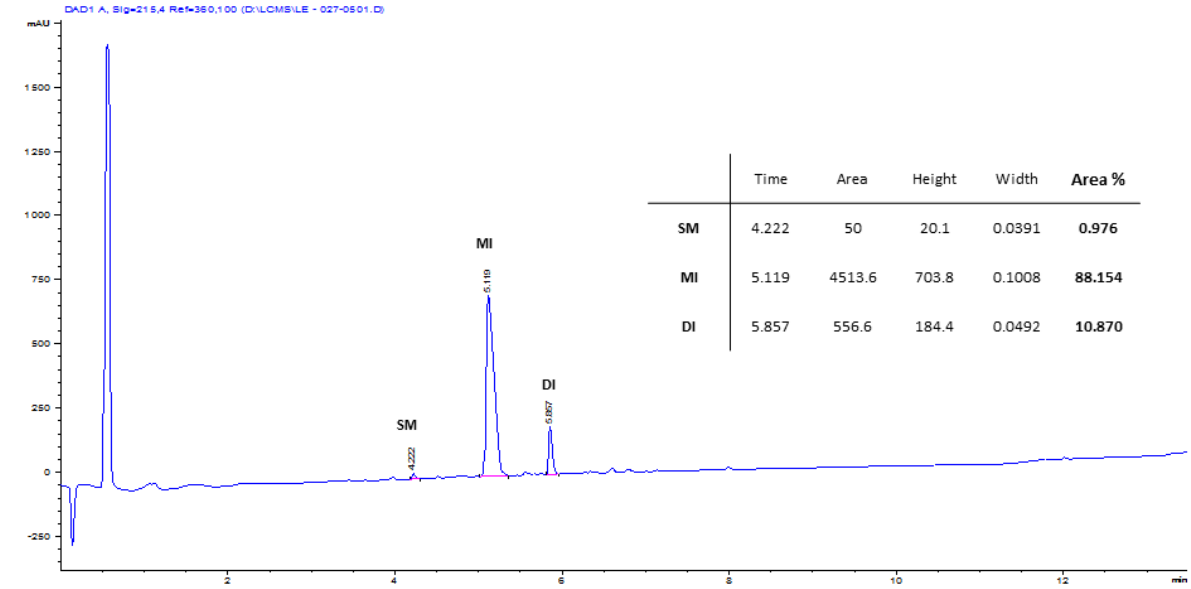

	Time	Area	Height	Width	Area %
SM	4.222	50	20.1	0.0391	**0.976**
MI	5.119	4513.6	703.8	0.1008	**88.154**
DI	5.857	556.6	184.4	0.0492	**10.870**

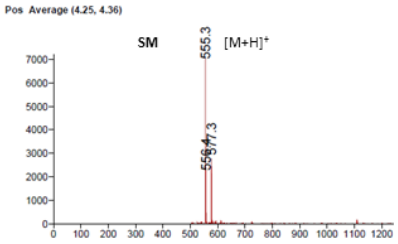

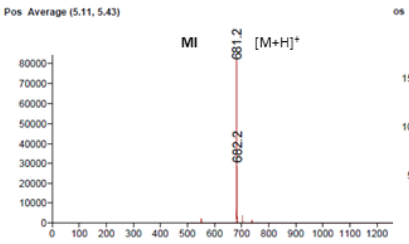

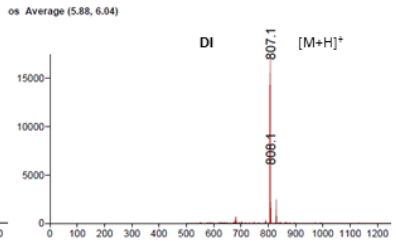

Goserelin

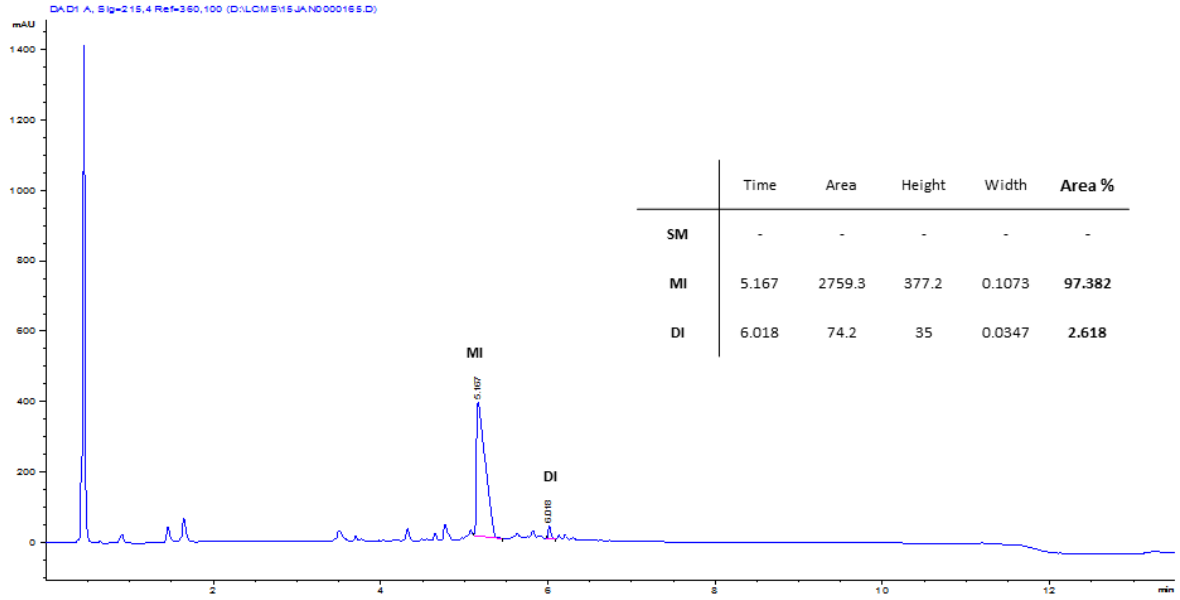

	Time	Area	Height	Width	Area %
SM	-	-	-	-	-
MI	5.167	2759.3	377.2	0.1073	**97.382**
DI	6.018	74.2	35	0.0347	**2.618**

Starting material was not detected

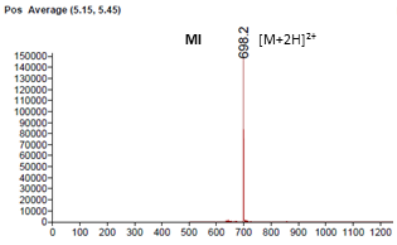

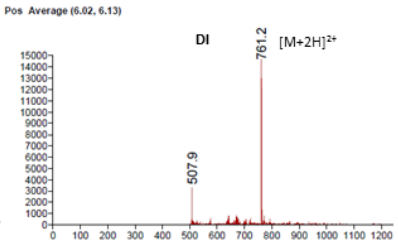

[Tyr^0]-Bradykinin

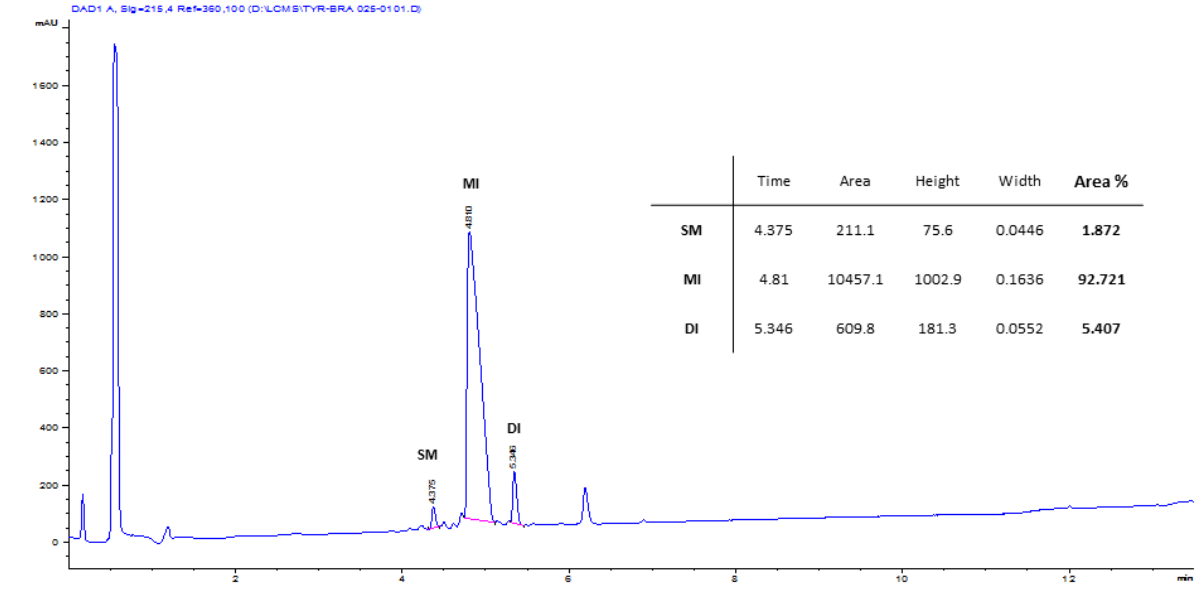

	Time	Area	Height	Width	Area %
SM	4.375	211.1	75.6	0.0446	**1.872**
MI	4.81	10457.1	1002.9	0.1636	**92.721**
DI	5.346	609.8	181.3	0.0552	**5.407**

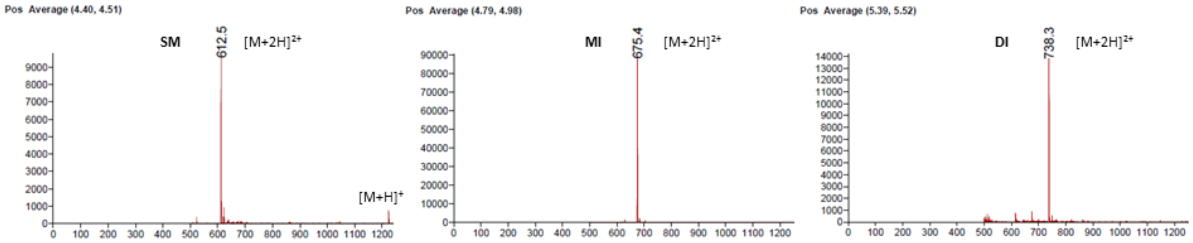

Angiotensin III

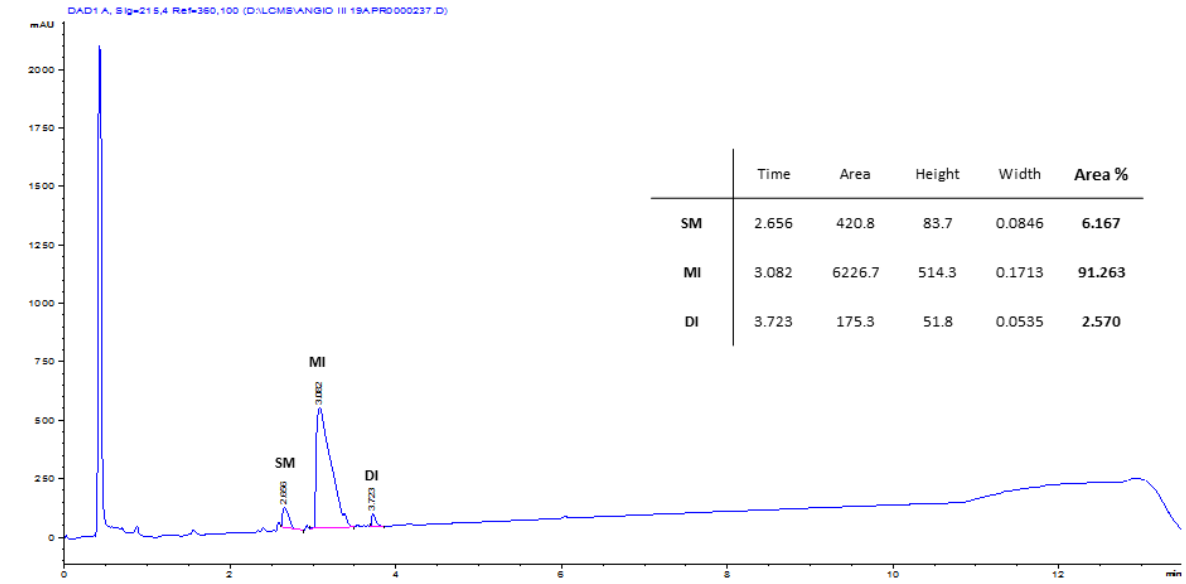

	Time	Area	Height	Width	Area %
SM	2.656	420.8	83.7	0.0846	**6.167**
MI	3.082	6226.7	514.3	0.1713	**91.263**
DI	3.723	175.3	51.8	0.0535	**2.570**

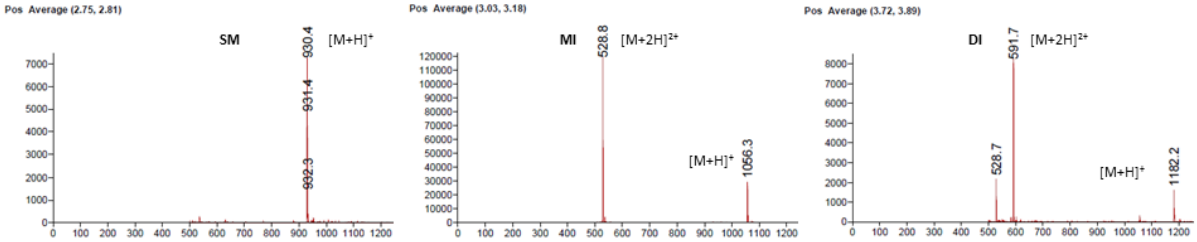

ACP fragment (65-74)

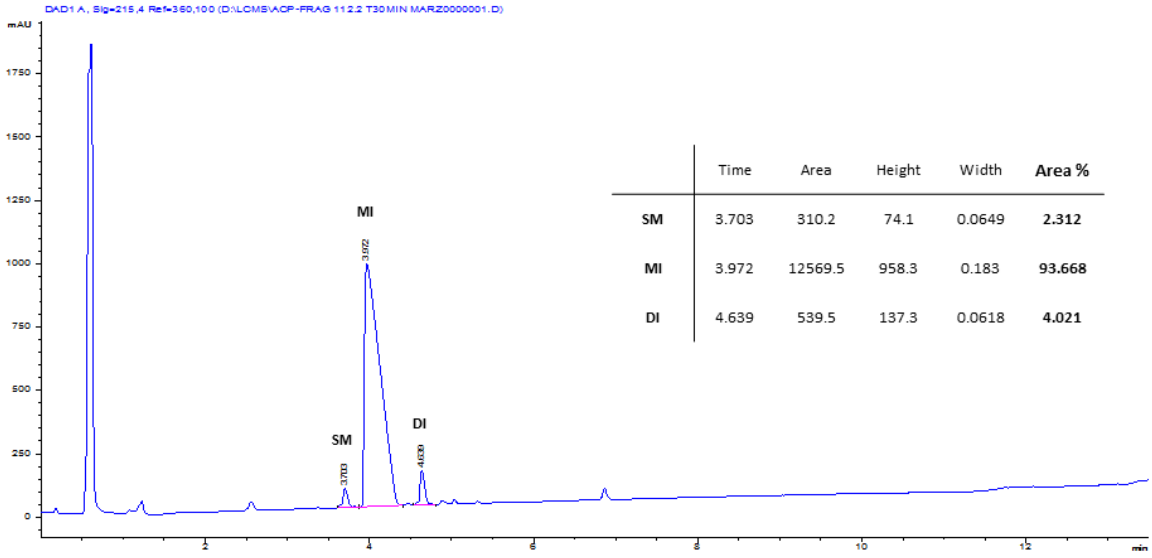

	Time	Area	Height	Width	Area %
SM	3.703	310.2	74.1	0.0649	**2.312**
MI	3.972	12569.5	958.3	0.183	**93.668**
DI	4.639	539.5	137.3	0.0618	**4.021**

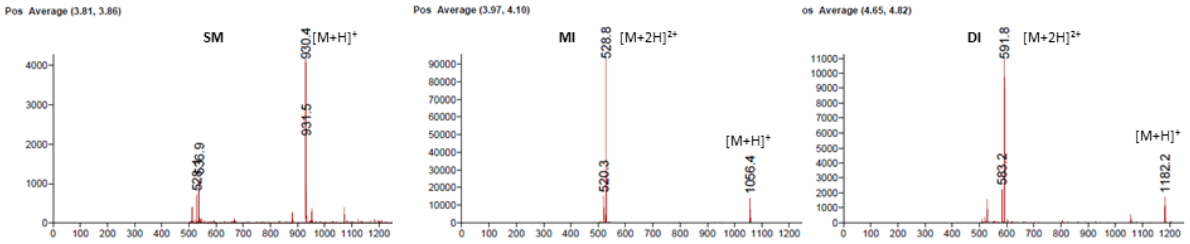

AcMeYVAD-CHO

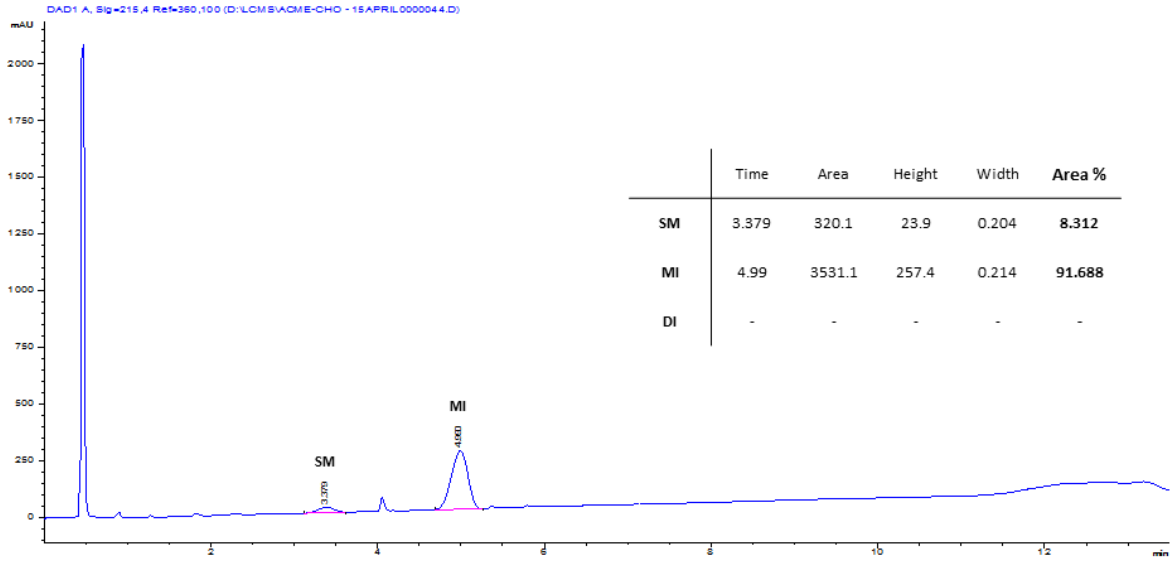

	Time	Area	Height	Width	Area %
SM	3.379	320.1	23.9	0.204	**8.312**
MI	4.99	3531.1	257.4	0.214	**91.688**
DI	-	-	-	-	-

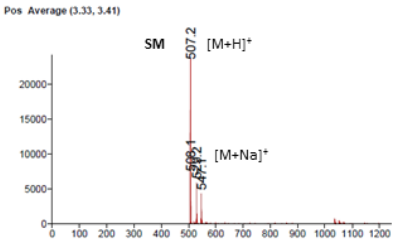

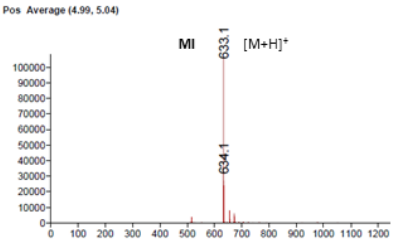

Di-iodinated product was not detected

Tocinoic acid

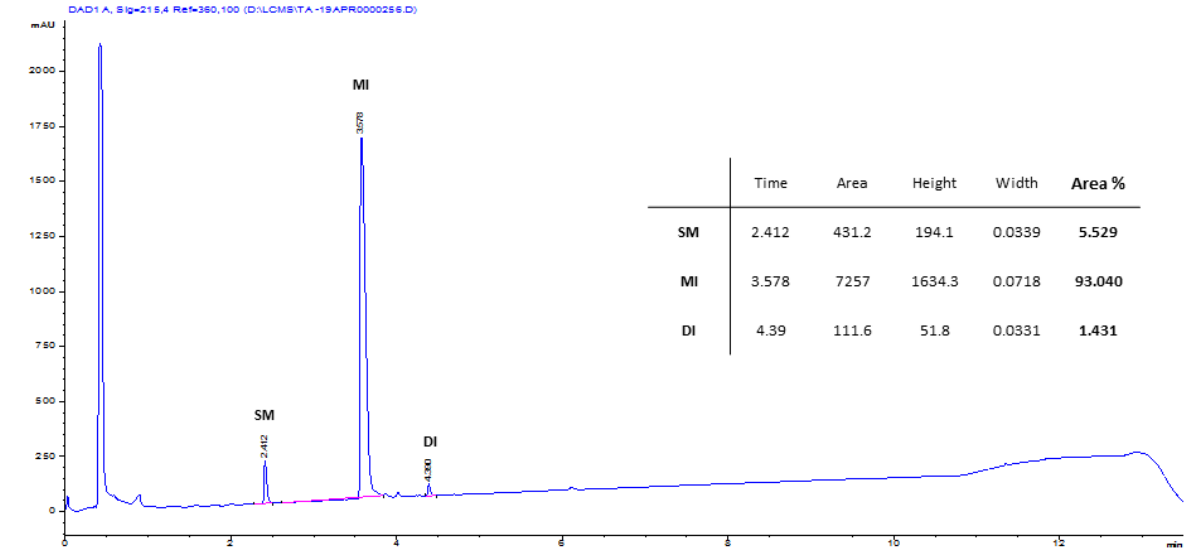

	Time	Area	Height	Width	Area %
SM	2.412	431.2	194.1	0.0339	**5.529**
MI	3.578	7257	1634.3	0.0718	**93.040**
DI	4.39	111.6	51.8	0.0331	**1.431**

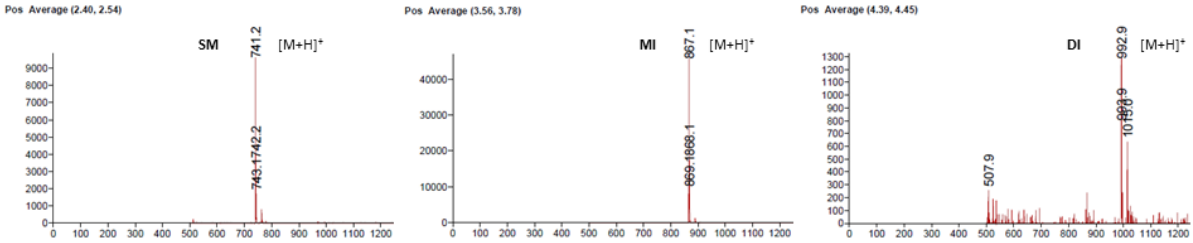

[Tyr^{8}]-Substance P

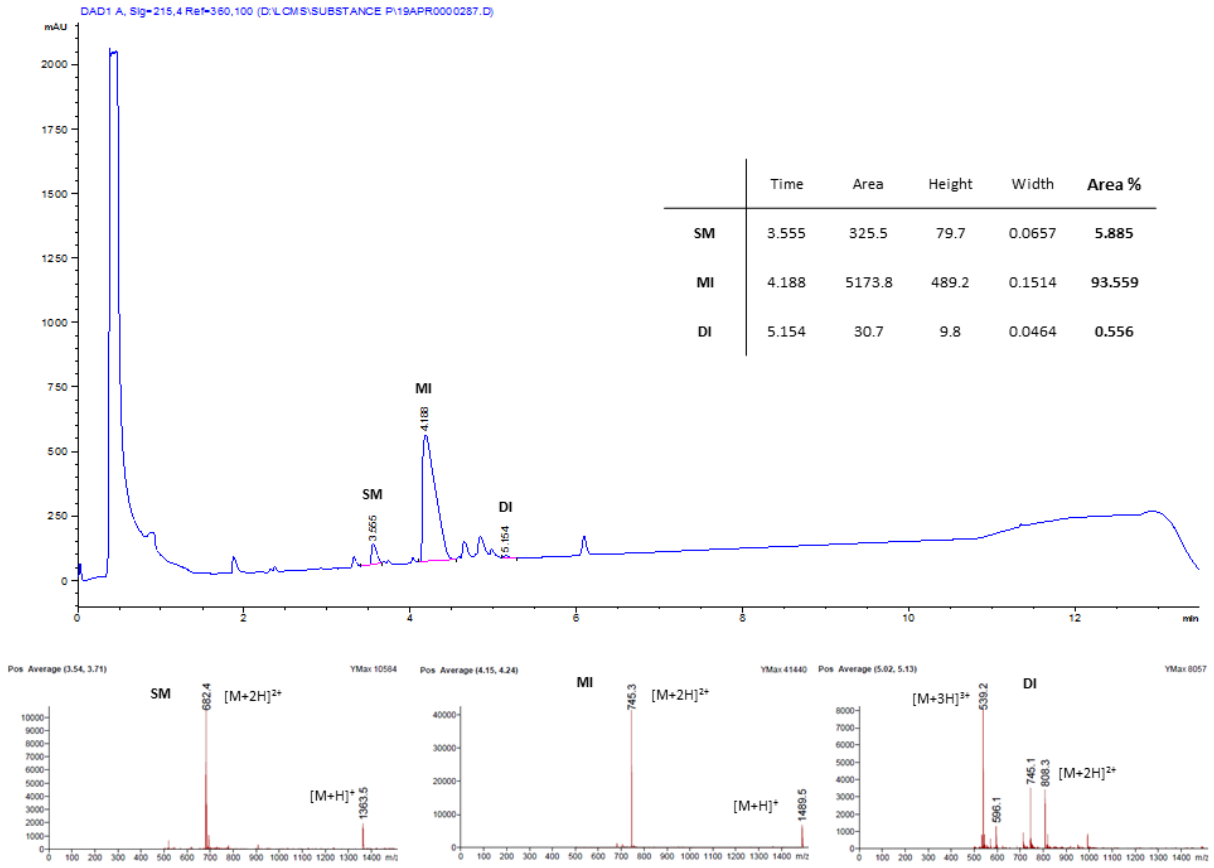

	Time	Area	Height	Width	Area %
SM	3.555	325.5	79.7	0.0657	**5.885**
MI	4.188	5173.8	489.2	0.1514	**93.559**
DI	5.154	30.7	9.8	0.0464	**0.556**

Human GLP-1 (7-37)

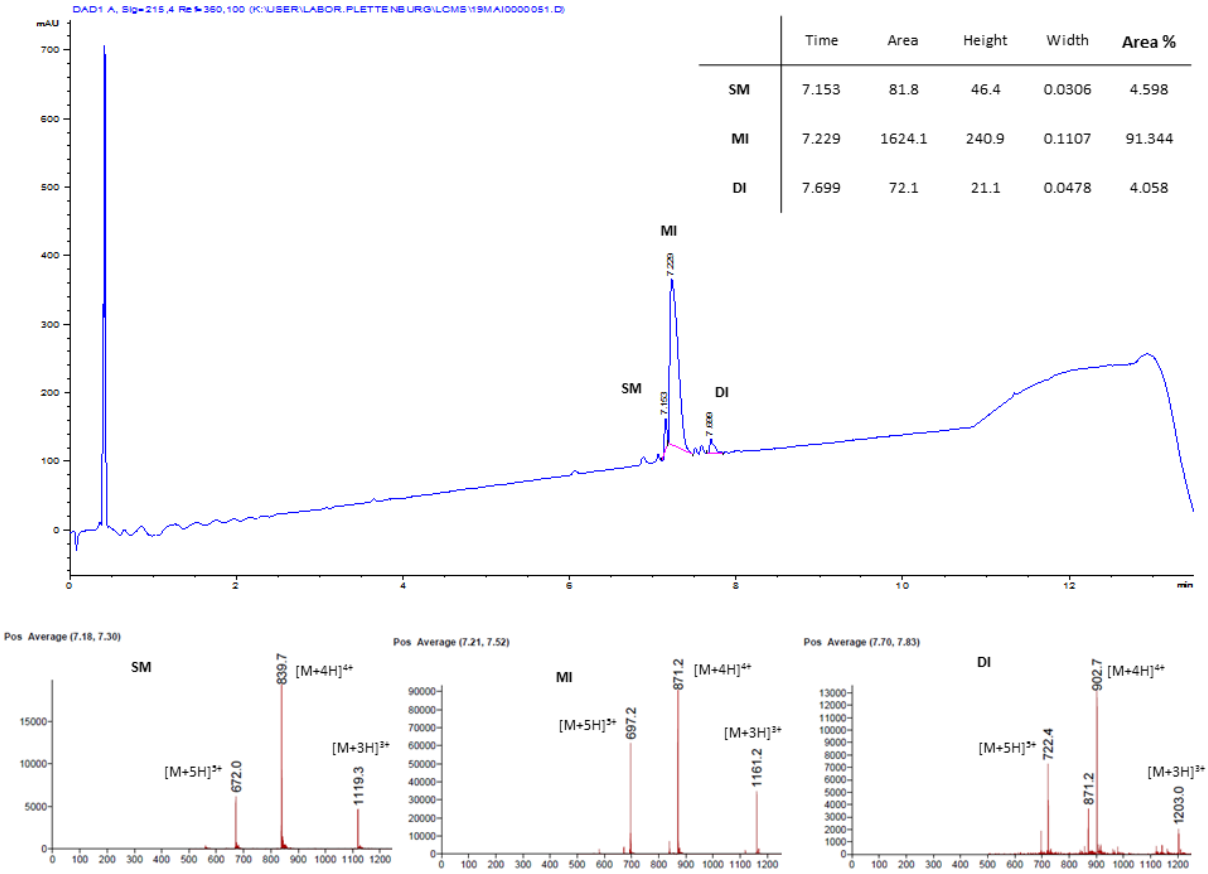

	Time	Area	Height	Width	Area %
SM	7.153	81.8	46.4	0.0306	4.598
MI	7.229	1624.1	240.9	0.1107	91.344
DI	7.699	72.1	21.1	0.0478	4.058

Mono-iodination of Cyclo(RGDyK)

Cyclo(RGDyK) (1.02 mg, 1.18 µmol) was dissolved in 500 µL of DCM and 125 µL of TFA. Then were added dropwise 33 µL of a 50 mM iodination stock solution (1.65 µmol, 1.4 eq.) (stock solution freshly prepared: 29.1 mg of Selectfluor were dissolved in 1.6 mL of ACN before the addition of 12.5 mg of NaI). The reaction mixture was allowed to stir at room temperature for 15 minutes. Two other additions of iodination solution (2 x 5 µL, 2 x 0.25 eq.) were needed to reach the following final ratio: SM: 5.5% - MI: 88.3% - DI: 6.2%. The reaction mixture was then evaporated under reduced pressure (TFA was co-evaporated three times with DCM) and redissolved in water/acetonitrile (1/1) before being submitted to HPLC (purification performed on Agilent Zorbax Rx C18, gradient: see general methods). The collected fraction was lyophilized to afford the desired product Cyclo(RGD[mono-iodo]yK) (m= 0.88 mg, 0.90 µmol, 77 % yield).

^{1}H NMR (700 MHz, d_6-DMSO, 308 K) δ: 1.10 (p, 2H), 1.36 (m, 2H), 1.45 (m, 4H), 1.57 (br, 1H), 1.72 (br, 1H), 2.39 (dd, 1 H), 2.70 (m, 4H), 2.78 (dd, 1H), 3.08 (q, 2H), 3.24 (dd, 1H), 3.94 (m, 1H), 4.04 (dd, 1H), 4.16 (q, 1H), 4.34 (q, 1H), 4.63 (q, 1H), 6.77 (d, 1H, J = 8.2 Hz), 6.87 (dd, 1H, J = 8.2, 2.0 Hz), 7.44 (d, 1H, J = 2.0 Hz), 7.52 (t, 1H), 7.61 (d, 1H), 7.68 (br, 3H), 8.00 (d, 1H), 8.09 (d, 1H), 8.11 (d, 1H), 8.44 (q, 1H), 10.10 (s, 1H), 12.20 (s, 1H).

^{13}C NMR (175 MHz, d_6-DMSO, 308 K) δ: 22.4, 25.1, 26.4, 28.5, 30.6, 35.0, 35.9, 38.6, 40.3, 43.2, 48.8, 51.8, 54.3, 54.5, 84.1, 114.6, 129.1, 130.2, 138.9, 155.0, 156.6, 169.4, 169.9, 170.5, 171.1, 171.5, 171.8.

HRMS (ESI-TOF) Calcd for $C_{27}H_{40}IN_9O_8$: 745.2054; Found: 745.2078.
UPLC-MS rt: 3.257 min (Gradient 2).

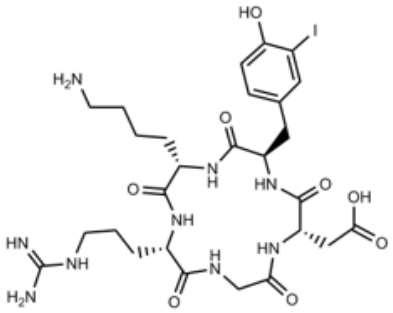

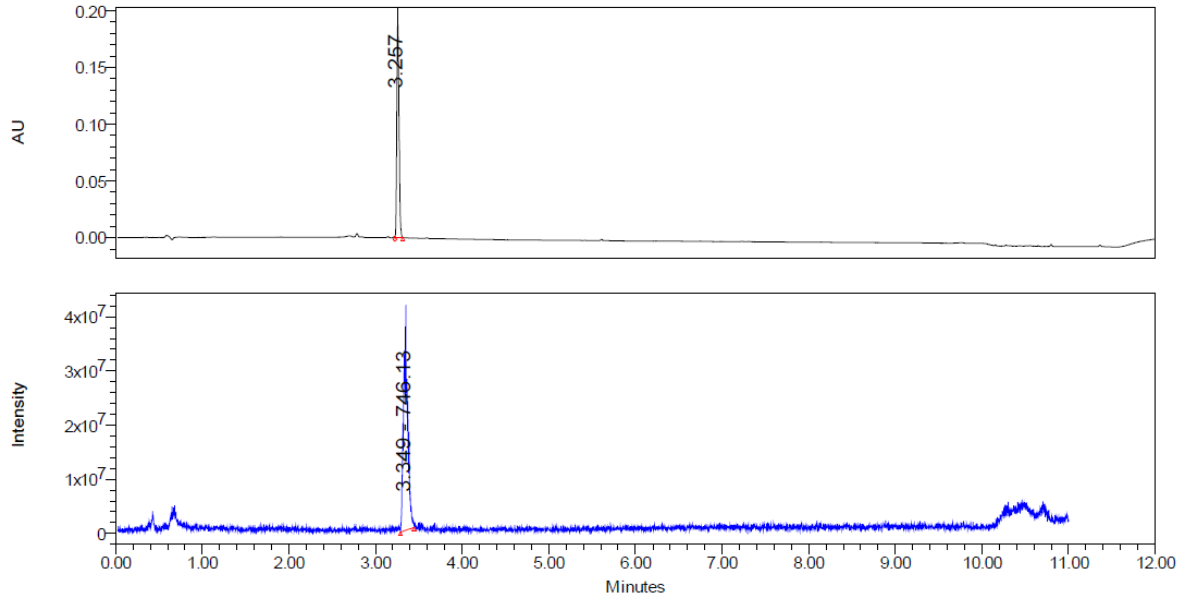

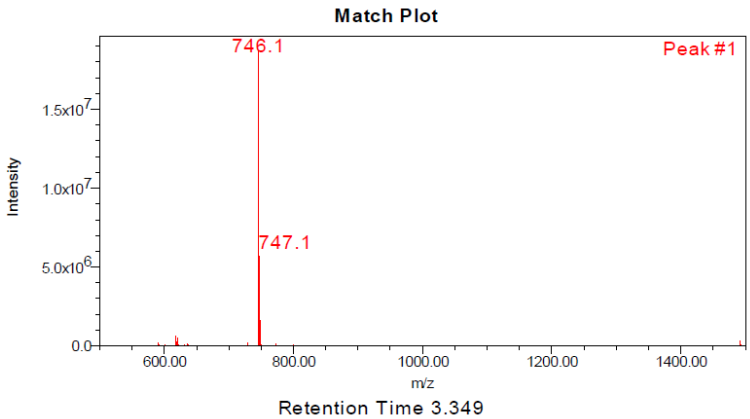

Mono-iodination of Leucin-Enkephalinamide (8)

Leucin-Enkephalinamide (36.0 mg, 64.9 µmol) was dissolved in 26 mL of DCM and 6.5 mL of TFA. Then were added dropwise 1.8 mL of a 50 mM iodination stock solution (91 µmol, 1.4 eq.) (stock solution freshly prepared: 50.0 mg of Selectfluor were dissolved in 2.8 mL of ACN before the addition of 21.0 mg of NaI). The reaction mixture was allowed to stir at room temperature for 15 minutes. Two other additions of iodination solution (2 x 320 µL, 2 x 0.25 eq.) were needed to reach the following final ratio: SM: 1.0% - MI: 88.2% - DI: 10.8%. The reaction mixture was then evaporated under reduced pressure (TFA was co-evaporated three times with DCM) and redissolved in water/acetonitrile (1/1) before being submitted to HPLC (purification performed on Xbridge Prep C18, gradient: see general methods). The collected fraction was lyophilized to afford the desired product [mono-Iodo]-Leucin-Enkephalinamide (27.3 mg, 40.1 µmol, 62 % yield).

^{1}H NMR (500 MHz, d_6-DMSO, 300 K) δ: 0.84 (d, 3H), 0.88 (d, 3H), 1.47 (m, 2H), 1.57 (m, 1H), 2.53 (s, 1H), 2.80 (dd, 1H), 2.87 (dd, 1H), 3.02 (dd, 1H), 3.45 (q, 1H), 3.61 (dd, 1H), 3.70 (m, 3H), 4.18 (m, 1H), 4.49 (m, 1H), 6.77 (d, 1H, J = 8.2 Hz), 6.97 (s, 1H), 7.03 (dd, 1H, J = 8.2, 2.0 Hz), 7.17 (m, 1H), 7.25 (d, 4H, J = 4.4 Hz), 7.53 (d, 1H, J = 2.0 Hz), 7.96 (d, 1H, J = 8.2 Hz), 8.07 (d, 1H, J = 8.2 Hz), 8.11 (t, 1H, J = 5.6 Hz), 8.18 (s, 1H), 8.30 (s, 1H), 10.10 (br, 1H).

^{13}C NMR (125 MHz, d_6-DMSO, 300 K) δ: 21.56, 23.02, 24.19, 37.28, 38.53, 40.80, 41.90, 42.02, 50.99, 54.09, 55.77, 84.36, 114.64, 126.26, 128.04, 129.17, 130.40, 130.62, 137.78, 139.22, 155.08, 163.38, 168.75, 169.10, 170.69, 173.76, 173.88.

HRMS (ESI-TOF) Calcd for $C_{28}H_{38}IN_6O_6$: 681.1892; Found: 681.1891.

UPLC-MS rt: 3.878 min (Gradient 1).

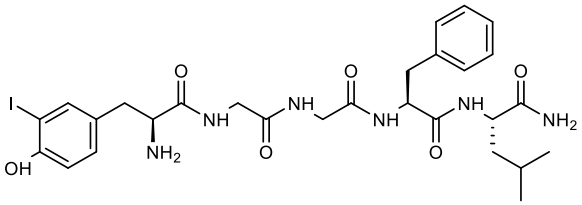

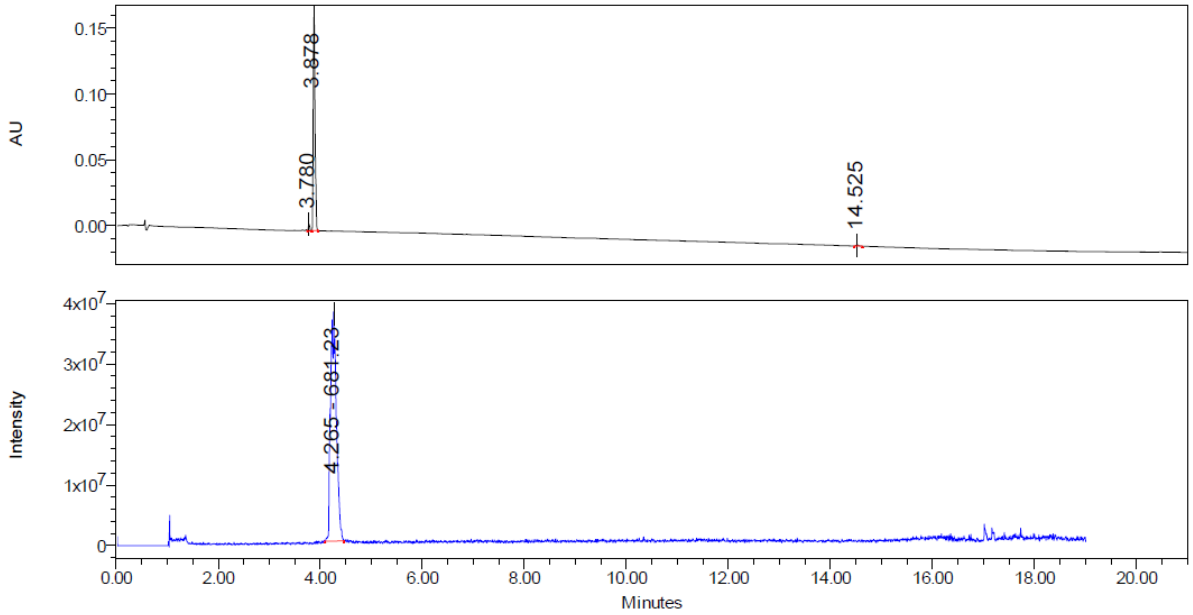

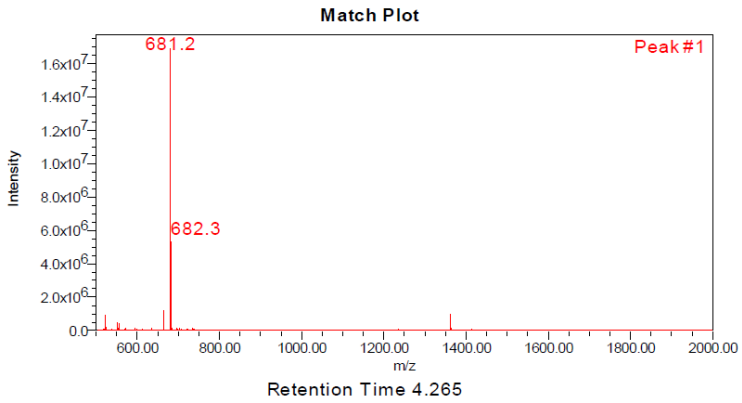

Mono-iodination of [Tyr^0]-Bradykinin

[Tyr^0]-Bradykinin (1.58 mg, 1.29 µmol) was dissolved in 740 µL of DCM and 180 µL of TFA. Then were added dropwise 36 µL of a 50 mM iodination stock solution (1.80 µmol, 1.4 eq.) (stock solution freshly prepared: 29.1 mg of Selectfluor were dissolved in 1.6 mL of ACN before the addition of 12.5 mg of NaI). The reaction mixture was allowed to stir at room temperature for 15 minutes. Two other additions of iodination solution (2 x 6.5 µL, 2 x 0.25 eq.) were needed to reach the following final ratio: SM: 1.9% - MI: 92.7% - DI: 5.4%. The reaction mixture was then evaporated under reduced pressure (TFA was co-evaporated three times with DCM) and redissolved in water/acetonitrile (1/1) before being submitted to HPLC (purification performed on Agilent Zorbax Rx C18, gradient: see general methods). The collected fraction was lyophilized to afford the desired product [mono-Iodo-Tyr^0]-Bradykinin (1.46 mg, 0.93 µmol, 72 % yield).

^{1}H NMR (500 MHz, d_6-DMSO, 300 K) δ: 1.43 (m, 1H), 1.51 (m, 5H), 1.61 (m, 2H), 1.70 (m, 2H), 1.79-2.05 (br, 9H), 2.18 (m, 1H), 2.72 (m, 2H), 2.79 (dd, 1H), 2.89 (dd, 1H), 2.96 (dd, 1H), 3.11 (m, 5H), 3.51 (m, 2H), 3.62 (m, 8H), 3.99 (m, 1H), 4.20 (m, 1H), 4.26 (dd, 1H), 4.30 (dd, 1H), 4.49 (m, 1H), 4.50-4.62 (m, 4H), 5.36 (s, 1H), 6.78 (d, 1H, J = 8.2 Hz), 7.00 (dd, 1H, J = 8.2, 2.0 Hz), 7.15-7.30 (m, 10H), 7.51 (d, 1H, J = 2.0 Hz), 7.56 (t, 1H), 7.61 (t, 1H), 7.70 (d, 1H), 7.94 (m, 2H), 8.08 (br, 2H), 8.13 (d, 1H), 8.31 (d, 1H), 8.66 (d, 1H), 10.31 (s, 1H), 12.72 (s, 1H).

^{13}C NMR (125 MHz, d_6-DMSO, 300 K) δ: 23.72, 24.43, 24.52, 25.09, 27.90, 28.12, 28.58, 28.81, 29.08, 35.47, 37.26, 37.72, 40.27, 40.47, 41.67, 46.82, 46.90, 50.01, 51.49, 52.60, 53.12, 53.38, 53.45, 57.63, 59.44, 59.60, 61.73, 84.78, 114.66, 126.26, 126.29, 126.90, 127.97, 128.02, 129.10, 129.13, 130.71, 137.57, 137.68, 139.39, 155.85, 156.66, 156.74, 167.52, 168.48, 168.50, 169.63, 170.04, 170.85, 170.95, 170.96, 171.77, 173.08.

HRMS (ESI-TOF) Calcd for $C_{59}H_{81}IN_{16}O_{13}$: 1348.5214; Found: 1348.5255.

UPLC-MS rt: 2.664 min (Gradient 1).

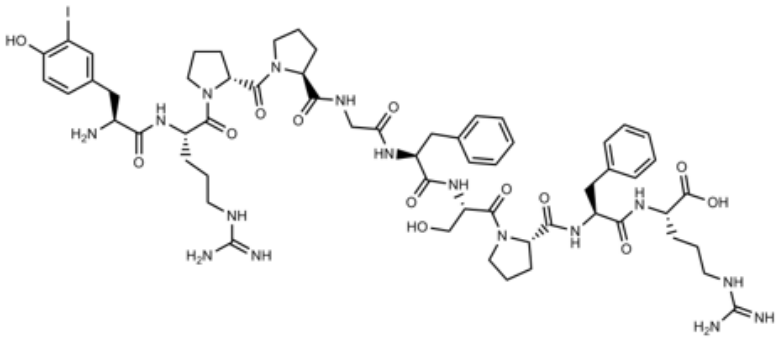

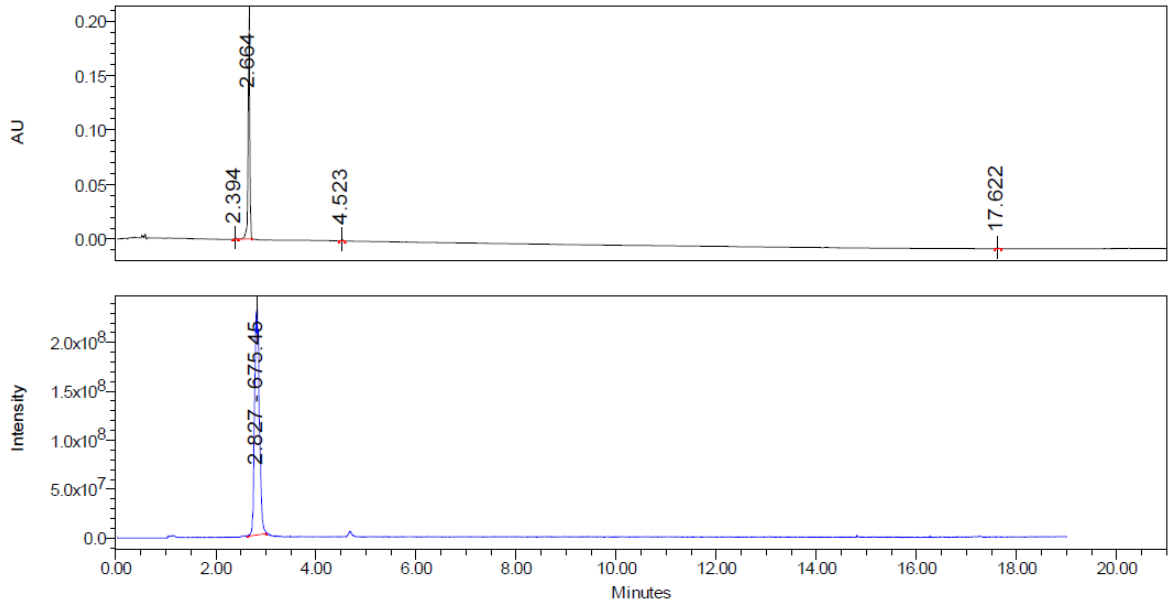

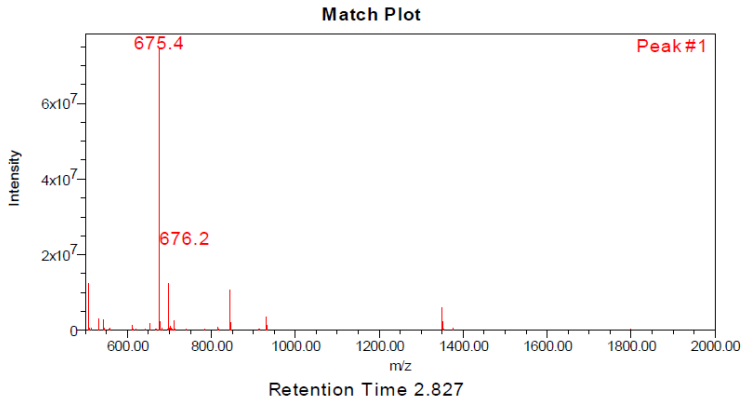

Mono-iodination of Angiotensin III

Angiotensin III (20.0 mg, 15.7 µmol) was dissolved in 8.5 mL of DCM and 2.0 mL of TFA. Then were added dropwise 440 µL of a 50 mM iodination stock solution (22.0 µmol, 1.4 eq.) (stock solution freshly prepared: 14.8 mg of Selectfluor were dissolved in 830 µL of ACN before the addition of 6.9 mg of NaI). The reaction mixture was allowed to stir at room temperature for 15 minutes. Three other additions of iodination solution (3 x 80 µL, 3 x 0.25 eq.) were needed to reach the following

final ratio: SM: 6.2% - MI: 91.3% - DI: 2.5%. The reaction mixture was then evaporated under reduced pressure (TFA was co-evaporated three times with DCM) and redissolved in water/acetonitrile (1/1) before being submitted to HPLC (purification performed on Xbridge Prep C18, gradient: see general methods). The collected fraction was lyophilized to afford the desired product [mono-Iodo]-Angiotensin III (14.9 mg, 11.6 µmol, 74 % yield).

^{1}H NMR (500 MHz, d_6-DMSO, 300 K) δ: 0.75 (d, 3H), 0.77 (t, 3H), 0.79 (d, 3H), 0.84 (d, 3H), 1.05 (p, 1H), 1.36 (m, 1H), 1.46 (m, 2H), 1.64 (m, 4H), 1.77 (br, 2H), 1.99 (m, 2H), 2.59 (dd, 1H), 2.77 (dd, 1H), 2.85 (dd, 1H), 2.93 (dd, 1H), 3.07 (m, 4H), 3.46 (br, 1H), 3.61 (m, 1H), 3.87 (br, 1H), 4.15 (t, 1H), 4.27 (m, 2H), 4.38 (dd, 1H), 4.49 (m, 1H), 4.79 (br, 1H), 6.75 (d, J = 8.4 Hz, 1H), 7.08 (m, 2H), 7.17 (m, 1H), 7.23 (m, 5H), 7.38 (br, 1H), 7.60 (m, 2H), 7.99 (s, 1H), 8.01 (s, 1H), 8.10 (br, 4H), 8.35 (d, 2H), 8.41 (d, 2H), 8.93 (br, 1H), 10.17 (s, 1H), 14.19 (br, 1H).

^{13}C NMR (125 MHz, d_6-DMSO, 300 K) δ: 10.85, 15.19, 17.57, 19.19, 24.10, 24.25, 24.28, 26.30, 28.62, 29.13, 31.11, 35.77, 36.62, 37.01, 40.12, 46.99, 47.7, 51.72, 53.83, 53.93, 56.65, 57.12, 59.87, 84.27, 114.41, 117.1, 126.2, 128.00, 129.17, 130.29, 130.36, 133.8, 137.88, 138.97, 155.02, 156.71, 168.22, 170.48, 170.85, 170.97, 171.43, 172.55.

HRMS (ESI-TOF) Calcd for $C_{46}H_{66}IN_{13}O_8$: 1055.4202; Found: 1055.4242.

UPLC-MS rt: 4.481 min (Gradient 2).

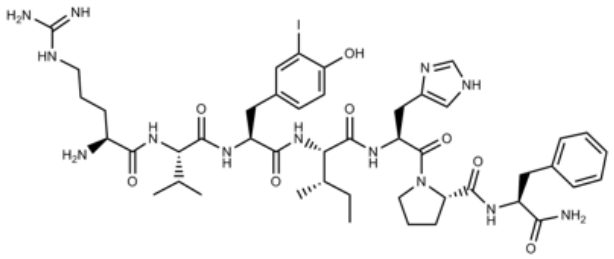

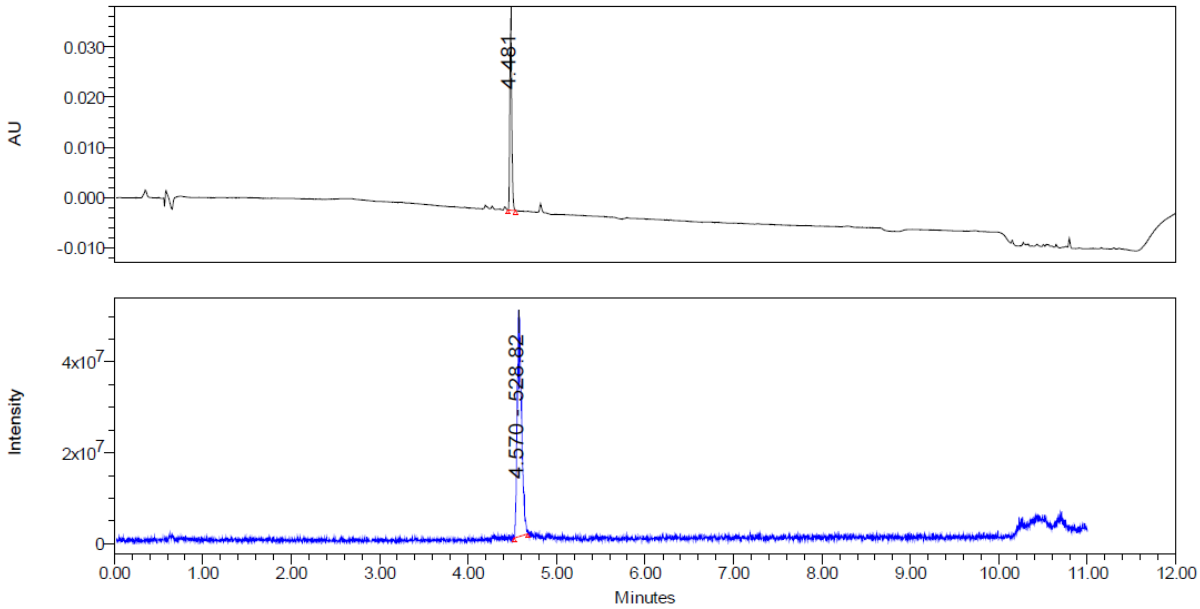

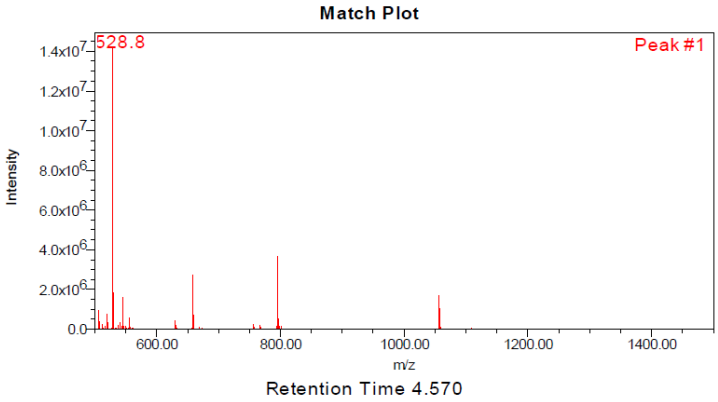

Mono-iodination of ACP-fragment 65-74 (11)

ACP fragment 65-74 (18.0 mg, 15.3 µmol) was dissolved in 6.0 mL of DCM and 1.5 mL of TFA. Then were added dropwise 428 µL of a 50 mM iodination stock solution (21.4 µmol, 1.4 eq.) (stock solution freshly prepared: 15.3 mg of Selectfluor were dissolved in 860 µL of ACN before the addition of 7.0 mg of NaI). The reaction mixture was allowed to stir at room temperature for 15 minutes. Two other additions of iodination solution (2 x 45 µL, 2 x 0.1 eq.) were needed to reach the following final ratio: SM: 2.3% - MI: 93.7% - DI: 4.0%. The reaction mixture was then evaporated under reduced pressure (TFA was co-evaporated three times with DCM) and redissolved in water/acetonitrile (1/1) before being submitted to HPLC (purification performed on Xbridge Prep C18, gradient: see general methods). The collected fractions were lyophilized to afford the desired product [mono-Iodo]-ACP fragment 65-74 (11.5 mg, 9.7 µmol, 63 % yield).

^{1}H NMR (500 MHz, d_6-DMSO, 295 K) δ: 0.73 (d, 3H), 0.76 (t, 3H), 0.80 (m, 6H), 0.91 (d, 3H), 0.92 (d, 3H), 1.00 (m, 1H), 1.06 (m, 1H), 1.17 (d, 3H), 1.18 (d, 3H), 1.35 (m, 1H), 1.43 (m, 1H), 1.66 (m, 2H), 1.76 (m, 1H), 1.87 (m, 1H), 2.03 (m, 1H), 2.13 (m, 2H), 2.43 (m, 1H), 2.51 (m, 1H), 2.62 (m, 3H), 2.84 (dd, 1H), 3.58 (m, 3H), 4.09 (t, 1H), 4.12 (t, 1H), 4.28 (m, 1H), 4.32 (m, 2H), 4.44 (m, 2H), 4.51 (m, 1H), 6.74 (d, J = 8.2 Hz, 1H), 6.84 (s, 1H), 6.99 (br, 1H), 7.02 (dd, J = 8.2, 1.8 Hz, 1H), 7.14 (s, 1H), 7.19 (s, 1H), 7.28 (s, 1H), 7.46 (s, 1H), 7.52 (d, J = 1.8 Hz, 1H), 7.67 (d, 1H), 7.77 (d, 1H), 8.04 (m, 5H), 8.10 (d, 1H), 8.17 (m, 2H), 8.28 (d, 1H), 8.52 (d, 1H), 10.07 (s, 1H), 12.35 (s, 1H).

^{13}C NMR (125 MHz, d_6-DMSO, 295 K) δ: 11.08, 11.11, 15.15, 15.27, 17.07, 17.79, 18.22, 18.33, 24.01, 24.45, 28.02, 29.89, 31.29, 35.96, 36.27, 36.43, 36.57, 36.99, 42.41, 47.97, 48.02, 49.54, 49.92, 52.07, 53.94, 56.6, 57.18, 57.25, 84.22, 114.49, 130.19, 130.34, 139.1, 155.01, 167.63, 170.29, 170.47, 170.6, 170.83, 171.01, 171.07, 171.11, 171.65, 171.82, 171.86, 171.91, 173.73.

HRMS (ESI-TOF) Calcd for $C_{47}H_{74}IN_{13}O_{15}$: 1187.4472; Found: 1187.4526.

UPLC-MS rt: 3.774 min (Gradient 1).

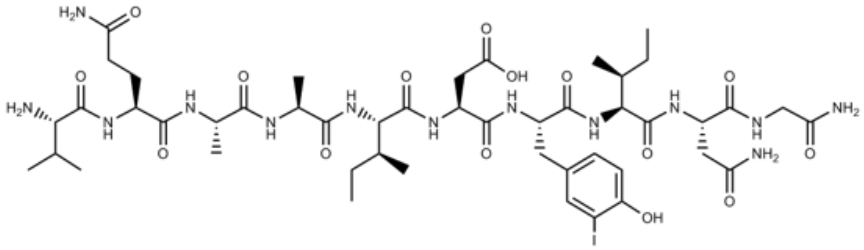

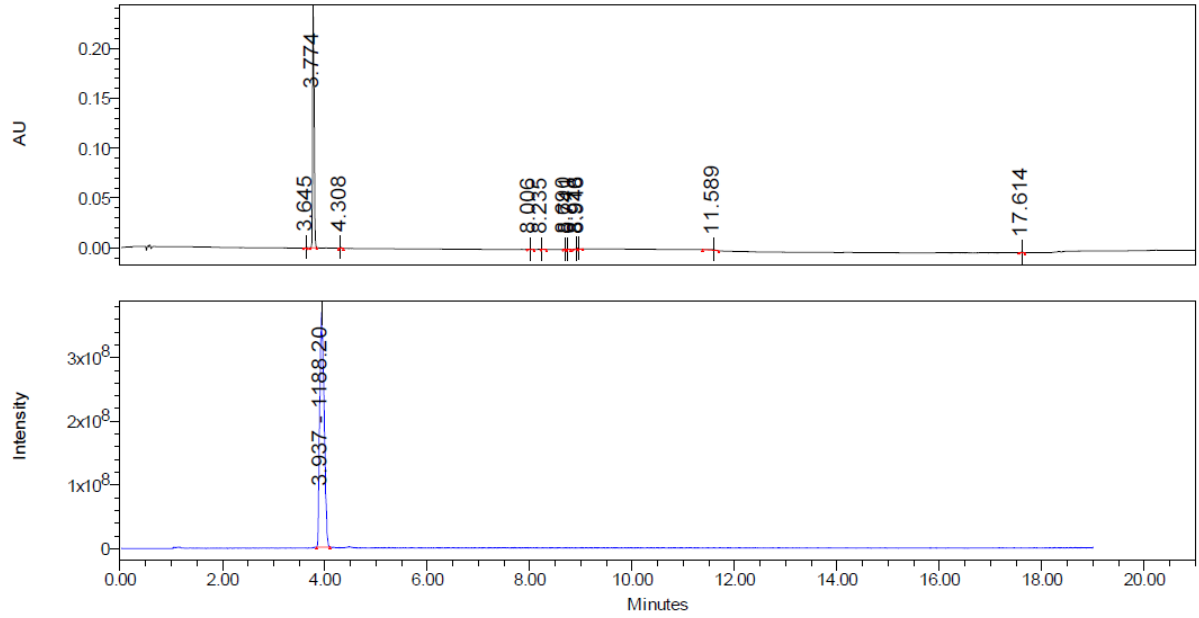

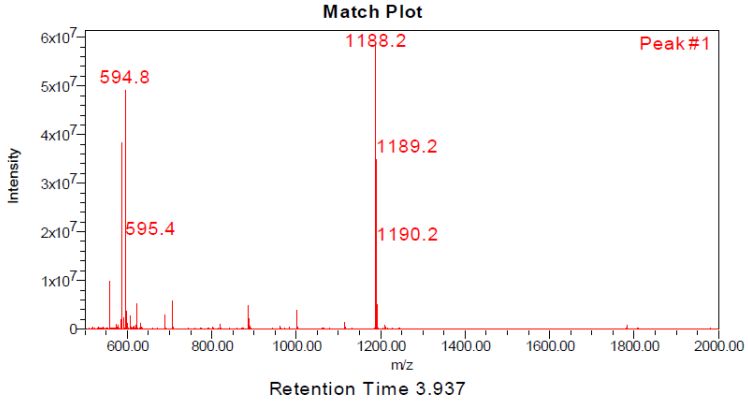

Mono-iodination of [Tyr^8]-Substance P (7)

[Tyr^8]-Substance P (3.0 mg, 2.2 µmol) was dissolved in 1.4 mL of DCM and 300 µL of TFA. Then were added dropwise 60 µL of a 50 mM iodination stock solution (3.0 µmol, 1.4 eq.) (stock solution freshly prepared: 15.0 mg of Selectfluor were dissolved in 840 µL of ACN before the addition of 7.2 mg of NaI). The reaction mixture was allowed to stir at room temperature for 15 minutes. Three other additions of iodination solution (3 x 15 µL, 3 x 0.35 eq.) were needed to reach the following final

ratio: SM: 5.9% - MI: 93.6% - DI: 0.5%. The reaction mixture was then quenched with 400 µL of reducing cocktail (freshly prepared: KI (10 mg) and ascorbic acid (10 mg) were sonicated in 500 µL of TFA for 10 minutes) and evaporated under reduced pressure (TFA was co-evaporated three times with DCM). The crude was dissolved in water/acetonitrile (1/1) before being submitted to HPLC (purification performed on Agilent Zorbax Rx C18, gradient: see general methods). The collected fractions were lyophilized to afford the desired product [mono-Iodo-Tyr^{8}]-Substance P (2.9 mg, 1.6 µmol, 72 % yield).

^{1}H NMR (700 MHz, d_6-DMSO, 295 K) δ: 0.84 (d, 3H), 0.88 (d, 3H), 1.39 (m, 2H), 1.47 (m, 2H), 1.51 (m, 1H), 1.54 (m, 2H), 1.61 (m, 3H), 1.67-1.77 (m, 6H), 1.78-1.88 (m, 6H), 1.91 (m, 3H), 2.03 (m, 4H), 2.11 (m, 4H), 2.38 (m, 1H), 2.45 (m, 1H), 2.67 (dd, 1H), 2.75 (m, 3H), 2.92 (m, 2H), 3.13 (m, 2H), 3.60 (m, 2H), 3.72 (m, 3H), 4.15 (m, 3H), 4.23 (m, 1H), 4.30 (m, 2H), 4.43 (m, 4H), 6.77 (d, 1H, J = 8.2 Hz), 6.87 (s, 2H), 7.08 (m, 2H), 7.15 (m, 3H), 7.19 (m, 3H), 7.32 (s, 2H), 7.58 (d, 1H, J = 1.8 Hz), 7.69 (t, 1H), 7.77 (br, 3H), 7.84 (d, 1H), 7.97 (t, 2H), 8.01 (t, 2H), 8.18 (br, 3H), 8.23 (t, 1H), 8.27 (d, 1H), 8.31 (d, 1H), 10.10 (s, 1H).

^{13}C NMR (175 MHz, d_6-DMSO, 295 K) δ: 14.65, 21.59, 21.84, 23.13, 23.62, 24.12, 24.67, 24.68, 26.56, 27.11, 27.39, 27.90, 29.03, 29.22, 29.70, 30.12, 31.48, 31.57, 31.59, 36.18, 37.50, 38.58, 40.22, 40.70, 41.99, 49.88, 47.04, 50.43, 50.48, 51.21, 51.76, 52.30, 52.80, 54.13, 54.29, 59.24, 59.83, 84.28, 114.63, 126.20, 128.04, 129.11, 130.22, 130.33, 137.59, 139.21, 155.10, 156.79, 166.84, 168.64, 170.38, 170.87, 170.92, 170.98, 171.30, 171.93, 172.04, 173.08, 174.19, 174.24.

HRMS (ESI-TOF) Calcd for $C_{63}H_{97}IN_{18}O_{14}S$: 1488.6197; Found: 1488.6244.

UPLC-MS rt: 2.555 min (Gradient 1).

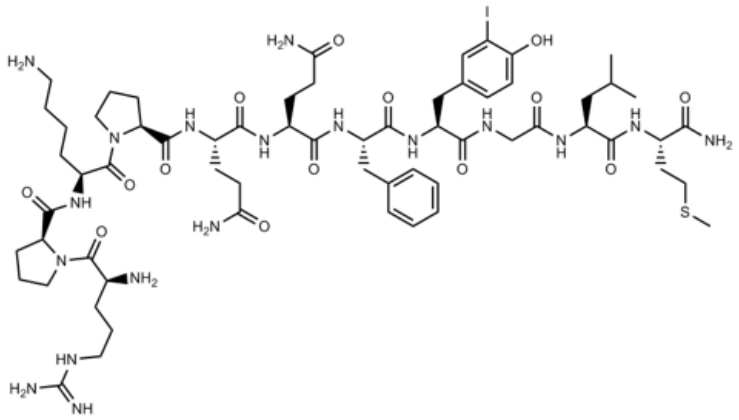

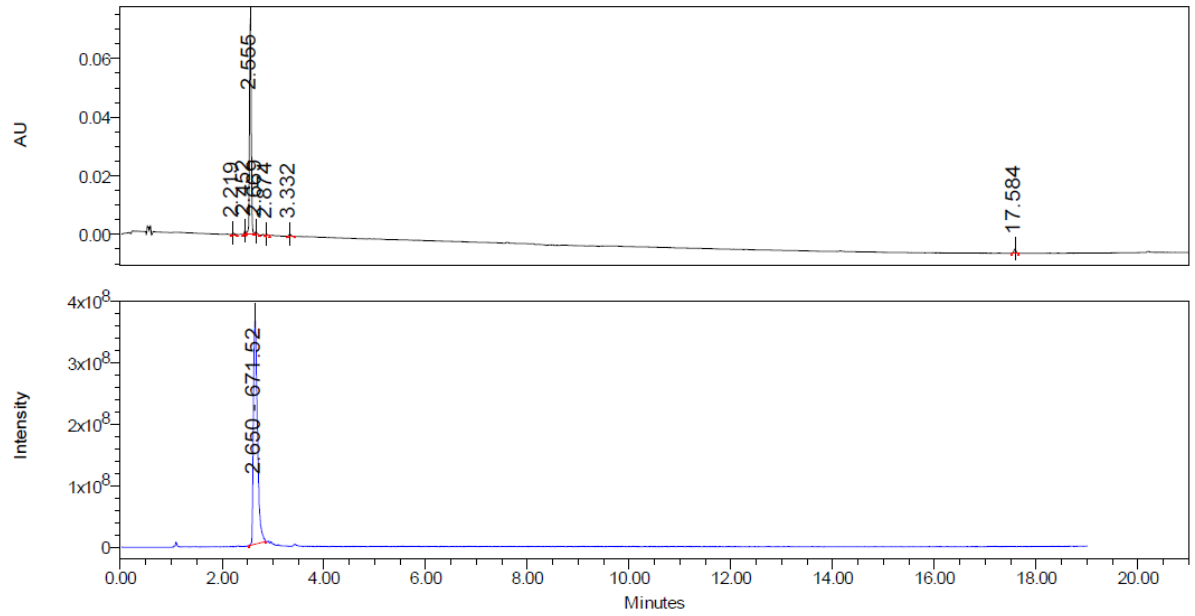

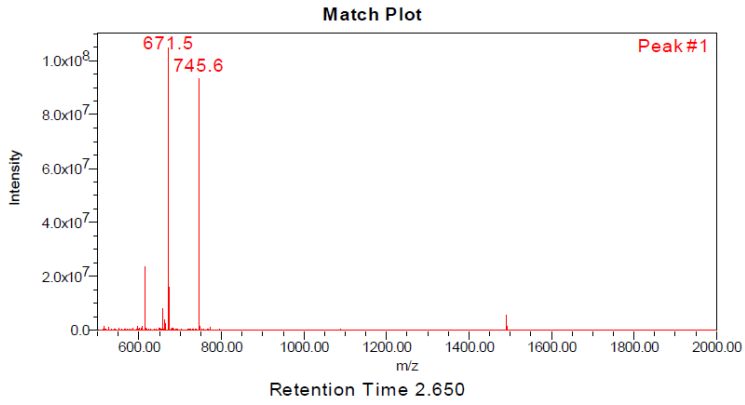

Mono-iodination of GLP-1(7-37)

GLP-1(7-37) (40.0 mg, 11.9 µmol) was dissolved in 5.6 mL of DCM and 1.4 mL of TFA. Then were added dropwise 330 µL of a 50 mM iodination stock solution (3.0 µmol, 1.4 eq.) (stock solution freshly prepared: 15.0 mg of Selectfluor were dissolved in 840 µL of ACN before the addition of 7.2 mg of NaI). The reaction mixture was allowed to stir at room temperature for 15 minutes. Two other additions of iodination solution (2 x 55 µL, 3 x 0.25 eq.) were needed to reach the following final ratio: SM: 4.6% - MI: 91.3% - DI: 4.1%. The reaction mixture was then evaporated under reduced pressure (TFA was co-evaporated three times with DCM). The crude was dissolved in water/acetonitrile (1/1) before being submitted to HPLC (purification performed on Waters Acquity CSH C18, gradient: see general methods). The collected fractions were lyophilized to afford the desired product [mono-Iodo]-GLP-1(7-37) (21.5 mg, 6.2 µmol, 52 % yield).

HRMS (ESI-TOF) Calcd for $C_{151}H_{227}IN_{40}O_{47}$ $[M+3H]^{3+}$ 1741.2900; Found: 1741.2999.

UPLC-MS rt: 6.217 min (Gradient 1).

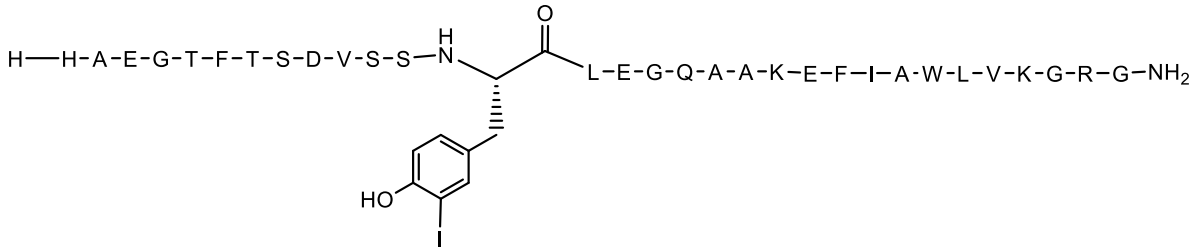

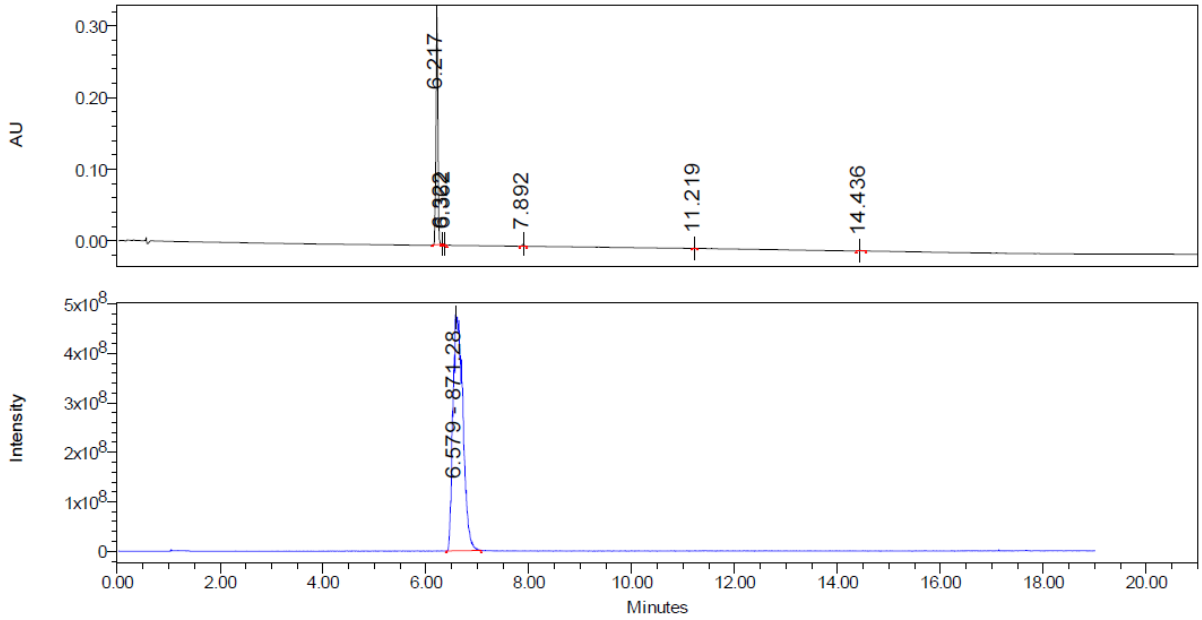

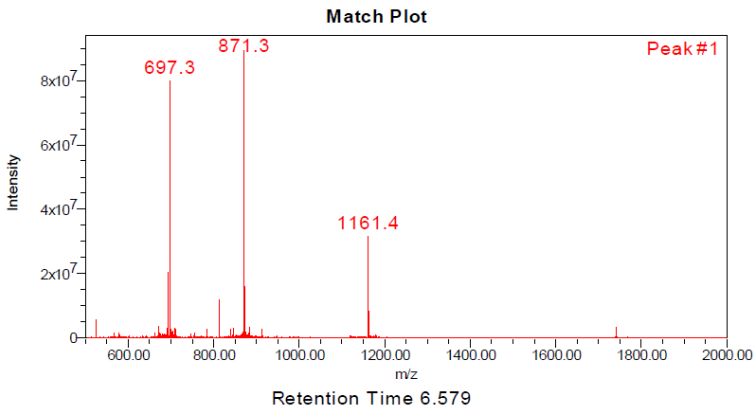

Synthesis of Amino-PEG$_2$-Dansyl

Dansyl chloride (100 mg, 370 µmol) was dissolved in 1.0 mL of DCM before the addition dropwise of tert-butyl(2-(2-(2-aminoethoxy)ethoxy)ethyl)carbamate (105 µL, 445 µmol) previously dissolved in 1 mL of DCM. The mixture was allowed to stir at room temperature for 2 hours. Reaction was monitored by LC-MS. The mixture was then diluted with 4 mL of brine, washed with water three times before being dried over magnesium sulfate and filtered. Subsequently 450 µL of TFA were added to the mixture (~10% v/v DCM) to induce Boc deprotection. After 15 min, LC-MS showed completion of reaction. The mixture was evaporated under reduced pressure and redissolved in acetonitrile and water before lyophilization to afford the desired product as pale yellow oil (201 mg,

346 µmol, 93 % yield).
^{1}H NMR (400 MHz, d_6-DMSO, 295 K) δ: 1.28 (s, 1H), 2.07 (s, 1H), 2.84 (s, 6H), 2.96 (m, 5H), 3.56 (m, 4 H), 4.60 (s, 1H), 5.37 (br s, 3H), 5.75 (br s, 1H), 7.27 (d, J=7.46 Hz, 1H), 7.61 (m, 2H), 7.72 (br s, 3H), 7.99 (t, J=5.81, 5.81 Hz, 1H), 8.11 (dd, J=7.34, 0.98 Hz, 1H), 8.30 (d, J=8.68 Hz, 1H), 8.47 (d, J=8.44 Hz, 1H).
^{13}C NMR (150 MHz, d_6-DMSO, 300 K) δ: 38.54, 42.16, 45.06 (2C), 66.58, 69.01, 69.30, 69.43, 115.13, 119.23, 123.56, 127.75, 128.00, 128.99, 129.03, 129.27, 136.21, 151.17.
HRMS (ESI-TOF) Calcd for $C_{18}H_{27}N_3O_4S$: 382.1795; Found: 382.1795.

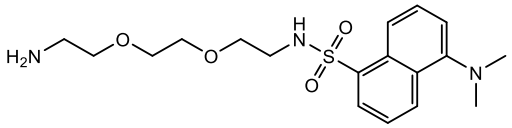

Synthesis of Boronic pinacol ester-PEG$_2$-Dansyl (9)
4-Carboxylphenylboronic acid pinacol ester (31 mg, 125 µmol), DIEA (45 µL, 258 µmol) and propylphosphonic anhydride T3P (75 µL, 125 µmol - 50% wt. solution in ethyl acetate) were dissolved in 1 mL of DCM and stirred at room temperature for 5 minutes before the dropwise addition of amino-PEG$_2$-Dansyl (60 mg, 104 µmol) and DIEA (45 µL, 258 µmol) previously dissolved in 750 µL of DCM. The reaction mixture was allowed to stir at room temperature. After 30 min, LC-MS showed completion of reaction. The crude was evaporated under reduced pressure and purified via silica gel chromatography (0->100% EtOAc/Hept – product eluted around ~80% EtOAc/Hept) to afford the desired product as a yellow oil (39 mg, 64 µmol, 62 % yield).
^{1}H NMR (400 MHz, d_6-DMSO, 295 K) δ: 1.17 (m, 1 H), 1.31 (s, 12 H), 1.91 (s, 1 H), 1.99 (s, 1 H), 2.50 (u), 2.82 (s, 6 H), 2.94 (q, J=5.83, 5.83, 5.83 Hz, 2 H), 3.28 (m, 4 H), 3.45 (u), 4.03 (q, J=7.17, 7.17, 7.17 Hz, 1 H), 7.24 (d, J=7.46 Hz, 1 H), 7.59 (m, 2 H), 7.74 (m(para), 2 H), 7.83 (m(para), 2 H), 8.11 (dd, J=7.34, 0.98 Hz, 1 H), 7.98 (t, J=5.81, 5.81 Hz, 1 H), 8.28 (d, J=8.68 Hz, 1 H), 8.44 (d, J=8.56 Hz, 1 H), 8.52 (t, J=5.50, 5.50 Hz, 1 H).
^{13}C NMR (150 MHz, d_6-DMSO, 300 K) δ: 24.65(4C), 39.51, 42.20, 45.03(2C), 68.72, 68.93, 69.29, 69.38, 83.89(2C), 115.05, 119.21, 123.50, 126.47(2C), 127.71, 127.97, 129.01, 129.03, 129.24, 134.21(2C), 136.32, 136.80, 151,27, 165.99.
The carbon directly bonded to boron could not be detected due to quadrupolar relaxation.

HRMS (ESI-TOF) Calcd for $C_{31}H_{43}BN_3O_7S$ $[M+Na]^+$ 634.2734; Found: 634.2737.

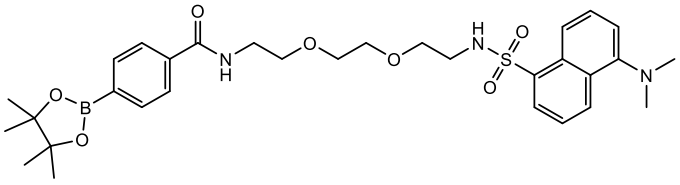

Synthesis of Boronic pinacol ester-PEG$_3$-azide (12)

4-carboxylphenylboronic acid pinacol ester (200 mg , 806 µmol), DIEA (422 µL, 2.42 mmol) and propylphosphonic anhydride T3P (720 µL, 1.21 mmol – 50% wt. solution in ethyl acetate) were dissolved in 500 µL of DCM and was allowed to premix at room temperature for 5 minutes before the dropwise addition of amino-PEG$_3$-azide (211 mg, 968 µmol) previously dissolved in 500 µL of DCM . The reaction was stirred at room temperature for 10 minutes. Reaction was monitored by LC-MS. The crude was dissolved in 5 mL of DCM and 5 mL of 0.5M HCl aqueous solution, washed twice with water (2x5mL) before being dried with magnesium sulfate, filtered and evaporated under reduced pressure to afford the desired product as a white powder (308 mg, 687 µmol, 85 % yield).

^{1}H NMR (400 MHz, d$_6$-DMSO, 295 K) δ: 0.94 (m, 1 H), 1.31 (s, 12 H), 1.48 (m, 1 H), 2.50 (u), 3.23 (br s, 1 H), 3.44 (br s, 1 H), 3.53 (d, J=4.65 Hz, 9 H), 3.57 (m, 4 H), 7.79 (m(para), 4 H), 8.55 (t, J=5.50, 5.50 Hz, 1 H).

^{13}C NMR (150 MHz, d$_6$-DMSO, 300 K) δ: 24.65(4C), 39.51, 49.95, 68.78, 69.18, 69.57, 69.64, 69.73, 69.76, 83.89(2C), 126.49(2C), 134.21(2C), 136.84, 166.00.

The carbon directly bonded to boron could not be detected due to quadrupolar relaxation.

HRMS (ESI-TOF) Calcd for $C_{21}H_{34}BN_4O_6$ $[M+Na]^+$ 471.2389; Found: 471.2388.

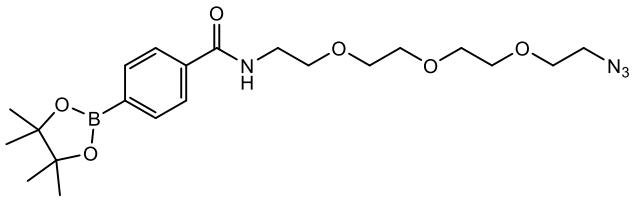

Synthesis of Dansyl-PEG$_2$-Leucin Enkephalinamide (10) - Suzuki-Miyaura Cross-coupling

Preparation of the Pd catalyst was performed as described by Chalker *et al*[2]. Briefly, 2-amino-4,6-dihydroxypyrimidine disodium (7.6 mg, 44 µmol) was dissolved in 440 µL of water by stirring for 2 minutes in a water bath preheated to 65°C. To the resulting solution was added $Pd(OAc)_2$ (5.0 mg, 22 µmol). The mixture was stirred vigorously at 65°C for 30 minutes to give a homogenous yellow-orange solution. After cooling to room temperature, the stir bar was removed to give the catalyst stock solution 50 mM in Pd(II).

In a 1.5 mL Eppendorf tube, [mono-Iodo]-Leucine Enkephalinamide (1.0 mg, 1.50 µmol) was dissolved in 75 µL of water and 75 µL of dioxane before the addition of glycerol (50 µL), K_2HPO_4 (1M aqueous stock solution, 45 µL, 45 µmol) and boronic pinacol ester-PEG$_2$-Dansyl (**9**) (50 mM stock solution in dioxane, 45 µL, 2.25 µmol). Prior and after the addition of $Pd(OAc)_2.L_2$ (50 mM aqueous stock solution, 75 µL, 3.75 µmol) the mixture was bubbled with argon for 10 minutes. The resulting solution was capped and stirred at 38°C for 12 hours on an Eppendorf Thermomixer (1300 rpm). The reaction was monitored by LC-MS. The crude mixture was quenched with 1 mL of a 1M HCl aqueous solution before being submitted to HPLC (purification performed on Agilent Zorbax Rx C18, gradient: see general methods). The collected fractions were lyophilized to afford the desired product Dansyl-PEG$_2$-Leucine Enkephalinamide (0.55 mg, 0.53 µmol, 35 % yield).

HRMS (ESI-TOF) Calcd for $C_{53}H_{67}N_9O_{11}S$: 1038.4754; Found: 1038.4753.

UPLC-MS rt: 6.793 min (Gradient 1).

Max Abs/Em - / 506 nm (absorption <400 nm cannot be measured with our device)

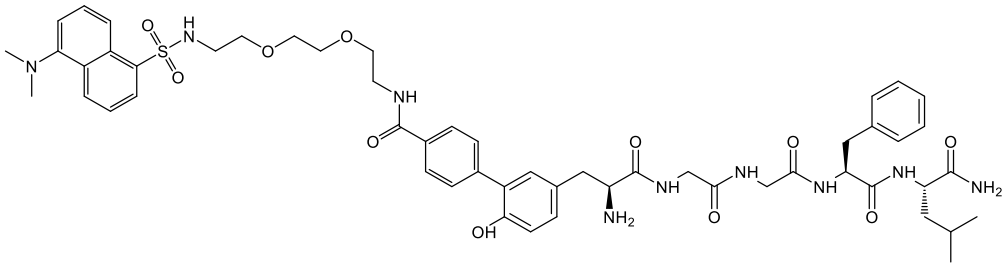

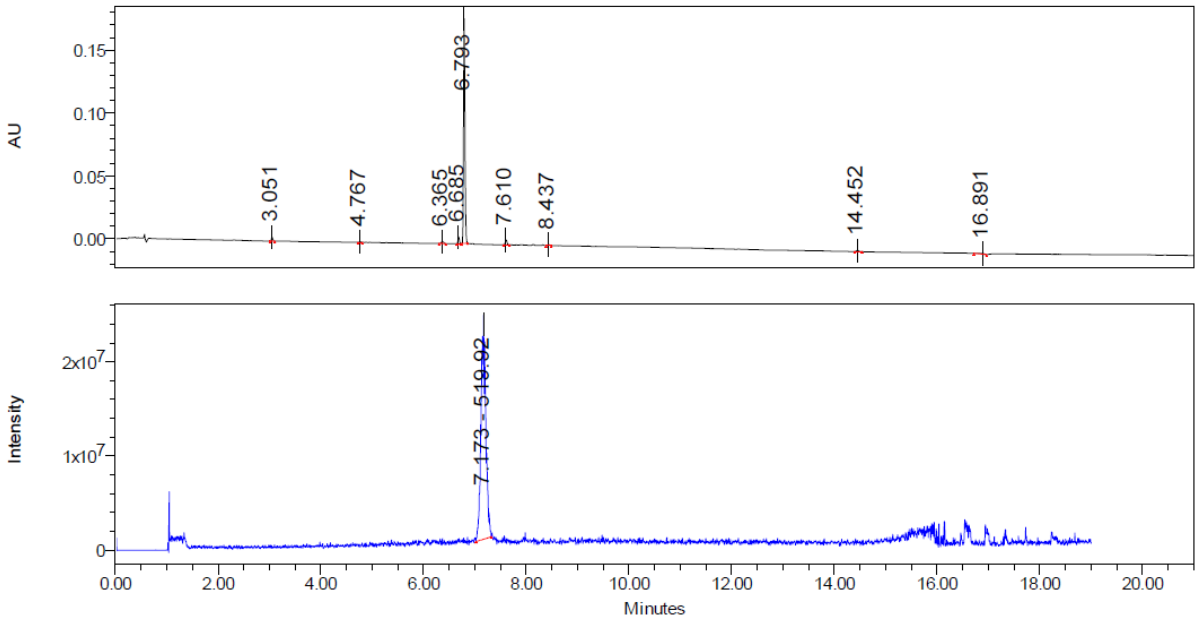
AU
0.15
0.10
0.05
0.00
3.051
4.767
6.365
6.685
6.793
7.610
8.437
14.452
16.891
Intensity
2x10^7
1x10^7
0
7.173 - 519.92
0.00
2.00
4.00
6.00
8.00
10.00
12.00
14.00
16.00
18.00
20.00
Minutes

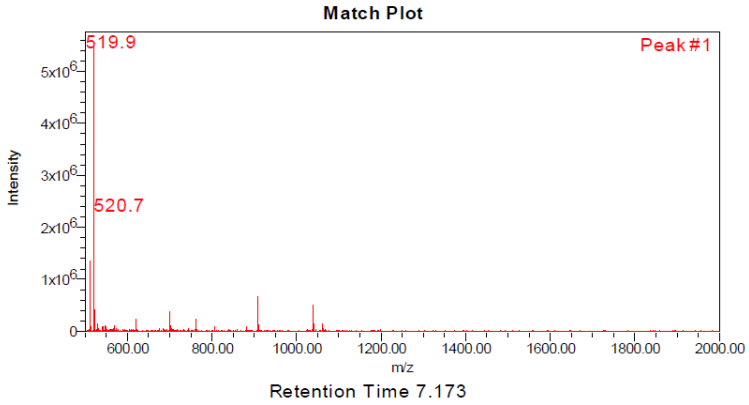
Match Plot
519.9
Peak #1
520.7
Intensity
5x10^6
4x10^6
3x10^6
2x10^6
1x10^6
0
600.00
800.00
1000.00
1200.00
1400.00
1600.00
1800.00
2000.00
m/z
Retention Time 7.173

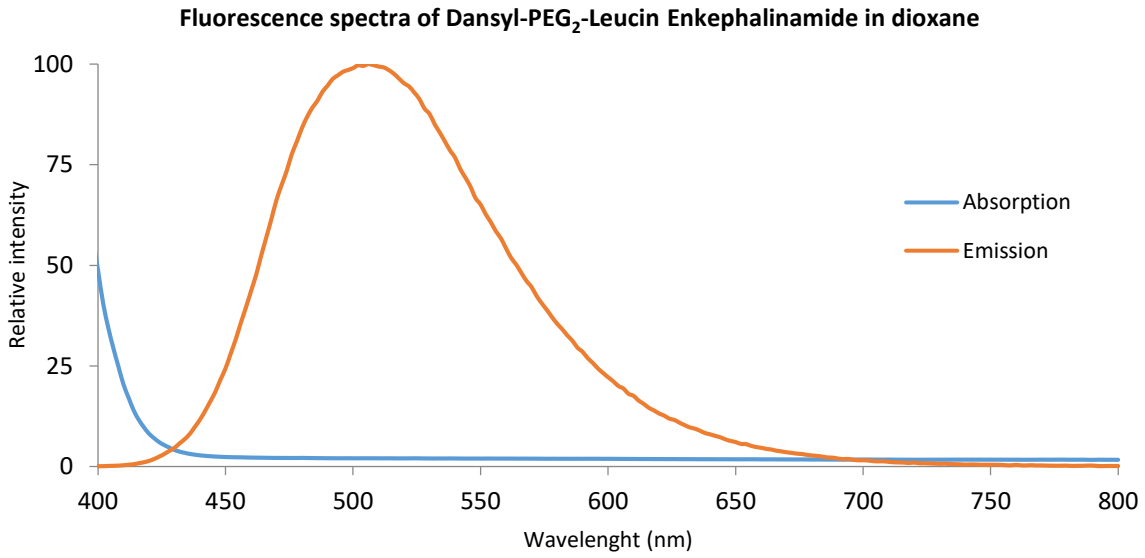

Synthesis of Azido-PEG$_3$-ACP fragment (65-74) - Suzuki-Miyaura Cross-coupling

In a 1.5 mL Eppendorf tube, [mono-Iodo]-ACP fragment (65-74) (2.43 mg, 2.05 µmol) was dissolved in 100 µL of water and 100 µL of dioxane before the addition of glycerol (50 µL), K_2HPO_4 (1M aqueous stock solution, 50 µL, 50 µmol) and boronic pinacol ester-PEG$_3$-azide (**12**) (50 mM stock solution in dioxane, 75 µL, 3.75 µmol). Prior and after the addition of $Pd(OAc)_2.L_2$ (50 mM aqueous stock solution, 80 µL, 4.0 µmol) the mixture was bubbled with argon for 10 minutes. The resulting solution was capped and stirred at 38 °C for 12 hours on an Eppendorf Thermomixer (1300 rpm). The reaction was monitored by LC-MS. The crude mixture was quenched with 1mL of a 1M HCl aqueous solution before being submitted to HPLC (purification performed on Agilent Zorbax Rx C18, gradient: see general methods). The collected fractions were lyophilized to afford the desired product Azido-PEG$_3$-ACP fragment (65-74) (1.68 mg, 1.22 µmol, 59 % yield).

HRMS (ESI-TOF) Calcd for $C_{62}H_{95}N_{17}O_{19}$: 1380.6917; Found: 1380.6899.

UPLC-MS rt: 4.950 min (Gradient 1).

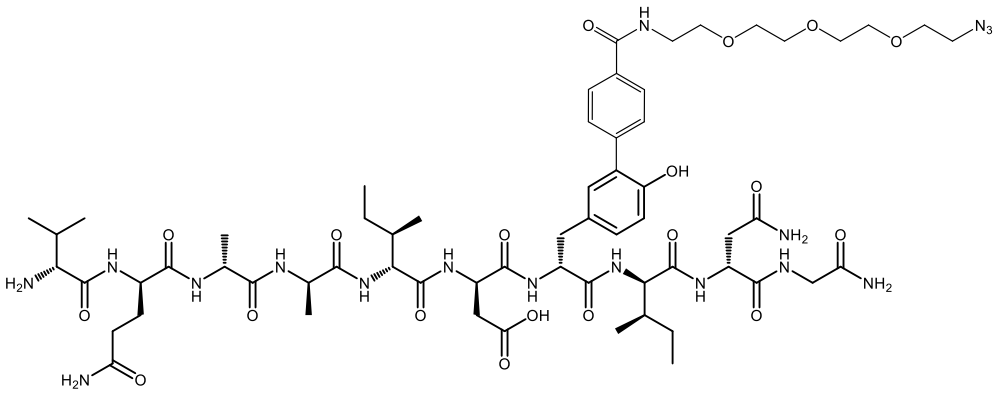

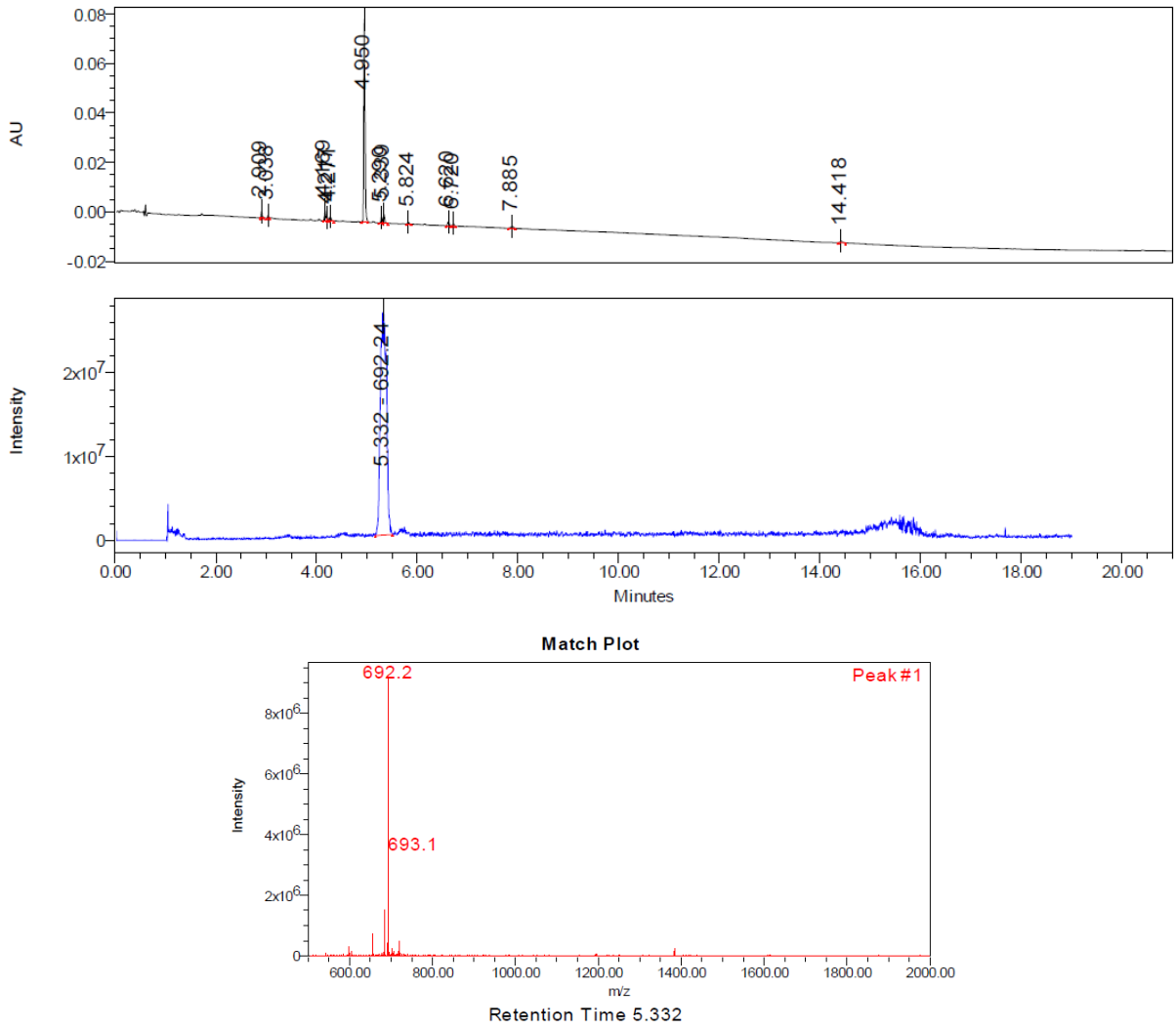

Synthesis of Alexa Fluor 488-PEG$_3$-ACP fragment (65-74) (13) – CuAAC

Azido-PEG$_3$- ACP fragment (65-74) (1.68 mg, 1.22 µmol) was dissolved in 200 µL of water and 100 µL of tBuOH before the addition of Alkyne-Alexa Fluor 488 (1.0 mg, 1.29 µmol). Copper sulfate (50 mM stock solution in water, 3 µL, 0.15 µmol), Cu-ligand THPTA[3] (200 mM stock solution in water, 3 µL, 0.60 µmol) and ascorbic acid (100 mM stock solution in water, 7.5 µL, 0.75 µmol) were premixed together before being added to the reaction mixture. The resulting solution was stirred at 38°C in a Thermomixer (1300 rpm) for 12 hours. The reaction was monitored by LC-MS. The crude mixture was dissolved in water/ACN before being submitted to HPLC (purification performed on Agilent Zorbax Rx C18, gradient: see general methods). The collected fractions were lyophilized to afford the desired product as an orange powder Alexa Fluor488-PEG$_3$-ACP fragment (65-74) (1.48 mg, 0.76 µmol, 62 % yield).

HRMS (ESI-TOF) Calcd for $C_{86}H_{112}N_{20}O_{29}S_2$ $[M+2H]^{2+}$ 977.8760; Found: 977.8803.

UPLC-MS rt: 5.009 min (Gradient 1).

Max Abs/Em 494/524 nm.

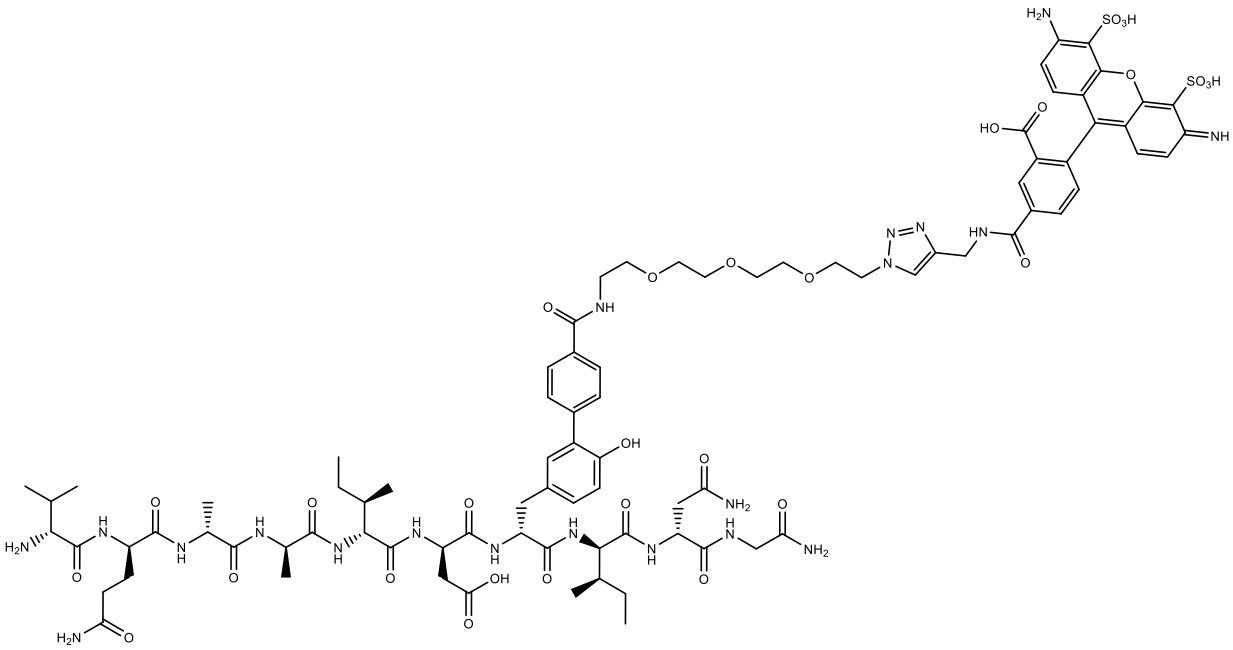

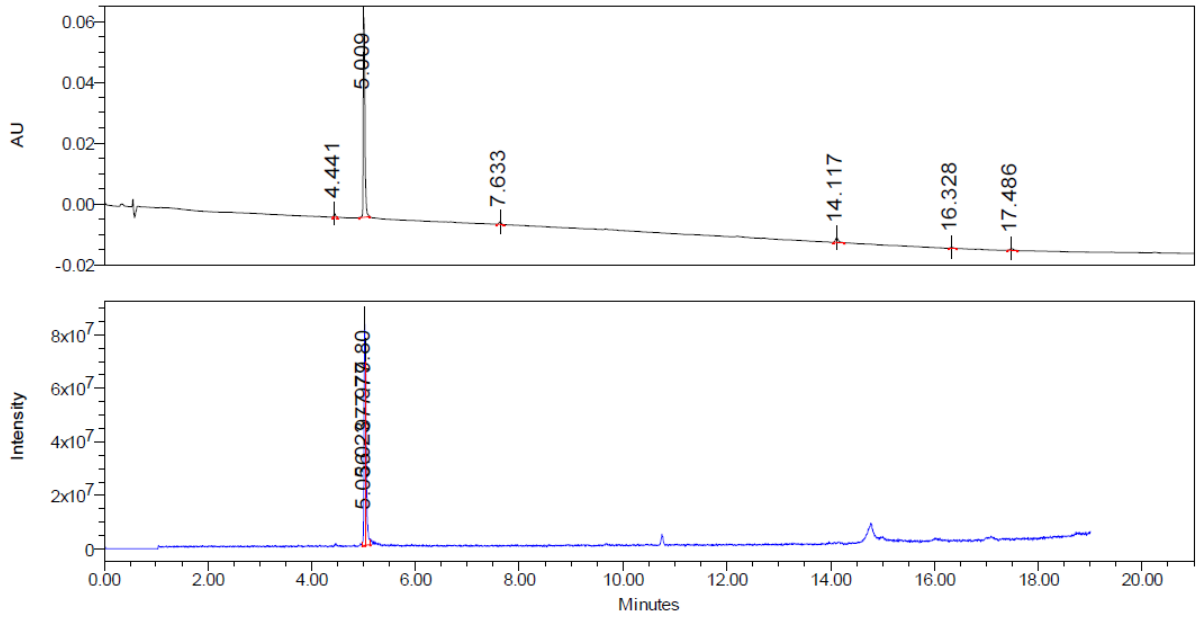
AU
0.06
0.04
0.02
0.00
-0.02
5.009
4.441
7.633
14.117
16.328
17.486
Intensity
8x10^7
6x10^7
4x10^7
2x10^7
0
0.00
2.00
4.00
6.00
8.00
10.00
12.00
14.00
16.00
18.00
20.00
Minutes

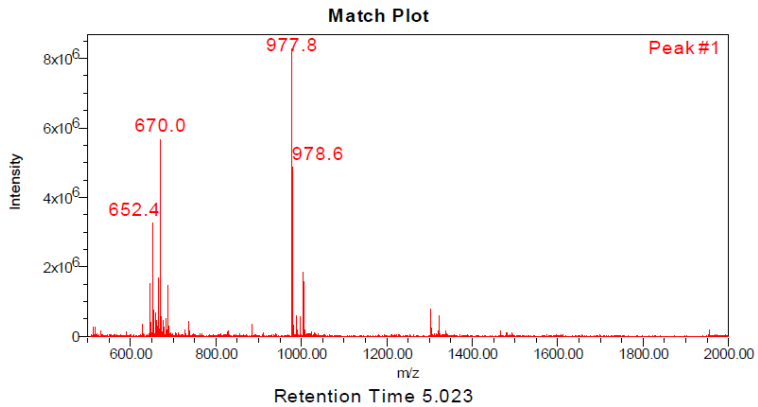
Match Plot
977.8
Peak#1
670.0
978.6
652.4
Intensity
8x10^6
6x10^6
4x10^6
2x10^6
0
600.00
800.00
1000.00
1200.00
1400.00
1600.00
1800.00
2000.00
m/z
Retention Time 5.023

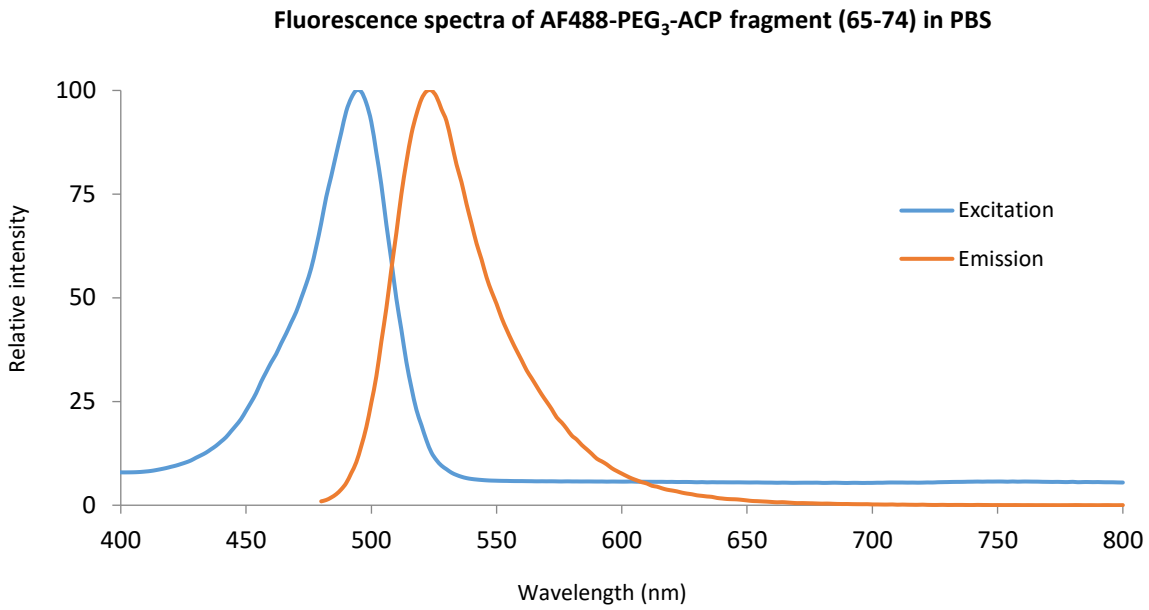
Fluorescence spectra of AF488-PEG3-ACP fragment (65-74) in PBS
Relative intensity
100
75
50
25
0
400
450
500
550
600
650
700
750
800
Wavelength (nm)
Excitation
Emission

NMR Spectra and proton assignment of mono-iodinated peptides

[mono-iodo] Leucine Enkephalinamide

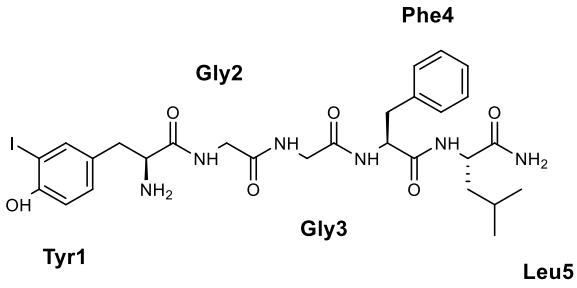

^{1}H NMR (500 MHz, d_6-DMSO, 300 K) and ^{13}C NMR (125 MHz, d_6-DMSO, 300 K).

		^{1}H	^{13}C
Tyr-1	NH_3^+	broad	-
	α	3.46	55.77
	β	2.86/2.51	38.53
	γ	-	130.62
	δ1	7.53	139.22
	δ2	7.03	130.40
	ε1	-	84.36
	ε2	6.78	114.64
	ζ	-	155.08
	ζ-OH	~ 10.1 (broad)	-
	C’	-	173.76
Gly-2	NH	8.30	-
	α	3.73	42.02
	C’	-	169.10
Gly-3	NH	8.12	-
	α	3.73/3.61	41.90
	C’	-	168.75
Phe-4	NH	8.08	-

	α	4.50	54.09
	β	3.04/2.80	37.28
	γ	-	137.78
	δ	7.25	129.17
	ε	7.25	128.04
	ζ	7.18	126.26
	C’	-	170.69
Leu-5	NH	7.95	-
	α	4.20	50.99
	β	1.47	40.80
	γ	1.57	24.19
	δ	0.88	23.02
	δ’	0.83	21.56
	C’	-	173.88
	NH_2	7.08/6.97	-

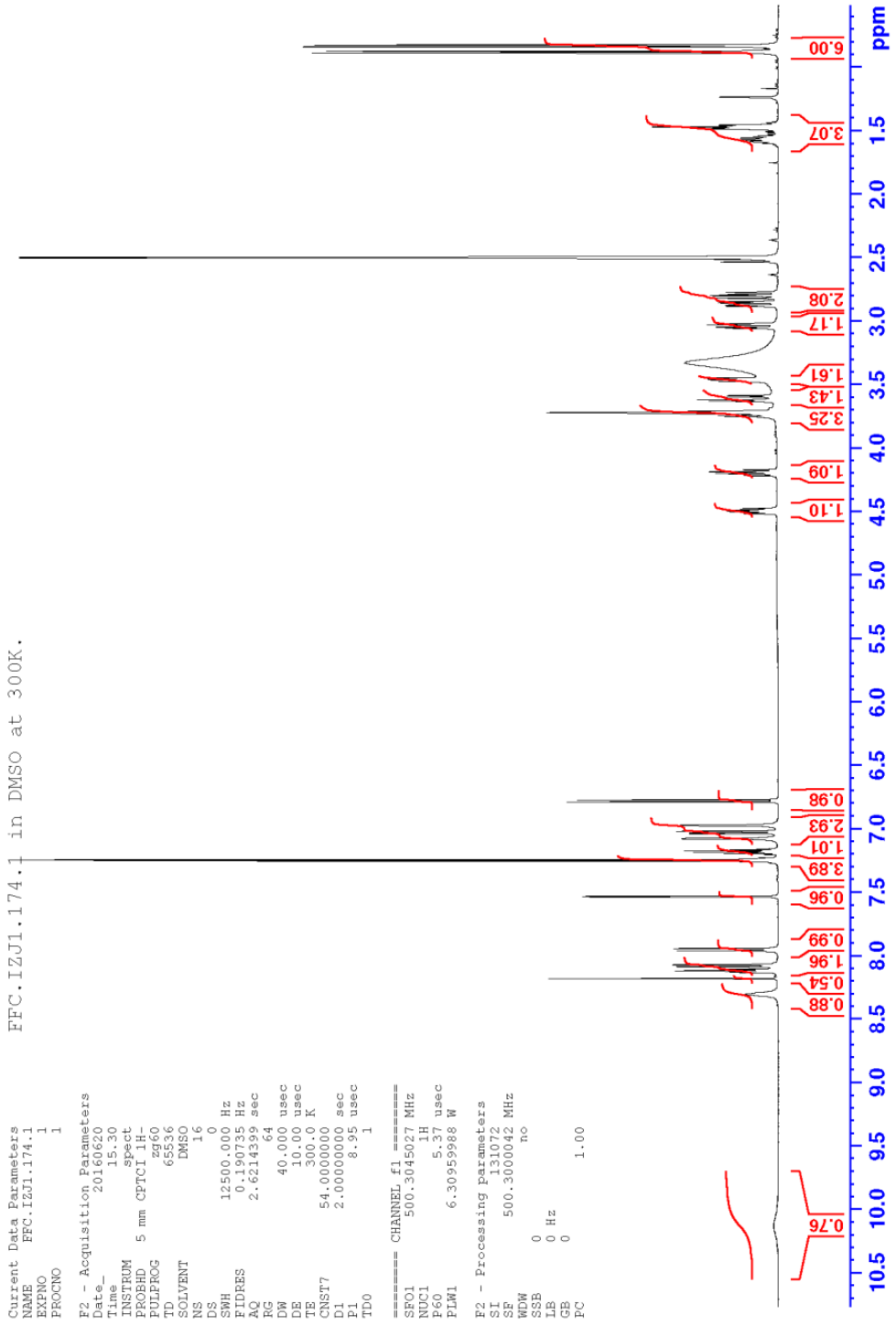
FFC.IZJ1.174.1 in DMSO at 300K.
Current Data Parameters
NAME FFC.IZJ1.174.1
EXPNO 1
PROCNO 1
F2 - Acquisition Parameters
Date_ 20160620
Time_ 15.30
INSTRUM spect
PROBHD 5 mm CPTCI 1H-
PULPROG zg60
TD 65536
SOLVENT DMSO
NS 16
DS 0
SWH 12500.000 Hz
FIDRES 0.190735 Hz
AQ 2.6214399 sec
RG 64
DW 40.000 usec
DE 10.00 usec
TE 300.0 K
CNST7 54.0000000
D1 2.00000000 sec
P1 8.95 usec
TD0 1
======== CHANNEL f1 ========
SFO1 500.3045027 MHz
NUC1 1H
P60 5.37 usec
PLW1 6.30959988 W
F2 - Processing parameters
SI 131072
SF 500.3000042 MHz
WDW no
SSB 0
LB 0 Hz
GB 0
PC 1.00
0.76
0.88
0.54
1.96
0.99
0.96
3.89
1.01
2.93
0.98
1.10
1.09
3.25
1.43
1.61
1.17
2.08
3.07
6.00
ppm

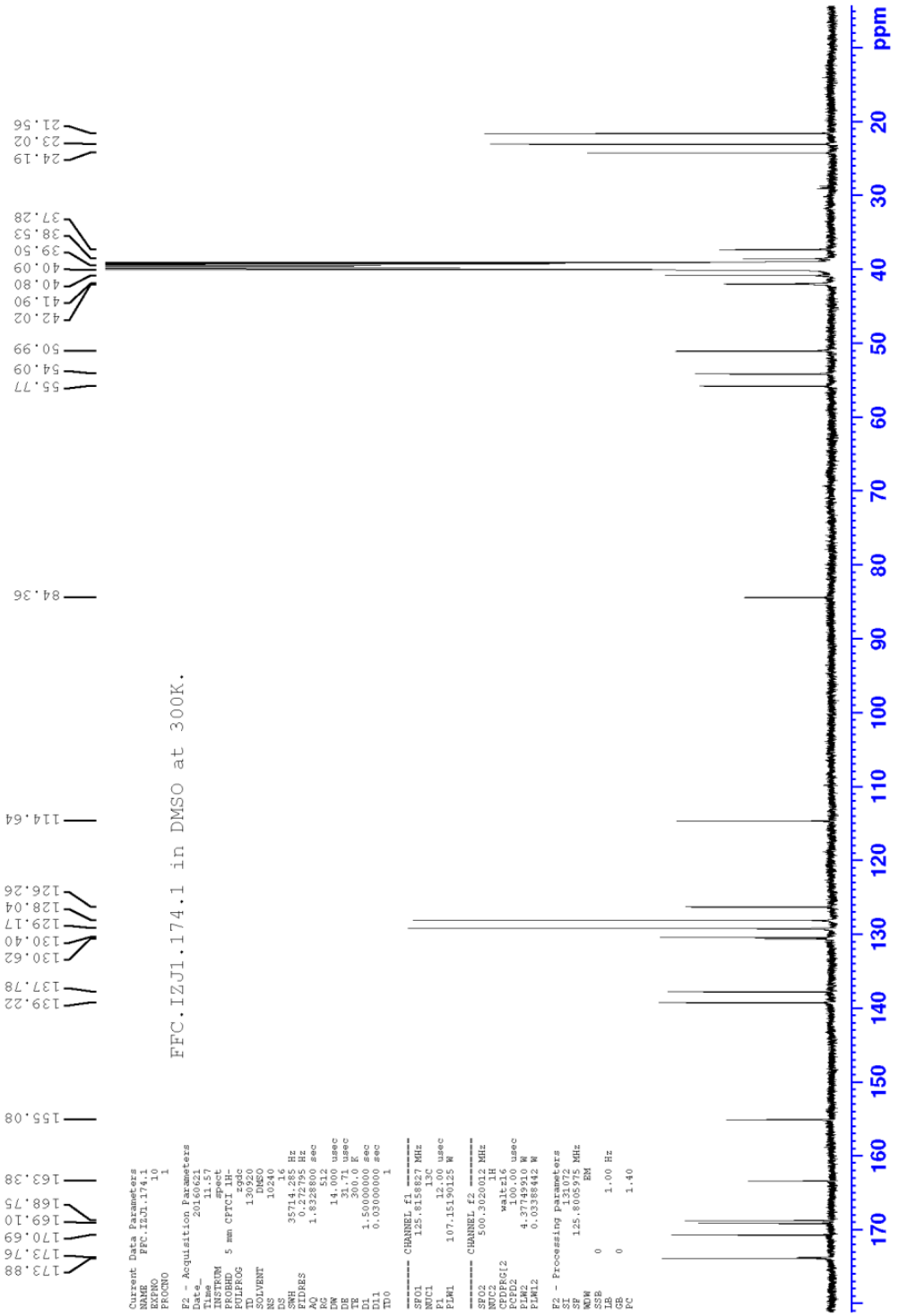
FFC.IZJ1.174.1 in DMSO at 300K.
ppm

Cyclo(RGD[mono-iodo]yK)

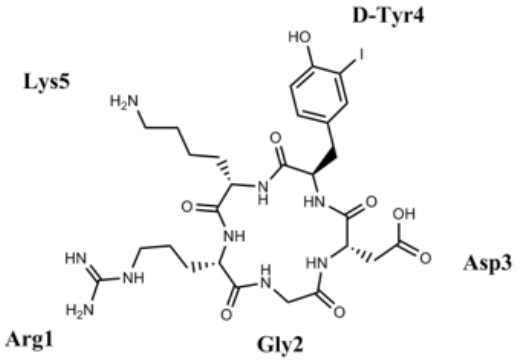

^{1}H NMR (700 MHz, d_6-DMSO, 308 K) and ^{13}C NMR (175 MHz, d_6-DMSO, 308 K).
Chemical shifts are referenced to the solvent signals (^{1}H: 2.50 ppm, ^{13}C: 39.50 ppm). At 308K a better dispersion of the amide signals (Asp-3 and Lys-5) has been obtained.

	^{1}H	^{13}C
Arg-1		
NH	7.61	-
α	4.16	51.84
β	1.71/1.48	28.48
γ	1.37	25.11
δ	3.09	40.26
ε	7.52	-
ζ	-	156.61
C’	-	171.10
Gly-2		
NH	8.44	-
α	4.04/3.24	43.22
C’	-	169.45
Asp-3		
NH	8.09	-
α	4.64	48.81
β	2.71/2.39	35.04

γ	(OH: ~12.2)	171.52
C’	-	169.93
D-Tyr-4		
NH	8.00	-
α	4.34	54.51
β	2.78/2.69	35.89
γ	-	129.81
δ1	7.44	138.93
δ2	6.97	130.21
ε1	-	84.14
ε2	6.77	114.61
ζ	-	155.02
ζ-OH	10.10	-
C’	-	170.54
Lys-5		
NH	8.11	-
α	3.94	54.38
β	1.58/1.43	30.62
γ	1.10	22.42
δ	1.46	26.41
ε	2.71	38.62
ζ	7.69	-
C’	-	171.82

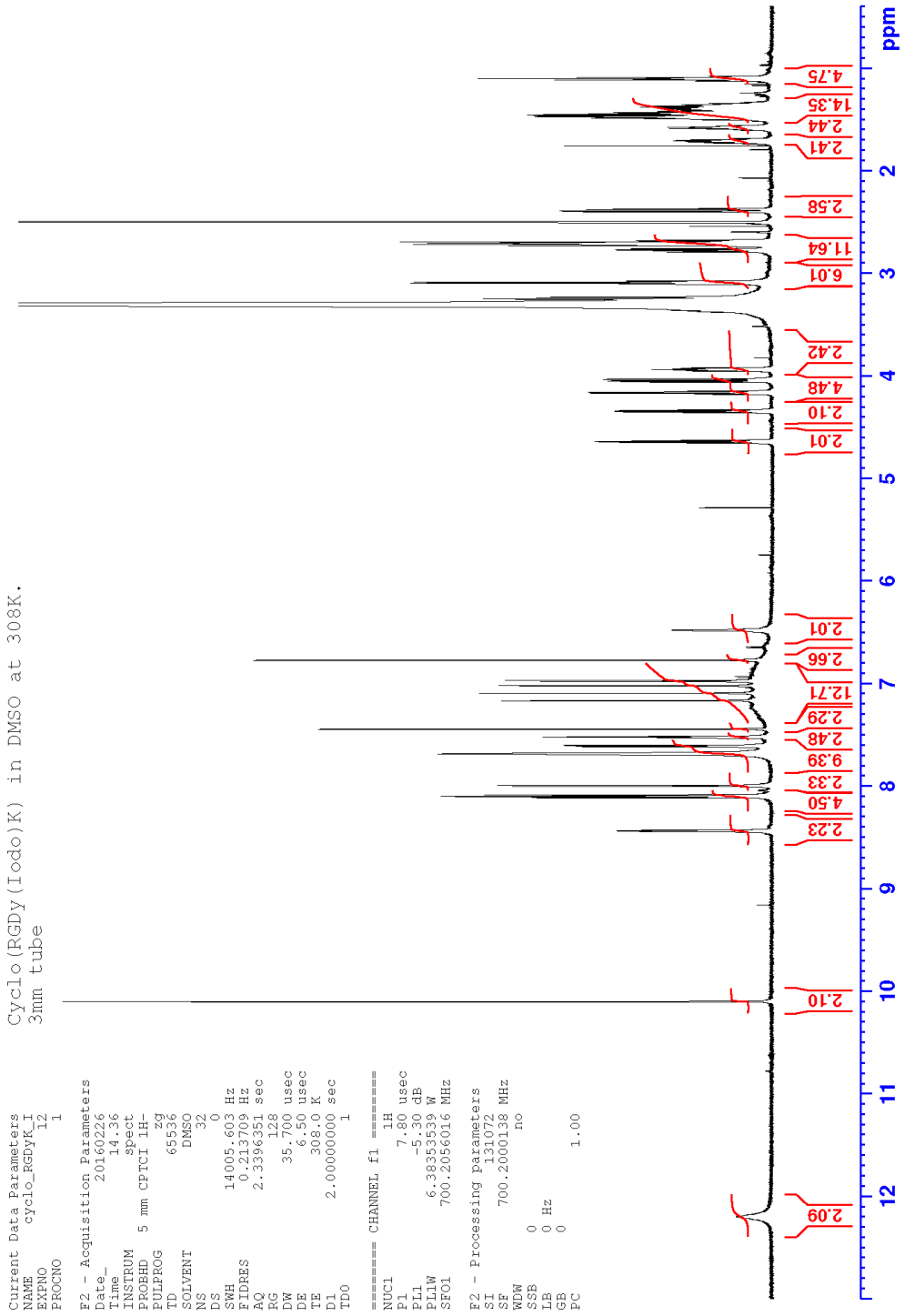
Cyclo(RGDy(Iodo)K) in DMSO at 308K.
3mm tube
Current Data Parameters
NAME cyclo_RGDyK_I
EXPNO 12
PROCNO 1
F2 - Acquisition Parameters
Date_ 20160226
Time 14.36
INSTRUM spect
PROBHD 5 mm CPTCI 1H-
PULPROG zg
TD 65536
SOLVENT DMSO
NS 32
DS 0
SWH 14005.603 Hz
FIDRES 0.213709 Hz
AQ 2.3396351 sec
RG 128
DW 35.700 usec
DE 6.50 usec
TE 308.0 K
D1 2.00000000 sec
TD0 1
======== CHANNEL f1 ========
NUC1 1H
P1 7.80 usec
PL1 -5.30 dB
PL1W 6.38353539 W
SFO1 700.2056016 MHz
F2 - Processing parameters
SI 131072
SF 700.2000138 MHz
WDW no
SSB 0
LB 0 Hz
GB 0
PC 1.00
2.09
2.10
2.23
4.50
2.33
9.39
2.48
2.29
12.71
2.66
2.01
2.01
2.10
4.48
2.42
6.01
11.64
2.58
2.41
2.44
14.35
4.75
ppm
12
11
10
9
8
7
6
5
4
3
2

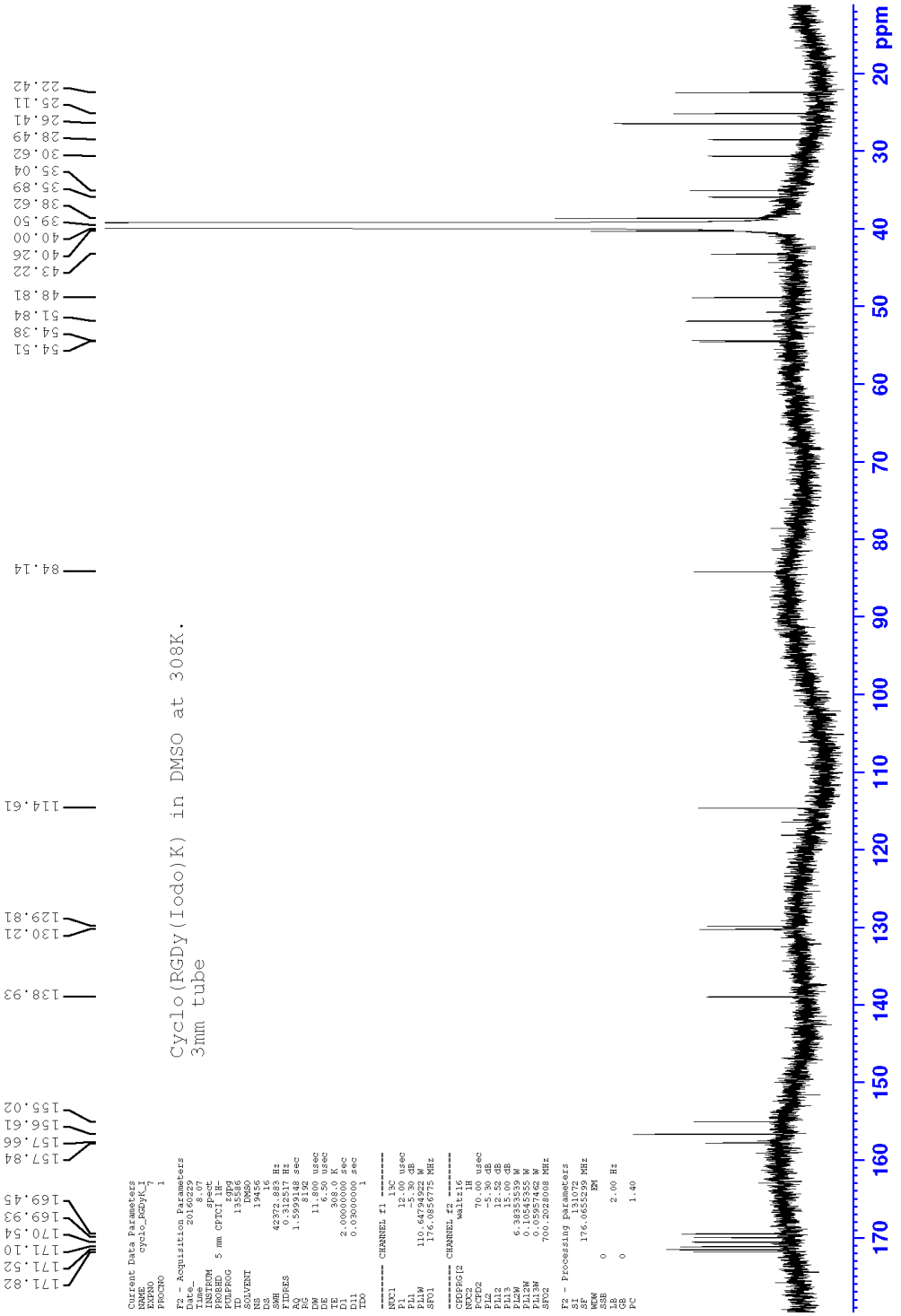
Cyclo(RGDy(Iodo)K) in DMSO at 308K.
3mm tube
ppm

[mono-Iodo-Tyr^0]-Bradykinin

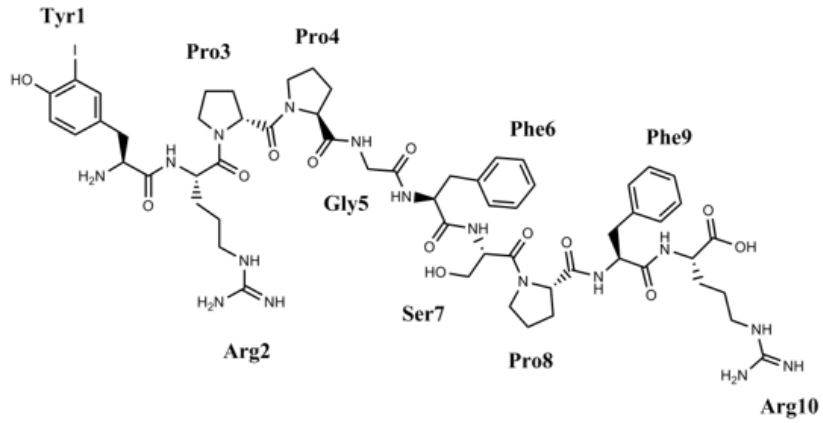

^{1}H NMR (500 MHz, d_6-DMSO, 300 K) and ^{13}C NMR (125 MHz, d_6-DMSO, 300 K).

	^{1}H	^{13}C
Tyr-1		
NH_3^+	8.08	-
α	3.99	53.12
β	2.89/2.79	35.44
γ	-	126.90
δ1	7.51	139.39
δ2	7.00	130.71
ε1	-	84.78
ε2	6.78	114.66
ζ	-	155.84
ζ-OH	10.31	-
C’	-	167.52
Arg-2		
NH	8.66	-
α	4.49	49.98
β	1.69/1.50	28.54

γ	1.53	24.41
δ	3.08	40.47
ε	7.61	-
ζ	-	156.73
C′	-	(a)
Pro-3		
α	4.58	57.63
β	2.18/1.84	27.87
γ	1.87	24.49
δ	3.60/3.48	46.90
C′	-	169.63
Pro-4		
α	4.26	59.44
β	2.00/1.81	29.05
γ	1.93/1.89	24.41
δ	3.66/3.58	46.81
C′	-	171.77
Gly-5		
NH	7.96	-
α	3.63	41.67
C′	-	168.48 (or 168.50) (a)
Phe-6		
NH	7.93	-
α	4.57	53.38
β	2.96/2.73	37.68
γ	-	137.57
δ	7.19	129.13
ε	7.24	128.02

ζ	7.18	126.29
C’	-	170.96 (b)
Ser-7		
NH	8.31	-
α	4.58	
β	3.63	61.73
β-OH	5.36	-
C’	-	(a)
Pro-8		
α	4.30	59.60
β	1.88/1.60	28.77
γ	1.70/1.43	23.72
δ	3.61/3.51	46.90
C’	-	170.84
Phe-9		
NH	7.70	-
α	4.54	53.45
β	3.08/2.72	37.23
γ	-	137.68
δ	7.24	129.10
ε	7.24	127.97
ζ	7.18	126.26
C’	-	170.95 (b)
Arg-10		
NH	8.13	-
α	4.20	51.46
β	1.79/1.64	28.09
γ	1.51	25.06

δ	3.12	40.27
ε	7.56	-
ζ	-	156.65
C’	-	173.08

(a) Could not be assigned

(b) Might be interchanged

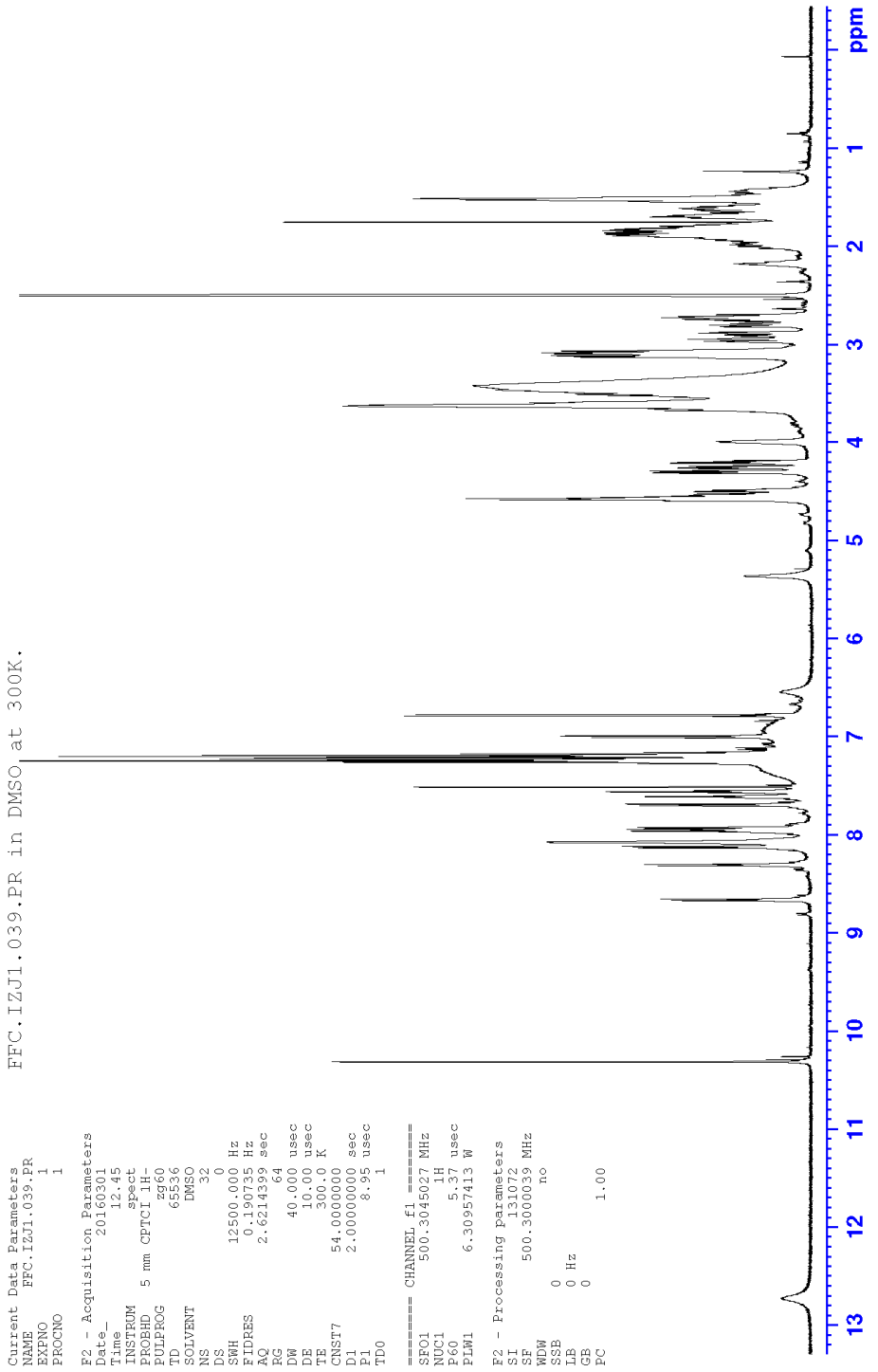
FFC.IZJ1.039.PR in DMSO at 300K.
Current Data Parameters
NAME FFC.IZJ1.039.PR
EXPNO 1
PROCNO 1
F2 - Acquisition Parameters
Date_ 20160301
Time_ 12.45
INSTRUM spect
PROBHD 5 mm CPTCI 1H-
PULPROG zg60
TD 65536
SOLVENT DMSO
NS 32
DS 0
SWH 12500.000 Hz
FIDRES 0.190735 Hz
AQ 2.6214399 sec
RG 64
DW 40.000 usec
DE 10.00 usec
TE 300.0 K
CNST7 54.0000000
D1 2.00000000 sec
P1 8.95 usec
TD0 1
======== CHANNEL f1 ========
SFO1 500.3045027 MHz
NUC1 1H
P60 5.37 usec
PLW1 6.30957413 W
F2 - Processing parameters
SI 131072
SF 500.3000039 MHz
WDW no
SSB 0
LB 0 Hz
GB 0
PC 1.00
13
12
11
10
9
8
7
6
5
4
3
2
1
ppm

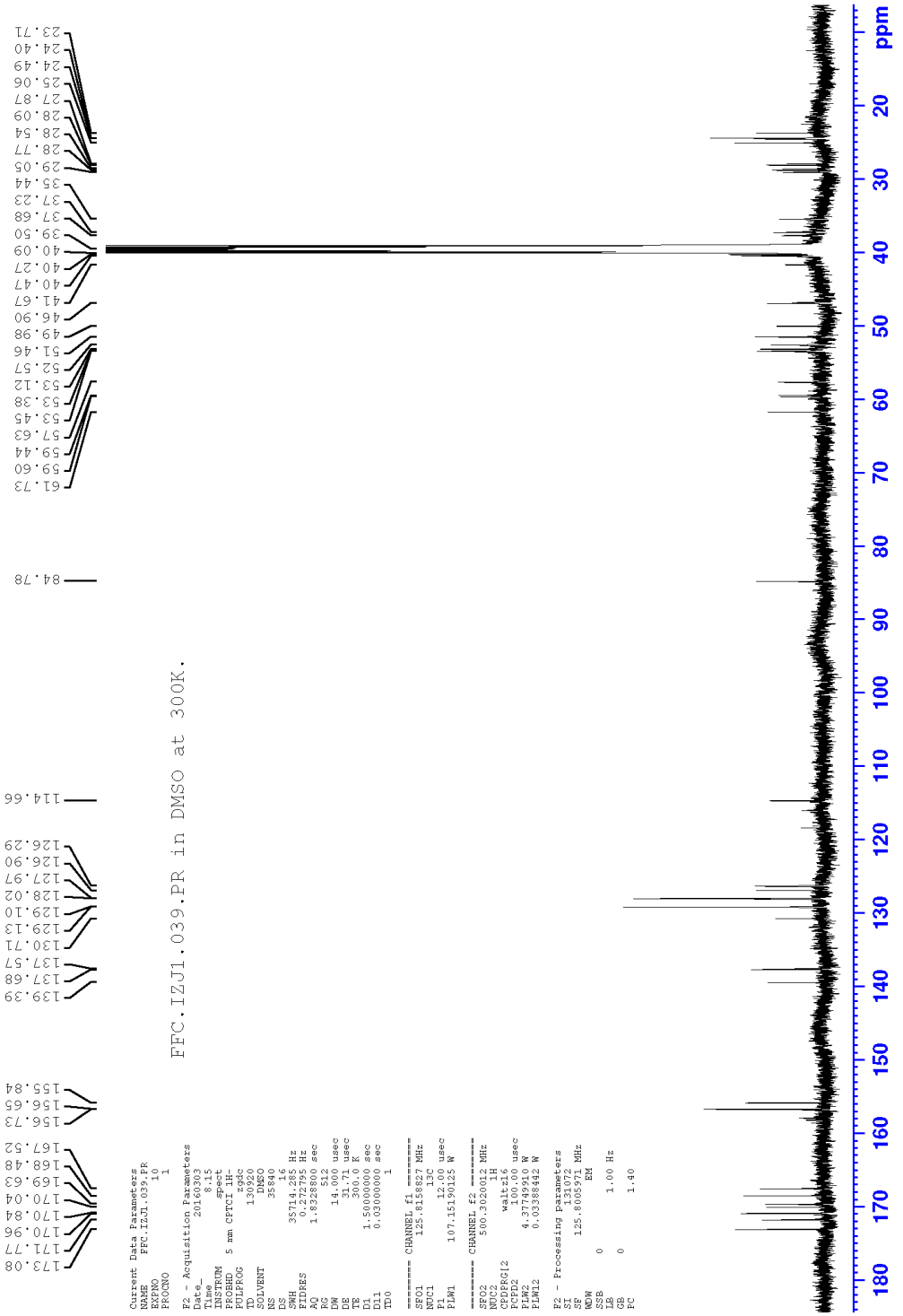
FFC.IZJ1.039.PR in DMSO at 300K.
ppm

[mono-Iodo]-Angiotensin III

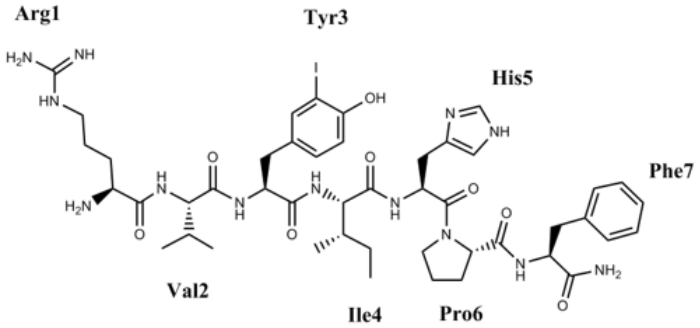

^{1}H NMR (500 MHz, d_6-DMSO, 300 K) and ^{13}C NMR (125 MHz, d_6-DMSO, 300 K).

	^{1}H	^{13}C
Arg-1		
NH_3^+	8.12	-
α	3.87	51.72
β	1.64	28.62
γ	1.46	24.28
δ	3.09	40.12
ε	7.60	-
ζ	-	156.71
C’	-	168.22
Val-2		
NH	8.35	-
α	4.27	57.12
β	2.02	31.11
γ	0.84	19.19
γ'	0.79	17.57
C’	-	170.48
Tyr-3		

NH	8.10	-
α	4.50	53.93
β	2.77/2.59	35.77
γ	-	130.29
δ1	7.60	138.97
δ2	7.09	130.36
ε1	-	84.27
ε2	6.75	114.41
ζ	-	155.02
ζ-OH	10.17	-
C′	-	170.97
Ile-4		
NH	8.00	-
α	4.15	56.65
β	1.66	36.62
β-Me	0.75	15.19
γ	1.36/1.05	24.10
δ	0.77	10.85
C′	-	170.85
His-5		
NH	8.41	-
α	4.79	~ 47.7 (broad)
β	3.05/2.93	~ 26.3 (broad)
γ	-	(a)
δ	7.38 (broad)	~ 117.1 (broad)
ε	~ 8.9 (very broad)	~ 133.8 (broad)
ε-NH_2^+	~ 14.2 (broad)	-
C′	-	(a)

Pro-3		
α	4.26	59.87
β	1.98/1.69	29.13
γ	1.77	24.25
δ	3.63/3.46	46.99
C’	-	171.43
Phe-9		
NH	~ 8.01 (very broad)	-
α	4.38	53.83
β	3.05/2.85	37.01
γ	-	137.88
δ	7.23	129.17
ε	7.23	128.00
ζ	7.17	126.20
C’	-	172.55
NH_2	7.26/7.09	-

(a) Could not be assigned due to extreme line broadening

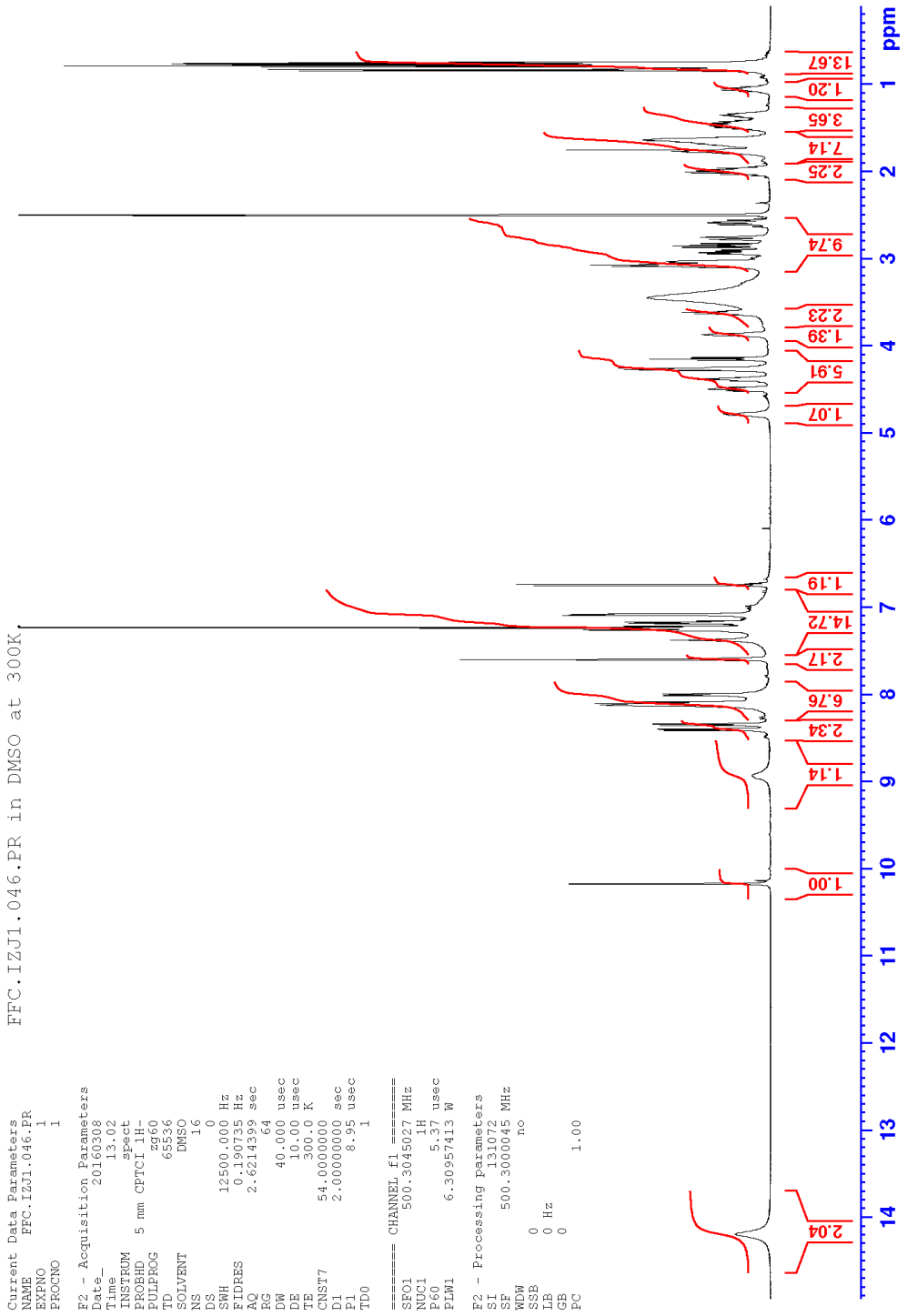
FFC.IZJ1.046.PR in DMSO at 300K
Current Data Parameters
NAME FFC.IZJ1.046.PR
EXPNO 1
PROCNO 1
F2 - Acquisition Parameters
Date_ 20160308
Time_ 13.02
INSTRUM spect
PROBHD 5 mm CPTCI 1H-
PULPROG zg60
TD 65536
SOLVENT DMSO
NS 16
DS 0
SWH 12500.000 Hz
FIDRES 0.190735 Hz
AQ 2.6214399 sec
RG 64
DW 40.000 usec
DE 10.00 usec
TE 300.0 K
CNST7 54.0000000
D1 2.00000000 sec
P1 8.95 usec
TD0 1
======== CHANNEL f1 ========
SFO1 500.3045027 MHz
NUC1 1H
P60 5.37 usec
PLW1 6.30957413 W
F2 - Processing parameters
SI 131072
SF 500.3000045 MHz
WDW no
SSB 0
LB 0 Hz
GB 0
PC 1.00
13.67
1.20
3.65
7.14
2.25
9.74
2.23
1.39
5.91
1.07
1.19
14.72
2.17
6.76
2.34
1.14
1.00
2.04
ppm

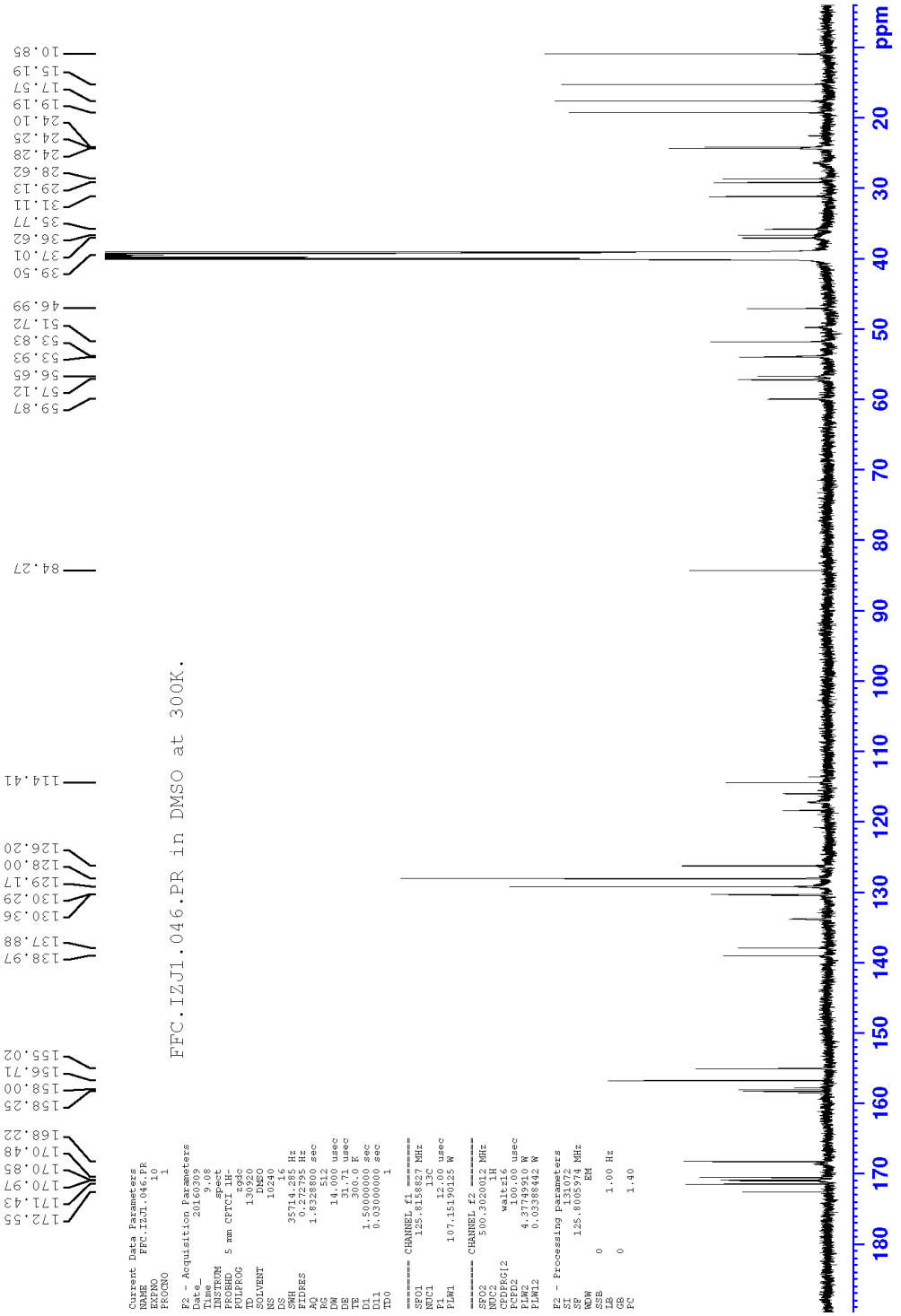
FFC.IZJ1.046.PR in DMSO at 300K.
ppm

[mono-Iodo]-ACP fragment 65-74

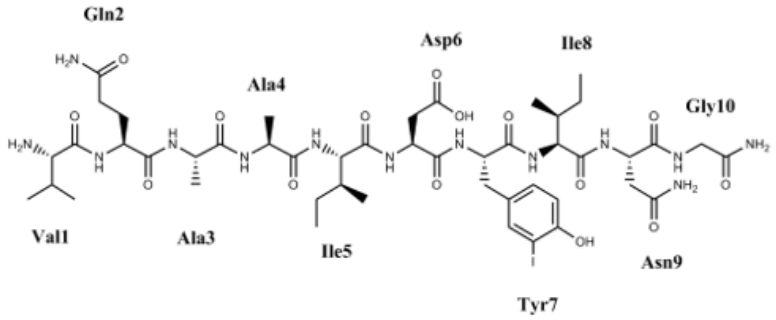

^{1}H NMR (500 MHz, d_6-DMSO, 295 K) and ^{13}C NMR (125 MHz, d_6-DMSO, 295 K).

		^{1}H	^{13}C
Val-1	NH_3^+	8.04	-
	α	3.60	57.25
	β	2.03	29.89
	γ	0.92	18.33
	γ′	0.91	17.70
	C′	-	167.63
Gln-2	NH	8.53	-
	α	4.33	52.07
	β	1.87/1.76	28.02
	γ	2.13	31.29
	δ	-	173.73
	δ-NH_2	7.29/6.84	-
	C′	-	170.29
Ala-3	NH	8.18	-
	α	4.28	47.97
	β	1.18	18.22
	C′	-	171.86

Ala-4	NH	8.11	-
	α	4.32	48.02
	β	1.17	17.79
	C’	-	171.91
Ile-5	NH	7.69	-
	α	4.13	56.60
	β	1.65	36.99
	β-Me	0.73	15.27
	γ	1.35/1.00	24.01
	δ	0.76	11.11
	C’	-	170.60
Asp-6	NH	8.17	-
	α	4.51	49.54
	β	2.62/2.43	36.27
	γ	-	171.65
	C’	-	170.47

The amide protons of Ala3 and Asp6 overlap at 300K.

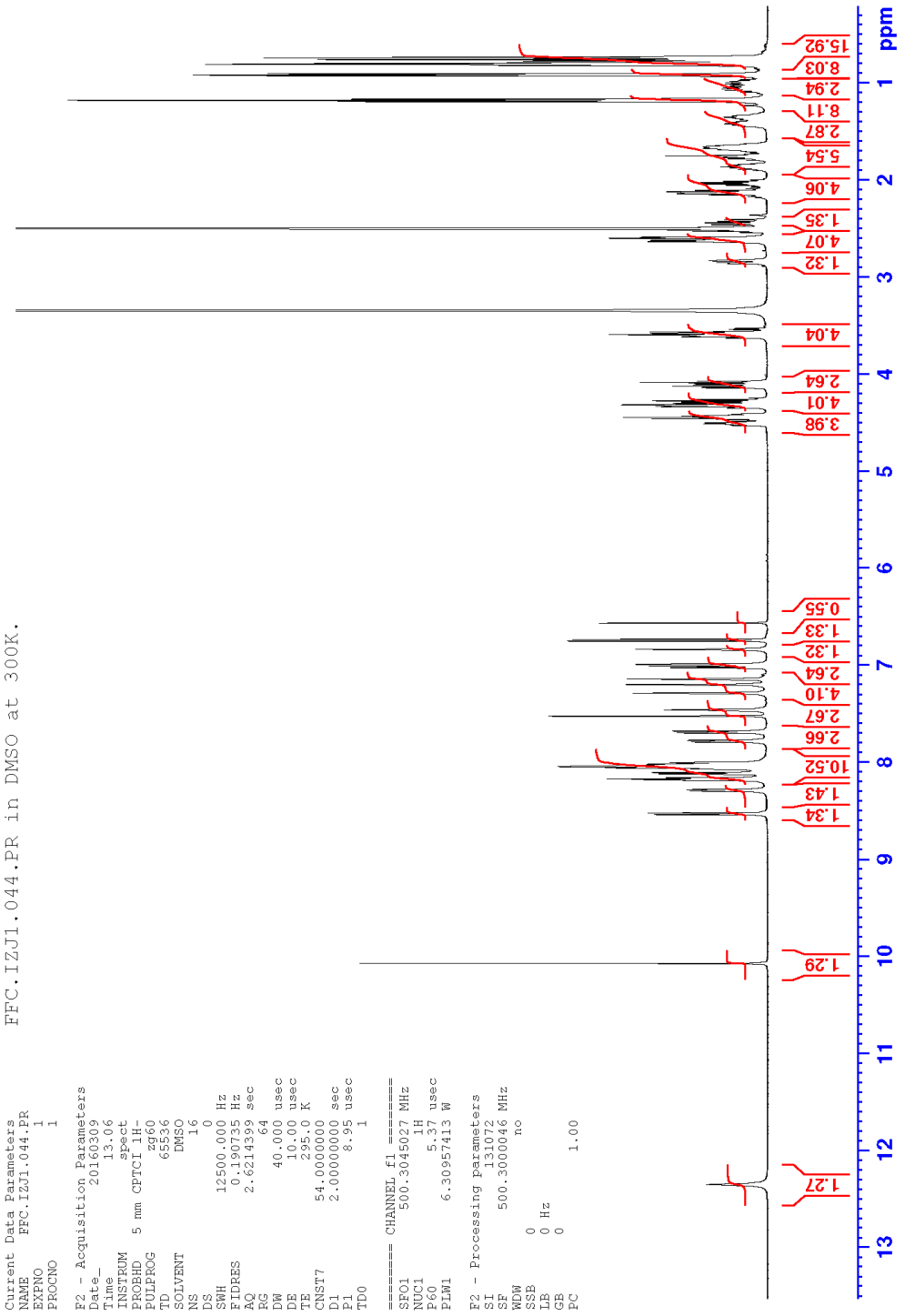
FFC.IZJ1.044.PR in DMSO at 300K.
Current Data Parameters
NAME FFC.IZJ1.044.PR
EXPNO 1
PROCNO 1
F2 - Acquisition Parameters
Date_ 20160309
Time_ 13.06
INSTRUM spect
PROBHD 5 mm CPTCI 1H-
PULPROG zg60
TD 65536
SOLVENT DMSO
NS 16
DS 0
SWH 12500.000 Hz
FIDRES 0.190735 Hz
AQ 2.6214399 sec
RG 64
DW 40.000 usec
DE 10.00 usec
TE 295.0 K
CNST7 54.0000000
D1 2.00000000 sec
P1 8.95 usec
TD0 1
======== CHANNEL f1 ========
SFO1 500.3045027 MHz
NUC1 1H
P60 5.37 usec
PLW1 6.30957413 W
F2 - Processing parameters
SI 131072
SF 500.3000046 MHz
WDW no
SSB 0
LB 0 Hz
GB 0
PC 1.00
15.92
8.03
2.94
8.11
2.87
5.54
4.06
1.35
4.07
1.32
4.04
2.64
4.01
3.98
0.55
1.33
1.32
2.64
4.10
2.67
2.66
10.52
1.43
1.34
1.29
1.27
ppm

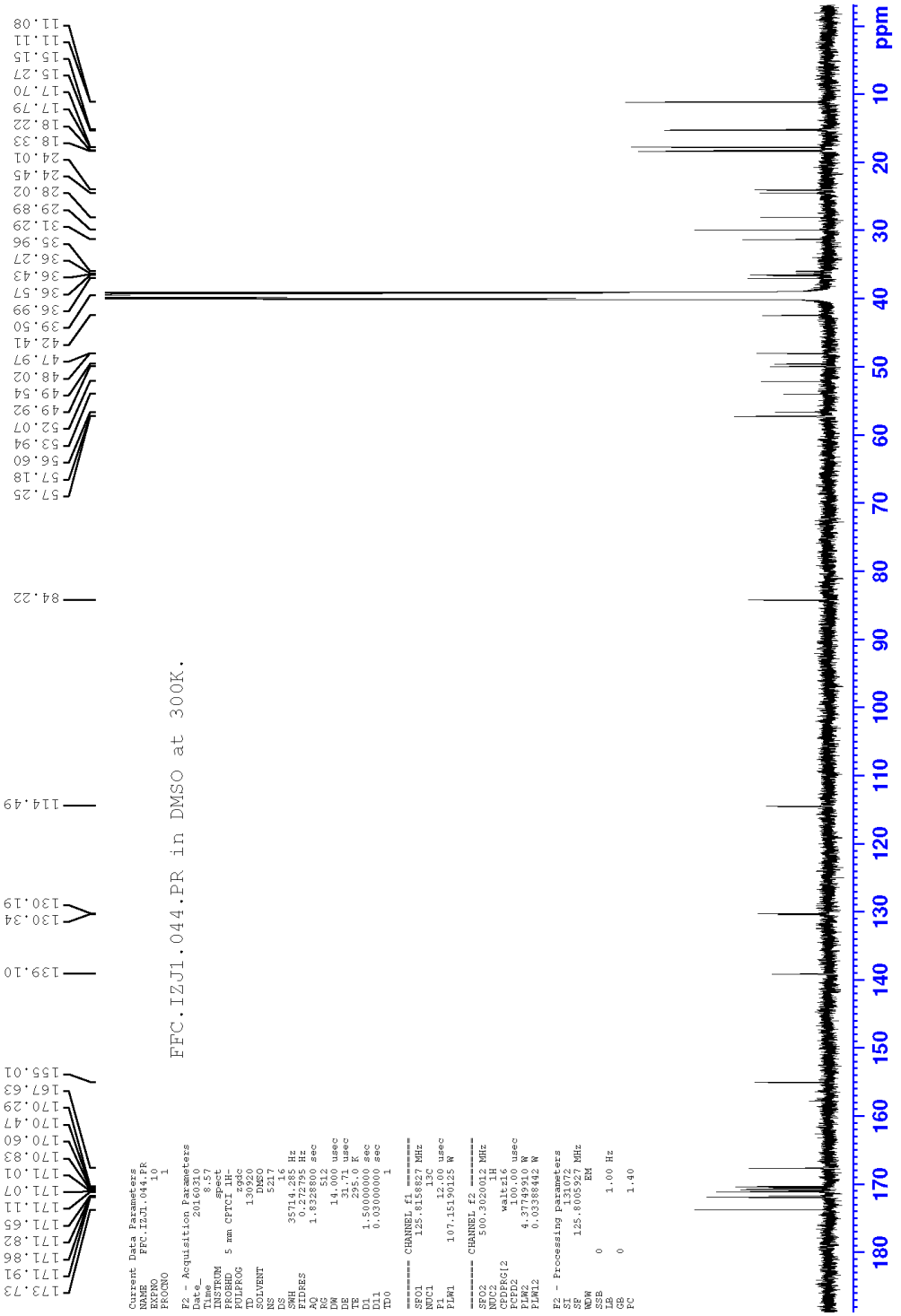
FFC.IZJ1.044.PR in DMSO at 300K.
ppm

[mono-Iodo-Tyr^{8}]-Substance P

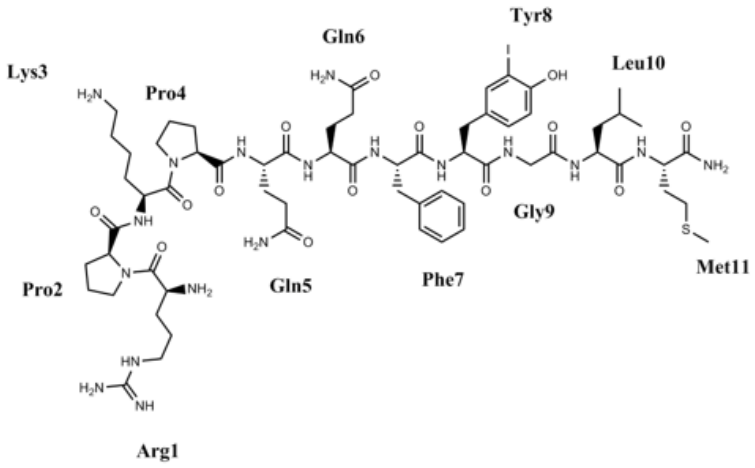

^{1}H NMR (700 MHz, d_6-DMSO, 295 K) and ^{13}C NMR (175 MHz, d_6-DMSO, 295 K).

		^{1}H	^{13}C
Arg-1	NH_3^+	8.18	-
	α	4.16	50.48 (a)
	β	1.76/1.70	27.11
	γ	1.62	23.62
	δ	3.13	40.22
	ε	7.69	-
	ζ	-	156.79
	C′	-	166.84
Pro-2	α	4.43	59.24
	β	2.11/1.75	29.22
	γ	1.91/1.83	24.66
	δ	3.70/3.46	47.04
	C′	-	170.98
Lys-3	NH	8.31	-
	α	4.43	50.43 (a)
	β	1.70/1.51	30.12

	γ	1.39	21.84
	δ	1.54	26.56
	ε	2.75	38.58
	ζ	7.77	-
	C′	-	170.38
Pro-4	α	4.30	59.83
	β	2.09/1.82	29.03
	γ	1.92/1.85	24.66
	δ	3.60/3.57	46.88
	C′	-	172.04
Gln-5	NH	8.27	-
	α	4.12	52.80
	β	1.85/1.73	27.39
	γ	2.12	31.48
	δ	-	174.24
	NH_2	7.32/6.87	-
	C′	-	174.24
Gln-6	NH	7.85	-
	α	4.15	52.30
	β	1.81/1.71	27.90
	γ	2.04	31.57
	δ	-	174.19
	NH_2	7.33/6.87	-
	C′	-	170.87
Phe-7	NH	7.97	-
	α	4.42	54.13
	β	2.93/2.74	37.50
	γ	-	137.59

	δ	7.15	129.11
	ε	7.19	128.04
	ζ	7.14	126.20
	C′	-	170.92
Tyr8	NH	8.03	-
	α	4.42	54.29
	β	2.90/2.67	36.18
	γ	-	130.22
	δ1	7.58	139.21
	δ2	7.08	130.33
	ε1	-	84.28
	ε2	6.77	114.63
	ζ	-	155.10
	ζ-OH	10.09	-
	C′	-	171.30
Gly-9	NH	8.23	-
	α	3.73	41.99
	C′	-	168.64
Leu-10	NH	8.02	-
	α	4.29	51.21
	β	1.47	40.70
	γ	1.61	24.12
	δ	0.88	23.13
	δ′	0.84	21.59
	C′	-	171.93
Met-11	NH	7.98	-
	α	4.23	51.76
	β	1.92/1.81	31.59

γ	2.45/2.38	29.70
δ	2.02	14.65
C’	-	173.08
NH_2	7.21/7.07	-

(a) Might be interchanged

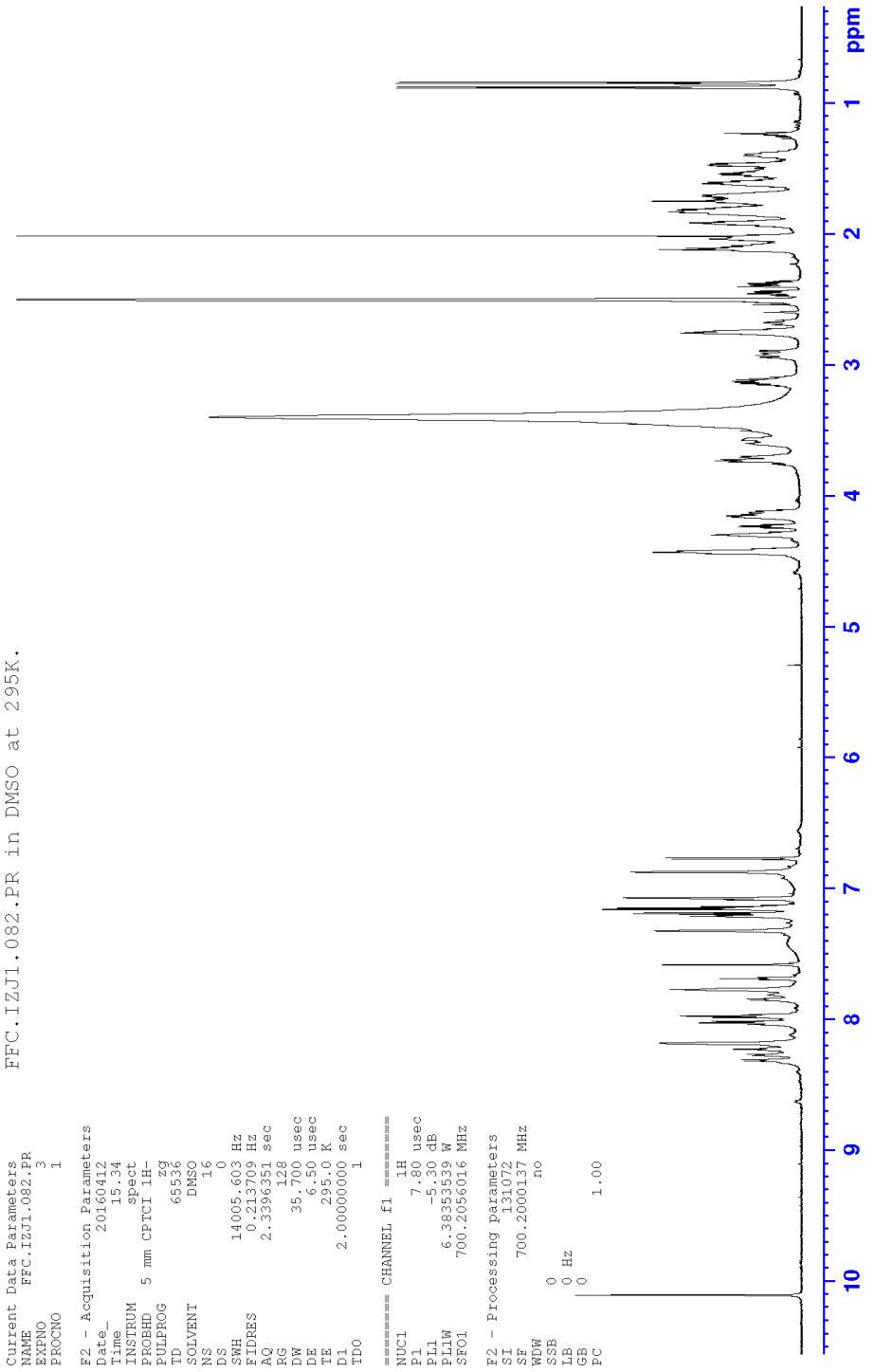
FFC.IZJ1.082.PR in DMSO at 295K.
Current Data Parameters
NAME FFC.IZJ1.082.PR
EXPNO 3
PROCNO 1
F2 - Acquisition Parameters
Date_ 20160412
Time 15.34
INSTRUM spect
PROBHD 5 mm CPTCI 1H-
PULPROG zg
TD 65536
SOLVENT DMSO
NS 16
DS 0
SWH 14005.603 Hz
FIDRES 0.213709 Hz
AQ 2.3396351 sec
RG 128
DW 35.700 usec
DE 6.50 usec
TE 295.0 K
D1 2.00000000 sec
TD0 1
======== CHANNEL f1 ========
NUC1 1H
P1 7.80 usec
PL1 -5.30 dB
PL1W 6.38353539 W
SFO1 700.2056016 MHz
F2 - Processing parameters
SI 131072
SF 700.2000137 MHz
WDW no
SSB 0
LB 0 Hz
GB 0
PC 1.00
10
9
8
7
6
5
4
3
2
1
ppm

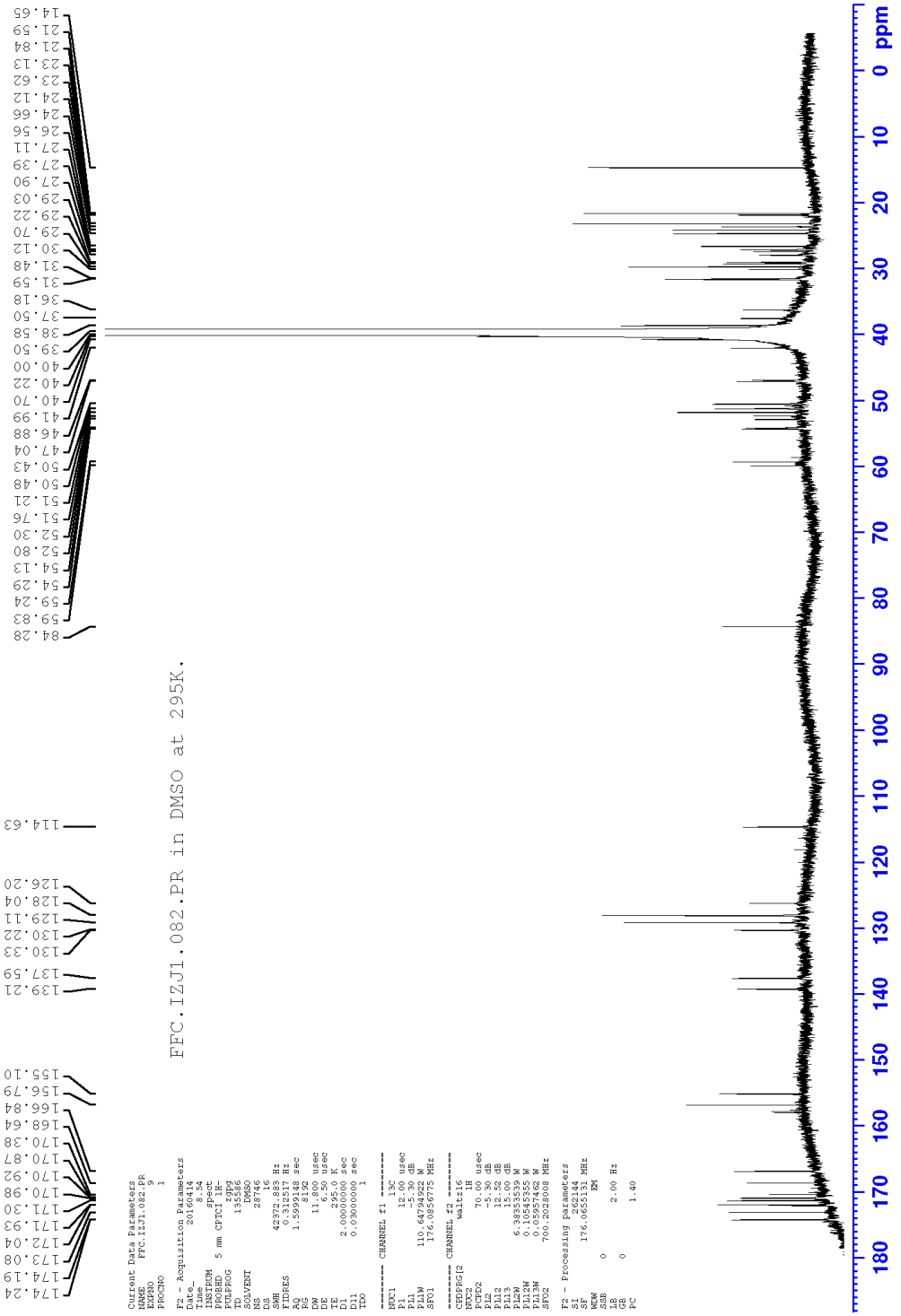
FFC.IZJ1.082.PR in DMSO at 295K.
0 ppm

Supporting References

1. J. M. Collins, K. A. Porter, S. K. Singh and G. S. Vanier, *Organic letters*, 2014, **16**, 940-943.
2. J. M. Chalker, C. S. Wood and B. G. Davis, *J. Am. Chem. Soc.*, 2009, **131**, 16346-16347.
3. V. Hong, S. I. Presolski, C. Ma and M. Finn, *Angewandte Chemie International Edition*, 2009, **48**, 9879-9883.

Chapter 5

General discussion and future perspective

Diabetes mellitus is a worldwide disease which has reached pandemic levels, affecting 1 in 11 adults in 2015, a total of 415 million people.[1] This is a major healthcare problem because the disease increases the risk of heart failure, stroke, and microvascular complications such as blindness, renal malfunction, and peripheral neuropathy. Consequently, diabetes imposes a severe economic burden on governments and individuals due to the demand for multi-modal treatment and the serious complications associated with the chronic nature of the disease. Today, putting aside bariatric surgery which is limited to a few extreme cases (extremely overweight T2D patients - with a body mass index greater than 35, and who are unresponsive to existing medical therapies) or the replacement of the lost β-cells by islet transplantation for T1D (which is also only temporary as autoimmunity persists), no cure for diabetes exists.

Pancreatic β-cells are the only mammalian cells capable of producing and releasing insulin, which regulates blood glucose uptake in peripheral tissues. They are extraordinarily well-tuned sensors: insulin secretion must not only be sufficient in quantity to elicit effects in target tissues (restraining glucose output by the liver and promoting glucose uptake into muscle and fat), but secretion must also be appropriately timed: delayed release of normal amounts of hormone is associated with hyperglycemia. As well, to achieve tighter homeostasis, insulin release has to be well-controlled to anticipate glucose rises and prevent persistent glucose elevations, which is possible as healthy β-cells feature some form of glucose memory. Diabetes is characterized by frequent hyperglycemia, which is a result of insufficient insulin in the body. As depicted in Figure 1, this is caused by either the auto-immune destruction of β-cells (for T1D) or a decrease in β-cell mass and function over time (for T2D). While much research has been conducted since the discovery of Langerhans islets, the pathogenesis of diabetes is still poorly understood, and further studies are required to provide a more accurate picture of the disease. Notably, even though factors such as increasing urbanization, aging populations, obesity, and falling levels of physical activity are known to contribute to rising levels of diabetes, the etiology of the decline in β cell mass and function remains to be elucidated.

How many functional β-cells are needed to maintain euglycemia and remain healthy? Trying to answer this question highlights the complexity of the interplay between β-cell mass and their sensing and secretory capacities. A surprising finding is that even after 50 years, residual amounts of functional β-cells were detected in a majority of type 1 diabetic patients,[2] which indicates that autoimmune-mediated β-cell destruction is for unknown reasons incomplete. Calculations based on the daily rate of insulin release in a nondiabetic individual suggest that as few as 40% of β-cells would be sufficient for adequate glucose control.[3] This figure is supported by the observation that patients who underwent a 50% partial pancreatectomy only had a small change in glucose tolerance.[4] Therefore, it seems that the remaining β-cells are capable of compensating for the increased insulin secretory burden by intensifying their production, but, to what extent and for how long before showing signs of failure of metabolic control is still unclear. Because no longitudinal and quantitative studies of β-cell mass in man exist, it is uncertain whether individuals with T2D start with a defect in their β-cell mass or if this develops as a consequence of sustained hyperglycemia. A non-invasive method for determining β-cell mass based on imaging could help answer these questions. Such a method would undoubtedly enable further understanding and elucidation of the pathogenesis of diabetes. Additionally, β-cell imaging would be useful for additional applications such as monitoring the success of islet transplantation and the viability of the graft.

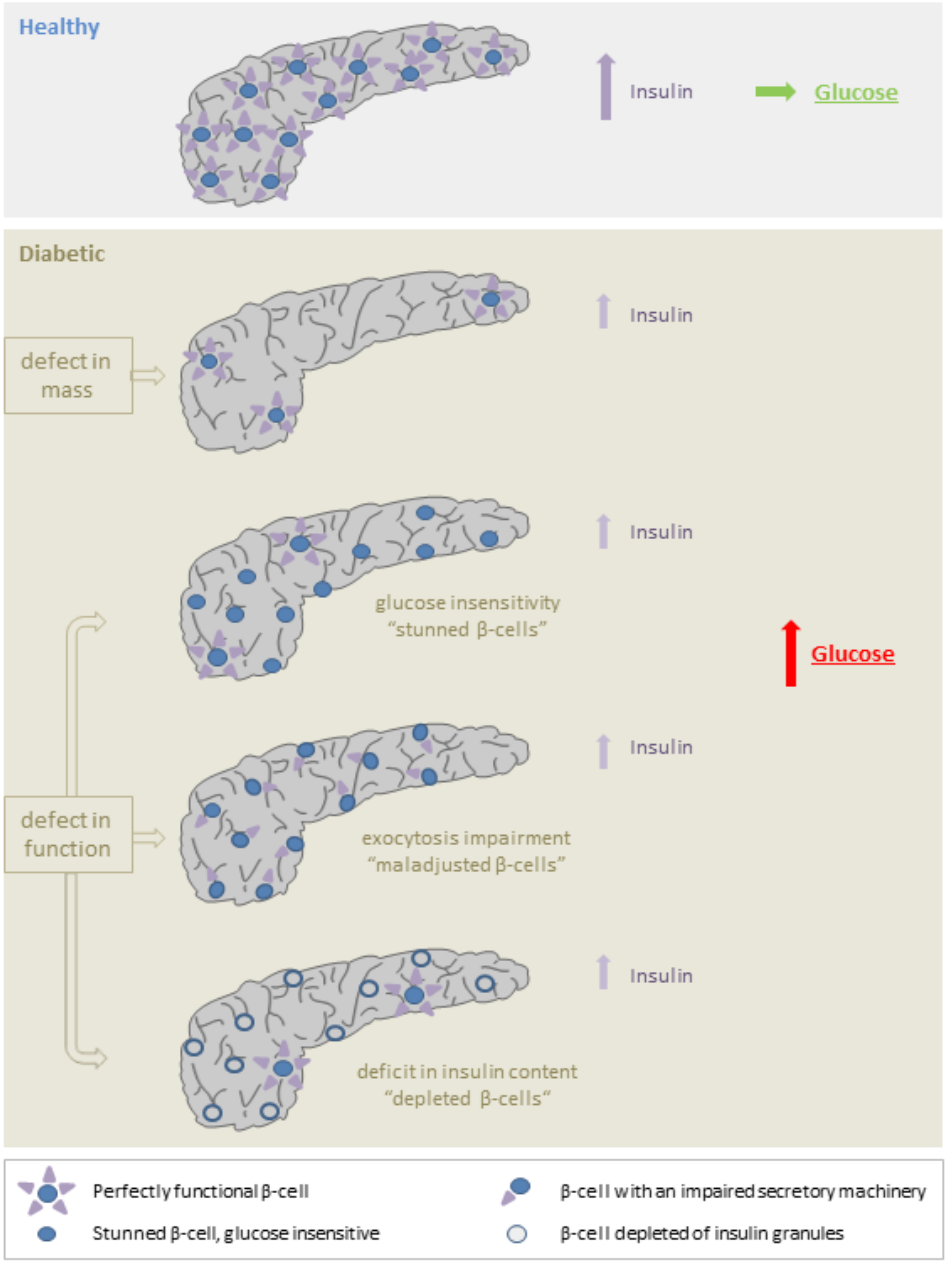

Figure 1 Loss of β-cell mass and function are the hallmarks of the development of both T1D and T2D. Defects in β-cell mass, resulting from an auto-immune reaction is a feature of T1D, but is also observed in late stages T2D. The of defects in function can be many i) A loss of sensing receptor expression,[5] or inactivation of key transcription factors,[6] producing "stunned" β-cells that temporarily stop responding to glucose[7] ii) High and prolonged exposure to free fatty acids leads to an alteration in the colocalization of Ca^{2+} channels and secretory granules. Consequently, although the calcium channels continue to open, the resulting increase in $[Ca^{2+}]_i$ occurs at the ''wrong'' location and fails to evoke secretion.[8] Aberrant granule docking[9] or a lack of ZnT8 zinc transporter expression[10] were also reported as sources of exocytosis impairment iii) In response to gradual cell exhaustion depletion of insulin content arises, or as a defense mechanism in response to a high-fat diet β-cells can undergo dedifferentiation[11] or autophagy[12]. The above-described cases are schematic, most of the T2D patients suffer from both a defect in mass and defects in function of a various nature.

This thesis describes the design, the synthesis and the characterization of fluorescent probes and radioactive tracers targeting the free fatty acid receptor (FFAR1-GPR40). This receptor is highly and predominantly expressed at the surface of the β-cells, but was never examined as a potential target for β-cell imaging. Lipids have complex effects on β-cell function: in the short term, free fatty acids potentiate glucose-induced insulin secretion, and in the long term, they are suspected to induce lipotoxicity. Hence, the FFAR1-GPR40 - as one receptor of the "fat sensor" family – could play a crucial role in the biology of β-cells. When it was deorphanized in 2003, the corresponding mRNA levels were evaluated to characterize the tissue distribution of the receptor. Although regarded as good surrogates in general, there are cases where the mRNA levels do not correlate with the level of the receptor protein it encodes. Accordingly, the development of FFAR1-GPR40 targeting molecules with high specificity is of great interest to enable direct and reliable FFAR1-GPR40 detection.

Development of a fluorescent FFAR1-GPR40 targeting probe

The novel probe was prepared by attaching a fluorescent molecule to the scaffold of TAK-875, a synthetic ligand which binds the FFAR1 with high affinity and selectivity. When optimizing the linker and the fluorophore moiety, we selected a short length amine-containing linker conjugated to Alexa Fluor 488. It was observed that fluorescent dyes with negative charge, such as the di-sulfonated Alexa Fluor 488, showed better specificity compared to dyes with neutral or positive charges. The new probe was shown to specifically label FFAR1-GPR40, and the target was successfully visualized at low nanomolar concentration on transfected HEK293 cells overexpressing the receptor using live cell microscopy. When the probe was used on cells expressing endogenous levels of the receptor such as MIN6 or INS1E, signal amplification based on antibodies was needed to boost the fluorescent signal and enable target detection, as receptor abundance was low. However, a possible alternative to the amplification protocol is the utilization of fluorescence-activated cell sorting (FACS) for the detection of cells expressing FFAR1-GPR40. With the help of this much more sensitive method, we were able to demonstrate that the probe shows detectable binding to FFAR1-GPR40 not only in overexpressing HEK293 cells, but also in MIN6 cells. Finally, it was confirmed that the developed probe still behaves as a FFAR1-GPR40 agonist, activating the receptor and stimulating insulin secretion in a glucose-dependent manner. As the reliability of the antibody based method for FFAR1-GPR40 detection has recently been challenged, the novel fluorescent probe, with the scaffold of a small molecule, provides a new tool for studying the receptor. Interestingly, shortly after submission of our initial manuscript, two other fluorescent probes were reported by two independent research groups underscoring the high interest for FFAR1-GPR40.[13, 14] All such probes were designed using a similar approach, but the two groups used them for different purposes than ours (Figure 2). While we focused on β-cell imaging, the group of Christiansen *et al.* developed their probe (TUG-905 analog labeled with NBD) to establish a bioluminescence resonance energy transfer (BRET)-based binding assay to measure the affinity of selected FFAR1 agonist.[13] Similarly, the group of Ren *et al.* utilized their fluorescent probe (TAK-875 analog labeled with FITC) to assess the binding affinity of free fatty acids to FFAR1-GPR40, but using an assay based on flow cytometry.[14]

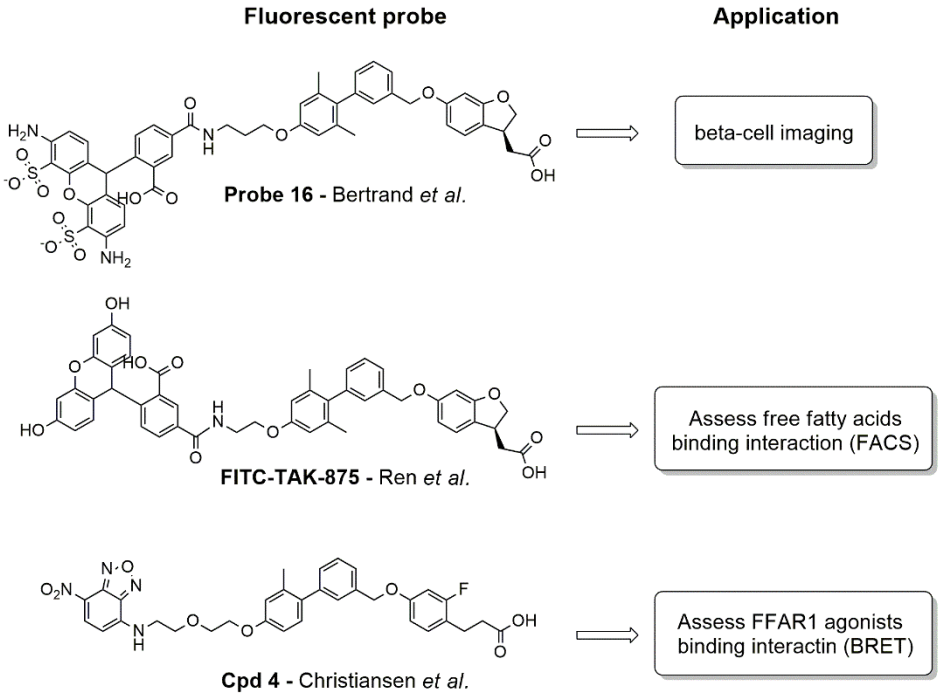

Figure 2 Structures of FFAR1-targeting fluorescent probes and their different applications.

Utilization of the above-described fluorescent probe for *in vivo* imaging in humans is unsuitable due to the light limited depth of penetration through skin and other biological tissue. However, by replacing the UV-visible fluorophore with a fluorophore absorbing and emitting in the near-infrared (NIRF) region, we were able to use non-invasive IVIS imaging to visualize FFAR1-GPR40 on BALB/c nude mice with subcutaneous FFAR1-GPR40 xenografts. Probe uptake 18 hours post-injection was greater in FFAR1-GPR40 xenografts compared to non-transfected xenografts lacking FFAR1-GPR40 expression (mouse 2 and mouse 5), or to control mice injected with PBS (mouse 10), as shown in Figure 2. To our disappointment, blocking experiments failed to reduce probe uptake in FFAR1-GPR40 xenografts (mouse 7), which possibly could be explained by a higher metabolization rate, or by quicker excretion, of the non-labeled blocking compound. However, due to the small number of animals this study remains very preliminary. More experiments are needed to conclude on the ability of the NIRF-probe to selectively target and image the receptor *in vivo*. These data result from a collaboration with Selen Ekim supervised by Prof. Martin Gotthardt from the Nuclear Medicine Department of the Radboud UMC, Nijmegen, The Netherlands.

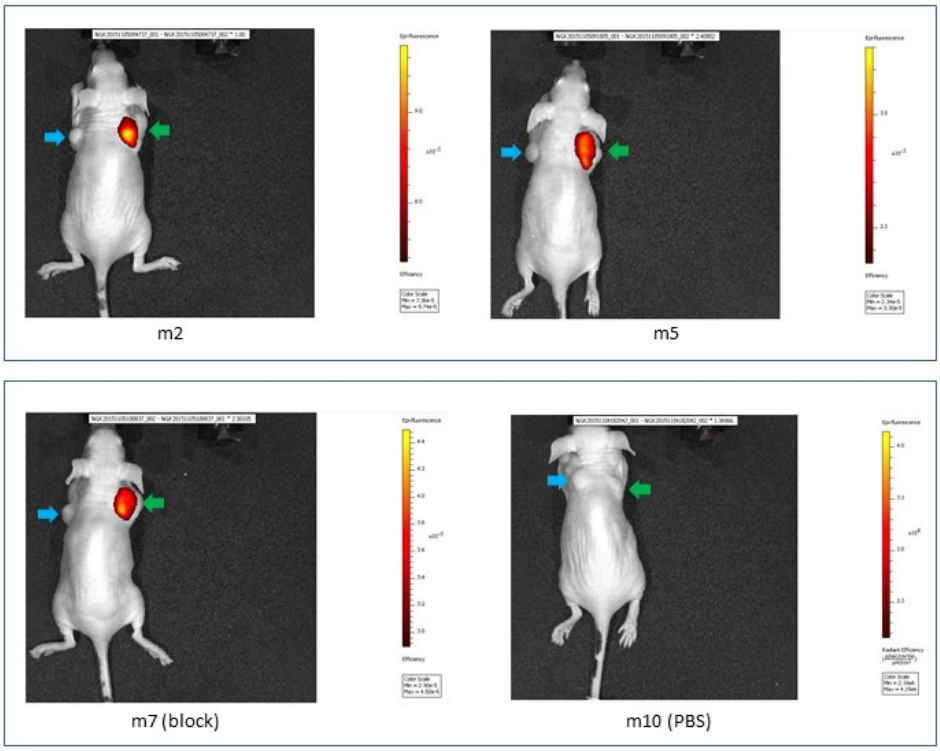

Figure 3 IVIS imaging of BALB/c nude mice with subcutaneous FFAR1-GPR40 xenografts, 18h post injection of the NIRF-probe. For each animal: on the left flanks (blue arrows – negative control) non-transfected xenografts, on the rights flanks (green arrows) FFAR1-GPR40 xenografts. Upper panel: the NIRF-probe accumulated preferably on the FFAR1-GPR40 xenografts. Lower panel (controls): blocking experiment failed to reduce the uptake of the probe on FFAR1-GPR40 xenografts (left) – injection of PBS vehicle shows no detectable fluorescent signal (right).

Development of a radioactive FFAR1-GPR40 targeting tracer

As already mentioned, methods based on optical imaging are not suitable for β-cell imaging *in vivo* in humans, therefore we sought to develop a FFAR1-GPR40 radioligand as potential tracer for PET-imaging. We first performed the tritiation of TAK-875 to get a model compound for *in vitro* binding evaluation studies on transfected HEK293 cells overexpressing the receptor of interest. Based on the encouraging results obtained with the tritiated compound, which showed a preference for binding to cells expressing FFAR1-GPR40, we developed a fluorinated analog of TAK-875. This latter derivative showed similar agonistic activity to the parent compound TAK-875 in a FLIPR-Ca^{2+} functional assay. After preliminary experiments to find suitable labeling reaction conditions that used potassium fluoride as a non-radioactive fluoride source, we implemented the radiolabeling which was achieved in reasonable radiochemical yield using azeotropically dried no-carrier-added [^{18}F], which was activated by a potassium carbonate-Kryptofix 2.2.2 system. Low expression of the receptor on the surface of primary cells and the high lipophilicity of the tracer might both limit its utility. Accordingly, further characterization of the [^{18}F]-tracer is needed and is currently ongoing in *in vitro* and *in vivo* studies, whose outcome will be reported in due course.

Targeting FFAR1-GPR40 for β-cell imaging & other purposes

Targeting FFAR1-GPR40 represents a new option as a detectable and functional putative β-cell marker. Being able to follow another β-cell specific receptor type besides GLP-1R, which is well established, will complement available information and may provide new insights in disease pathogenesis. Importantly, with concerns about potential downregulation of some receptors (such as GLP-1R) in the course of the disease, it might be useful for the islet biology community to define a set of several β-cell specific biomarkers. This set of markers, useful to generate a characteristic *fingerprint* could, for instance, include a combination of genes (Nkx6.1 - protein Nk6.1 homebox), transcription factors (Pdx1 - pancreatic duodenal homebox 1), ion transporters (ZnT8 - zinc transporter 8), ion channels (K_{ir}6.2 - a major subunit of the ATP-sensitive K^+ channel), membrane proteins (TMEM 27- transmembrane protein 27), and G protein-coupled receptors (GLP-1R, FFAR1-GPR40), among others. The positive detection of a combination of these markers could confirm β-cell identity, even if one marker is missing. Relying on such a fingerprint would allow more consistent studies on β-cell and could result in a more comprehensive understanding of β-cell biology. In the case of a cell presenting an insulin secreting dysfunction (one example described in Figure 1), *e.g.* due to ZnT8 expression failure, we can easily assume that a ZnT8 targeting antibody will fail to detect this cell as a β-cell – even if this cell is loaded with insulin.[10] Similarly, a cell not detected by an Exendin-scan targeting the GLP-1R, may simply be an exhausted β-cell that has downregulated the receptor for some reason, but which is still capable of relevant glucose-stimulated insulin secretion.

Aside from β-cell biology, it is suggested that FFAR1-GPR40 may be implicated in the control of breast cancer cell growth by fatty acids, and that FFAR1-GPR40 could provide a link between fat and cancer.[15] Indeed, existence of functional FFAR1-GPR40 was detected in MCF-7, a human breast cancer cell line.[16] The availability of a FFAR1-GPR40 fluorescent probe and a radioactive probe could be useful in detecting the receptor and elucidating its role in the development of breast cancer.

Collectively, all these promising results should encourage researchers to further develop and characterize FFAR1-GPR40 targeting probes and tracers in order to: i) confirm with high confidence that FFAR1-GPR40 is a β-cell specific marker, ii) to determine their suitability for non-invasive β-cell imaging, iii) to verify their potential for other applications such as breast cancer imaging.

Functional β-cell imaging, a crucial complement to β-cell mass imaging

The three most clinically advanced tracers for β-cell imaging to date, namely [^{111}In]-Exendin, [^{18}F]-FP-DTBZ and [^{11}C]-5-HTP,[17] are restricted to detecting β-cells based on the presence or not of their molecular targets (respectively GLP-1R, VMAT2 and DDC). As shown on Figure 1, there are many possible functional defects in insulin-producing cells, any combination of these may be responsible for diabetes. Therefore, in order to complement the tools available for evaluating β-cell mass, new imaging modalities examining β-cell function are desperately needed to better understand progression of the disease. Examples of approaches aimed at imaging β-cell function include the use of Zn^{2+} chelators, Mn^{2+}-enhanced MRI (MEMRI) or superoxide ion detection by chemiluminescence.
Exploiting the fact that Zn^{2+} is co-released with insulin during secretion, the group of Li *et al.* developed a new Zn^{2+} chelator called *ZIMIR*, which displays robust fluorescence enhancement on Zn^{2+} chelation.

With this novel probe, they were able to image the exocytotic activity of dispersed single primary cells, as well as of intact islets.[18]

Manganese ions Mn^{2+} can significantly enhance the contrast of MRI by entering stimulated β-cells through calcium channels. Mn^{2+}-enhanced MRI was successfully used to detect the decline in β-cell mass in a rodent model of T1D, as pancreatic MEMRI signals dropped with progress of the disease.[19]

Superoxide anion O_2^- is produced during normal cellular respiration and plays key roles in cellular physiology. As a consequent of utilizing mitochondrial-derived reactive oxygen species as signaling molecules during the process of insulin secretion, and of having an unusually low expression of some scavenger enzymes, β-cells possess very high superoxide anion concentrations. Interestingly, in response to variation in glucose concentrations, dynamic changes in cellular O_2^- concentration were observed: hyperglycemia was correlated with diminution of the chemiluminescent signal. The small molecule coelenterazine, by generating a chemiluminescence fluorescent signal in a superoxide anion levels-dependent fashion, acts as an *in vitro* and *in vivo* reporter of intracellular O_2^- concentration. Using O_2^- detection with coelenterazine, the group of Bronsart *et al.* recently showed that chemiluminescence correlates with a loss of functional β-cell in NOD diabetic mouse model, which is one of the predominant models for T1D. Although the chemiluminescence-based approaches are limited to small animal imaging (as all optical imaging methods – see above), they might prove to be very useful for dynamic and longitudinal studies.[20]

Future perspectives for β*-cell imaging and how it could support novel therapeutic options*

It is critical that islets maintain adequate β-cell mass and function in response to various fluctuations in demand. For this purpose, β-cells adapt to fit the appropriate requirements. To do so, they can increase the overall β-cell mass via a number of processes: proliferation (replication of β-cells), neogenesis (differentiation from non- β-cells), hyperplasia (increased β-cell number) and hypertrophy (increased β-cell size). In contrast, if needed, β-cell regulation can occur via death (through apoptosis, necrosis, autophagy, and ferroptosis), hypoplasia (decreased β-cell number) and hypotrophy (decreased β-cell size).[21] Novel therapies will not be restricted to those that achieve euglycemia, but will include those that change the course of the disease by reversing the processes of β-cell failure. We can assume that new antidiabetic drugs will possess β-cell protective action, exert proliferation, or will even be able to restore impaired function. As an example, researchers from the Genomics Institute of the Novartis Research Foundation reported in 2015 an orally available small molecule inducing human adult β-cell proliferation. Islets treated with the new drug retained functionality *in vitro* and after transplantation into diabetic mice.[22] Such small-molecule inducer of β-cell proliferation was exploited in a delivery strategy which leveraged the tissue specificity of the β-cell imaging agent DTBZ.[23] Within the booming field of regenerative medicine, new promises for diabetes treatment have emerged. A group from Harvard described a scalable differentiation protocol that can generate hundreds of glucose-responsive β-cells from human pluripotent stem-cells.[24] They show hallmarks of mature β-cells such as variation of intracellular Ca^{2+} in response to glucose, the packaging of insulin into secretory granules, and demonstrating insulin release after sequential glucose challenges *in vitro*. Transplantation of these cells ameliorates hyperglycemia in diabetic mice. To verify and validate the

above-mentioned claims (actual preservative action or β-cell proliferation after compound treatment, actual expression of β-cell marker for differentiated cells etc.) β-cell imaging will have a central role.

Finally, it was recently reported that β-cells may be divided in two subcategories: those that express the *Fltp* gene, and those that do not. This gene encodes the protein Flattop, a Wnt/planar cell polarity effector and reporter gene involved in the acquisition of tissue polarity and 3D architecture. The proliferation-competent (*Fltp*$^{-}$) cells were distinguished from the mature ones (*Fltp*$^{+}$) by distinct molecular, physiological, functional and ultrastructural features.[25] Interestingly, the proliferation-competent cells (*Fltp*$^{-}$), accounting for around 20% of the total β-cell number, showed the ability to differentiate into mature ones (*Fltp*$^{+}$). This pool of (*Fltp*$^{-}$) cells could represent an interesting therapeutic target, if they can be induced into mature and functional β-cells in diabetic patients. In this case β-cell imaging could again prove to be valuable if it is able to distinguish between these two kinds of cell subpopulations. This would enable the monitoring of proliferation-competent (*Fltp*$^{-}$) cells as they convert into mature functional β-cells (*Fltp*$^{+}$).

Discovering new labeling methods as fuel for novel bioimaging probes and tracers

Incorporation of conjugation sites into small peptides can be easily achieved by selection of appropriately functionalized amino acid building blocks for solid phase peptide synthesis, however selective functionalization of isolated peptides and proteins not containing protecting groups still remains a challenging task. Among the naturally occurring amino acids, the most commonly used for bioconjugation are cysteine and lysine as they are potent nucleophiles. However, the high abundance of lysine on protein surfaces makes specific acylation challenging and non-oxidized cysteines are less frequently displayed on protein surfaces. Therefore we focused on the development of an additional modification technique targeting tyrosine as an alternative to the widely used amino acids lysine and cysteine. We devised a new method for the mild and effective mono-iodination of tyrosine residues in fully unprotected peptides. This method is highly chemoselective and compatible with a wide variety of functional groups. The introduced iodine can subsequently serve as a handle for further functionalization, such as introduction of fluorescent dyes, and thus be used for the labeling of isolated peptides. By extending chemical options to modify peptides and proteins, the possibilities to design and synthetize novel bioimaging probes are multiplied, and chances to find the best tools to decipher complex biological process are maximized.

Conclusion

The development of ideal imaging tools will be the result of achievements from the fields of both biology and chemistry. While the finding of an ideal target specifically expressed by β-cells will arise from innovative molecular biologists, the design and synthesis of probes and tracers, and the discovery of new fluorescent dyes or optimized (radio)labeling methods, will be the task of talented organic chemists. Combining forces and exchanging knowledge at the interface of chemistry and biology will be of paramount importance, and even a prerequisite, to eventually reach the ambitious goal of selective and non-invasive β-cell imaging. This could play a key role in combating one of today's most widespread yet poorly understood diseases, diabetes.

"Connaître, ce n'est point démontrer, ni expliquer. C'est accéder à la vision."

Antoine de Saint Exupéry

References

[1] International-Diabetes-Federation. (2015) Diabetes Atlas - Seventh edition.
[2] Keenan, H. A., Sun, J. K., Levine, J., Doria, A., Aiello, L. P., Eisenbarth, G., Bonner-Weir, S., and King, G. L. (2010) Residual insulin production and pancreatic β-cell turnover after 50 years of diabetes: Joslin Medalist Study, *Diabetes 59*, 2846-2853.
[3] Ashcroft, F. M., and Rorsman, P. (2012) Diabetes mellitus and the β cell: the last ten years, *Cell 148*, 1160-1171.
[4] Menge, B., Schrader, H., Breuer, T., Dabrowski, Y., Uhl, W., Schmidt, W., and Meier, J. (2009) Metabolic consequences of a 50% partial pancreatectomy in humans, *Diabetologia 52*, 306-317.
[5] Thorens, B., Wu, Y., Leahy, J. L., and Weir, G. C. (1992) The loss of GLUT2 expression by glucose-unresponsive beta cells of db/db mice is reversible and is induced by the diabetic environment, *Journal of Clinical Investigation 90*, 77.
[6] Guo, S., Dai, C., Guo, M., Taylor, B., Harmon, J. S., Sander, M., Robertson, R. P., Powers, A. C., and Stein, R. (2013) Inactivation of specific β cell transcription factors in type 2 diabetes, *The Journal of clinical investigation 123*, 3305-3316.
[7] Ferrannini, E. (2010) The stunned β cell: a brief history, *Cell metabolism 11*, 349-352.
[8] Hoppa, M. B., Collins, S., Ramracheya, R., Hodson, L., Amisten, S., Zhang, Q., Johnson, P., Ashcroft, F. M., and Rorsman, P. (2009) Chronic palmitate exposure inhibits insulin secretion by dissociation of Ca 2+ channels from secretory granules, *Cell metabolism 10*, 455-465.
[9] Ohara-Imaizumi, M., Nishiwaki, C., Kikuta, T., Nagai, S., Nakamichi, Y., and Nagamatsu, S. (2004) TIRF imaging of docking and fusion of single insulin granule motion in primary rat pancreatic β-cells: different behaviour of granule motion between normal and Goto–Kakizaki diabetic rat β-cells, *Biochemical Journal 381*, 13-18.
[10] Wijesekara, N., Dai, F., Hardy, A., Giglou, P., Bhattacharjee, A., Koshkin, V., Chimienti, F., Gaisano, H., Rutter, G., and Wheeler, M. (2010) Beta cell-specific Znt8 deletion in mice causes marked defects in insulin processing, crystallisation and secretion, *Diabetologia 53*, 1656-1668.
[11] Talchai, C., Xuan, S., Lin, H. V., Sussel, L., and Accili, D. (2012) Pancreatic β cell dedifferentiation as a mechanism of diabetic β cell failure, *Cell 150*, 1223-1234.
[12] Ebato, C., Uchida, T., Arakawa, M., Komatsu, M., Ueno, T., Komiya, K., Azuma, K., Hirose, T., Tanaka, K., and Kominami, E. (2008) Autophagy is important in islet homeostasis and compensatory increase of beta cell mass in response to high-fat diet, *Cell metabolism 8*, 325-332.
[13] Christiansen, E., Hudson, B. D., Hansen, A. H., Milligan, G., and Ulven, T. (2016) Development and characterization of a potent free fatty acid receptor 1 (FFA1) fluorescent tracer, *Journal of medicinal chemistry 59*, 4849-4858.
[14] Ren, X.-M., Cao, L.-Y., Zhang, J., Qin, W.-P., Yang, Y., Wan, B., and Guo, L.-H. (2016) Investigation of the Binding Interaction of Fatty Acids with Human G Protein-Coupled Receptor 40 Using a Site-Specific Fluorescence Probe by Flow Cytometry, *Biochemistry 55*, 1989-1996.
[15] Hardy, S., St-Onge, G. G., Joly, É., Langelier, Y., and Prentki, M. (2005) Oleate promotes the proliferation of breast cancer cells via the G protein-coupled receptor GPR40, *Journal of Biological Chemistry 280*, 13285-13291.
[16] Yonezawa, T., Katoh, K., and Obara, Y. (2004) Existence of GPR40 functioning in a human breast cancer cell line, MCF-7, *Biochemical and biophysical research communications 314*, 805-809.
[17] Eriksson, O., Laughlin, M., Brom, M., Nuutila, P., Roden, M., Hwa, A., Bonadonna, R., Gotthardt, M. (2016) In vivo imaging of beta cells with radiotracers: state of the art, prospects and recommendations for development and use, *Diabetologia 59*, 1340-1349

[18] Li, D., Chen, S., Bellomo, E. A., Tarasov, A. I., Kaut, C., Rutter, G. A., and Li, W.-h. (2011) Imaging dynamic insulin release using a fluorescent zinc indicator for monitoring induced exocytotic release (ZIMIR), *Proceedings of the National Academy of Sciences 108*, 21063-21068.
[19] Antkowiak, P. F., Stevens, B. K., Nunemaker, C. S., McDuffie, M., and Epstein, F. H. (2013) Manganese-enhanced magnetic resonance imaging detects declining pancreatic β-cell mass in a cyclophosphamide-accelerated mouse model of type 1 diabetes, *Diabetes 62*, 44-48.
[20] Bronsart, L. L., Stokes, C., and Contag, C. H. (2016) Chemiluminescence imaging of superoxide anion detects beta-cell function and mass, *PloS one 11*, e0146601.
[21] Cerf, M. E. (2013) Beta cell dysfunction and insulin resistance, *Frontiers in endocrinology 4*.
[22] Shen, W., Taylor, B., Jin, Q., Nguyen-Tran, V., Meeusen, S., Zhang, Y.-Q., Kamireddy, A., Swafford, A., Powers, A. F., and Walker, J. (2015) Inhibition of DYRK1A and GSK3B induces human [beta]-cell proliferation, *Nature communications 6,* 8372.
[23] Hao, X., Jin, Q., Va, P., Li, C., Shen, W., Laffitte, B., and Wu, T. Y. (2016) Pancreas-Specific Delivery of beta-Cell Proliferating Small Molecules, *ChemMedChem 11*, 1129-1132.
[24] Pagliuca, F. W., Millman, J. R., Gürtler, M., Segel, M., Van Dervort, A., Ryu, J. H., Peterson, Q. P., Greiner, D., and Melton, D. A. (2014) Generation of functional human pancreatic β cells in vitro, *Cell 159*, 428-439.
[25] Bader, E., Migliorini, A., Gegg, M., Moruzzi, N., Gerdes, J., Roscioni, S. S., Bakhti, M., Brandl, E., Irmler, M., Beckers, J., Aichler, M., Feuchtinger, A., Leitzinger, C., Zischka, H., Wang-Sattler, R., Jastroch, M., Tschop, M., Machicao, F., Staiger, H., Haring, H. U., Chmelova, H., Chouinard, J. A., Oskolkov, N., Korsgren, O., Speier, S., and Lickert, H. (2016) Identification of proliferative and mature β-cells in the islets of Langerhans, *Nature 535*, 430-434.

Summary

The aim of the studies reported in this thesis was twofold: first, we sought to design, synthesize and characterize novel fluorescent probes and radioactive tracers for noninvasive β-cell imaging. Second, we desired to develop a new methodology for the bioorthogonal labeling of peptides for the synthesis of imaging probes.

Chapter 1 is a general introduction which presents diabetes and the associated complications, its prevalence, the main sub-categories of the disease, and its daunting economic impact. The determinants of diabetes, especially type 2 diabetes, consist of a matrix of genetic and environmental factors that interact with one another, and even though an unhealthy lifestyle (such as sedentarity, a high sugar and fat diet) and obesity are widely suspected to promote the disease, the exact causes are still unclear. Notably, what exactly happens to the mass and function of the pancreatic β-cells - -the only cells of the body capable of secreting insulin - during the onset and the progression of the disease is still poorly understood. Therefore, new tools are urgently needed to study and get better insights into the physiopathology of diabetes, and β-cell imaging could be highly valuable for this purpose. Several probes and tracers for β-cell imaging have been described; the most promising are exendin-4 analogs targeting the cell surface GLP-1 receptor, and dihydrotetrabenazine derivatives which bind the type 2 vesicular monoamine transporter. However, some shortcomings and challenges still hamper their use for *in vivo* β-cell mass determination in humans. Consequently, the search for alternative targets and probes with ideal properties for accurate imaging of β-cell mass should continue. We introduce in Chapter 1 the free fatty acid receptor 1 (FFAR1-GPR40), which is highly and predominantly expressed at the surface of the β-cells, as a new potential target for β-cell imaging.

Accordingly, in **Chapter 2** is described the design, the synthesis and the characterization of the first fluorescent probes targeting the FFAR1-GPR40. The novel probe was prepared by attaching a fluorescent molecule to the scaffold of TAK-875, a synthetic ligand which binds the FFAR1 with high affinity and selectivity. It was determined that the key moiety involved in receptor interaction was the dihydrobenzofuran carboxylic acid and that modifying the 4'-position of the terminal biphenyl ring would not affect binding affinity. Various linkers of different length were examined: a short amine-containing linker was selected because it was well tolerated and it enabled convenient conjugation with the dyes, most of them being commercially available as amine-reactive N-hydroxysuccinimide esters. It was also observed that fluorophores with neutral or positive charges showed high membrane labeling, giving higher nonspecific signal in comparison to negatively charged fluorophores such as Alexa Fluor 488. Consequently, further biological characterizations were carried out with the Alexa Fluor 488 conjugate. The new probe was shown to specifically label FFAR1-GPR40, the target was successfully visualized at low nanomolar concentration on transfected HEK293 cells overexpressing the receptor using live cell microscopy. When the probe was used on cells expressing endogenous levels of the receptor such as MIN6 or INS1E, signal amplification based on antibodies was needed to detect the target. Finally, it was verified that the developed probe still behaves as a FFAR1-GPR40 agonist, activating the receptor and stimulating insulin secretion in a glucose-dependent manner. As the reliability of the method for FFAR1-GPR40 detection based on antibodies was recently challenged, the novel fluorescent probe, with the scaffold of a small molecule, provides a new tool for studying the receptor. Although utilization of fluorescent probes is limited to *in vitro* imaging, it represents a new option to detect an important functional putative β-cell marker.
Optical imaging using fluorescent probes has a very high resolution, but the restriction of the approach lies in the depth of penetration in tissue, which is limited to a few millimeters for dyes in the visible range, and to 2-3 cm for near-infrared fluorophores. This precludes the imaging of internal organs,

such as the pancreas, from outside the body in humans. On the other hand, imaging methods such as positron emission tomography (PET) or single-photon emission computed tomography (SPECT) are extremely sensitive and are not limited by penetration depth. Therefore, we envisioned using a FFAR1-GPR40 ligand as a potential tracer for *in vivo* examinations, this work is reported in **Chapter 3**. The first tritiation of TAK-875, a synthetic ligand which binds the FFAR1-GPR40 with high affinity and selectivity, is reported. The [^{3}H]-TAK-875 was used as a model compound for *in vitro* binding evaluation studies on transfected HEK293 cells overexpressing FFAR1-GPR40. The tritiated analog showed a binding signal sevenfold higher for cells expressing the receptors compared to cells lacking expression of the target. Based on these positive results, the design of a [^{18}F]-tracer started with the modification of TAK-875 and the introduction of a suitable labeling position. As already mentioned above, modifications at the 4'-position of the terminal biphenyl ring are well tolerated in terms of agonistic activity and binding affinity, we thus used the phenol side chain to introduce a tosylate leaving group as precursor for [^{18}F]-introduction. The fluoride labeled derivative showed similar agonistic activity to the parent compound TAK-875 in a FLIPR-Ca^{2+} functional assay. After preliminary experiments to find suitable labeling reaction conditions using KF as a non-radioactive fluoride source, we implemented the radiolabeling with [^{18}F] which was achieved in reasonable radiochemical yield and was transferred to an automated, cassette-based radiosynthesis module. Further characterization of the [^{18}F]-tracer is ongoing in *in vitro* and *in vivo* studies, whose outcome will be reported in due course.

Progress in the development of new imaging probes is made possible by research endeavors in biology, for instance through identification of new cellular targets for imaging, but progress is also thanks to a strong contribution from research in chemistry. Notably, chemists have discovered fluorophores with enhanced photo-chemical properties used in the field of optical imaging. In the field of nuclear medicine, they have also helped in the elaboration of new chelators with superior complexation features, and have developed more efficient and high-yielding radiolabeling protocols. The design and synthesis of both [^{111}In]-Exendin, [^{18}F]-FP-DTBZ and [^{11}C]-5-HTP benefited from these innovations, which were accomplished by chemists. Therefore, **Chapter 4** focuses on the development of a new methodology for the labeling of fully unprotected peptides. While most conjugation strategies rely on the reactivity of lysine or cysteine, these approaches can be limited by the high abundance of lysine on protein surfaces, or by the fact that cysteins are very often involved in non-reactive disulfide bridges. Consequently we aimed at exploiting tyrosine, as an alternative labeling option, to functionalize peptides and proteins. A new method for the mild and effective mono-iodination of tyrosine is reported. The combination of sodium iodide and Selectfluor in dichloromethane supplemented with trifluoroacetic acid allows the introduction of a single iodine atom in *ortho* position of the phenol ring. This method is highly chemoselective and compatible with a wide variety of functional groups, as verified on numerous biologically active peptides such as derivatives of Leu-Enkephalimanide, Angiotensin, Bradykinin, Oxytocin, and GLP-1(7-37) among others. Using the reactivity of the mono-iodo peptides, conjugation with fluorophore building blocks was performed via Suzuki-Miyaura cross-coupling, which serves as an example of bio-imaging probe synthesis. These findings will prove to be a useful additional tool in the arsenal of bioconjugation chemistry, notably for peptides obtained by isolation from natural sources (an important example of such a peptide is Exendin-4, which was originally isolated from the salivary glands of the Gila Monster) rather than through chemical synthesis, or where lysine and free cysteine are not available for labeling.

Finally, in **Chapter 5** all the results described in this thesis are summarized and discussed, together with the latest discoveries in β-cell biology and the potential future perspectives in β-cell imaging.

Samenvatting

Het doel van de studies beschreven in dit proefschrift was tweeledig: ten eerste wilden we nieuwe fluorescente probes en radioactieve tracers ontwerpen, synthetiseren en karakteriseren om op niet invasieve wijze β-cellen in beeld te brengen. Ten tweede wilden we graag een nieuwe methodologie ontwikkelen voor het bioorthogonaal labelen van peptiden voor de synthese van imaging probes.

Hoofdstuk 1 is een algemene introductie over diabetes en de bijbehorende complicaties, de prevalentie, de voornaamste subcategorieën van de ziekte, en de ontmoedigende economische impact. De factoren die bepalen of iemand diabetes krijgt, en dan vooral type 2 diabetes, bestaan uit een matrix genetische factoren en omgevingsfactoren die interactie hebben met elkaar. En ondanks dat een ongezonde levensstijl (weinig bewegen, een dieet met veel suiker en vet) en zwaarlijvigheid ervan verdacht worden de ziekte te stimuleren, zijn de exacte oorzaken nog steeds onduidelijk. Bijvoorbeeld wat er precies gebeurt met de massa en functie van β-cellen in de alvleesklier – de enige cellen in het lichaam die insuline kunnen produceren - tijdens het ontstaan en de ontwikkeling van de ziekte, is nog niet bekend. Daarom zijn er met spoed nieuwe tools nodig om de fysiopathologie van diabetes beter te kunnen bestuderen en begrijpen, en β-cel imaging kan voor dit doel van grote waarde zijn. Verschillende probes en tracers voor β-cel imaging zijn beschreven; de meest veelbelovende zijn exendin-4 analoga die binden aan de GLP-1 receptor op het celoppervlak, en dihydrotetrabenazine derivaten die binden aan de type 2 vesiculaire monoamine transporter. Toch zijn er een aantal tekortkomingen en uitdagingen aan deze tracers die hun gebruik voor *in vivo* β-cel massa in mensen hinderen. Daarom zal de zoektocht naar alternatieve targets en probes met ideale eigenschappen voor accurate beeldvorming van β-cel massa nog doorgaan. We introduceren in Hoofdstuk 1 de free fatty acid receptor 1 (FFAR1-GPR40), die in hoge mate tot expressie komt op het oppervlak van β-cellen, als nieuwe potentiële target voor β-cel imaging.

In **Hoofdstuk 2** wordt het ontwerpen, synthetiseren en karakteriseren van de eerste fluorescente probes beschreven die de FFAR1-GPR40 targeten. De nieuwe probe is gemaakt door een fluorescent molecuul aan een scaffold van TAK-875 te binden, een synthetische ligand die met hoge affiniteit en selectiviteit bindt aan FFAR1. We hebben bepaald dat de dihydrobenzofuran carboxyl zuur de belangrijkste groep is voor de interactie met de receptor en dat het modificeren van de 4’ positie van de terminale biphenyl ring geen effect heeft op de affiniteit van de binding. Linkers van verschillende lengte zijn onderzocht: een korte amine bevattende linker werd geselecteerd, omdat deze goed getolereerd werd en de linker zorgde voor goede conjugatie met de dyes, waarvan de meeste commercieel beschikbaar waren als amine reactieve N-hydroxysuccinimide esters. We hebben ook gezien dat fluorophoren met neutrale of positieve ladingen hogere membraan binding lieten zien, waardoor een hoger aspecifiek signaal werd gezien in vergelijking met negatief geladen flourophoren, zoals Alexa Fluor 488. Daarom zijn verdere biologische karakteriseringen uitgevoerd met het Alexa Fluor 488 conjugaat. De nieuwe probe bond specifiek aan FFAR1-GPR40 en het werd succesvol in beeld gebracht in een laag nanomolaire concentratie met microscopie op getransfecteerde HEK293 cellen die de receptor tot overexpressie brengen. Toen we de probe gingen testen op cellen met een endogeen niveau van receptor expressie zoals MIN6 of INS1E, was er een amplificatie van het signaal nodig met antilichamen om het target te detecteren. Uiteindelijk hebben we geverifieerd dat de ontwikkelde probe zich nog steeds gedraagt als een FFAR1-GPR40 agonist, en dus nog steeds de

receptor activeert en de insuline secretie stimuleert op een glucose afhankelijke manier. Omdat de betrouwbaarheid van de methode om FFAR1-GPR40 te detecteren met behulp van antilichamen recent in twijfel is getrokken, vormt de nieuwe fluorescente probe, met de scaffold van een klein molecuul, een nieuwe tool om de receptor te bestuderen. Ondanks dat het gebruik van fluorescente probes gelimiteerd is tot *in vitro* imaging, biedt dit een nieuwe optie om een belangrijke functionele β-cel marker te detecteren.

Optical imaging met fluorescente probes heeft een hele hoge resolutie, maar een sterke beperking van deze benadering is de penetratiediepte in weefsel, die beperkt is tot een paar millimeter voor dyes in zichtbare bereik, en 2-3 cm voor near-infrared fluorophoren. Dit sluit beeldvorming van interne organen in het menselijk lichaam uit, zoals de alvleesklier. Echter, beeldvormende technieken zoals positron emission tomography (PET) en single-photon emission computed tomography (SPECT) zijn extreem gevoelig en zijn niet gelimiteerd door penetratiediepte. Daarom wilden we een FFAR1-GPR40 ligand ontwerpen voor *in vivo* gebruik. Dit werk is beschreven in **Hoofdstuk 3**. De eerste tritiatie van TAK-875, een synthetisch ligand dat bindt aan FFAR1-GPR40 met hoge affiniteit en selectiviteit, is beschreven. [^{3}H]-TAK-875 is gebruikt als een modelverbinding voor *in vitro* bindings experimenten met getransfecteerde HEK293 cellen die FFAR1-GPR40 tot overexpressie brengen. Het getritieerde analoog toonde een zeven keer hogere binding op getransfecteerde cellen in vergelijking met cellen die de receptor niet to expressie brengen. Gebaseerd op deze positieve resultaten zijn we gestart met het ontwerpen van een [^{18}F]-tracer door modificatie van TAK-875 en de introductie van een geschikte positie voor labeling. Zoals hierboven al werd beschreven, werden modificaties aan de 4’ positie van de terminale biphenyl ring goed getolereerd met betrekking tot agonistische activiteit en bindingsaffiniteit. Daarom gebruikten we de phenol side chain om een tosylate leaving group te introduceren als een precursor voor de introductie van [^{18}F]. Het derivaat gelabeld met fluoride toonde vergelijkbare agonistische activiteit als het oorspronkelijke TAK-875 in een FLIPR-Ca2+ functioneel essay. Na preliminaire experimenten om geschikte labeling condities te vinden waarbij we KF gebruikten als een niet radioactieve bron, implementeerden we de radioactieve labeling met [^{18}F] met een goede radiochemische opbrengst in een geautomatiseerde radiosynthese module met cassettes. Er wordt nog gewerkt aan verdere karakterisering van de [^{18}F]-tracer in verschillende *in vitro* en *in vivo* studies, waarvan de uitkomst nog gerapporteerd zal worden.

Vooruitgang in de ontwikkeling van nieuwe imaging probes wordt mogelijk gemaakt door onderzoeksinspanningen in de biologie, bijvoorbeeld door de identificatie van nieuwe cellulaire targets voor beeldvorming, maar vooruitgang is ook te danken aan een sterke contributie uit het veld van de chemie. Zo hebben chemici fluorophoren ontdekt met versterkte fotochemische eigenschappen die gebruikt worden in het veld van de optical imaging. In het veld van de nucleaire geneeskunde hebben ze ook geholpen in de ontwikkeling van nieuwe chelatoren met superieure complexerende kenmerken. Ook hebben ze protocollen ontwikkeld voor radiolabeling die efficiënter zijn en een hogere opbrengst opleveren. Het ontwerp en de synthese van zowel [^{111}In]-Exendin, [^{18}F]-FP-DTBZ en [^{11}C]-5-http hebben geprofiteerd van deze innovaties, die zijn bereikt door chemici. Daarom focust **Hoofdstuk 4** op de ontwikkeling van een nieuwe methodologie voor de labeling van volledig onbeschermde peptiden. De meeste conjugatiestrategieën gebaseerd zijn op de reactiviteit van lysine

of cysteine. Echter, deze benadering kan gelimiteerd zijn door hoge aanwezigheid van lysine op eiwit oppervlakken, of door het feit dat cysteines erg vaak betrokken zijn bij de vorming van niet reactieve disulfidebruggen. Derhalve zijn wij gaan kijken naar de mogelijkheden van tyrosine als een alternatieve optie voor labeling om peptiden en eiwitten te funtionaliseren. Een nieuwe methode voor de milde en effectieve mono-iodinatie van tyrosine is beschreven. De combinatie van natriumiodide en Selectfluor in dichloromethaan gesupplementeerd met trifluorazijnzuur biedt de mogelijkheid van een introductie van een enkel iodine atoom in ortho positie op de fenol ring. Deze methode is sterk chemoselectief en compatibel met een grote variëteit aan functionele groepen, zoals geverifieerd bij vele biologisch actieve peptiden, zoals onder andere derivaten van Leu-Enkephalimanide, Angiotensin, Bradykinin, Oxytocin, and GLP-1(7-37). Door gebruik te maken van de reactiviteit van de mono-iodo peptiden, voerden we conjugaties uit met fluorophore building blocks via Suzuki-Miyaura cross-coupling, dat dient als een voorbeeld van de synthese van een bio-imaging probe. Deze resultaten zullen bewijzen dat dit een nuttige additionele tool is in het arsenaal van bioconjugatie chemie, vooral voor peptiden die worden verkregen door isolatie uit natuurlijke bronnen (een belangrijk voorbeeld hiervan is het peptide Exendin-4, dat geïsoleerd wordt uit de speekselklieren van het Gilamonster) in plaats van door chemische synthese, of wanneer lysine en vrij cysteine niet beschikbaar zijn voor labeling.

Uiteindelijk worden in **Hoofdstuk 5** alle resultaten beschreven in dit proefschrift samengevat en bediscussieerd, aangevuld met de laatste ontdekkingen in β-cel biologie en de potentiële toekomstperspectieven in β-cel imaging.

List of publications

Romain Bertrand, Andrea Wolf, Yuri Ivashchenko, Matthias Löhn, Matthias Schäfer, Mark Brönstrup, Martin Gotthardt, Volker Derdau and Oliver Plettenburg. *Synthesis and Characterization of a Promising Novel FFAR1/GPR40 Targeting Fluorescent Probe for beta cell imaging*. ACS Chemical Biology, 2016, 11 (6), pp 1745-1754. DOI: 10.1021/acschembio.5b00791.

Romain Bertrand, Isabel Hamp, Mark Brönstrup, Remo Weck, Mario Lukacevic, Andras Polyak, Tobias Ross, Martin Gotthardt, Oliver Plettenburg and Volker Derdau. *Synthesis of GPR40 targeting ^{3}H- and ^{18}F probes towards selective beta cell imaging*. Journal of Labelled Compounds and Radiopharmaceuticals, 2016, June 10, Epub ahead of print. DOI: 10.1002/jlcr.3412.

Romain Bertrand, Michael Wagner, Volker Derdau and Oliver Plettenburg. *Mild and selective mono-iodination of unprotected peptides as initial step for the synthesis of bioimaging probes*. ACS Bioconjugate Chemistry, 2016, *27* (10), pp 2281–2286**.** DOI: 10.1021/acs.bioconjchem.6b00461.

The work described in **Chapter 2** was highlighted in a “Spotlight” article of ACS Chemical Research in Toxicology, written by Abigail Druck Shudofsky. *Small molecule fluorescent probe selectively binds a beta cell functional marker allowing in vitro imaging*. ACS Chemical Research in Toxicology, 2016, 29 (6), pp 941–942.

Acknowledgements

The research leading to these results has received funding from the People Program (Marie Curie Actions) of the European Union's Seventh Framework Program FP7/2007-2013/under REA Grant Agreement No. 289932.

I would first like to express my sincere gratitude to everyone who, directly or indirectly, has contributed to the work presented in this thesis.

My PhD project was part of *BetaTrain* - a Marie Curie Initial Training Network for Excellence in Molecular Imaging in Diabetes. This was an extraordinary opportunity which enabled me to travel across Europe, to attend international conferences, and to rub shoulders with both talented students from all over the globe, and with experts with cutting-edge expertise in the field of beta cell/diabetes imaging and image processing.

Therefore, I thank wholeheartedly Prof. Martin Gotthardt, my mentor from the Radboud University of Nijmegen, The Netherlands and the coordinator of the *Beta Train* consortium. Thanks for being at the origin of such an incredible program which combined soft skills courses and high-quality scientific trainings. I am convinced that these latter will be very valuable to me and to all the ESR involved in *Beta Train*. If the program was a success, this is also thanks to the amazing work of Annemarie Eek and Nicoline Geverink, they both contributed to the coordination and the organization of the meetings. Special thanks to Annemarie for translating the Samenvatting.

I was really glad to meet the fellows: Stefanie, Filippo, Josie, Pim, Saba, Vineetha, Greg, Andrea, Shweta, Sandeep, and Janne. We had great fun together during the consortium meetings in Copenhagen, Prague, Frankfurt, Nijmegen, Geneva, and Umea. I wish you guys all the best for the future.

Special mention goes to Max, Rita, Selen and Wael, who I had the chance to directly collaborate with. Exchanging ideas, planning experiments together, blending chemistry and biology, this was really one of the things I enjoyed the most.

During my PhD, I performed three secondments in Nijmegen, The Netherlands, and one in Leuven, Belgium. Therefore, I would like to thank all the people for their help and their kind welcome from both the Nuclear Department of the Radboud University: Stefanie Willekens, Selen Ekim, Wael Arabi Eter, Desiree Bos, Annemarie Eek, Maarten Brom and Martin Gotthardt; and from the moSAIC of the K.U. Leuven: Rita Ribeiro, Shweta Saini, and Uwe Himmelreich. I discovered and learned a lot of new things with you.

Thanks to all collaborators and co-authors: Prof. Ulf Ahlgren from the Centre of Molecular Medicine of Umeå University, and Mario Lukacevic, Andras Polyak, and Prof. Tobias Ross from the Department of Nuclear Medicine of the Hannover Medical School.

This thesis work has been carried out at Sanofi, in the R&D Diabetes Division / Research & Translational Medicine, on the Industriepark of Höchst - Frankfurt am Main, Germany.

Working over the last three years at Sanofi has been both a real pleasure and a highly valuable experience. My first thanks go to my colleagues: Horst Kleine, Miriam Tiefenbach, Wenskowsky Lea, Dr. Stefan Petry but also Reiner Simonis, Daniela Schultheis, Antje Müller, Patrick Denner and Arne Krack, Lothar Hornung, Dr. Albert Sanchez, Dr. Felix Gnerlich, Doris Deseyve, Armin Müller, and Jenny Schubert for the friendly welcome and your great help. I am also very grateful to all the interns who were involved in the projects: Dominique Treder, Antje Hutwelker, Romain Vauchel, and Isabel Hamp - working with each of you was a very enriching experience but most importantly, a lot of fun. I would

also like to thank the people from the Peptide department: Reiner Loder, Sascha Rauch, Ludger Wäss, Alma Sadikovic, Claudia Schneider, and Katrin Schlitt; from the NMR department: Dr. Michael Kurz, Dr. Maic Fredesdorf, Nicole Hörl, and Ute Messinger; from the Purification department: Richarda Hennig, Thorsten Zeisberg, and Steffen Kohlitz; from the Radiochemistry department: Remo Weck, Dr. Wolfgang Holla and Dr. Jens Atzrodt; from the analytical department: Thomas Wendrich, Ana Villar Garea, Nicola Jacoby and Christian Ehrmann; from the Biology department: Dr. Matthias Lohmann, Dr. Jürgen Dedio, Birgit Herzog, Inge Kress-Fischer, Angelika Sabel, Dr. Klaus Steinmeyer, Dr. Yuri Ivashchenko and Dr. Matthias Schäfer. Thanks to Dr. Mark Brönstrup and Dr. Pablo Juretschke for the initial coordination. My project would not have been possible without the help of all the above-mentioned people.

Thanks a lot for the very kind welcome of the players of the Sanofi Soccer team: Caka, Darius, Benni, Oli, Marc, Erwin, Alex, Patrick, Bodo, Norbert, Felix, Albert, and of course mon collègue bordelais Patrice. That was a lot of fun!

Many thanks to Dr. Michael Wagner and Dr. Stefan Petry for giving me the opportunity to dive into the chemistry of peptides and fatty acids, and for all the useful advice during the group meetings.

Many thanks to Dr. Andrea Wolf for teaching me cell culture, for explaining me the basis of microscopy and for having devoted time to help me with on various projects.

Many thanks to Dr. Meltsje de Hoop for the fruitful discussions and the novel ideas. I am also very grateful for the great training on confocal microscopy and the efforts invested on characterizing the fluorescent probes together with Fabian Reinisch.

Many thanks to Dr. Matthias Löhn and his coworkers for their great help with the animal experiments, the isolation of islets, and the cell sorting. I always felt warmly welcomed in Matthias' lab and I really appreciated our discussions and your very positive mindset.

Special thanks to Dr. Haiyu Hu for your precious advice during my first months in the company, for the training on SPPS, for the chinese lessons, and of course, for the very nice bike.

Special thanks to Dr. Seth Jones for proofreading my last article and my thesis, for correcting my English, and for explaining the subtelties of your language. Beyond than, thanks for being such a nice colleague to discuss and work with. Good luck for your research work at Sanofi and … for the baby ☺!

Special thanks to Dr. Elsa Pflimlin for creating such a musical and pleasant atmosphere at work. The two years spent in the same office will remain as very good memories. Merci pour tes conseils et ton soutien dans les moments difficiles. En espérant que nos chemins se croiseront à nouveau dans le futur. Peut-être sous le soleil de San Diego ou la pluie de Paris.

Very special mention goes to my two enthusiastic and amazing supervisors: Prof. Oliver Plettenburg & Dr. Volker Derdau. You have been both great supervisors and instructors. I really benefited from your advice and expertise; by your sides, I had the chance to learn about chemistry, biology and radiochemistry but also about pharmaceutical research and development, molecular imaging and medicine. Not many Ph.D projects involve working in such a multi-disciplinary environment and I am very happy I embarked upon this project with you. I am particularly grateful for their guidance, their patience, their constant support, and their trust in my work, especially during moments of doubts. In der Hoffnung, dass sich unsere Wege eines Tages wieder kreuzen!

Volker, many thanks for your kind and useful supervision, notably during the last months, it meant a lot to me. I hope you will get as much fun with your new Ph.D student as we had together. Ein ganz großes und herzliches Dankeschön!

Oliver, many thanks for opening my mind to many different disciplines and for having nurtured my curiosity - you always encouraged me to go beyond. I wish you all the best for your new adventure in Hannover and Munich. Ich drücke Dir ganz fest die Daumen!

Cette thèse n'aurait pas été possible sans le soutien de mes proches. Merci à tous mes amis de Pessac, de Bordeaux, de Montpellier, de Francfort et d'ailleurs. Nos retrouvailles à travers l'Europe, ou à la maison, pour un molkky, pour une shisha, pour un jorky, ou simplement pour boire des coups, m'ont ressourcé et m'ont donné beaucoup de force pour continuer à avancer. Merci à Jojo, Felix et surtout à Kevin pour avoir organisé cette magnifique mission en Egypte dont on se souviendra longtemps. Un grand merci à Mathieu pour avoir accepté de concevoir la couverture de cette thèse.
Mention toute particulière à mes ami(e)s chers : Tati mon inséparable partenaire de crime, Simon KM, Rouffy, Mehdi, Marie, Romain KB, Mamy Laure, Guigui, Bédou, Claire R., Tiphaine, Claire N., Chlo, Bobby et Mimi qui sont venus (ou revenus) me rendre visite à Francfort.

Bien évidemment, un immense merci à ma famille pour m'avoir soutenu et donné du courage. Dans les moments de doutes et de remise en question, vous avez toujours été présents. La prophétie raconte que j'étais destiné à faire un métier avec un uniforme. Papa, Maman, j'espère que devenir un chercheur en blouse blanche vous rendra fier.

Enfin, un merci très spécial à Marion et Gustavo qui m'ont accompagné au long de cette aventure allemande. Votre présence à mes côtés a rendu le quotidien très joyeux. Je garderai un magnifique souvenir de mon passage à Francfort, et c'est en très grande partie grâce à vous. Mille mercis !
Um agradecimento muito especial para Marion e Gustavo que me acompanhou durante toda esta aventura alemã. A sua presença comigo fez os dias mais alegre. Eu mantenho uma maravilhosa memória da minha visita em Frankfurt, e isso é grande parte graças a você. Da parte do koalinha para o sapinho. Muito obrigado !

Cette thèse est dédiée à la mémoire de mon amie Lise Deval, rencontrée pendant mes travaux de recherche. Originaires de Bordeaux, le destin aura croisé nos chemins à Francfort pour nouer une amitié trop brutalement interrompue. Ton sourire, ta pétillante joie de vivre et ta gentillesse ne seront jamais oubliés. Repose en paix.

About the author

Romain Bertrand was born in Neuilly sur Seine, France on September 29th 1989. He grew up in Pessac, a city close to Bordeaux, in southwestern France. In 2007, he graduated from the Lycée Pape Clément in Pessac before enrolling in preparatory classes in Lycée Montaigne in Bordeaux. In 2009, he entered the National Graduate School of Chemistry in Montpellier (ENSCM), where he obtained his Bachelor in Science degree, with a special focus on organic chemistry. He next moved to Philadelphia, USA in 2011-2012 to perform a Co-op program and joined the Heart Failure Medicinal Chemistry department of GlaxoSmithKline in King of Prussia, USA. In 2012, he returned to Montpellier to finalize the ENSCM curriculum and graduated as a chemical engineer in 2013. In parallel, he received a "Chemistry for the biomolecules of life" Master in Science degree. The same year, he started a PhD project at Sanofi in Frankfurt am Main, Germany, under the supervision of Dr. Volker Derdau and Prof. Oliver Plettenburg, registered at the Radboud University Medical Center in Nijmegen, the Netherlands, with Prof. Martin Gotthardt as the academic mentor. The PhD program, *Beta Train*, was part of a prestigious Marie Curie initial training network for excellence in molecular imaging in diabetes, funded by the European Union's seventh framework program. *Beta Train* brought together experts with cutting-edge expertise in the field of β-cell-diabetes imaging and image processing. His PhD research focused on the synthesis and characterization of novel fluorescent probes and radioactive tracers for β-cell imaging, as well as on the development of a new method for the labeling of peptide towards the synthesis of bio-imaging probes. This research resulted in the present thesis.